A TRUNCATED AXIAL SKELETON:

THE EVOLUTIONARY LOSS (AND REAPPEARANCE)

OF VERTEBRAE IN ANURANS

by

Gregory R. Handrigan

Submitted in partial fulfillment of the requirements
for the degree of Doctor of Philosophy

at

Dalhousie University
Halifax, Nova Scotia
July 2006

Your file Votre référence
ISBN: 978-0-494-19587-1
Our file Notre référence
ISBN: 978-0-494-19587-1

DALHOUSIE UNIVERSITY

To comply with the Canadian Privacy Act the National Library of Canada has requested that the following pages be removed from this copy of the thesis:

Preliminary Pages

Examiners Signature Page (pii)

Dalhousie Library Copyright Agreement (piii)

Appendices

Copyright Releases (if applicable)

TABLE OF CONTENTS

LIST OF FIGURES

LIST OF FIGURES

(continued)

LIST OF TABLES

ABSTRACT

A defining feature of modern anurans (frogs and toads) is their truncated vertebral column. In most, the axial skeleton comprises no more than 9 pre-sacral vertebrae, a single sacral vertebra, and, post-sacrally, the urostyle. Tadpoles from one anuran family, Megophryidae, deviate from this pattern in bearing up to 30 supernumerary vertebral centra in their tails. The osteology and ontogeny of the expanded caudal skeleton of megophryids varies widely within the family, but for all genera, supernumerary vertebrae are resorbed at metamorphosis, presumably by osteoclastic degradation.

A potential molecular candidate underlying the expansion of the tail skeleton of megophryids and its reduced state in other anurans is the gene *Pax1*. *Pax1*$^{-/-}$ mutant mice exhibit loss of ventral vertebral elements, including centra and intervertebral discs. To explore a role for the gene in vertebral column development in anurans, I identified the *Xenopus laevis* ortholog, *XlPax1*, and characterized its developmental expression. The gene is strongly expressed in the pharyngeal endoderm and at lower levels in the sclerotomes, the precursors of vertebrae. This pattern is consistent with amniotes and corroborates a role for *Pax1* in vertebral development in anurans. Given the observation of *XlPax1* transcripts in the tail of *X. laevis*, however, I downplay *Pax1*'s role in caudal vertebral agenesis in anurans.

To explore the molecular basis for the axial truncation of the anuran presacral skeleton, I identified and characterized a second *X. laevis* gene, *XlGdf11*. In the mouse, *Gdf11* has been implicated as a posteriorizing factor, regulating the expression boundaries of *Hoxc* genes and, upon genetic knock-out, causing dramatic posteriorization of the axial skeleton. In *X. laevis*, *XlGdf11* is strongly expressed at the rostral end and also in the tail bud, the site of axial and paraxial tissue progenitors. Furthermore, genetic loss-of-function studies showed that *XlGdf11* is important for the normal formation of the antero-posterior axis; however, the gene does not appear to act through its predicted downstream targets, the *Hox* genes, in carrying out this function.

Collectively, these data underscore both the role of conserved molecular pathways in development and the potential of these pathways to generate novel morphologies.

LIST OF ABBREVIATIONS AND SYMBOLS USED

λ	wavelength
[*gene*]$^{-/-}$	homozygous mouse mutant for particular gene
12/101	1° antibody against early skeletal muscle
3'	3' end of nucleotide sequence
5'	5' end of nucleotide sequence
ANOVA	Analysis of Variance
BLAST	Basic Local Alignment Search Tool
BMP	Bone Morphogenetic Protein
bp	base pair
CAS	California Academy of Sciences
CRAM	Cranial reduction and axial malformation
cDNA	complementary DNA
ddH_2O	distilled, deionized water
DEPC	diethylpyrocarbonate
EST	expressed sequence tag
F	*F*-distribution
FMNH	Field Museum of Natural History
EtOH	ethanol
I,II,…	presacral vertebrae of anurans
ISH	*in situ* hybridization
MMR	Marc's Modified Ringers
MNHN	Muséum National d'Histoire Naturelle
MO	morpholino
n	sample size
NCBI	National Center for Biotechnology Information
NIBB	National Institute for Basic Biology, Japan
p	probability value of a statistical test
PS1,2,…	post-sacral centra of megophryid tadpoles
PSM	presomitic mesoderm
ROM	Royal Ontario Museum
RT-PCR	reverse transcriptase polymerase chain reaction
TGF-β	Tranforming Growth Factor Beta
UPGMA	Unweighted Pair Group Method, Arithmetic Mean
UTR	untranslated region of mRNA
X[*gene*]	*Xenopus* ortholog of a gene
XlGdf11	orthologous *Gdf11* gene in *Xenopus laevis*
XlGdf11	orthologous *Gdf11* protein in *Xenopus laevis*
XlPax1	orthologous *Pax1* gene in *Xenopus laevis*
XlPax1	orthologous *Pax1* protein in *Xenopus laevis*
ZRC	Raffles Museum of Singapore

ACKNOWLEDGEMENTS

Special thanks to Richard Wassersug for his unflagging faith in my abilities as a scientist.

Thank you to my labmates and friends in the Wassersug lab: JoAnne Phillips, Kerri Oseen, Dr. Irena Rot, Christopher Taylor, Monika Fejtek, Lesley Roberts, Dr. Einas al-Eisa, Gillian Gouchie, Michelle Brett, Jamilia Maimaiti, and Josie Todd.

Sincerest thanks as well to my mentors Drs. Vett Lloyd and Brian Hall and members, alumni, and friends of their labs, especially Dr. Andy Haigh, William MacDonald, Tara Edwards, Lori McEachern, Neely Vincent, Matthew Vickaryous, Tim Fedak, Michelle Connolly, Lisa Budney, Dr. Tamara Franz-Odendaal, Dr. Wendy Olson, Andrew Gillis, Donna Krailo, and Dr. Eckhard Witten. This project never would have got off the ground without your help.

The following people each contributed in some non-trivial way to the work presented in this thesis and deserve acknowledgement: Alexander Haas, Peter Vize, Anne Maglia, Barb Banbury, Naoto Ueno, Stephane Grosjean, Jinzhong Fu, Gunter Wagner, Anna Urban, Xiaolan Zhou, Leon Browder, Jill Johnston, Gary Sisson, Victor Rafuse, Frank Smith, Anne Louise MacDonald, Ira Blitz, Sashko Damjanovski, Boris Kablar, Jonathan Slack, Richard Harland, Ian Paterson and members of the Gene Probe Lab; the curatorial staff at the AMNH, CAS, FMNH, MNHN, ROM, and the Raffles Museum of Singapore.

Special thanks to Dr. Richard Elinson for generously agreeing to read this thesis.

Finally, I would like thank my parents and brothers as well as my friends Gerard Murphy, Dolly Wadhwa, Daniel Basquill and Prabakaran Soundararajan, for their encouragement and distraction over the past 5 years.

CHAPTER 1:

GENERAL INTRODUCTION

The fundamental question of my doctoral research relates to the underlying adaptive, developmental and molecular forces that led to the evolutionary truncation of the anuran axial skeleton. In other words, why do frogs and tadpoles lack caudal vertebrae and why is their presacral skeleton so truncated?

I have already discussed these two questions at length in a paper I co-authored with Dr. Richard Wassersug, titled 'The anuran *Bauplan*: A review of the adaptive, developmental and ontogenetic underpinnings of frog and tadpole morphology.' This paper, which is currently in press in the journal *Biological Reviews of the Cambridge Philosophical Society*, is presented herein as chapters 2, 4 and 7.

My reason for splitting this manuscript into three separate, non-adjacent chapters is that the original research presented in the intervening chapters, 3, 5 and 6, represents direct extensions of ideas raised in the review:

Chapter 3 describes the identification and characterization of the *Xenopus laevis* ortholog of *Pax1*. In amniotes, this gene is integral to the development of centra, the vertebral components missing from the tails of most larval anurans. Based on the observed conservation of sequence and expression profile of *XlPax1* compared to the amniote orthologs, I hypothesize that *XlPax1* is indeed a regulator of vertebral development in *X. laevis*. The presence of transcripts at caudal levels in *X. laevis* tadpoles, however, suggests a less significant role for *Pax1* in caudal vertebral agenesis.

In chapter 5, I describe the identification and characterization of another *X. laevis* gene, *XlGdf11*. Amniote orthologs of *Gdf11* have been shown to organize the trunk vertebral column by delineating the expression of a battery of *Hox* genes. *XlGdf11*, thus, represents a good candidate gene for studying the anteriorization of the presacral skeleton that has occurred during anuran evolution. The expression pattern of *XlGdf11*, as visualized by *in situ* hybridization, corroborates a role for the gene in axial patterning in *X. laevis*. Molecular gain- and loss-of-function studies, however, indicate that *XlGdf11* may not function alone or perhaps in a different manner in regulating *Hox* expression boundaries than in amniotes.

Finally, in chapter 6, I deal with an unusual anuran family, Megophryidae, in which tadpoles of several genera bear supernumerary vertebral centra in their tails. This skeletal morphology starkly contrasts that of all other anurans, which present only rudimentary neural arch elements post-sacrally. I survey 9 megophryid genera, identifying at least 5 that share this novel morphology. Among these genera, there is great variation in the number of caudal vertebrae as well as in the modes of ossification. In all cases, however, vertebrae are resorbed at metamorphosis, and the typical, reduced anuran post-sacral skeleton is reclaimed. I correlate the appearance of caudal centra in megophryids with their unusual riparian ecology and speculate as to the underlying developmental and molecular bases.

The third and final segment of the Handrigan & Wassersug review is included in Chapter 7, where I cull the specific conclusions raised in Chapters 2 and 4 into a general

discussion about the nature of *Bauplan* and its role in driving morphological evolution. Finally, in the general conclusion to this dissertation (Chapter 8), I consider my original research findings in the broader contexts of *Bauplan* and evolutionary-developmental biology.

CHAPTER 2:

THE ANURAN *BAUPLAN*

The contents of this chapter together with chapters 4 and 7 are currently in press in the journal *Biological Reviews of the Cambridge Philosophical Society* as:

Handrigan, G. R. & Wassersug, R. J. The anuran *Bauplan*: A review of the adaptive, developmental, and genetic underpinnings of frog and tadpole morphology, 100 manuscript pages.

2.1 INTRODUCTION

Anurans (frogs, toads and tadpoles) are characterized by a biphasic life history with distinct larval and adult phases joined by a major metamorphic event (*i.e.,* indirect development). Tadpoles and post-metamorphic anurans differ in most respects, including habitat, diet, behavior, and physiology. Morphological differences are particularly striking; tadpoles have globular bodies and long, flexible tails, whereas adults completely lack a tail and have stout bodies with well-developed limbs. At the same time, tadpoles and frogs share some key features in common, such as a truncated axial skeleton and absence of caudal vertebrae, which confer adaptive benefits on both life stages. What is more, these features are very tightly conserved across the order—virtually all tadpoles and frogs have them.

In his review of anuran phylogeny, Griffiths (1963) noted this "extreme morphological uniformity" and went as far as to say that anurans are "the most easily diagnosed of all vertebrate groups." In the following review, I qualify these statements by pinpointing several diagnostic anuran characters and discussing at length their adaptive implications, and ontogenetic and genetic bases. My focus lies primarily with those features common to both tadpole and adult and thus particularly integral to the anuran *Bauplan.*

2.2 *BAUPLAN* AND ITS NESTS

The term *Bauplan* (German transl. 'blueprint', 'ground plan'; n. pl. *Baupläne*) has been with us for 50 years, although its conceptual origins extend back to the work of Buffon and Cuvier (Hall, 1996). *Bauplan* has been variously conceptualized as: "the basic organizational plan common to higher taxa at the level of the phylum, order or class," "the suite of characters that unites members at higher taxonomic levels", and "all the morphological features from conception to death [shared by higher taxa]" (Hall, 1996; pp. 224-226; see references therein for original source). I draw especial attention to the latter as it underscores the continuity of life history and thus integrates larval and adult phases into a single *Bauplan* concept. In other words, transient ontogenetic features as well as fixed adult characters fit under the umbrella of *Bauplan*. This is particularly appropriate when discussing animals with complex life histories, such as anurans.

In my view, a *Bauplan* is characterized by a suite of derived, diagnostic features that are shared by (and possibly unique to) members of a higher, monophyletic taxon. The vertebrate *Bauplan*, for example, would include features of the phylotypic period (*e.g.*, notochord, tail bud), a mineralized skeleton, and the neural crest among others. Generally speaking, *Bauplan* characters are synonymous with synapomorphies—both describe and unite animals within a clade. A *Bauplan* designation, however, holds broader implications; it not only defines a taxon, but also the lifestyle of its members. Also implicit in *Bauplan* are the evolutionary and developmental mechanisms that established and have subsequently maintained the generalized morphology of a taxon.

Anurans fit neatly within the vertebrate *Bauplan* as outlined above. As a readily-diagnosable group, however, they also have their own *Bauplan*. Similarly, *Baupläne* can be assigned to bats, cetaceans, turtles, snakes and other higher, diagnosable vertebrate taxa. These sub-Vertebrata *Baupläne* are not distinct from the vertebrate *Bauplan*, but nested within it—*Unterbaupläne* (Hall, 1996). This hierarchical aspect makes the *Bauplan* concept a useful tool for high-level taxonomy, particularly in the delineation of phyla (for examples see: Brusca & Brusca, 1990; Nielsen, 2003).

Unterbaupläne can diverge considerably from each other—compare snakes and frogs—but generally do not deviate beyond the morphological bounds of the overarching *Bauplan*. For instance, vertebrates display much variation in skeletal morphology, but no vertebrate has completely *done away with* its skeleton. The morphological bounds of a *Bauplan* are set by constraints, which emerge from the inherent biases of development, and the canalizing effect of phyletic history (Hall, 1996). Thus, *Bauplan* is a window into the mechanisms at work in major morphological evolution (*i.e.*, macroevolution) and, through unifying and organizing higher taxa, provides a framework in which to study these mechanisms.

I do not offer here a complete character list of the anuran *Bauplan*. Instead, I have deliberately ignored many features, such as the hinged pelvic apparatus and broad fenestral cranial skeleton, in order to focus on these three: 1) absence of caudal vertebrae, 2) a truncated axial skeleton, and 3) elongated tarsal elements. I address, in turn, the

evolutionary origins, adaptive implications, and genetic and ontogenetic bases of each; and then synthesize these points into a general discussion of the origins of vertebrate morphological diversity as well as the utility of the *Bauplan* concept in clarifying the roles—and interplay—of development and ecology in determining diversity. To begin, I discuss the tails of anurans, which nominally lack them.

2.3 'AN-URA': MISSING A TAIL

In conventional use, the term 'tail' denotes *a segmented extension of the body beyond the anus* (Young, 1962; Handrigan, 2003). By this definition, all frogs and toads are rightly considered anural—they have highly compact bodies that terminate at the vent (anus). This is even the case for the tailed frog *Ascaphus truei* (for a photograph of this species and others mentioned throughout, please visit AmphibiaWeb: http://elib.cs.berkeley.edu/aw/). Adults of this basal anuran species are endowed with a tail-like albeit stubby appendage. Whereas the 'tail' of *Ascaphus* has some musculature consistent with a caudal origin, it is, in fact, an intromittant organ; *i.e.*, an unsegmented, cloacal extension that facilitates internal fertilization (van Dijk, 1959; Brown, 1989).

Tadpoles, however, are most certainly not anural: Their elongate tails extend well beyond the anus and are the primary means of motility up until metamorphosis. Tails are even seen in anurans that do not have a free-living larval phase (*e.g.*, *Eleutherodactylus*), but instead of propelling the animal they have been co-opted for other uses, including gas exchange in select species (Townsend & Stewart, 1985; Callery, Fang & Elinson, 2001).

In all cases, the functionality of the tail is lost in adult anurans, along with the tail itself. Clearly, the focus was on the latter when the label 'Anura' was first applied to the taxon.

The tadpole tail is an *incomplete* extension of the body—it comprises all axial structures except for the vertebral column, which terminates at the level of the anus in nearly all anurans. The serially-arranged muscles of the tadpole tail, the myotomes, instead work against a thick, rigid notochord. Curiously, caudal vertebrae are present in larvae of the genus *Megophrys* (Griffiths, 1956; 1963; see Fig. 2.1) and in closely related genera within the family Megophryidae (Haas, Hertwig & Das, 2006; pers. obs.). These vertebrae are quite rudimentary, consisting of mere centra without corresponding neural arches, and vary greatly in number among genera. In the extreme, the larvae of *Leptobrachella mjobergi*, which burrow into gravel at the bottom of streams, bear 25+ caudal vertebrae that almost reach the tail tip (Haas *et al.*, 2006; see below). Adult megophryids lack these extra vertebrae.

2.4 Enter the *Bauplan*

Along with the tail, the anuran trunk has also seen an evolutionary reduction in its vertebral complement, with no more than nine presacral vertebrae in *Ascaphus* and as few as five or six in some pipids, such as *Hymenochirus* (Fig. 2.2). Frogs and toads have a third fewer vertebrae between skull and sacrum than most tetrapods. The few (2-4) vertebrae found posterior to the sacrum in anurans, larval megophryids a notable exception, are incomplete and fused in the adult.

The 'telescoping' of the vertebral column and the coincident loss of an adult tail occurred *pari passu* with the appearance of anurans. The earliest identified (ca. 250 million years ago) frog-like fossil species, *Triadobatrachus massinoti*, bore an axial skeleton consisting of up to 14 pre-sacral, rib-bearing vertebrae and a tail comprising at least six discrete vertebrae (Rage & Roček, 1989). By the Early Jurassic, the pre-sacral complement had been reduced to ten (Báez & Basso, 1996; compared to the eight originally reported by Estes & Reig, 1973) and the tail reduced to a coccyx fused to an elongate urostyle as exemplified by the early frog *Vieraella herbsti* (Estes & Reig, 1973). An elongate urostyle also characterized the earliest frog *Prosalirus bitis*, which predates *V. herbsti* by 10-15 million years; however, the number of presacral vertebrae in this species is unknown (Shubin & Jenkins, 1995; Jenkins & Shubin, 1998). Among extant taxa, the coccyx consists of 2-4 fused post-sacral vertebrae (Fig. 2.3). Only the dorsal portions, the neural arches, of these vertebrae are seen prior to metamorphosis. Vertebral bodies (centra) are almost never seen, except in some megophryid larvae.

Further novelties ushered in by *Prosalirus* and *Vieraella* and retained by modern anurans are elongate tarsal bones in the hindlimb (Estes & Reig, 1973; Shubin & Jenkins, 1995; Jenkins & Shubin, 1998). The moderately elongated tarsals of *Triadobatrachus* and the Lower Permian *Doleserpeton* suggest, however, that this limb elongation had begun much earlier (R. Carroll, pers. comm.). These typically nodular elements in other amphibians have been lengthened in anurans to resemble the more proximal hindlimb bones, the tibia and the fibula (see insets in Fig. 2.2). Elongate tarsal bones have

otherwise only been described in the saltatory prosimian primates galagos and tarsiers (Emerson, 1985; Blanco, Misof & Wagner, 1998).

The anuran *Bauplan* was thus established by the time *Prosalirus* and *Vieraella* evolved, and, in the subsequent 200 million years, it has seen relatively minor modification. The reduced post-sacral skeleton, short trunk, and elongate tarsals that served the early Jurassic anurans have been retained in modern frogs. In the following section, I review the adaptive implications of these *Bauplan* characters.

2.5 The Bauplan at Work

Frogs and toads are largely saltatory animals. Like kangaroos, prosimian primates, and other jumping vertebrates, they propel themselves by the synchronized extension of their hindlimbs. In frogs, however, this gait is ballistic and episodic rather than cursorial as in kangaroos where the centre of mass maintains a nearly constant velocity and the tail counter-levers the mass of the rest of the body (see Hutchinson, 2004 for a recent review). Frog jumping contrasts directly with the undulatory, fluid locomotion seen in most other vertebrates, whether they are swimming in water or walking and running on land (Emerson, 1985).

Anuran saltation likely evolved in a riparian environment, at the interface between land and water, as an effective escape mechanism (Gans & Parsons, 1966). According to Emerson (1985, p. 58), "[jumping has the ecological effects of] quickness and

unpredictability, as well as height and distance." Faced with a threat, a frog on the shore could easily escape to the safety of water in a single bound. A swift and long jump may also prove useful to a frog in catching food (Gans & Parsons, 1966).

2.5.1 The adult: built for jumping

Various features of their morphology well suit adult anurans for jumping: large hindlimb muscles, reduced forelimbs, an ilio-sacral hinge apparatus, a fenestral (hence lightweight) skull, and the three characters that form the focus of this paper: a missing tail, truncated vertebral column, and elongate hindlimbs (Emerson, 1985).

Hindlimb muscles are the anuran motor. Muscle fibers within the hindlimbs are maximally activated during a jump and operate at optimal sarcomere length and shortening velocity (Lutz & Rome, 1994; Peplowski & Marsh, 1997; Roberts & Marsh, 2003). The bones of the anuran hindlimb, including the elongate tarsal elements, provide an extensive scaffold with additional attachment sites on which the muscles can act.

Other jumping specializations of the anuran *Bauplan* ensure the efficient use of the power generated by the hindlimbs. A frog can jump farther when its center of mass is in line with the propulsive force (Emerson, 1979; 1985). When the center of mass is not in line with the thrust vector, torque is generated, and the body rotates, abbreviating the jump. In the pre-jump, flexed position of the hindlimbs, the long axis of the femur of a frog is flexed ventrally in reference to the vertebral column. Simple extension of the hindlimbs

would pitch the snout downward. However, compensatory dorsiflexion at the ilio-sacral joint brings the anterior part of the frog's body in line with the pelvic girdle and the propulsive force generated by the hindlimbs. A frog is thus able to jump farther and with greater control (Emerson, 1979; 1985).

The rationale for why anuran saltation is more efficient with a short, compact torso and concurrently no tail can be understood in light of basic biomechanics. The longest distance any large mass projectile will travel occurs with a takeoff angle of ~45°. This angle can be achieved more easily when the body is short. A longer torso would necessitate proportionately longer front limbs to elevate the head. That, in turn, would add mass, which would increase the cost of locomotion. A short torso in saltatory anurans thus requires only short forelimbs, which cost little, but also add little or nothing to thrust during jumping. A longer body in and of itself would require more muscle activity to resist axial bending and torque while in flight, adding, again, to the cost of locomotion.

A tail, if it were retained after metamorphosis, would obstruct depression of the vent, when the head is elevated at the start of a jump. The cost to a frog of having a tail in tow was demonstrated experimentally by Wassersug and Sperry (1977). They found that anurans in the middle of metamorphic climax jumped farther when their tails were surgically removed. With a tail remnant still present, the froglets could not raise their snouts to 45°. The tail neither facilitated pushing off straight at the start of the jump nor provided propulsion during the aerial phase of the jump—it merely added mass. Thus,

removal of the tail either by surgery (as in Wassersug & Sperry, 1977) or by natural metamorphosis seems to improve terrestrial locomotor performance for anurans.

2.5.2 The tadpole: built for swimming and metamorphosis

A short, tailless torso appears to facilitate saltation for the adult frog, but then why should anurans have a tailed tadpole? The tadpole tail, as a midline axial propeller, permits undulatory aquatic locomotion, which is more efficient for sustained locomotion in the water than a saltatory frog kick (Wassersug, 1989). In lacking an osseous skeleton, the typical tadpole tail is more flexible than that of most fishes. As a result, it provides tadpoles with the ability to rapidly fold themselves in half and to turn 180° in a fraction of a body length (Hoff & Wassersug, 2000). This "folding" of the tadpole at the beginning of a turn is further facilitated by the core feature of the anuran *Bauplan*, the short torso. Tadpoles have very high angle acceleration and extremely short turning radii, which may help them escape predation (Wassersug, 2001). Hydrodynamically, however, the flexible tadpole tail is not as efficient as that of fishes of comparable size (Liu, Wassersug & Kawachi, 1996; 1997).

One advantage of the tadpole's vertebraeless tail is that it can be eliminated quickly at the time of metamorphosis. Rapid regression of the tail is important in the transition because an anuran that has both forelimbs exposed and the tadpole tail still present has neither efficient aquatic nor terrestrial locomotion (Wassersug & Sperry, 1977). Anurans at metamorphic climax consequently experience exceptionally high levels of predation

(Arnold & Wassersug, 1978). This, in turn, has led to selection for rapid metamorphosis. Wassersug (1989) and Hoff and Wassersug (2000) have suggested that having no skeletal elements in most of the tail and support only in the form of a notochord facilitates rapid absorption of the tail and thus rapid transition from the larval to adult lifestyle.

Hoff and Wassersug (2000) did not discuss the problematic group of megophryid frogs, which are exceptions to this story; *i.e.*, their tadpoles have ossified vertebrae in their tails (Fig. 2.1). The extreme example is the *Leptobrachella* larva with 25+ caudal vertebrae (Haas *et al.*, 2006). *Leptobrachella* tadpoles live in an unusual environment and have an exceptional lifestyle—they are active burrowers in gravel. The vertebrae in their tails provide a strong skeleton to anchor muscles that must be recruited to generate thrust for burrowing through a resistant substrate. By having the musculoskeletal machinery for active burrowing, these anurans can hide out of the range of most predators that otherwise attack tadpoles. But they pay a price: The environment in which they live is low in primary productivity, and nutrient acquisition must be slow for *Leptobrachella* tadpoles. It is not known how long these tadpoles take to metamorphose, but it is likely to be substantially longer than for normal pond tadpoles of comparable size.

2.6. Building the *Bauplan*

If a short vertebral column and a truncated tail are key to the anuran *Bauplan*, how is this morphology achieved through modification of the more general vertebrate developmental program? In this section, I detail the development and genetic regulation of the somites,

a sub-population of the mesoderm. Somites are the building blocks of the axial skeleton and thus are central to the evolution of the anuran *Bauplan*. Here I compare somite development in amphibians with other vertebrates in order to highlight discrepancies that may account for the divergent axial morphology of the Anura. I begin with the vertebrate archetype.

2.6.1 From somites to vertebrates

The vertebral column, its associated musculature, and the dorsal dermis all arise from somites. These coalescences of mesoderm cells are arranged as bilateral pairs flanking the neural tube and notochord along the length of the trunk and tail. Somites are formed with the sequential, cranio-caudal division of the segmental plate, located in the tail bud (Christ & Wilting, 1992; Christ & Ordahl, 1995). The presomitic mesoderm (PSM) of the plate is covertly segmented into bilaminar mesenchymal discs, which gradually condense and epithelialize to form the somites.

Similar covert segments, called somitomeres, are thought to occur in the heads of vertebrates—rostrally abutting the segmented paraxial mesoderm, although their existence has been called into question (Wachtler & Jacob, 1986; Freund *et al.*, 1996; Pourquié, 2001; Kuratani, 2005). Somitomeres do not segregate, but are thought to disperse and contribute to various tissues of the head, such as voluntary muscles and dermis. Vertebrate taxa appear to have a characteristic number of somitomeres (reviewed

by Jacobson, 1988; see his Table 1). Both anurans and urodeles appear to have four, whereas *Gallus*, *Mus*, and the snapping turtle *Cheledra* each have seven.

Somitomeres should not be confused with their immediate, and very real, caudal neighbors, the occipital somites, which segregate and epithelialize like their post-cranial counterparts and ultimately contribute to the occipital bone of the skull. Five occipital somites are found in amniotes (Burke *et al.*, 1995), whereas cyclostomes have none (Augier, 1931). The number of occipital somites in amphibians is contentious. Augier (1931) counted three, whereas Chung and colleagues (1989) described four degenerating myotomes in the cranium of *Xenopus laevis*, which they denoted, from rostral to caudal, W, X, Y and Z. Of the four, only somite Z is clearly posterior to the otic vesicle and has a discernible sclerotome (see their Fig. 2B). Immediately caudal to Z is their "somite 1", which is purported to form the first trunk vertebra. This is also at odds with the findings of Smit (1953), who counted only three degenerative somites and assigned a cervical fate to the *first* post-otic somite, Chung *et al.*'s 'Z'. I use Smit's system in the current study (see Table 1) to be consistent with papers cited throughout (*e.g.*, Burke *et al.*, 1995; Lombardo & Slack, 2001).

2.6.2 Somite compartmentalization

In response to inductive signals emanating from adjacent axial and paraxial structures and overlying ectoderm, somites differentiate into discrete compartments as different in cell morphology as they are in cell fate (Christ & Wilting, 1992; Christ & Ordahl, 1995).

Dorsally, a dermomyotome arises from somitic cells that temporarily retain their epithelial character. This compartment will ultimately form both dermis and muscle, but more immediately, a myotome. This secondary somitic compartment forms as cells at the lips of a dermomyotome proliferate, delaminate, and move underneath the compartment (Buckingham, 2001; Brent & Tabin, 2002). Once in a myotome, cells arrange themselves longitudinally and fuse with their cranio-caudal neighbors, forming myotubes that span the entire length of a somite. Medial and lateral lips give rise to epaxial (dorsal) and hypaxial (ventral) muscle, respectively. Myotome development in the zebrafish diverges slightly from this generalized vertebrate pattern: Myogenic adaxial cells, initially flanking the notochord, migrate radially towards the surface ectoderm and concurrently elongate to form mononuclear myotubes (DeVoto *et al.*, 1996; Stickney, Barresi & DeVoto, 2000; Costa *et al.*, 2003).

At occipital, cervical and limb/fin axial levels in amniotes and zebrafish, a distinct population of myogenic precursors, marked by the expression of the gene *lbx1*, de-epithelializes from lateral dermomyotome. These cells migrate from somites to become the muscles of the limb, tongue, and diaphragm (Brand-Saberi & Christ, 1999; Neyt *et al.*, 2000; Buckingham, 2001; Galis, 2001; Brent & Tabin, 2002). At inter-limb/fin levels, muscle progenitors arise directly from epithelial extensions of the myotome. A similar mechanism is employed in appendicular myogenesis in chondrichthyan fishes. In both cases, myoblasts derived from the myotomal extensions do not express *lbx1*, suggesting novel molecular regulation not involving that gene (Neyt *et al.*, 2000).

Dermomyotome's ventral counterpart, sclerotome, arises as cells of the somite wall undergo an epithelial-to-mesenchymal transition and migrate towards the midline. Sclerotomes subsequently divide into rostral and caudal halves, which regroup with sclerotomal cells of neighboring somites and condense around the notochord to form the perichordal tube, the precursor of vertebral bodies and intervertebral discs. This regrouping is called resegmentation. The dense regions of the tube, called perichordal rings, are slightly out of phase with the myotome; they undergo chondrogenesis and subsequently ossify to form the vertebrae as well as rib portions (Christ & Wilting, 1992; Christ, Huang & Wilting, 2000; Pugener, 2002).

In teleosts, the notochord contributes plays a second role in vertebral body development apart from its primary role as a source of inductive signals for the adjacent tissues. Fleming and colleagues (2004) showed that centra of zebrafish neither form via a cartilaginous intermediate nor contain osteoblasts (as labeled by alkaline phosphatase). Rather, centra appear to arise from bone-forming matrix secreted by the notochord. As yet, this mechanism of vertebral development has not been described for any other vertebrate.

2.6.3 A different take: Somite development in amphibians

Somite development in amphibians more or less adheres to the scheme described for amniotes above (Youn and Malacinski, 1981; Keller, 2000; Martin & Harland, 2001). Differences do exist, however, and they provide insight into the developmental basis and

evolutionary history of the anuran *Bauplan*. The first discrepancy addressed here is an inevitability of the biphasic amphibian life history.

2.6.3.1 Decoupled axial and appendicular development in amphibians

In most tetrapods, the axial and appendicular systems develop concurrently. Somites differentiate following neurulation and contribute muscle-forming precursors to the outgrowing limb bud. In amphibians, however, appendicular development is relatively delayed—limb outgrowth does not begin until days or weeks after the somites have undergone terminal differentiation. The decoupling of axial and appendicular development has prompted some (Galis, Wagner & Jorkusch, 2003) to suggest that the amphibian limb bud has evolved as a self-organizing module, capable of autonomous growth and regeneration independent of extrinsic involvement, such as myogenic cells from somite. By this scenario, the limb bud would recruit myogenic cells from adjacent, differentiated muscle tissues (Galis, 2001; Galis *et al.*, 2003).

An alternative scenario has limb muscle precursors migrating from the somite to the limb field, the precursor to the bud, as in other tetrapods, but 'lying in wait'. Martin and Harland (2001; 2006) have shown that muscle progenitors do indeed de-epithelialize from the somite and migrate ventro-laterally in *Xenopus laevis*. Unexpectedly, though, the myoblasts appear to contribute to musculature of *both* the body wall and the limbs (Martin & Harland, 2001; 2006). They noted *lbx1* expression in precursors of the *rectus abdominus* as well as in the limb bud (stage 53). The apparent dual contribution of

migrating myoblasts to the body wall and limbs is at odds with other studied vertebrates, which rely on myotomal extensions at either inter-limb/fin levels or along the entire body axis.

Whereas this work paints a compelling picture, it awaits confirmation by cell-tracing analysis. Tentative tracing work by Satoh and colleagues (2005) gave contradictory results. Using a Cre-LoxP-labeling system, they followed migrating myoblasts until stage 55—two beyond Martin and Harland's study—and found no labeled cells in the limb buds. As the authors concede, however, the labeling system is imperfect, accounting for only 50-80% of myogenic cells in the somite, and may be missing the pool of appendicular myoblasts. A more precise, long-term cell-tracing system is needed to resolve this ambiguity.

Whatever the mechanism for delayed limb development, a functional implication is that it reduces drag on the swimming tadpole (Dudley, King & Wassersug, 1991; Liu *et al.*, 1996; 1997)

2.6.3.2 Myotome development

I now turn my attention to the details of somite compartmentalization and development in amphibians. The myotome is the best studied of the amphibian somitic compartments. In urodelean amphibians, as represented by *Ambystoma*, *Cynops*, and *Pleurodeles*, this population of muscle precursors makes up the greater part of the epithelial somite

(Malacinski *et al.*, 1989; Keller, 2000). Myotome cells, which are initially mononucleate, form somite-spanning, multinucleate myocytes in a manner akin to other vertebrates—cranio-caudal expansion and fusion with adjacent cells (Youn & Malacinski, 1981).

Myotome development in anurans, however, is quite variable. Among the few genera examined, no less than three distinct mechanisms have been identified (Hamilton, 1969; Kiełbówna, 1981; Youn & Malacinski, 1981; for review see Keller, 2000; especially Fig. 14). The myotomal cells of *Pelobates* and the neobatrachians *Rana* and *Bufo*, like those of urodeles and amniotes, fuse with cranio-caudal neighbors to form elongate, multinucleate myocytes. In the model anuran *X. laevis*, however, myotome development is particularly derived: Mononucleated myocytes, initially oriented perpendicular to the cranio-caudal axis, rotate through 90° to traverse the length of the somite (Hamilton, 1969; especially Fig. 5C). Multinucleation, which does not appear to involve cell fusion in *Xenopus*, occurs later in development at stage 45 (as per Nieuwkoop & Faber, 1956). Delayed multinucleation is also a feature of myotome development in *Bombina* and *Gastrotheca*. In these genera, initially polymorphic myocytes elongate and interdigitate to span the somite and subsequently undergo nuclear division. This parallels the events of myotome development in zebrafish (DeVoto *et al.*, 1996; Stickney *et al.*, 2000; Costa *et al.*, 2003).

No clear phylogenetic trend emerges from this survey (Fig. 2.4). The presence of mononuclear myotubules in both zebrafish and archaeobatrachid frogs (*e.g.*, *Xenopus*, *Bombina*), however, suggests that this may approximate the ancestral vertebrate

condition. The similarities between urodeles, amniotes, and neobatrachid frogs would then represent convergencies. In any case, the diversity of mechanisms of myotome development suggests that it is a dynamic process, capable of enlisting a range of cell behaviors to achieve a common end, namely, cranio-caudally oriented myotubules. A broader survey of myotome development in amphibians, especially the much neglected caecilians, and other vertebrate taxa would reveal the true breadth of the variation and the inherent flexibility of the vertebrate *Bauplan*.

2.6.3.3 The rest of the somite

The other two somitic compartments in anurans, the dermatome and sclerotome, have received less attention than their muscle-forming counterpart. They present, however, some interesting departures from the vertebrate archetype that reflect and perhaps underlie the novel axial morphology that characterizes the anuran *Bauplan*.

An amphibian dermatome segregates from the dorso-lateral pole of a somite as myotomal cells elongate. Dermatomal cells are round in shape, arranged in a single layer that underlies the dorsal epithelium and cover a myotome like a blanket (Keller, 2000). Hamilton (1969) contends that the blanket is continuous across somites, but Youn and Malacinski (1981) suggest that it is segmented as in other vertebrates. Little else has been discussed in the literature regarding the dermatome.

The first convincing visualization of sclerotomes in an amphibian, a urodele, was provided by Detwiler (1937), who distinguished a cryptic population from neural crest cells by vital-dying and localized it to the immediate vicinity of the notochord. Mookerjee (1931) and Mookerjee & Das (1939) had previously inferred sclerotome development in anurans from histology, later confirmed by Brustis, Landsmann & Gipouloux (1976) and Youn & Malacinski, (1981). Sclerotomal cells segregate from the ventro-medial corner of a somite as myotome forms. Shortly after, scattered layers of sclerotomal cells can be found adjacent to the spinal cord and notochord, where they differentiate into fibrous connective tissue of the perichordal tube and rings, which, in turn, give rise to cartilaginous precursors by either epichordal or perichordal modes (Fig. 2.5). Dorsally, bilateral sclerotomal populations abutting the perichordal layer proliferate, chondrify and expand to encase the spinal cord, forming the neural arches. [Mookerjee (1931) and Mookerjee & Das (1939) used Gadow's (1896) now defunct term 'basidorsals' to denote these neural-arch-forming populations. They are more appropriately termed 'neural arch centers'.]

Whereas the perichordal rings are alternately arranged with the segmental musculature, there is no evidence to suggest that resegmentation, the recombination of adjacent, rostral-caudal sclerotomal halves, occurs in anurans (Wake, 1970). Resegmentation is similarly equivocal in salamanders (Wake & Lawson, 1973) and in teleosts (Morin-Kensicki, Melancon & Eisen, 2002; Fleming, Keynes & Tannahill, 2004). It may, however, occur in caecilians (Williams, 1959; Wake & Wake, 2000), which seem to

share more in common with amniotes than anurans, salamanders and other anamniotes when it comes to vertebral development (Malacinski *et al.*, 1989).

In anurans and urodeles, as in zebrafish, the sclerotome is dwarfed by the myotome (Williams, 1959; Wake, 1970). *X. laevis* has especially small sclerotomes, each merely a few mesenchymous cells in the vicinity of the notochord (Brustis *et al.*, 1976; Youn and Malacinski, 1981, especially Fig. 2C; Malacinski *et al.*, 1989, especially Fig. 2A; Keller, 2000). Ironically, and like amniotes, members of the third amphibian order, the limbless, elongate caecilians, have relatively large sclerotomes and diminutive myotomes, not to mention a greatly expanded complement of somites (Williams, 1959; Wake, 1970; 1980; Wake & Wake, 2000).

A broad survey of relative somitic compartment size across the Vertebrata may uncover some interesting correlations central to their overarching *Bauplan.* Is an extensive appendicular system, such as the long, heavily-muscled hindlimbs of anurans, correlated with larger myotomes compared to sclerotomes? Conversely, do elongate, limbless vertebrates, such as caecilians as well as snakes, skinks, and cetaceans, generally bear larger sclerotomes than myotomes? As I point out in the following section, somite compartmentalization is a dynamic process that can be easily perturbed in favor of sclerotome or dermomyotome formation.

2.6.4 Genetic specification of the somite

Secreted signals emanating from midline structures establish the dorso-ventral axis of the somite and, in turn, delineate the boundaries of future somitic compartments. The surface ectoderm and the roof plate of the neural tube are both sources of Wnt molecules (Wnt1, Wnt3a, Wnt4, Wnt6, and Wnt7a), whereas the notochord and floor plate secrete Sonic hedgehog (Shh) (Brent & Tabin, 2002; Christ, Huang & Scaal, 2004). Signal diffusion creates opposing, antagonistic gradients that span a somite. At high concentrations in the immediate vicinity of the source, Wnt and Shh molecules act as dorsalizing and ventralizing signals, respectively. Wnt molecules induce expression of *Pax3* and *Pax7* in dorsal epithelial cells that will form dermomyotome (Goulding, Lumsden & Gruss, 1993; Goulding, Lumsden & Paquett, 1994; Williams & Ordahl, 1994). In response to Shh from the notochord and floor plate, the genes *Pax1*, *Pax9*, *Mesenchymal forkhead 1*, *Scleraxis*, and *Twist* are up-regulated in cells of the ventral somite, the future sclerotome (Christ *et al.*, 2004). At the convergence of the gradients, where neither signal is particularly strong, cells show expression of the myogenic progenitor markers *MyoD* and *Myf5*. They will eventually de-epithelialize to form the myotome (Brent & Tabin, 2002).

2.6.4.1 Somite proportions

The relative proportion of the epithelial somite that contributes to a particular compartment depends on the balance of dorsal and ventral signals. Perturbing either gradient, by surgical or genetic manipulation, can result in preferential expansion of one

somitic compartment at the expense of another. Transplanting an additional notochord, a source of ventralizing Shh signal, into the paraxial mesoderm, for example, causes sclerotomes to enlarge and the dermomyotomes to recede (Brand-Saberi *et al.*, 1993; 1996; Pourquié *et al.*, 1993). Conversely, ectopically grafting *Wnt*-expressing cells adjacent to the notochord promotes *Pax3* and *MyoD* expression in the ventral somite and expansion of the dermomyotome; *Pax1* expression and the sclerotomal cell complement are concomitantly diminished (Wagner *et al.*, 2000). Retroviral-mediated *Wnt* over-expression in the paraxial mesoderm produces a similar effect (Capdevila, Tabin & Johnson, 1998).

In each of the preceding examples, somitic cell fate has been reassigned and discrepancies in compartment size are not due to changes in the rate of cell proliferation or apoptosis. That said, recent work by Galli and colleagues (2004) points to a role for *Wnt-3a* in the proliferation of dorsal/dermomyotomal cells. Chick embryos electroporated with *Wnt-3a* exhibit mediolateral expanded dermomyotome and myotome, with no significant change in the number of *Pax1*-positive sclerotomal cells.

In none of these experiments were the manipulated embryos examined post-hatching. It would be interesting to see the effects of perturbing compartment size on gross morphology. For instance, might smaller dermomyotomes and hence reduced appendicular contribution lead to limb reduction?

2.6.4.2 Sclerotome specification in anamniotes

Conceivably, the small sclerotomes of anurans, urodeles and teleosts are the product of attenuated or 'drowned out' inductive signal from the notochord/floor plate. Because sclerotome development in amphibians is poorly described, however, general conclusions drawn for anamniotes are largely from teleost studies.

Genetic perturbation of Hedgehog (Hh) signaling in zebrafish suggests that the somitic compartments of teleosts are as malleable as those of amniotes. The exact role of Hh signaling in zebrafish sclerotome development, however, is ambiguous. Blocking Hh with constitutively active protein kinase A produces the same effect as over-expressing Hh: a reduction in the number of sclerotomal cells. Conversely, the pertussis toxin, a mild Hh blocker, induces sclerotome expansion at the expense of muscle progenitors (Hammerschmidt & McMahon, 1998; Stickney *et al.*, 2000). Further work is needed to resolve this ambiguity and extend the discussion to amphibians.

Hedgehog signaling aside, sclerotome specification in zebrafish seems to adhere faithfully to the amniote program. Expression profiles for the orthologs of *Pax9*, *twist*, and other recognized sclerotome markers are consistent with those of avians and mammals (Nornes *et al.*, 1996; Stickney *et al.*, 2000; Fleming *et al.*, 2004). One glaring omission, however, is the lack of a clone of *Pax1*, one of the fundamental mediators of the axial inductive signal, cell proliferation, and chondrogenesis in the sclerotome. This was also the case for anurans until I identified a *Xenopus* ortholog of the gene.

In the following chapter, I describe the identification and characterization of *XlPax1*, the *Xenopus laevis* ortholog of *Pax1*. This gene is particularly relevant to the discussion at hand as it is a definitive molecular marker of the sclerotome in vertebrates and a key regulator of early vertebral development. *Pax1*-deficient mice, for example, lack ventral vertebral portions, including the centra and intervertebral discs, along the entire length of the column (Wallin *et al.*, 1994). This reduced axial skeleton calls to mind the post-sacral skeleton of most anurans. In Chapter 3, I explore whether the developmental expression of *XlPax1* corroborates a role for the gene in building the caudal skeleton of *X. laevis*. Subsequently, in Chapter 4, I embark on a more general discussion of vertebral preclusion in anurans, returning briefly to *Pax1* and considering potential roles for other players in vertebral formation.

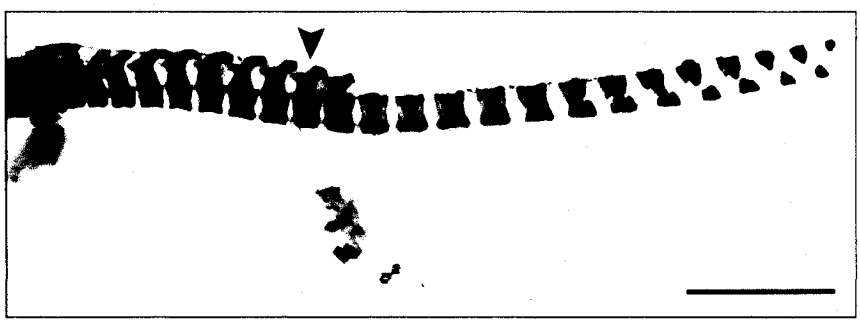

Figure 2.1 Post-cranial skeleton of the tadpole of *Megophrys nasuta* (stage 36). Specimen was cleared and stained with alizarin red and alcian blue for bone and cartilage, respectively. Along with *Leptobrachella* and several other megophryid genera, *Megophrys* bear supernumerary post-sacral vertebral centra—14 in this species. The arrowhead indicates the sacral vertebra. Specimen (ZRC 1.1543) was provided by the Raffles Museum, Singapore and staged according to Gosner (1960). Scale bar equals 4 mm.

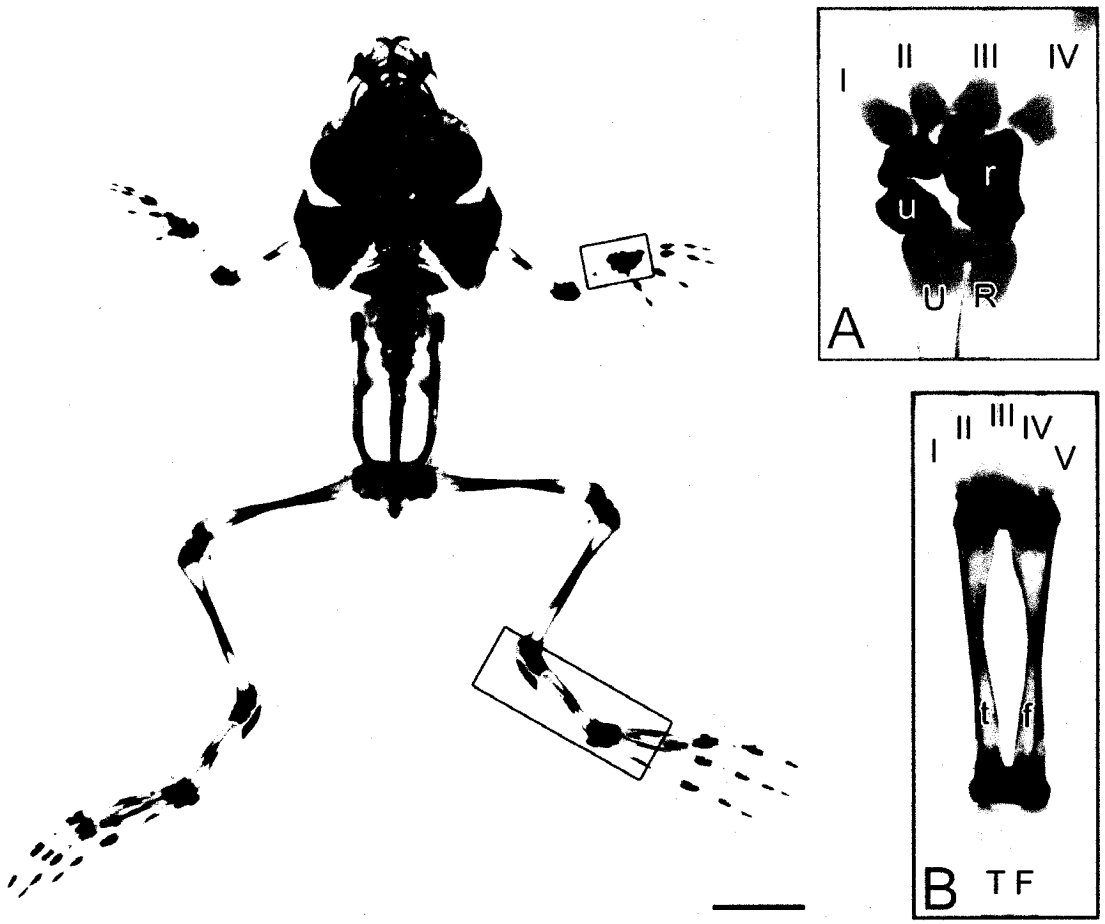

Figure 2.2 Juvenile of the pipid *Hymenochirus boettgeri* cleared and stained for bone and cartilage. Its axial skeleton, among the shortest in the vertebrate world, consists of 8 discrete skeletal elements: 6 pre-sacral vertebrae, 1 sacral vertebra, and the urostyle. Insets: (Top) Distal forelimb elements with highlighted carpals. R, radius; U, ulna; r, radiare; u, ulnare; I-IV, phalanges. (Bottom) Distal hindlimb elements with highlighted tarsals. The tibiare (t) and fibulare (f) are both greatly expanded in anurans. T, tibia; F, fibula; I-V, phalanges. Scale bar equals 2 mm.

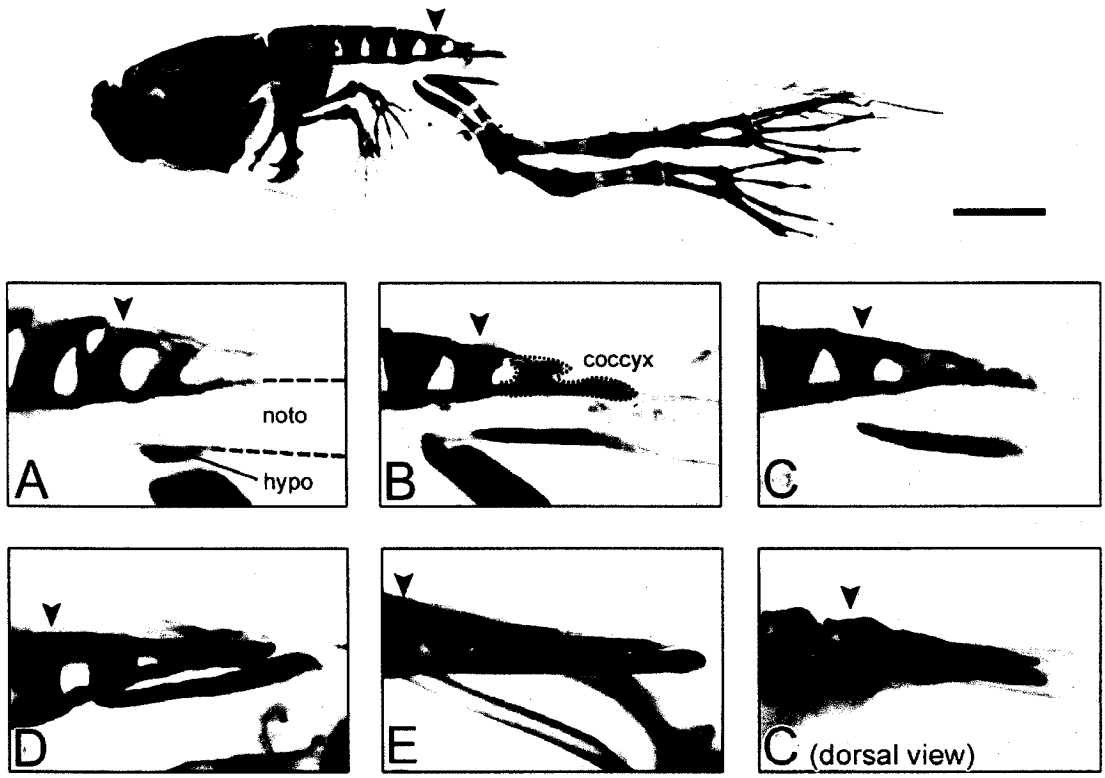

Figure 2.3 Urostyle development in *Hymenochirus boettgeri*. Top: Stage-44 *H. boettgeri* with 8 discrete vertebral elements terminating immediately posterior to the sacrum (arrowhead). Unlike various megophryid species (see Fig. 2.1), *H. boettgeri* bears no osseous elements in its tail. A-E: Ontogenetic series (from Gosner stages 39-46) showing post-sacral skeletal development in *H. boettgeri*. The hypochord (hypo) chondrifies rostro-caudally (and will later ossify). Concurrently, the notochord (noto) collapses, bringing the chondrified hypochord in close contact with the coccyx (outlined in B), a fused series of post-sacral neural arch elements. In pipids and most other anurans, the hypochord and coccyx fuse syntostically. Scale bar equals 2 mm.

Figure 2.4 A partial phylogeny of the Anura. Anurans are conventionally divided into two groups, the 'archaic' Archaeobatrachia and the more 'advanced' Neobatrachia. In this tree I have condensed the latter into two clades, the Ranoidea and Hyloidea, which each compromise numerous families. Anurans originated during the Mesozoic represented here by the proto-frog *Triadobatrachus massinoti* followed approximately 50 million years later by the early anurans *Vieraella herbsti* and *Prosalirus bitis*. Daggers denote these fossil species and broken lines depict their presumed affinities with contemporary anurans. Somitic myotubes arise by at least three distinct modes in anurans; colored circles on tree branches represent the mode for particular clades where this has been investigated. In *Bombina* and hyloids (*e.g.*, *Gastrotheca*), mononuclear myocytes interdigitate and elongate (E) to span the somite (Kiełbówna, 1981). However, in *Pelobates* and the ranoids *Rana* and *Bufo*, elongate myotubes are formed by the rostro-caudal fusion (F) of neighbouring myocytes. Myotube rotation (R), in which mononuclear myocytes initially perpendicular to the longitudinal axis reorient themselves 90˚, has been described only in the pipid *Xenopus laevis* (Hamilton, 1969). The presence of mononuclear myocytes in *Xenopus* and the fellow archaeobatrachid *Pelobates* as well as the teleost *Danio* suggests that this may be the ancestral vertebrate condition; however, this hypothesis is only weakly corroborated by my phylogeny. Tree is adapted from Frost *et al.* (2006).

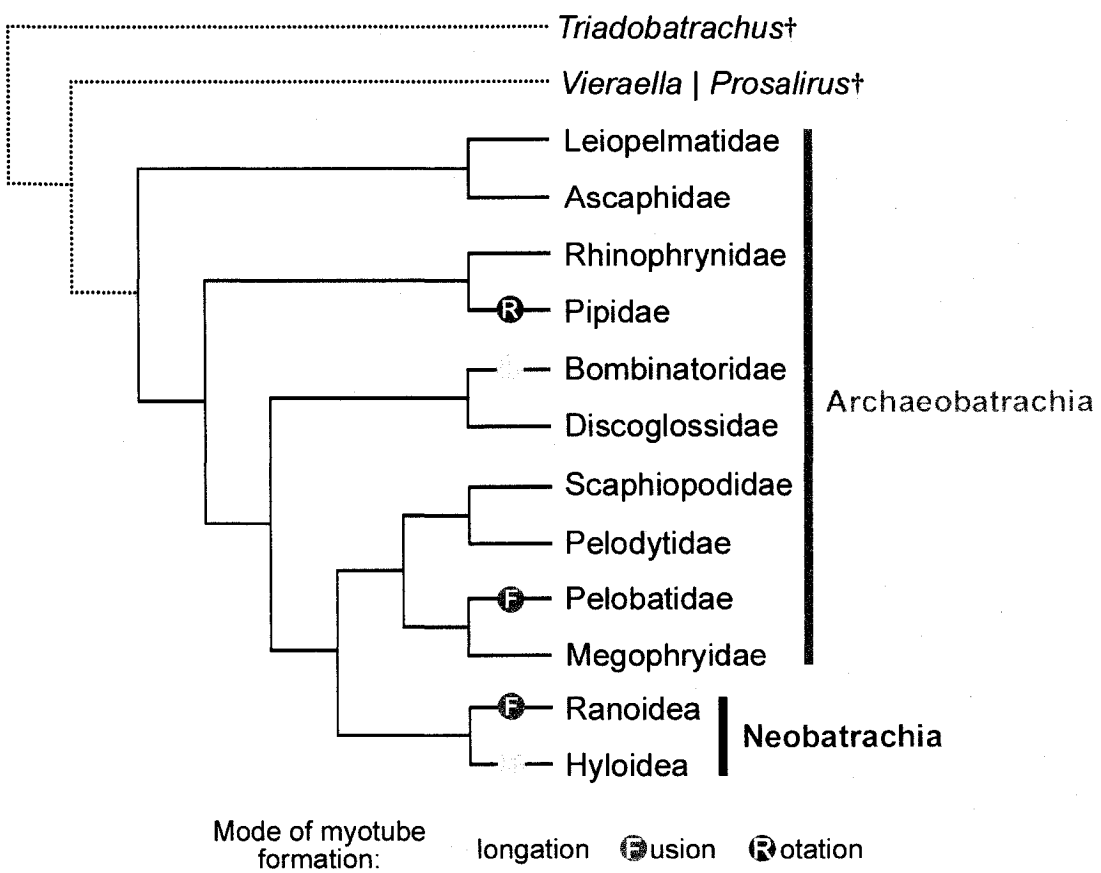
Triadobatrachus†
Vieraella | Prosalirus†
Leiopelmatidae
Ascaphidae
Rhinophrynidae
Pipidae
Bombinatoridae
Discoglossidae
Scaphiopodidae
Pelodytidae
Pelobatidae
Megophryidae
Ranoidea
Hyloidea
Archaeobatrachia
Neobatrachia
Mode of myotube formation:
longation
usion
otation

Figure 2.5 Vertebral development in anurans. Orientation sketch (far left) shows a hypothetical developmental series of somites (S) flanking the notochord (n) and neural tube (NT). Somite 1 has just segregated from the segmental plate and somites 2-5 are progressively older (and more differentiated). Following segregation, epithelial somites undergo compartmentalization (1), forming the sclerotome and myotome. [I refrain from using the term 'dermomyotome' here as it is not clear whether the myotome and dermatome arise from the same somitic compartment in anurans.] Myotomal cells retain their epithelial character, whereas cells of the sclerotome undergo an epithelial-to-mesenchymal transition, migrate medially (2), and then condense around the notochord along its entire length to form the perichordal tube (3). The tube is expanded at intervertebral levels (3 bottom), forming perichordal rings, which give rise to the intervertebral discs; vertebrae form between the rings (3 top). Vertebral centra (c) and intervertebral discs (i.d.) arise by one of two ossification modes. By the perichordal mode (P), the perichordal tube chondrifies (cartilage cells in blue) and subsequently ossifies (pink dotting) around the entire circumference of the notchord; this mode is seen in the families Rhinophrynidae and Ascaphidae. Epichordal ossification (E) of the centra and discs, however, occurs only on the dorsal surface of the notochord. Ventrally, the tube remains fibrous and the notochord undergoes degeneration (Discoglossidae); in the Pipidae and Pelobatidae the ventral perichordal tube chondrifies, but subsequently degenerates (not shown). Neural arch elements (n.a.) and the transverse processes (t.p.) arise from sclerotomal cells that do not contribute to the perichordal tube.

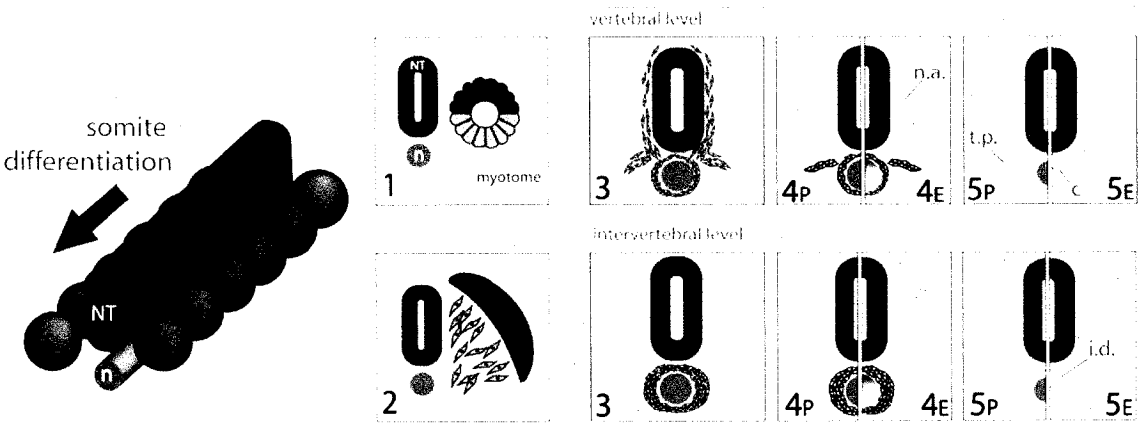
somite
differentiation
NT
n
NT
n
myotome
1
vertebral level
3
n.a.
4P
4E
t.p.
5P
c
5E
intervertebral level
2
3
4P
4E
i.d.
5P
5E

CHAPTER 3:

DEVELOPMENTAL EXPRESSION OF *XlPax1*

3.1 SUMMARY

Pax genes encode transcription factors that regulate organogenesis in vertebrates. Specifically, *Pax1* controls the development of pharyngeal arches and the axial skeleton. I have identified a full-length cDNA clone that represents a presumptive ortholog of *Pax1* in *Xenopus laevis* (*XlPax1*). The putative protein bears an octapeptide sequence and a highly conserved paired domain, which shares 98% and 96% sequence identity with that of other Pax1 and Pax9 orthologs, respectively. Sequence alignment and phylogenetic analysis consistently group XlPax1 with other vertebrate Pax1 orthologs to the exclusion of Pax9, strongly suggesting that it represents the *X. laevis Pax1* ortholog.

I have profiled the expression of *XlPax1* by RT-PCR and *in situ* hybridization (ISH) analysis. RT-PCR reveals that transcripts are up-regulated during the neural-fold stage, when somite segregation commences. Whole-mount ISH shows strong *XlPax1* expression in the facial mesenchyme and the pharyngeal pouches (I-IV) and weaker, segmented expression in the somites. Cross-sectional ISH pinpoints transcripts to the pharyngeal endoderm and to somitic cells immediately adjacent to the notochord, representing the sclerotome. These data corroborate a role for *XlPax1* in the development of the axial skeleton of *X. laevis*. I suggest that *Pax1* may contribute to the lack of caudal vertebral centra in *X. laevis* and other anurans, but the precise underlying mechanism is unknown.

3.2 INTRODUCTION

Pax genes constitute a family of nine members that encode transcription factors bearing a single DNA-binding paired domain. This motif is higly conserved (>90% identity) between both orthologous and paralogous *Pax* family members. Outside of the paired domain, however, there is greater structural variability within the family, which comprises four sub-groups. The Group I genes *Pax1* and *Pax9* together differ from other family members by not encoding a homeodomain. They have retained, however, the conserved octapeptide sequence, which is thought to interact with other proteins in regulating gene trans-activation (Underhill, 2000).

Pax genes are broadly expressed during vertebrate embryogenesis (Strachen and Read, 1994). *Pax1*, the focus of this report, is strongly expressed in the sclerotomes, the precursors of vertebrae and intervertebral discs, and the developing limbs of chick and mouse embryos. Expression is also seen at the head, specifically in the facial mesenchyme, the pharyngeal pouches and pouch derivatives (Deutsch, Dressler & Gruss, 1988; Peters, Doll & Niessing, 1995; Wallin *et al.*, 1996). This expression pattern is closely mirrored by fellow Group I gene, *Pax9* (Neubuser, Koseki & Balling, 1995).

Pax1 function has been best characterized in the developing axial skeleton, where it regulates cell proliferation and chondrogenic specification in the sclerotome (Koseki *et al.*, 1993; Wallin *et al.*, 1994; Ebensperger *et al.*, 1995; Peters *et al.*, 1999; Rodrigo *et al.*, 2003). In $Pax1^{-/-}$ double homozygous mutant mice, sclerotome cells fail to condense and

chondrify, precluding the formation of vertebral bodies, intervertebral discs, and rib portions. Confirming a synergistic interaction between *Pax1* and *Pax9* during axial development, the double homozygous mouse mutant displays even more dramatic skeletal reduction (Peters *et al.*, 1999). Parallels can be drawn between the incomplete vertebral column of the these mutants with that of anurans, which lacks vertebral centra at the caudal level.

To elucidate a potential role for *Pax1* in the development of the reduced anuran axial skeleton, I have profiled the developmental expression of a *Pax1* in the African clawed frog *Xenopus laevis*. The gene, *XlPax1*, encodes a 358 amino-acid polypeptide, which shares strong sequence identity with vertebrate orthologs of Pax1 as well as Pax9. The early expression pattern of *XlPax1* closely parallels that of other vertebrates. Specifically, transcripts are found in the pharyngeal endoderm, facial mesenchyme, and in the medial portion of somites, corresponding to the sclerotome. I discuss these findings in light of the unusually truncated axial skeleton that characterizes anurans (also see Chapter 4, sections 4.3.1 and 4.3.2).

3.3 Materials and Methods

3.3.1 Clone identification

Querying the NIBB XDB *Xenopus laevis* EST database (http://xenopus.nibb.ac.jp/) by tBLASTx with the *Mus musculus* ortholog of *paired box gene 1* (NCBI Accession #

AAK01146) yielded one highly similar clone, XL085n23. It was derived from a cDNA library constructed from tailbud-staged embryos and was directionally-cloned with *Eco*RI (5' end) and *Xho*I (end 3') into the plasmid pBluescript SK-. Following completion of a Materials Transfer Agreement, XL085n23 was received from NIBB as a dried sample on filter paper.

3.3.2 Clone amplification

To generate sufficient template quantities for subsequent sequencing and transcription reactions, subcloning efficiency DH5α competent *E. coli* cells (Invitrogen # 18265-017) were transformed with XL085n23 as per the manufacturer's specifications. The transformed cells were plated on ampicillin-treated agar plates and incubated overnight at 37°C. Individual bacterial colonies were further incubated in Luria-Burtani liquid medium (for this and other solution recipes see Sambrook, Fritsch & Maniatis, 1989) and, on the following day, plasmid DNA was recovered by a mini-prep protocol (as per Sambrook *et al.*, 1989). To confirm success of the transformation and to determine the precise size of the clone inserts, 5μL of each sample was digested for 2 hours using *Eco*RI (Fermentas # ER0271) and then the linearized template examined by electrophoresis on a 1% agarose gel. XL085n23 represented a 1.65 kb insert in pBluescript SK-. Following further purification using a GFX spin column (GE Healthcare # 27-9602-01), clone stocks were quantified by spectrophotometry (λ = 260nm) and then placed at -20°C for long-term storage.

3.3.3 Sequencing and analysis

XL085n23 was sequenced using oligonucleotides (Alpha DNA, Montreal, Quebec; http://www.alphadna.com) against the generic M13 primer sites of pBluescript SK- and internal sites. The clone is full-length, containing an open-reading frame and 5' and 3' UTRs. Sequence data for XL031e11 was assembled and translated in GeneRunner (http://www.generunner.com/) and then deposited to GenBank (Accession # DQ667149; http://www.ncbi.nlm.nih.gov/entrez).

Using the software ClustalX (http://bips.u-strasbg.fr/fr/Documentation/ClustalX/), a multiple protein sequence alignment of XlPax1 with orthologous proteins was generated. Putative Pax1 sequences from each of the following vertebrates were used: *Bos taurus* (XP_617873), *Canis familiaris* (XP_542866), *Danio rerio* (XP_692791), *Homo sapiens* (NP_006183), *Mus musculus* (NCBI Accession # AAK01146) and *Rattus norvegicus* (XP_230663). The basic Clustal alignment was redrawn using the BoxShade Server (http://www.ch.embnet.org/software/BOX_form.html).

3.3.4 Phylogenetic tree construction

Neighbour-joining, UPGMA, parsimony, and maximum likelihood trees were generated based on the comparison of amino acid sequences of vertebrate homologs of Pax1 and Pax9 and the closely-related invertebrate homologs. [**Pax1/9s**: *Branchiostoma* (CAB42656), *Ciona* (NP_001027594), and *Halocynthia* (BAA74835). **Pax1s**: *Bos*

(XP_617873), *Canis* (XP_542866), *Coturnix* (AAB35064), *Danio* (XP_692791), *Homo* (NP_006183), *Mus* (AAK01146), and *Rattus* (XP_230663). **Pax9s**: *Bos* (XP_592227), *Callimico* (AAZ39857), *Callithrix* (AAZ39858), *Canis* (XP_547776), *Danio* (NP_571373), *Gallus* (NP_990243), *Homo* (NP_006185), *Leontopithecus* (AAZ39859), *Lepilemur* (AAZ39865), *Lethenteron* (BAB12396), *Macaca* (AAZ39855), *Mus* (NP_035171), *Pan* (AAZ39854), *Perodicticus* (AAZ39862), *Propithecus* (AAZ39866), *Ptychodera* (BAA78380), *Rattus* (BAE79272), *Saguinus* (AAZ39860), *Saimiri* (AAZ39856), *Takifugu* (AAG44703), *Tarsius* (AAZ39861), and *Xenopus* (AAH84222). **Outgroup root**: *Drosophila* Pox meso (P23757)]. All trees were generated with the PHYLIP 3.6 software suite (http://evolution.genetics.washington.edu/phylip.html) using a ClustalX alignment as the initial input.

3.3.5 RT-PCR

Expression of *XlPax1* transcripts was profiled by relative RT-PCR during early embryonic stages (Nieuwkoop & Faber 11-37). Total RNA was extracted from staged, unfixed *X. laevis* embryos using TRIzol reagent (as per manufacturer's instructions; Invitrogen # 15596-026), twice precipitated in ethanol, and then reconstituted in 30μL of DEPC-treated ddH_2O. Stock concentrations and purities were determined by spectrophotometry, 0.250 ug/uL working stolutions were aliquoted, and all samples were then placed at -80°C for long-term storage. A 245-bp segment of *XlPax1* mRNA was amplified using the Qiagen OneStep RT-PCR kit (Qiagen # 210210) with the primers 5'-agactgaggatcgtggagtt-3' (forward) and 5'-gaagtctgtccctgatttcc-3' (reverse) and the

following reaction conditions: 30 cycles; T_a = 54.0°C; [$MgCl_2$] = 1.5 mM. These conditions also permitted co-amplification of a 189-bp mRNA segment of *Histone H4*, a house-keeping gene routinely used to normalize reactions across stages (Steinbeisser *et al.*, 1995; forward: 5'-cgggataacattcagggt-3'; reverse: 5'-tccatggcggtaactgtc-3'). *XlPax1* and *Histone H4* amplicons were resolved by electrophoresis on a 3% agarose gel and visualized using SYBR-Green (Applied Biosystems # 4306736).

3.3.6 Embryo collection, culturing, and fixation

In vitro fertilization of *X. laevis* was carried out as per Sive, Grainger & Harland (2000). In brief, mature female frogs were administered 500-600 units of human chorionic gonadotropin to induce ovulation and egg-laying (HCG; Sigma-Aldrich # 8554). The next day (~12-16 hours later), unfertilized eggs were gently squeezed from females into a Petri dish. Following a quick wash in 0.4× MMR, 0.2 mL of a slurry of homogenized testes, extracted from a euthanized male frog, was added to the eggs for a minute. Within 20 minutes, fertilized eggs were dejellied by washing in 2% L-Cysteine (pH 7.8) for no more than 4 minutes. Once embryos had reached the appropriate stage, they were euthanized in 0.1% MS222 (Sigma-Aldrich # A5040), fixed in MEMFA (0.1M MOPS, 2mM EGTA, 1mM $MgSO_4$, 3.7% formaldehyde) for 2 hours at room temperature (or overnight at 4°C) and then transferred to 100% ethanol for long-term storage at -20°C.

3.3.7 RNA probe generation and *in situ* hybridization

Approximately 5 μg of extracted, column-purified XL085n23 DNA was linearized in overnight reactions with restriction endonucleases (for sense template: *Apa*I; antisense: *Eco*RI). Following digestion, templates were again purified, reconstituted in 20 μL DEPC-treated ddH_2O, and quantified by spectrophotometry. *XlPax1* RNA probes were generated using digoxigenin-labeled nucleotides (Roche # 11277073910) and T7 or T3 polymerases (Fermentas), for antisense and sense transcripts, respectively. Subsequently, probes were purified by LiCl precipitation, reconstituted in DEPC-treated water and stored at -80°C. Whole-mount *in situ* hybridization was carried out as per Sive, Grainger, & Harland (2000) with the following modifications: RNase T1 was omitted from the stringency washes, embryos were treated with proteinase K for up to 10 minutes, and CHAPS from the hybridization buffer. Bound probe was localized using an anti-digoxigenin, alkaline-phosphatase-conjugated antibody (Fab fragments, Roche # 11214667001) and visualized by chromogenic reaction with the substrate BM Purple (Roche # 11442074001).

3.3.8 Paraffin and vibratome sectioning

Xenopus embryos were processed for paraffin histology as per Sive, Grainger & Harland (2000). For vibratome-sectioning, embryos were embedded in 8% low-melting agarose (Sigma A9414) and cut at a thickness of 30 μm using. Sections were mounted on slides in 100% glycerol, cover-slipped, and then photographed.

3.3.9 Photography

Whole-mount *Xenopus* embryos were were photographed with a Zeiss Axiocam MRc digital camera attached to a Zeiss Stemi 2000-C stereoscope. For paraffin and vibratome sections, an Axioplan 2 microscope was used. Fluorescence images were taken using a Oimaging Qican Fast camera coupled with a Leica MZ FL III stereoscope.

3.4 RESULTS

3.4.1 Characterization and orthology

The clone XL085n23 contains a complete 1,074-bp open-reading frame flanked by 5' and 3' UTRs. Conceptual translation yielded a 358-amino acid protein bearing a conserved paired domain at segment 4-131 and an octapeptide sequence at 197-204 bp (Fig. 3.1). Overall, the putative protein shares high sequence identity with vertebrate homologs of both Pax1 and Pax9 (Table 3.1). To clarify the orthology of the clone, phylogenetic analysis based on a comprehensive multiple protein alignment of vertebrate and invertebrate Pax1/Pax9 homologs was carried out. Maximum-likelihood, parsimony and distance methods alike generated trees grouping XL085n23 with vertebrate orthologs of Pax1 to the exclusion of Pax9 orthologs (see Fig. 3.2 for a boot-strapped consensus tree and Fig. 3.3 for a representative UPGMA tree; other trees not shown). This strongly corroborates *Pax1* orthology for XL085n23, which will henceforth be referred to as

XlPax1. Aligning the presumptive XlPax1 protein sequence with vertebrate Pax1 orthologs shows divergence at two sites within the paired domain and one residue of the octapeptide (Fig. 3.4).

3.4.2 Developmental expression of *XlPax1*

XlPax1 transcripts are barely detectable by RT-PCR up until Nieuwkoop and Faber stage 15, at which time *Xenopus* embryos begin neurulation (Fig. 3.5A). Transcript levels are maintained at moderate levels until early tailbud stages, when a slight spike is detected. At stage 22, whole-mount *XlPax1* expression can be seen as bilateral streaks in the pharyngeal region. By the following stage, a second streak is emerging, and at stage 28, *XlPax1* is expressed as three bilateral pairs of vertical streaks, corresponding to the location of the branchial arches (Fig. 3.5B). Subsequent stages confirm that the rostralmost pair corresponds to the location of the facial mesenchyme, while the second and third pairs represent pharyngeal pouches 1 and 2, respectively. In frontal section through the pharynx, transcripts are clearly restricted to the pharyngeal endoderm, which everts laterally to form the pouches. A third pair of pouches has formed by stage 31 and a fourth and final pair is visible by stage 35, all expressing *XlPax1*.

XlPax1 transcripts are maintained at low levels in the somitic mesoderm throughout these stages (Fig. 3.5C). In cross-section, *XlPax1*expression is seen in the medial-most aspect of the somites, between the notochord and myotome (Fig. 3.6A,B). This corresponds to the location of sclerotome, the bone-forming compartment of the somite. In later stages

(Fig. 3.7), strong *XlPax1* expression persists in the pharynx, but its segmental pattern in the paraxial mesoderm is lost. This coincides with the development of sclerotomal mesoderm into the perichordal tube surrounding the notochord (Nieuwkoop & Faber, 1956). Accordingly, cross-sectional analysis confirms that transcripts are maintained peri-notochordally. During metamorphic climax, *XlPax1*expression is visible in the developing limbs. Transcripts are progressively restricted to the anterior, proximal aspect of both the fore- and hind-limbs (Fig. 3.7B; hindlimb data not shown).

3.5 Discussion

XlPax1, the *X. laevis* ortholog of *Pax1*, is highly conserved with other vertebrate orthologs with respect to its sequence and expression profile during development. The putative protein shares more than 70% overall sequence identity with other orthologs. This value increases to 96% within the conserved paired domain. Similarly, the *XlPax1* expression pattern in *X. laevis* closely mirrors that of other vertebrate orthologs. As in the mouse and chick, expression is in the pharyngeal pouches, facial mesenchyme, sclerotomes, and proximal limb (Deutsch *et al.*, 1988; Peters *et al.*, 1995; Wallin *et al.*, 1996).

A core question is whether the axial skeletal expression of *XlPax1* helps explain how anurans evolved their truncated vertebral column. The dramatically reduced post-sacral skeleton, which is a shared derived feature of the anuran *Bauplan* (see Chapter 2), predicts a similarly dramatic change in the expression or function of *Pax1*, a key

regulator of vertebral development. No such obvious disparity in expression, however, was observed here. This finding downplays a role for *XlPax1* in caudal vertebral agenesis in *X. laevis* and shifts the burden to *XlPax1*'s co-regulators (*e.g.*, *Pax9*) or its downstream targets, the more proximal regulators of chondrogenesis. Indeed, I show in Chapter 4 that the tail of *X. laevis* is negative for tenascin and collagen type II, two definitive markers of early cartilage formation.

A potential function for *XlPax1* in forming the vertebra-less tadpole tail should not be ruled out entirely. Subtle changes in the timing of gene expression may produce dramatic changes in morphology during ontogeny and evolution. While *XlPax1* is expressed in the tadpole tail of *X. laevis* in early tadpole stages, it is not clear how late in development the signal persists. Premature down-regulation of *XlPax1*, a key regulator of cell proliferation and chondrogenesis in the sclerotome, could possibly lead to caudal vertebral preclusion in anurans. In this scenario, sclerotomal cells may not reach the cell density required to form cartilaginous condensations, the precursors to vertebrae.

This scenario is premised, of course, on the assumption that *XlPax1* is functioning as it does in amniotes (*i.e.*, regulating cell proliferation). This may in fact not be the case. Sequence alignment reveals that XlPax1 diverges from other vertebrate orthologs at two residues within the the tightly-conserved paired domain and at one site within the octapeptide sequence (Fig. 3.4). Seo *et al.* (1998) have shown that single-site mutations within the paired domain can dramatically change the resulting motif's DNA-binding

capacity (Seo *et al.*, 1998) The divergent residues reported here could potentially have a great impact on the *XlPax1* normal function in development.

The precise role of *XlPax1* in the ontogeny of *X. laevis*—particularly in the caudal paraxial tissue—awaits elucidation by morpholino and RNA injection analyses. It would also be worthwhile to characterize the expression and function of fellow Group I gene *Pax9* (GenBank # AAH84222), which is known to synergistically operate with *Pax1* in vertebral formation in the mouse (Peters *et al.*, 1999).

Figure 3.1 Nucleotide and putative amino acid sequences of a cDNA clone (NIBB # XL085n23) corresponding to *XlPax1*. The open-reading frame encodes a polypeptide of 358 amino acids. The putative paired domain is boxed and the conserved octapeptide sequence is double-underlined.

```
ggcacgaggatcagatcaagttcgccattgcgctttttttgctggaggagaaggaaagcgcattgttatttggagtaatttagcg    84

cacggccctcctcctcatctggatactctggaaaataaaccctcgtcccatgtctatctgagccgctaaatttctgccgagcag   168

                                  M  E  Q  N  Y  G  E  V  N  Q  L  G  G  V                 14
cattgcgattcccatgttgcagcacggaATG GAA CAG AAT TAT GGC GAA GTG AAC CAG CTG GGA GGT GTG      238

F  V  N  G  R  P  L  P  N  A  I  R  L  R  I  V  E  L  A  Q  L                            35
TTT GTC AAT GGG AGA CCC CTG CCC AAT GCG ATC AGA CTG AGG ATC GTG GAG TTG GCG CAG CTG      301

G  I  R  P  C  D  I  S  R  Q  L  R  V  S  H  G  C  V  S  K  I                            56
GGG ATC AGG CCT TGC GAT ATC AGC CGA CAA TTG CGC GTC TCT CAC GGA TGT GTC AGT AAA ATC      364

L  A  R  Y  N  E  T  G  S  I  L  P  G  A  I  G  G  S  K  P  R                            77
CTG GCC CGT TAC AAC GAG ACC GGC TCT ATA TTG CCC GGG GCT ATC GGA GGC AGC AAA CCC AGA      427

V  T  T  P  T  V  V  K  H  I  R  D  Y  K  Q  G  D  P  G  I  F                            98
GTC ACC ACC CCC ACC GTA GTG AAA CAC ATC AGG GAC TAC AAA CAG GGC GAC CCC GGC ATC TTC      490

A  W  E  I  R  D  R  L  L  A  D  N  V  C  D  K  Y  N  V  P  S                           119
GCT TGG GAA ATC AGG GAC AGA CTT CTG GCA GAC AAC GTG TGC GAC AAG TAC AAC GTC CCC TCT      553

V  S  S  I  S  R  I  L  R  N  K  I  G  N  L  S  Q  P  N  Q  Y                           140
GTC AGC TCC ATC AGT CGG ATA TTA AGG AAT AAA ATC GGC AAC TTG TCT CAA CCC AAC CAG TAT      616

E  S  P  K  Q  S  P  S  Q  P  T  L  P  Y  N  P  L  Y  Q  Y  P                           161
GAG AGC CCC AAG CAG TCT CCA TCC CAG CCA ACG TTA CCC TAC AAC CCG CTG TAT CAG TAT CCC      679

Y  P  N  P  I  S  P  G  S  T  K  G  G  S  H  H  P  G  V  H  M                           182
TAC CCC AAT CCC ATC TCC CCT GGC TCT ACC AAG GGG GGC TCT CAT CAC CCA GGG GTG CAT ATG      742

P  T  G  H  V  N  I  A  R  Q  W  P  S  A  H  S  V  N  N  I  L                           203
CCC ACG GGA CAT GTC AAT ATT GCC AGG CAG TGG CCC TCG GCT CAT TCT GTC AAC AAC ATT CTG      805

G  I  R  Y  G  F  M  D  Q  S  P  I  A  G  T  E  G  S  V  Y  S                           224
GGG ATC CGG TAT GGA TTC ATG GAC CAA AGC CCT ATT GCC GGC ACC GAG GGC TCT GTG TAT TCT      868

P  K  M  E  D  W  A  S  V  N  R  S  G  F  P  G  S  Q  N  M  N                           245
CCA AAA ATG GAA GAC TGG GCC AGT GTC AAT CGA TCA GGC TTC CCT GGC AGT CAG AAT ATG AAC      931

G  L  E  K  S  V  V  E  P  D  I  K  Y  S  Q  S  A  S  S  L  S                           266
GGC CTG GAG AAA TCT GTG GTG GAG CCT GAT ATC AAA TAC TCA CAG TCG GCC TCC AGT CTC TCT      994

T  V  G  S  F  V  S  A  C  A  Y  P  T  S  N  Q  Y  G  V  Y  G                           287
ACA GTG GGC AGC TTT GTC TCA GCC TGT GCC TAC CCT ACC AGC AAC CAA TAT GGG GTT TAT GGC     1057

P  P  G  A  G  Y  V  P  P  G  H  H  W  Q  T  Q  G  S  P  L  G                           308
CCC CCA GGA GCT GGA TAC GTC CCC CCA GGA CAC CAC TGG CAG ACA CAG GGC AGT CCT CTC GGG     1120

H  S  V  T  V  H  G  G  D  I  A  A  P  V  T  F  K  H  R  E  V                           329
CAC AGC GTG ACG GTA CAT GGA GGT GAC ATT GCA GCC CCA GTG ACA TTC AAA CAC AGG GAA GTG     1183

V  N  R  K  P  N  S  P  I  I  K  I  P  E  T  L  S  N  V  H  G                           350
GTG AAC AGG AAA CCA AAC AGC CCT ATC ATA AAA ATC CCA GAG ACT TTG AGT AAC GTA CAT GGA     1246

L  P  L  P  A  S  S  S                                                                   358
CTT CCA CTC CCA GCT TCA TCC TCT TA acaacttcaaggcacccacaacagactttatgatggcggccccacatg     1321

tntgccttacggatcataccaggatggccttaaggtctgaatgtggaactggaccatgcaatccggacggcattctatcccaag    1405

anaaggggatgaaaaacaaactaaccttgccttgaggtaattaaagtggaacagttgaattaaaatttcctcccccctccttt    1489

cttttggttatttcctttccacctccctctcttcccctttctcatttgtttttttttacacccccttttctcaccacaatttgtcgc   1573

ccccgctttctcctctttgtataaatactggagaaga                                                   1610
```

Figure 3.2 An UPGMA consensus tree based on the comparison of full-length amino acid sequences of vertebrate homologs of Pax1 and Pax9. The protein Pox meso, a designated *Drosophila* homolog of Pax1 and Pax9 (Bopp *et al.*, 1989), was used as an outgroup root. XlPax1 groups with other vertebrate orthologs to the exclusion of Pax9 homologs. The numbers indicate the relative robustness of each node as assessed by boot-strap analysis (based on 100 replicates). See text for GenBank Accession numbers.

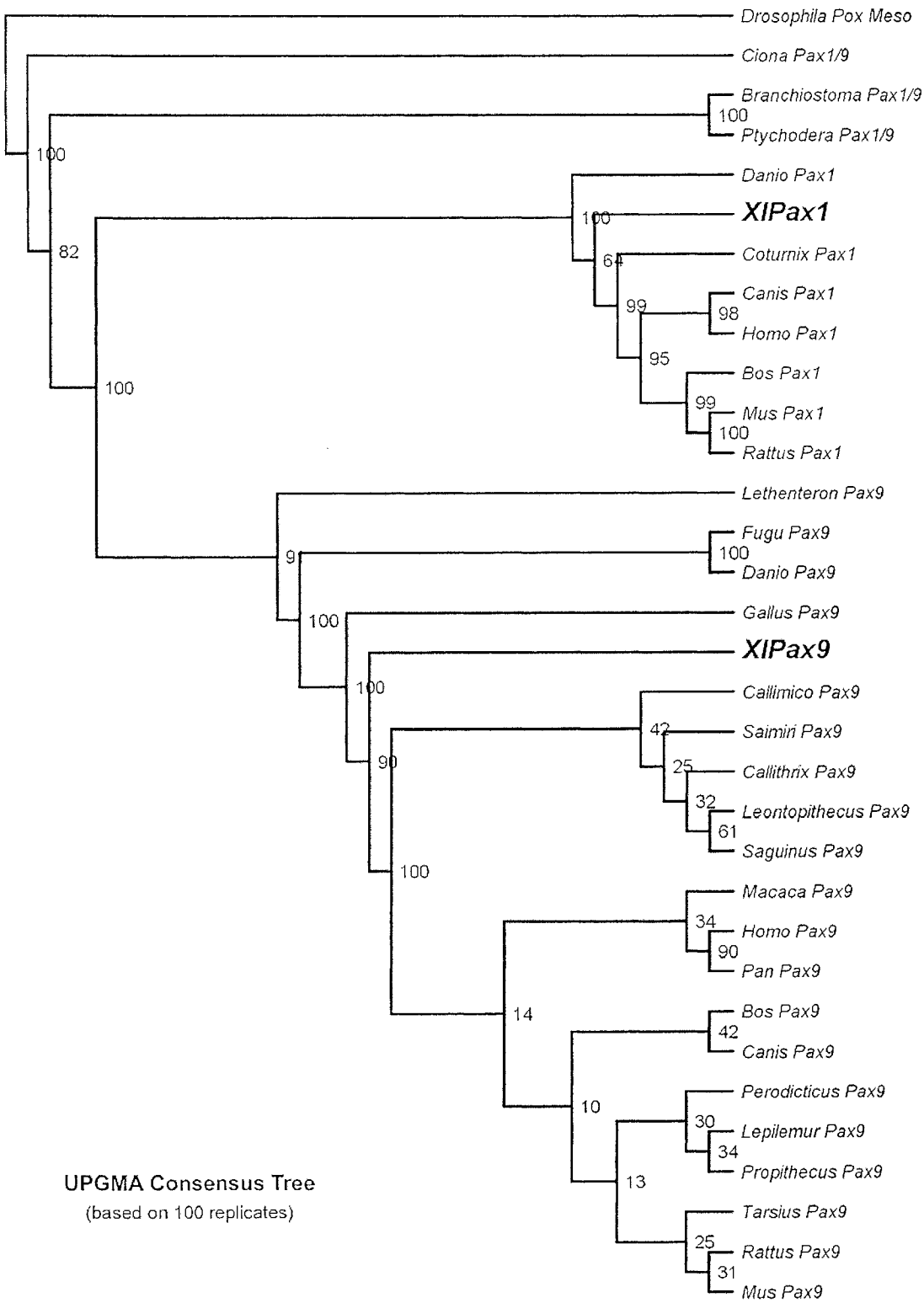

UPGMA Consensus Tree
(based on 100 replicates)

Figure 3.3 An UPGMA distance tree based on the comparison of full-length amino acid sequences of vertebrate homologs of Pax1 and Pax9. The protein Pox meso, a designated *Drosophila* homolog of Pax1 and Pax9 (Bopp *et al.*, 1989), was used as an outgroup. XlPax1 groups with other vertebrate Pax1 orthologs to the exclusion of Pax9 homologs. The scale bar indicates 0.1 amino acid substitutions per site. See section 3.3.4 for GenBank accession numbers.

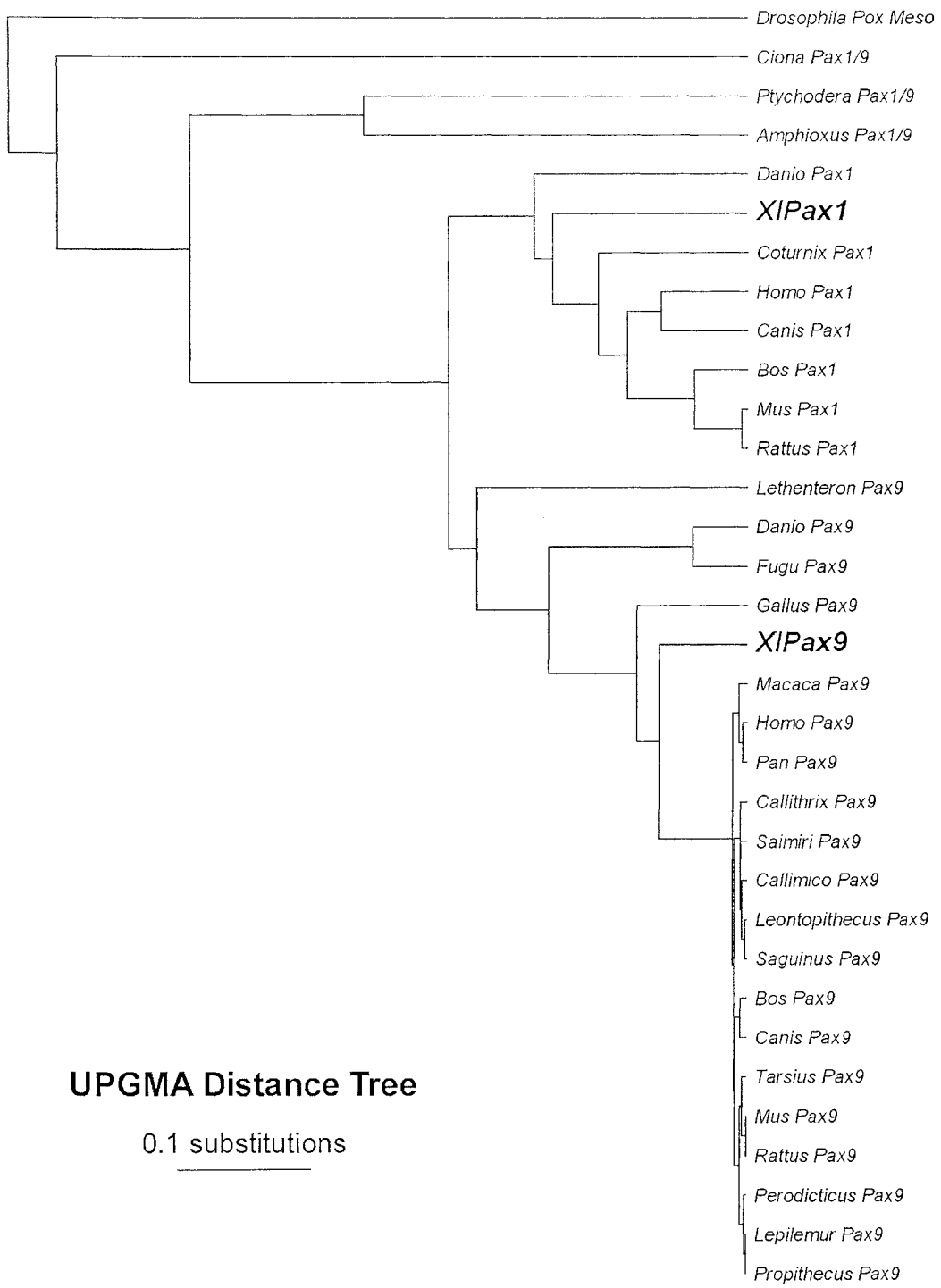
Drosophila Pox Meso
Ciona Pax1/9
Ptychodera Pax1/9
Amphioxus Pax1/9
Danio Pax1
XlPax1
Coturnix Pax1
Homo Pax1
Canis Pax1
Bos Pax1
Mus Pax1
Rattus Pax1
Lethenteron Pax9
Danio Pax9
Fugu Pax9
Gallus Pax9
XlPax9
Macaca Pax9
Homo Pax9
Pan Pax9
Callithrix Pax9
Saimiri Pax9
Callimico Pax9
Leontopithecus Pax9
Saguinus Pax9
Bos Pax9
Canis Pax9
Tarsius Pax9
Mus Pax9
Rattus Pax9
Perodicticus Pax9
Lepilemur Pax9
Propithecus Pax9
UPGMA Distance Tree
0.1 substitutions

Figure 3.4 Multiple protein alignment of predicted amino acid sequence of XlPax1 with orthologous vertebrate proteins. [*Mus musculus* (NCBI Accession # AAK01146), *Rattus norvegicus* (XP_230663), *Homo sapiens* (NP_006183), *Canis familiaris* (XP_542866), *Bos taurus* (XP_617873) and *Danio rerio* (XP_692791).] Amino acid residues highlighted in red represent the paired box domain and those in blue are the conserved octapeptide sequence. Asterisks indicate notably divergent residues.

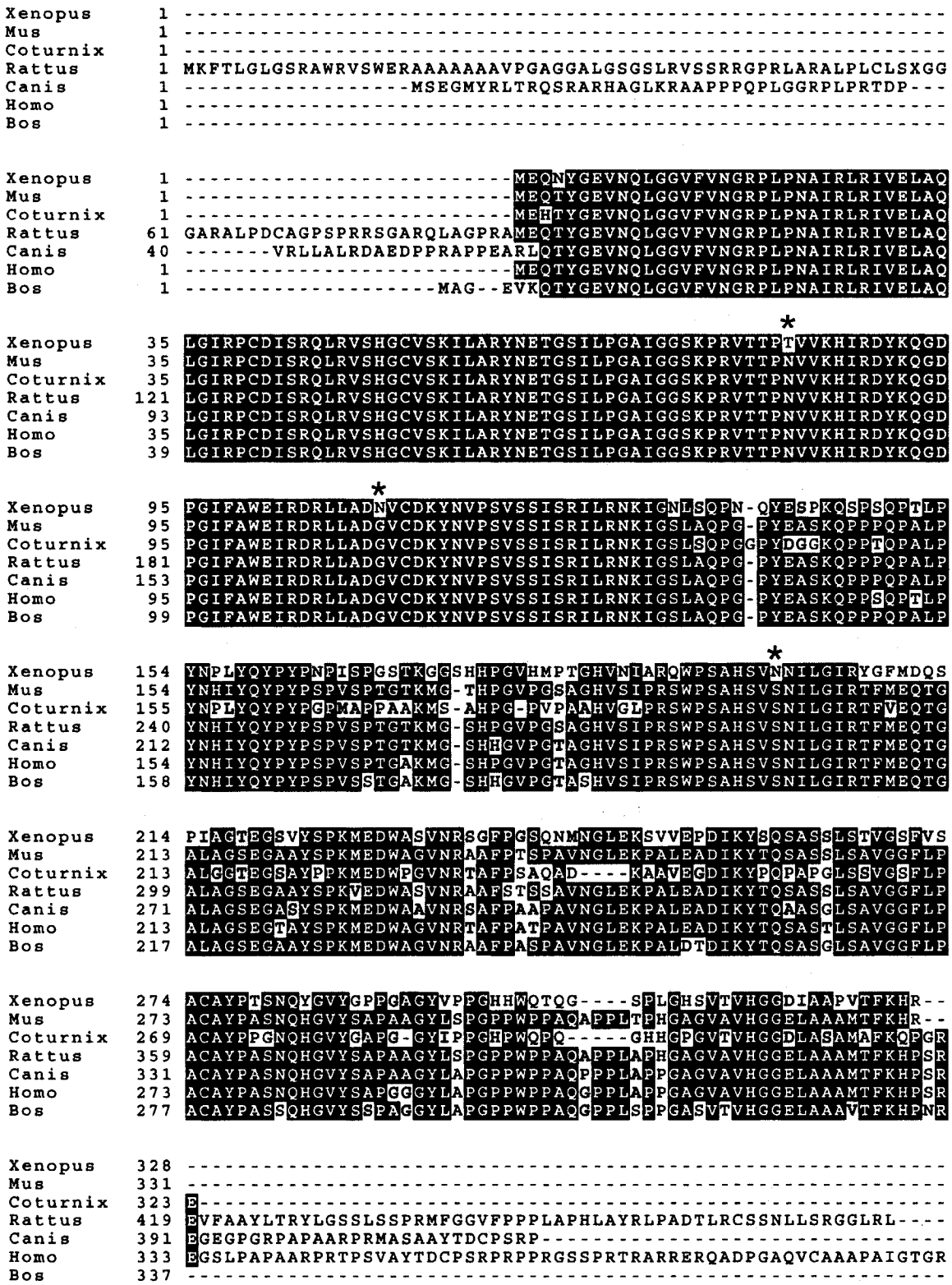
Xenopus 1 ----------
Mus 1 ----------
Coturnix 1 ----------
Rattus 1 MKFTLGLGSRAWRVSWERAAAAAAAVPGAGGALGSGSLRVSSRRGPRLARALPLCLSXGG
Canis 1 ----------MSEGMYRLTRQSRARHAGLKRAAPPPQPLGGRPLPRTDP---
Homo 1 ----------
Bos 1 ----------
Xenopus 1 ----------MEQNYGEVNQLGGVFVNGRPLPNAIRLRIVELAQ
Mus 1 ----------MEQTYGEVNQLGGVFVNGRPLPNAIRLRIVELAQ
Coturnix 1 ----------MEHTYGEVNQLGGVFVNGRPLPNAIRLRIVELAQ
Rattus 61 GARALPDCAGPSPRRSGARQLAGPRAMEQTYGEVNQLGGVFVNGRPLPNAIRLRIVELAQ
Canis 40 -------VRLLALRDAEDPPRAPPEARLQTYGEVNQLGGVFVNGRPLPNAIRLRIVELAQ
Homo 1 ----------MEQTYGEVNQLGGVFVNGRPLPNAIRLRIVELAQ
Bos 1 ----------MAG--EVKQTYGEVNQLGGVFVNGRPLPNAIRLRIVELAQ
Xenopus 35 LGIRPCDISRQLRVSHGCVSKILARYNETGSILPGAIGGSKPRVTTPTVVKHIRDYKQGD
Mus 35 LGIRPCDISRQLRVSHGCVSKILARYNETGSILPGAIGGSKPRVTTPNVVKHIRDYKQGD
Coturnix 35 LGIRPCDISRQLRVSHGCVSKILARYNETGSILPGAIGGSKPRVTTPNVVKHIRDYKQGD
Rattus 121 LGIRPCDISRQLRVSHGCVSKILARYNETGSILPGAIGGSKPRVTTPNVVKHIRDYKQGD
Canis 93 LGIRPCDISRQLRVSHGCVSKILARYNETGSILPGAIGGSKPRVTTPNVVKHIRDYKQGD
Homo 35 LGIRPCDISRQLRVSHGCVSKILARYNETGSILPGAIGGSKPRVTTPNVVKHIRDYKQGD
Bos 39 LGIRPCDISRQLRVSHGCVSKILARYNETGSILPGAIGGSKPRVTTPNVVKHIRDYKQGD
Xenopus 95 PGIFAWEIRDRLLADNVCDKYNVPSVSSISRILRNKIGNLSQPN-QYESPKQSPSQPTLP
Mus 95 PGIFAWEIRDRLLADGVCDKYNVPSVSSISRILRNKIGSLAQPG-PYEASKQPPPQPALP
Coturnix 95 PGIFAWEIRDRLLADGVCDKYNVPSVSSISRILRNKIGSLSQPGGPYDGGKQPPTQPALP
Rattus 181 PGIFAWEIRDRLLADGVCDKYNVPSVSSISRILRNKIGSLAQPG-PYEASKQPPPQPALP
Canis 153 PGIFAWEIRDRLLADGVCDKYNVPSVSSISRILRNKIGSLAQPG-PYEASKQPPPQPALP
Homo 95 PGIFAWEIRDRLLADGVCDKYNVPSVSSISRILRNKIGSLAQPG-PYEASKQPPSQPTLP
Bos 99 PGIFAWEIRDRLLADGVCDKYNVPSVSSISRILRNKIGSLAQPG-PYEASKQPPPQPALP
Xenopus 154 YNPLYQYPYPNPISPGSTKGGSHHPGVHMPTGHVNIARQWPSAHSVNNILGIRYGFMDQS
Mus 154 YNHIYQYPYPSPVSPTGTKMG-THPGVPGSAGHVSIPRSWPSAHSVSNILGIRTFMEQTG
Coturnix 155 YNPLYQYPYPGPMAPPAAKMS-AHPG-PVPAAHVGLPRSWPSAHSVSNILGIRTFVEQTG
Rattus 240 YNHIYQYPYPSPVSPTGTKMG-SHPGVPGSAGHVSIPRSWPSAHSVSNILGIRTFMEQTG
Canis 212 YNHIYQYPYPSPVSPTGTKMG-SHHGVPGTAGHVSIPRSWPSAHSVSNILGIRTFMEQTG
Homo 154 YNHIYQYPYPSPVSPTGAKMG-SHPGVPGTAGHVSIPRSWPSAHSVSNILGIRTFMEQTG
Bos 158 YNHIYQYPYPSPVSSTGAKMG-SHHGVPGTASHVSIPRSWPSAHSVSNILGIRTFMEQTG
Xenopus 214 PIAGTEGSVYSPKMEDWASVNRSGFPGSQNMNGLEKSVVEPDIKYSQSASSLSTVGSFVS
Mus 213 ALAGSEGAAYSPKMEDWAGVNRAAFPTSPAVNGLEKPALEADIKYTQSASSLSAVGGFLP
Coturnix 213 ALGGTEGSAYPPKMEDWPGVNRTAFPSAQAD----KAAVEGDIKYPQPAPGLSSVGSFLP
Rattus 299 ALAGSEGAAYSPKVEDWASVNRAAFSTSSAVNGLEKPALEADIKYTQSASSLSAVGGFLP
Canis 271 ALAGSEGASYSPKMEDWAAVNRSAFPAAPAVNGLEKPALEADIKYTQAASGLSAVGGFLP
Homo 213 ALAGSEGTAYSPKMEDWAGVNRTAFPATPAVNGLEKPALEADIKYTQSASTLSAVGGFLP
Bos 217 ALAGSEGAAYSPKMEDWAGVNRAAFPASPAVNGLEKPALDTDIKYTQSASGLSAVGGFLP
Xenopus 274 ACAYPTSNQYGVYGPPGAGYVPPGHHWQTQG----SPLGHSVTVHGGDIAAPVTFKHR--
Mus 273 ACAYPASNQHGVYSAPAAGYLSPGPPWPPAQAPPLTPHGAGVAVHGGELAAAMTFKHR--
Coturnix 269 ACAYPPGNQHGVYGAPG-GYIPPGHPWQPQ-----GHHGPGVTVHGGDLASAMAFKQPGR
Rattus 359 ACAYPASNQHGVYSAPAAGYLSPGPPWPPAQAPPLAPHGAGVAVHGGELAAAMTFKHPSR
Canis 331 ACAYPASNQHGVYSAPAAGYLAPGPPWPPAQPPPLAPPGAGVAVHGGELAAAMTFKHPSR
Homo 273 ACAYPASNQHGVYSAPGGGYLAPGPPWPPAQGPPLAPPGAGVAVHGGELAAAMTFKHPSR
Bos 277 ACAYPASSQHGVYSSPAGGYLAPGPPWPPAQGPPLSPPGASVTVHGGELAAAVTFKHPNR
Xenopus 328 ----------
Mus 331 ----------
Coturnix 323 E----------
Rattus 419 EVFAAYLTRYLGSSLSSPRMFGGVFPPPLAPHLAYRLPADTLRCSSNLLSRGGLRL----
Canis 391 EGEGPGRPAPAARPRMASAAYTDCPSRP----------
Homo 333 EGSLPAPAARPRTPSVAYTDCPSRPRPPRGSSPRTRARRERQADPGAQVCAAAPAIGTGR
Bos 337 ----------

Figure 3.5 Early *XlPax1* expression. (A) Temporal expression of *XlPax1* as detected by relative RT-PCR. Nearly undetectable at early stages, *XlPax1* transcript levels increase noticeably at stage 15 (asterisk) and again during tailbud stages (26+). (B) Rostral expression of *XlPax1*, first evident in pharyngeal pouch 1 (P1; arrowhead) at stage 22, subsequently expands to the facial mesenchyme (fm) and pharyngeal pouches 2-4 (P2-4). Frontal sections through the pharynx (right) show strong expression of *XlPax1* in the pharyngeal endoderm, which everts laterally to form the pouches. ba, branchial arch; ot, otic vesicle; phx, pharynx. Scale bar equals 0.5 mm. (C) Whole-mount expression. *XlPax1* expression persists in the head and somites (arrowheads in inset) from tailbud to tadpole stages.

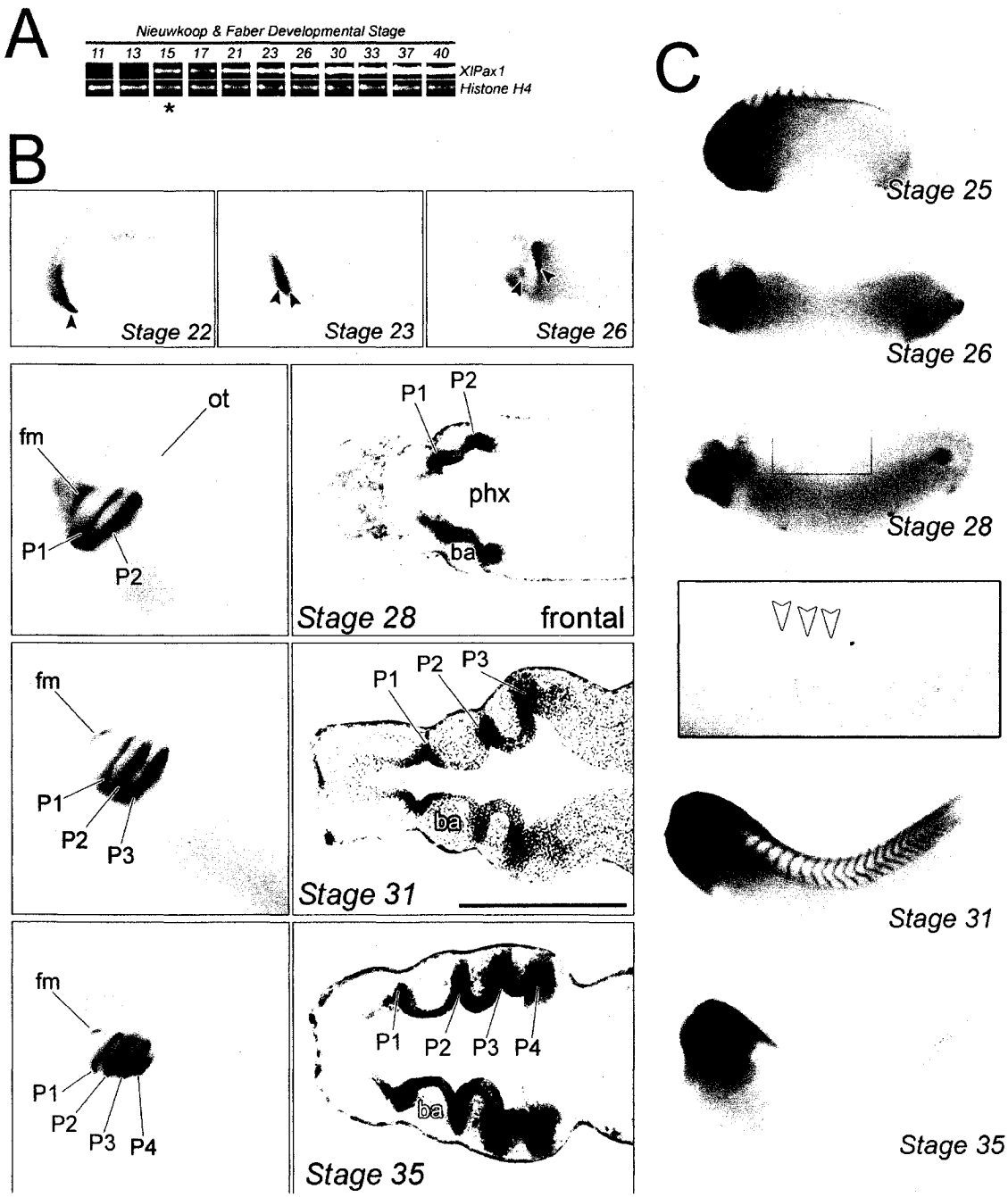
A
Nieuwkoop & Faber Developmental Stage
11 13 15 17 21 23 26 30 33 37 40
XlPax1
Histone H4
*
B
Stage 22
Stage 23
Stage 26
ot
fm
P1
P2
P1
P2
phx
ba
Stage 28
frontal
fm
P1
P2
P3
P1
P2
P3
ba
Stage 31
fm
P1
P2
P3
P4
P1
P2
P3
P4
ba
Stage 35
C
Stage 25
Stage 26
Stage 28
Stage 31
Stage 35

Figure 3.6 *XlPax1* expression in the somitic mesoderm. (A) In trunk cross-section, *XlPax1* transcripts (black arrowheads) are restricted to those cells between the notochord (n) and the myotome (myo; brown-staining in A2), corresponding to the sclerotome. nt, neural tube. (B) In frontal section, *XlPax1* is expressed in cells of the medial face of somites (outlined). Inset at left shows, in lateral view, *XlPax1* expression in trunk somites (arrowheads) of a partially-cleared embryo. Shown at the right, also in lateral view, is 12/101 labelling of trunk myotomes (white arrowheads). Scale bar = 0.5 mm.

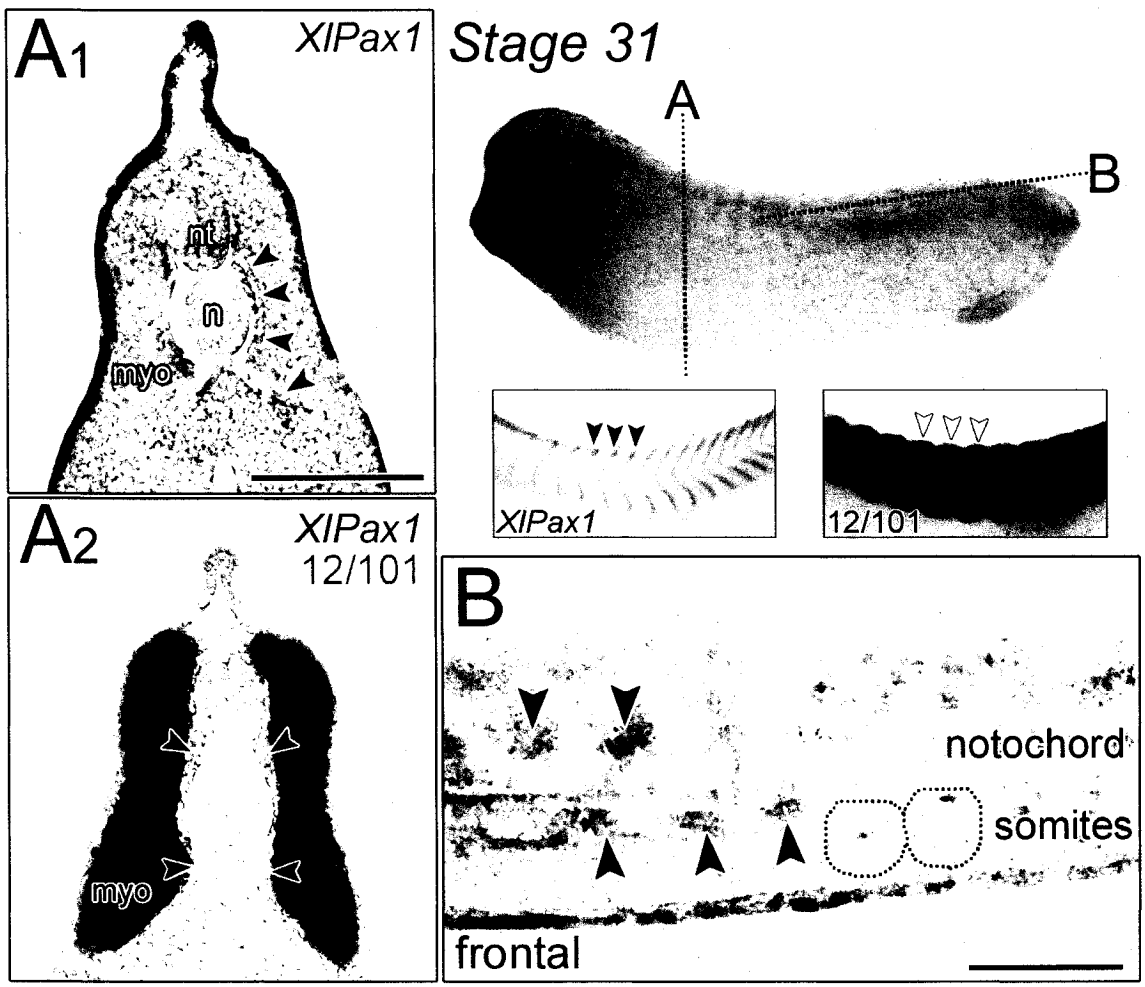
A1
XlPax1
nt
n
myo
Stage 31
A
B
XlPax1
12/101
A2
XlPax1
12/101
myo
B
notochord
somites
frontal

Figure 3.7 Late expression of *XlPax1*. (A) At stage 41, strong *XlPax1* expression can be seen in the pharyngeal endoderm (white arrow). More caudally, *XlPax1* transcripts (white arrowhead) persist in the peri-notochordal tissue despite the loss of the segmental character of expression visible in whole-mount at early stages (asterisks in inset). In all three sections, staining can be seen in the neural tube (black arrow). Similar staining was observed in the sense controls (data not shown), suggesting it is merely non-specific labelling. Black arrowheads indicate the level of successive transverse sections along the longitudinal axis. myo, myotome. (B) Forelimb expression of *XlPax1*. *XlPax1* transcripts, visible on the anterior face of the limb bud (white arrowheads), are restricted proximally by stage 53.

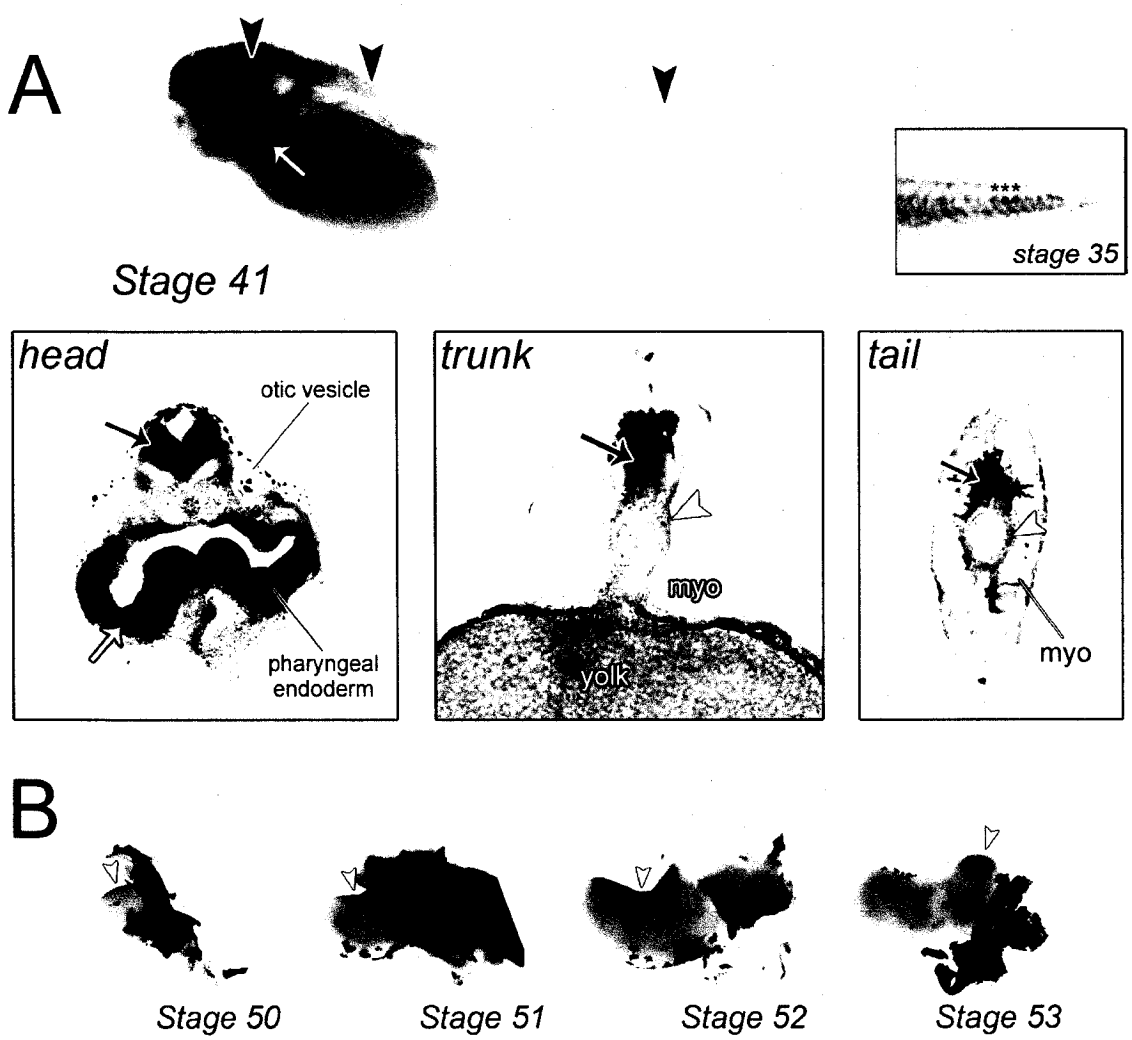
A
Stage 41
stage 35
head
otic vesicle
pharyngeal endoderm
trunk
myo
yolk
tail
myo
B
Stage 50
Stage 51
Stage 52
Stage 53

Table 3.1 Overall protein sequence identity between XlPax1 and select vertebrate orthologs of Pax1 and Pax9. See text for GenBank Accession numbers for each sequence.

Species	**Overall sequence identity shared with XlPax1**	
	Pax1	Pax9
Mus musculus	74%	58%
Rattus norvegicus	73%	57%
Homo sapiens	76%	59%
Danio rerio	70%	59%

CHAPTER 4:

HOW TO LOSE VERTEBRAE: VERTEBRAL FUSION AND PRECLUSION

The contents of this chapter together with chapters 2 and 7 are currently in press in the journal *Biological Reviews of the Cambridge Philosophical Society* as:

Handrigan, G. R. & Wassersug, R. J. The anuran *Bauplan*: A review of the adaptive, developmental, and genetic underpinnings of frog and tadpole morphology, 100 manuscript pages

AUTHOR'S NOTE

In the preceding chapter, I explored a potential role for the gene *XlPax1* in caudal vertebral agenesis in *Xenopus laevis*. Here, I delve more deeply into the larger question, returning briefly to *XlPax1*, but also implicating a host of other molecules, including tenascin and collagen type II, in vertebral loss in anurans. First, however, I address a second (albeit less important) route to vertebral loss in anurans, namely, the fusion of initially discrete vertebrae. Finally, I discuss the anteriorization of the anuran vertebral column that has occurred concomitantly with vertebral loss. I turn to the *Hox* genes and their upstream regulators as key factors in this dramatic reorganization that has led to the abbreviated anuran presacral vertebral column.

4. 1 Introduction

The reduced vertebral number of the anuran *Bauplan* can be attributed to two developmental processes: (1) the amalgamation of discrete vertebrae or vertebral rudiments during late ontogeny and (2) the loss of vertebral-forming capacity by caudal somites early in ontogeny.

4.2 Vertebral fusion

Vertebral fusion accounts for the loss of only a few vertebrae. In pipids, microhylids, and bufonids, the atlas and second vertebra fuse just before or at metamorphosis, reducing the number of presacral vertebrae from eight to seven or even six. In some *Dendrobates*, the first four presacral vertebrae are fused (Trueb, 1973). The pipids *Hymenochirus* and *Pipa*, both given to hyperossification, have a further reduced vertebral count due to fusion of the sacrum and neighboring vertebrae into a synsacrum (Pugener, 2002).

Beyond the sacrum, several rudimentary caudal vertebrae fuse to form the coccyx, a structure also present in avians (known as the pygostyle), apes, and humans (Pugener, 2002; Ročková & Roček, 2005). Subsequently, the urostyle is formed as the coccyx synostotically fuses with the ossified hypochord, a rod-like structure lying just under the notochord (see Fig. 2.3 for depiction of urostyle development in *Hymenochirus boettgeri*). A comparable structure to the hypochord has also been found in lancelets, lampreys, fishes and urodeles, but is curiously absent from amniotes, suggesting

secondary loss (see Löfberg & Collazo, 1997 and references cited therein). The embryonic (non-ossified) hypochord has been implicated in regulating the medial migration of angioblasts to form the dorsal aorta in vertebrates (Cleaver & Krieg, 1998). In anurans, the hypochord has also been commissioned to contribute to the adult skeleton.

Griffiths (1963) described the ossified hypochord as an outgrowth of the first post-sacral vertebra, whereas Mookerjee (1931) suggested that it arises from fused 'basiventrals'. More likely, however, the hypochord arises independently of the vertebral column, from a cell population not derived from the paraxial mesoderm. A recent recasting of the *Xenopus* mesodermal fate map convincingly shows that the hypochord is derived entirely from mesoderm arising in the superficial epithelial layer of the gastrula (Shook, Majer & Keller, 2004). Similarly, careful fate-mapping studies in the zebrafish by Warga & Nüsslein-Volhard (1999; endoderm) and Melby *et al.* (1996; mesoderm) also favor a mesodermal origin for the hypochord. These findings cast overwhelming doubt on Eriksson and Löfberg's (2000) assertion of an endodermal origin for the hypochord in *Danio* and encourage revisitation to Löfberg & Collazo's (1997) cell-labeling work with the axolotl, which evoked a similar origin.

The details of early hypochordal specification are being clarified. Zebrafish loss-of-function studies pinpoint members of the *Delta-Notch* signaling pathway as key players in the process (Latimer *et al.*, 2002). Specifically, *Notch* activation by *Delta* ligands from the paraxial mesoderm appears to divert midline precursor cells from a notochordal to hypochordal fate. Interestingly, the notochord has been implicated in the early formation

of the hypochord in *Xenopus*, perhaps providing an instructive signal. Cleaver, Seufert & Krieg (2000) showed that surgical ablation of the notochord leads to failure of hypochord development, whereas additional notochord grafts lead to enlargement of the structure. It should be noted, however, that these experiments are premised on an *endodermal* origin of the hypochord and thus may require reevaluation. Cleaver and colleagues (2000) also described the subsequent degeneration of the hypochord during tadpole stages, noting several hallmarks of apoptosis (*e.g.*, nuclear fragmentation). Of course, at immediately post-sacral levels, the hypochord avoids degradation and subsequently initiates a chondrogenic program (Fig. 2.3).

4.3 Mechanisms of vertebral preclusion

Of the approximately 50 somites segregated in anurans, only the most rostral form vertebrae in the majority of species (*Leptobrachella*, *Megophrys,* and several other megophryids are exceptions; Griffiths, 1963; Haas *et al.*, 2006; pers. obs.). Three possible scenarios may account for vertebral preclusion in most vertebrates:

1. *Sclerotomal segregation does not occur.* Presumptive skeletal precursors may be relegated to an alternative fate, such as myogenesis, due to absent or perturbed inductive signal.

2. *Sclerotome undergoes developmental arrest and regresses.*

3. *Chondrogenesis of sclerotome is precluded.* Sclerotomal cells initiate typical development, but are prevented from differentiating into cartilaginous precursors and eventually ossifying.

Scenario 1 probably holds for the ephemeral, embryonic tails of humans and birds. In both, initial caudal segmentation is followed by tail regression. Only the most proximal of the caudal somites form bone, which is eventually incorporated into the coccyx or pygostyle (Schoenwolf, 1981; O'Rahilly & Muller, 2003). For tadpole tails, however, Scenario 3 is probably the better summary of events. The demonstration of *XlPax1* transcripts in presumptive caudal somites (Fig. 4.1A, 3.5C, 3.7A) confirms that sclerotomes are segregated in the tail (hence Scenario 1 is invalid). Histological examination suggests that these caudal sclerotomes undergo some degree of differentiation, dismissing Scenario 2. Mookerjee (1931) described 'fibrous neural arches' that envelop the spinal cord and a perichordal tube encircling the notochord in the tails of *Rana*, *Bufo* and *Xenopus*. Bruns and Gross (1970) refer to a similar connective sheath that extends from the vertebral column, and was previously termed the 'skelatogeneous layer' by Noetzel (1895). However, its true origin cannot be determined without direct cell-tracing analysis. In any case, a few megophryid genera have circumvented each of these blocks and bear ossified vertebrae in their tails (Griffiths, 1956; 1963; Haas *et al.*, 2006).

4.3.1 Molecular blocks to vertebral chondrogenesis

Following sclerotome segregation and migration, the next step in vertebral formation is the appearance of cartilaginous condensations. These tight aggregates of mesenchymal cells are readily visible in histological preparations and can be visualized by the molecular markers tenascin, syndecan, and N-CAM (Hall & Miyake, 2000). Upon reaching a particular cell density, condensations differentiate into cartilage, an event heralded by the expression of *Sox9* and *collagen type II*. Should cell density fall shy of the threshold level, skeletogenesis does not proceed (Hall & Miyake, 2000). Arguably, the small size of anuran sclerotomes would make them more prone to such a fate than, say, the relatively larger sclerotomes of amniotes. Obviously, trunk sclerotomes are able to overcome this initial check and go on to form complete vertebrae. This compensatory feat may be the handiwork of those genes regulating cell proliferation in the sclerotome, including *Pax1*, *Pax9*, and *Bapx1* (see Hall & Miyake, 2000 for a comprehensive survey).

It is different story for caudal sclerotomes, which do not give rise to cartilage or bone (except in megophryid larvae). Not surprisingly, Mookerjee (1931) found no condensations ('basidorsals' and 'basiventrals') in the tails of *Rana*, *Bufo* or *Xenopus* and, accordingly, immunohistochemical analysis with the condensation marker tenascin is negative for the tail of late-stage *X. laevis* tadpoles (Fig. 4.1B).

The absence of cartilaginous condensations in the midline of the tadpole tail mirrors the phenotype of the *Pax1/Pax9* double homozygous mouse mutant, in which sclerotome

cells fail to condense and undergo chondrogenesis (Wallin *et al.*, 1994). The presence of *XlPax1* transcripts in presumptive caudal somites and perichordal tissue, however, rules out the complete attenuation of gene expression in the tail (Fig. 4.1A). Instead, transcript levels may be relatively lower than in trunk somites or expression may be down-regulated shortly after compartmentalization, thereby preventing sclerotome cells from proliferating and forming cartilaginous condensations. It remains to be seen whether *Pax9* is expressed in presumptive caudal somites. It is unlikely, however, that loss of *Pax9* expression in caudal somites could account for agenesis of vertebral bodies in the tadpole tail. Whereas *Pax9*-knockout dramatically exacerbates the axial defects of *Pax1*$^{-/-}$ mouse mutants, *Pax9* homozygous mutants themselves present no vertebral column defects (Peters *et al.*, 1995; 1998).

The liability may lie instead downstream with the targets of *Pax1* and *Pax9*, including *Bapx1*, *Sox9*, and *collagen type II*. Mice deficient for *Bapx1* present a phenotype very similar to *Pax*-deficient mutants, such as no cartilaginous condensations (Murtaugh, Chyung & Lassar, 1999; Murtaugh *et al.*, 2001; Rodrigo *et al.*, 2003; Christ, Huang & Scaal, 2004). Three *Bapx1* orthologs have been identified in *Xenopus*; however, only one, *koza*, is expressed in the somitic mesoderm (Newman *et al.*, 1997; Newman & Krieg, 1999; 2002). The expression profile of *koza* is otherwise not consistent with a role for the gene in shaping the anuran axial skeleton: There is no rostro-caudal asymmetry and transcripts are progressively restricted to peripheral myotome during early tadpole stages (Newman & Krieg, 2002).

Prospective roles are more likely for *Sox9* and *Collagen Type II*, which are both expressed in paraxial tissues in *Xenopus* (Su *et al.*, 1991; Bieker & Yazdani-Buicky, 1992; Spokony *et al.*, 2002). *In situ* hybridization analysis of the tail, however, shows that while *XSox9* transcripts are present in the ventral neuroepithelium, there is no sign of peri-notochordal expression (Fig. 4.1C). Similarly, immunohistochemistry using an antibody against Collagen type II shows no staining in paraxial tissues of the tail (Fig. 4.1B). Collectively, these data suggest that the very earliest stages of chondrogenesis are precluded in the tadpole tail, likely during the formation of cartilaginous condensations.

4.3.2 Dismantling the vertebra: insights into extinct and extant anuran forms

A model of *Pax*-mediated caudal vertebral preclusion in anurans cannot account for the absence of neural arches in most of the tadpole tail because these vertebral components, which circumscribe the neural tube, are retained in the *undulated* mouse mutant. In amniotes, dorsal neural arches, the laminae, arise from cells of the sclerotome that under the influence of bone morphogenetic protein- (BMP-) 4 secreted from the roof plate down-regulate *Pax1* in favor of *Msx1* expression (Ebensperger *et al.*, 1995; Christ *et al.*, 2004). Ventral neural arch elements, the pedicles, are specified by the paired homeobox gene *Uncx4.1*, which maintains condensation of the caudal sclerotomal half. Mice deficient for *Uncx4.1* lack pedicles as well as proximal ribs and transverse processes (Leitges *et al.*, 2000; Mansouri *et al.*, 2000).

Extrapolating these data to anurans, vertebral agenesis in the tadpole tail emerges as a disruption of a battery of specification pathways, each relying on inductive signals emanating from the notochord/floor plate complex. In amniotes, these signals are *Shh* and *noggin*. Together they induce and maintain gene expression in the developing sclerotome (Christ, Huang & Scaal, 2004). Disrupting the normal expression of each gene in the mouse results in concomitant changes in the expression of *Pax1*. While *Pax1* expression is not entirely eliminated in either mouse mutant, *noggin*-knockout leads to delayed expression of the gene, whereas *Shh*-knockout results in reduced *Pax1* transcript levels (Chiang *et al.*, 1996; McMahon *et al.*, 1998). In the homozygous *Shh* mutant, sclerotomes are markedly reduced in size and the axial skeleton, including both dorsal and ventral elements, does not form.

Orthologs of both genes are strongly expressed along the length of the notochord and floor plate well into tadpole stages in *Xenopus*, indicating that the sclerotome-inducing signal is indeed present in the future tail (Fig. 4.1C; Smith and Harland, 1992; Ekker *et al.*, 1995; Fletcher, Watson & Harland, 2004). Somitic cells, however, appear unable to respond appropriately to these signals.

The presence of caudal vertebral elements in some tadpoles suggests that the underlying machinery has been retained, at least partially, in anurans, but is latent in most species. A *Pax*-mediated pathway may be functioning in the tails of megophryid tadpoles, which bear only caudal centra; the lack of neural arch elements implies that normal *Msx1* and *Uncx-4.1* function has been perturbed. The curious absence of caudal intervertebral

discs, which are also *Pax*-mediated in amniotes, in megophyrids points to the further decoupling of dorsal vertebral elements (Christ *et al.*, 2004).

Decoupling of centrum and neural arch specification is also manifested in the evolution and ontogeny of the presacral anuran axial skeleton (Carroll *et al.*, 1999). The development of centra and neural arches are temporally offset during anuran ontogeny; both chondrogenesis and ossification of the arches precedes centra formation. As noted above, the delayed initiation of vertebral body development in tadpoles produces a condition very similar to the *undulated* mouse. Only when metamorphosis is complete are the ventral portions of vertebrae filled in. Carroll and colleagues (1999) point out that this pattern recapitulates the sequence of events during vertebrate evolution: centra first appeared in the Late Triassic with the teleosts—long after the appearance of vertebral arches in early jawed fishes.

The focus of the preceding discussion has been the vertebral unit and, specifically, the processes by which it forms and may be lost. In the following, I turn my attention to the vertebral column in its entirety—as a series of vertebrae of variable shape and size organized into discrete regions. I review the mechanisms that impose a global pattern onto the axial skeleton and how they have been modified to generate the broad range of axial morphologies seen in vertebrates, of which the truncated anuran vertebral column occupies one extreme.

4.4 *Hox* GENE REGULATION OF AXIAL PATTERNING

4.4.1 The '*Hox* code' and vertebrate axial diversity

The vast majority of an anuran's somites contribute to caudal structures. Paradoxically, many of these somites reside rostral to the anus ('trunk') until late tadpole stages (Nieuwkoop and Faber stages 35+). With the regression of the post-anal gut at stage 35 and concomitant caudal outgrowth, they are essentially displaced caudally in reference to the anus. However, Tucker and Slack (1995) confirmed by fate-map analysis that these trunk-cum-caudal somites are not respecified during this axial remodeling—they are caudal from the outset. In this case, the outset occurs before the somite is even formed. In vertebrates, the presomitic mesoderm (*i.e.*, segmental plate), from which somites bud, comprises prospective presacral, sacral and caudal regions distinguished by fate as well as gene expression. This was initially confirmed by heterotopic grafting experiments on chicken embryos; exchanging presumptive cervical or lumbar PSM with presumptive thoracic PSM, for example, results in ectopic rib formation (Kieny, Mauger & Sengel, 1972; Jacob, Christ & Jacob, 1975).

The *Hox* family genes are the primary patterning genes of the segmental plate in vertebrates (see papers cited in: Burke, 2000; Christ *et al.*, 2000). The expression profile of *Hox* paralogs within the plate (and the resulting somites) corresponds with their order in the chromosomal cluster; moving 3' to 5', anterior expression termini of the genes are staggered rostro-caudally.

Hox expression boundaries in the paraxial mesoderm coincide with morphological boundaries of the future axial skeleton (Burke, 2000; Gaunt, 2000). For example, the anterior border of *Hoxc6* marks the cervico-thoracic transition (and level of the pectoral girdle) in tetrapods. Comparing somitic levels of *Hoxc6* expression termini between vertebrates (see Table 4.1) reveals non-trivial differences. Somites 3, 8, 13, and 15 mark the expression of *Hoxc6* in the frog, mouse, turtle and chick, respectively (Gaunt, 1994; Burke *et al.*, 1995; Ohya, Kuraku & Kuratani, 2005). The expression boundary of the frog ortholog has been 'pushed forward' (anteriorized) relative to the termini of those of amniotes. Within this group, expression of the chick ortholog is 'pushed back' (posteriorized) compared to that of the mouse and turtle.

These boundary displacements correlate with the divergent cervical morphologies of these animals: Mice and turtles have fewer cervical vertebrae and relatively shorter necks than chicks, and a single cervical vertebra, the atlas, separates the pectoral girdle (the nearest proxy for the cervico-thoracic transition in the non-regionalized anuran trunk skeleton) from the cranium in frogs. Incidentally, pythons also bear only a single cervical vertebra and, predictably, exhibit anteriorized *Hoxc6* somitic expression (Cohn & Tickle, 1999).

The predictability of the code appears to break down for some *Hox* paralogs (Burke *et al.*, 1995). For example, the expression terminus of *Hoxd9* abuts the future lumbro-sacral transition in the mouse and chick, whereas the other *Hox9* gene expression boundaries line up neatly at the thoracic-lumbar boundary. Burke and colleagues (1995) suggested

that posteriorized *Hoxd9* expression is plesiomorphic and points to the absence of a thoracic-lumbar transition—or any overt regionalization—in the trunk of primitive tetrapods (as well as modern amphibians).

The code's predictability also appears to break down over the course of development. In many cases, *Hox* expression termini are not fixed, but regress caudally and are confined exclusively to the tail bud in later stages (see Lombardo & Slack, 2001 for example). The axial levels of *Hox* expression given above and throughout this paper represent the most static and anterior for each gene in each vertebrate.

4.4.2 Anteriorizing the anuran: *Hox* gene expression in frogs and toads

Along with the rostrally-displaced pectoral girdle, other aspects of the divergent anuran axial pattern may be ascribed to *Hox* anteriorization in the paraxial mesoderm. Slack and colleagues (Lombardo & Slack, 2001; Christen *et al.*, 2003) surveyed posterior *Hox* gene expression in *Xenopus* and revealed that termini have been anteriorized across the board (Table 4.1). Notably, *Hoxc10* and *Hoxd10*, both markers of the presacral-sacral transitional zone in tetrapods, have their expression termini at trunk somite 8—around 20 somites anterior relative to the chick (somite 26) and mouse (27) and eight anterior to the salamander (Carlson *et al.*, 2001). Accordingly, the sacrum and cranium of frogs are separated by no more than eight vertebrae, and the anuran trunk is dwarfed by that of all other vertebrates (Fig. 4.2).

Curiously, Lombardo and Slack (2001) described no paraxial expression for either *Hoxa9* or *d9* in *Xenopus*, despite strongly anteriorized expression for both genes in the neural tube. Intuitively, this makes sense, as the axial boundary designated by these genes in amniotes (*i.e.*, the thoracic-lumbar transition) is also missing in anurans. However, this finding remains surprising given the assumed conservation of the *Hox* code among vertebrates. Perhaps disruptions in the expression of individual *Hox* genes or even entire paralogous groups (*e.g.*, *Hox9* in anurans) constitute another route for axial diversity.

The premature termination of the vertebral column just beyond the sacrum may be the product of anteriorized expression of *Hoxb13*. Mice homozygous for loss-of-function mutations show overgrowth in all major structures derived from the tail bud, including the neural tube and the caudal vertebrae. This points to a role for *Hoxb13* as a general repressor of caudal development in the mouse and perhaps other vertebrates by mediating cell proliferation and apoptosis rates in the tail (Economides, Zeltser & Capecchi, 2003). A role for *Hoxb13* (and perhaps other *Hox13* paralogs) in constructing the vertebrae-less tadpole tail, however, assumes that the caudal axial skeleton is patterned independently of other segmental structures of the tail, such as the myomeres. Otherwise, caudal muscle would never be seen without corresponding bone.

Recent work from Fomenou and colleagues (2005) rejects this hypothesis. In an elegant series of somite-transplantation experiments, they demonstrated that the somitic compartments (*viz.*, sclerotome and dermomyotome) of the chick are tightly coupled with respect to global axial patterning. To summarize, *Hoxc6* expression and thoracic fate

were retained upon rotating and cervically-transplanting dorsal or ventral portions of presumptive thoracic somites. Thoracic sclerotomes (*i.e.*, ventral somite) were respecified to dermomyotomal fate in their new dorsal (cervical) position, but went on to form the scapula, a normal derivative of thoracic dermomyotomes. Therefore, the axial fate of all somitic cells is generic and fixed early on, but the intra-segmental fate of these cells depends entirely on local signals emanating from the notochord, neural tube and other adjacent tissues.

More recently, Iimura and Pourquié (2006) did uncover decoupling in the developing somite of the chick. Specifically, they showed that medial and lateral somitic compartments arise from separate precursor populations in the embryo. Furthermore, the lateral compartment imposes a global pattern on the medial compartment. It is important to note, however, that this work does not contradict that of Fomenou and colleagues (2005)—nor does it shed light on vertebral agenesis in the segmented tadpole tail—as both vertebrae and their associated muscle arise from the *medial* somitic compartment.

Returning to the tadpole tail, the lack of *individual* caudal vertebrae can be accounted for by the mechanisms outlined in the previous section. The absence of *the entire set* of caudal vertebrae, however, is the work of a currently unresolved mechanism of axial patterning. While an immediate role of *Hoxb13* and other 5' *Hox* genes in this process is unclear, these genes are among the first candidates that should be considered in addressing this issue.

Finally, anteriorized *Hox* expression may also account for the seeming reduction in the number of cranial mesodermal segments, both occipital somites and somitomeres, in anurans. Augier (1931) set the number of occipital somites in amphibians at three—two less than amniotes, but three more than cyclostomes (which bear none). Amphibians represented to Augier an intermediate step in a progressive "occipitalization" of trunk somites during vertebrate evolution from fish to amniotes.

In his recent review of cranium evo-devo, Kuratani (2005) acknowledged the variation in occipital somite number in vertebrates and implicated *Hox* genes in it. In amniotes, genes of the *Hox1*, *2*, and *3* paralogous groups regulate patterning of the occipital somites (Burke *et al.*, 1995). Whereas the role of these genes in the nervous system of anurans is well-characterized, there is scant data on a role in paraxial development. I suggest that expression termini of *Hox1*, *2*, and *3* have been posteriorized in amniotes relative to anurans. Such a scenario could also explain the apparently reduced somitomere count of anurans, which have almost half the number seen in mice, birds, turtles, and teleosts. Jacobson (1988) attributed the reduction to 2-to-1 somitomere fusion. Instead, somitomeric mesoderm may have been respecified to a somitic fate as *Hox* expression shifted rostrally during evolution. This discussion, however, is predicated on the authenticity of vertebrate somitomeres, a persistently contentious issue for developmental biologists.

Johnson *et al.* (2003) offer an alternative perspective. They suggest that the adoption of germ-cell predetermination in anurans may have facilitated the evolutionary

anteriorization of their body plan. In this mode, germ cells arise from the germ plasm, a portion of the zygotic cytoplasm sequestered into cells very early in development. In urodeles and zebrafish, however, germ cells are produced much later in development, in response to inductive signals in the posterior mesoderm of tailed embryos (*i.e.*, regulative germ cell production). Johnson and colleagues (2003) contend that the predetermination of germ cells enabled the posterior mesoderm to "more readily absorb mutations to axial patterning genes (such as *Hox* genes) that produce novel anteriorized phenotypes." In the case of urodeles and zebrafish, both with relatively posteriorized morphologies, similar mutations would risk terminating the germ line. Regulative germ-cell production may represent a developmental constraint to the evolution of anteriorized body plans in vertebrates. Experimental eradication of the germ line in *X. laevis* and coincident perturbation of *Hox* gene expression could test this hypothesis.

As tempting as it is to assign a *Hox* gene basis to the evolution of the anuran axial skeleton—and all axial diversity in vertebrates—it is also prudent to acknowledge the alternative scenario, *viz.*, that transposition of *Hox* gene expression occurred secondarily to changes in the axial skeleton, regulated by a separate genetic program. Bejder & Hall (2002) evoked such a scenario in their discussion of limblessness and axial elongation in cetaceans. The experimental demonstration that *Hox* genes *actively* regulate axial boundaries, however, rejects an entirely passive role for *Hox* genes in axial evolution. I review some of these experiments in the following section.

4.4.3 *Hox* patterning

Gene-targeting experiments in the mouse have confirmed that *Hox* genes actively specify somitic fate (along with the fate of other midline structures). For example, mice deficient for *Hoxc6* exhibit a homeotic transformation of the second thoracic vertebra into the first (Garcia-Gasca & Spyropolos, 2000). More dramatic phenotypes are seen in whole paralogous group knock-outs (Wellik and Capecchi, 2003); mice in which all *Hox11* paralogs (*a11*, *c11*, and *d11*) have been targeted exhibit homeotic transformation of all sacral vertebrae to a lumbar identity (a phenotype that evokes the sacrum-less caecilian vertebral column; Wake, 1980).

Presumably, anuran *Hox* genes function similarly in vertebral development as other vertebrate homologs, but diverge with respect to expression character. Their precise function, however, has been little investigated. The lack of gene-targeting technology for this group is no doubt to blame for this. *Hox* gene function can be approximated using a combination of 'knockdown' techniques, including antisense mRNA and morpholino injection. Perturbing the expression *Xenopus* ortholog of *Hoxc8* (*XHoxc8*) by the first method leads to axial truncation and severe (and likely secondary) edema in tadpole-stage embryos (Ko & Chung, 2003).

4.4.4 Regulating *Hox* gene expression

Changes in the somitic expression domains of *Hox* genes correlate with the broad array of axial morphologies demonstrated by vertebrates (Burke, 2000). What genetic

mechanisms mediate these interspecific shifts in *Hox* expression and, in turn, likely drove vertebrate axial evolution?

Enhancers are the most immediate regulators of *Hox* gene expression. These discrete, *cis*-regulatory elements control the rate, location, and timing of gene transcription in an embryo. In some elegant and continually unfolding work, Shashikant and colleagues (Belting, Shashikant & Ruddle, 1998; Shashikant *et al.*, 1998; Anand *et al.*, 2003; Shashikant *et al.*, 2004; Wang *et al.*, 2004) have dissected the promoter region of *Hoxc8* by gene-trap analysis. They have identified a 200-bp 'early enhancer region' that contains at least nine discrete enhancer elements; their combinatorial interaction regulates *Hoxc8* expression in vertebrate embryos. Discrepancies in the sequence and structuring (*i.e.*, location and orientation) of these elements may account for the divergent axial morphologies of vertebrates, as assayed by enhancer-swapping transgenic analysis. A 4-bp deletion in the whale early enhancer (compared to that of the mouse), for example, is manifested as posteriorized gene expression when the enhancer is used to drive reporter gene expression in transgenic mice. Conversely, teleost-enhancer-driven expression is markedly anteriorized relative to endogenous *Hoxc8* expression. An anuran enhancer would likely produce a similar effect.

Hox gene expression is also mediated by a host of upstream extrinsic factors, some of which may directly bind to *Hox* promoter elements. These include retinoic acid, activin, and various fibroblast growth factors (Cohn & Tickle, 1999; Burke, 2000). One of the more potent players is *growth/differentiation factor 11* (*Gdf11*), which encodes the

secreted molecule BMP-11 (Gamer *et al.*, 1999; Nakashima *et al.*, 1999). Gene-targeting experiments in mice have determined that BMP-11 functions as a posteriorizing signal in vertebral column patterning by defining the expression domains of *Hoxc6*, *Hoxc8*, *Hoxc10*, and *Hoxc11*, each of which is closely associated with major axial transitional zones (Table 4.1). Thus, mice deficient for *Gdf11* have 6-8 more trunk vertebrae—and correspondingly fewer caudal vertebrae—than their wild-type littermates, and call to mind the dachshund breed of dogs (McPherron, Lawler & Lee, 1999; Gad and Tam, 1999). Conceivably, the truncated vertebral column of anurans could be due to a heterochronic shift in *Gdf11* expression or higher endogenous levels of transcripts.

In the following chapter, I explore this hypothesis by describing the characterization of a *Xenopus laevis* ortholog of *Gdf11* (*XlGdf11*). This work documents the developmental expression of *XlGdf11* and directly tests a potential function for the gene in delineating *Hox* expression termini and, in turn, patterning the vertebral column in anurans.

4.5 Materials and Methods

4.5.1 Cryo-sectioning

Specimens sectioned for *in situ* hybridization were mounted and snap-frozen in OCT compound (Baxter # M7148-4) at -80°C; those for immunohistochemistry were first fixed in 4% paraformaldehyde (overnight at 4°C), briefly washed in PBS, and then equilibrated in 30% sucrose (4 hours at 4°C) prior to mounting in OCT. Cryo-sections were cut at 20-

40 µm using a Leica 2800E Frigocut Microtome Cryostat and collected on SuperFrost/Plus slides (Fisher # 12-550-15).

4.5.2 *In situ* hybridization on frozen sections

In situ hybridization was carried out on frozen tissue sections according to Schaeren-Wiemers & Gerfin-Moser (1993) with the following modifications: 1) sections were hybridized at 65°C instead of 72°C; 2) BM Purple was used as a chromogenic substrate in place of NBT/BCIP; and 3) sections were mounted using 100% glycerol. *XSox9* and *XShh* clones were acquired from Jean-Pierre Saint-Jeannet (University of Pennsylvania) and Stephen Ekker (University of Minnesota) and probes generated according to their instructions.

4.5.3 Immunohistochemistry on frozen sections

Immunohistochemistry was carried out on cryo-sections by the protocol of Pfaff *et al.* (1996). Tenascin was detected using Hybridoma antibody M1-B4 and collagen type II with Hybridoma II-II6B3. Both primary antibodies were diluted to 1:20 and detected by reacting DAB with a HRP-conjugated, goat anti-mouse secondary antibody (diluted to 1:200).

Figure 4.1 A survey of molecular regulators of vertebral development in the tadpole of *Xenopus laevis*. A. Whole-mount expression of the *X. laevis* ortholog of *Pax1* (NCBI Accession # DQ667149). In this stage-36 embryo, *XlPax1* transcripts (labeled purple) are expressed in a segmental pattern in the pharyngeal arches as well as in caudal somites (see inset), indicating that sclerotomes (asterisks) are segregated in the tadpole tail. B. Immunohistochemical detection (orange staining) of the proteins tenascin and collagen type II in paraxial tissues in frozen transverse sections at trunk (top row; Nieuwkoop & Faber stage 51) and tail (bottom; stage 56) levels. Tenascin, detected with Hybridoma antibody M1-B4 (1:20 1° dilution), is found in ventral perichordal tissue and in the periphery of the neural arches (na) and vertebral bodies (vb) in the trunk. Similarly, collagen type II (1:20 1° dilution; Hybridoma II-II6B3) is detected in the neural arches, forming centra, and dorsal to the notochord (nc). Neither protein, however, could be found at significant levels in paraxial tissues (arrowheads) at caudal levels using the very same antibodies and detection protocol. Chondrogenesis in the tail is thus precluded in its very earliest stage, namely, condensation formation. C. *In situ* hybridization analyses of expression of the genes *XShh* and *XSox9* in frozen transverse sections through the tadpole tail (stage 56). *XShh* is expressed in the ventral neural tube, confirming that an inductive axial signal for vertebral formation is indeed present in the tail. *XSox9* is expressed in the neuroepithelium, but not in the paraxial tissues; this is consistent with the absence of cartilage in the tadpole tail. Arrowheads indicate the localized expression of each gene in the neural tube (nt). myo, myotome; nc, notochord; na, neural arch; vb, vertebral body. *In situ* hybridization and immunohistochemistry were carried out as per Sive, Grainger & Harland (2000). Scale bars equal 0.5 mm.

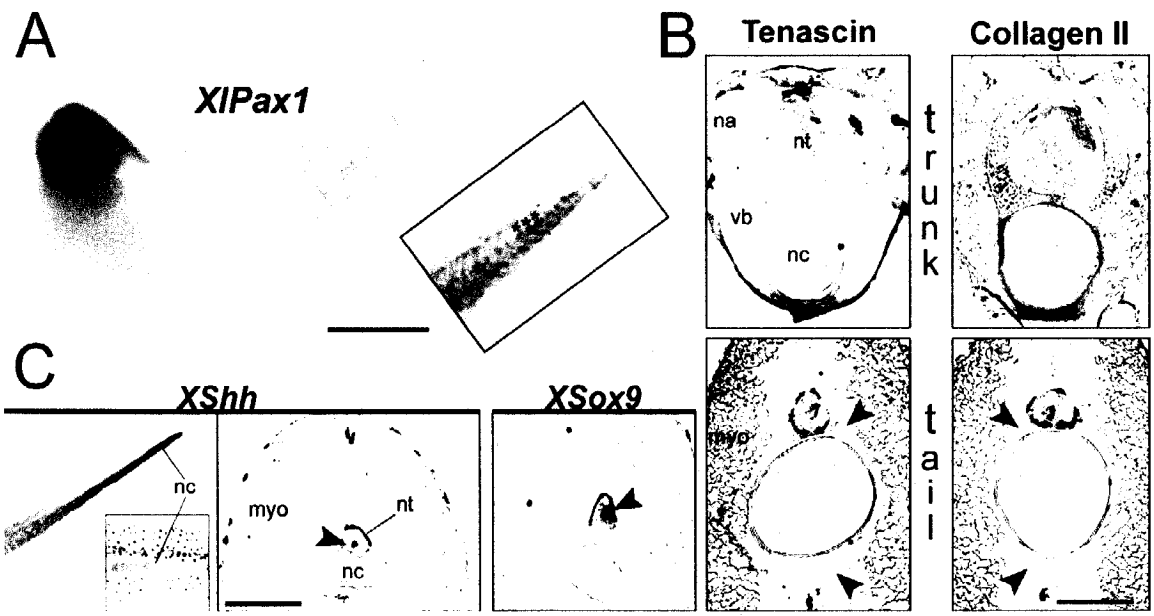
A
XlPax1
B
Tenascin
Collagen II
na
nt
vb
nc
trunk
tail
C
XShh
XSox9
nc
myo
nt
nc

Figure 4.2 *Hox* patterning of the tetrapod axial skeleton. *Hox* gene expression domains within the somitic mesoderm coincide with the morphological boundaries of the future vertebral column (regions are color-coded). For example, the anterior expression boundary of *Hoxc10* marks the future location of the sacrum in all tetrapods. Variation in the axial level of the sacrum in tetrapods can thus be correlated with shifts in the expression of *Hoxc10* (and its paralogs) in the somites (Burke *et al.*, 1995). In the amniotes *Mus* and *Gallus*, *Hoxc10* expression falls at trunk somite level 27 and 26, respectively. Expression has been shifted anteriorly in amphibians, terminating at the 16th trunk somite in *Ambystoma* (Carlson *et al.*, 2001) and the 8th in *Xenopus* (indicated by asterisk; Christen *et al.*, 2003). *Hox* expression appears to be generally anteriorized in *Xenopus* (see Table 4.1); this may account for the shortened trunk and absence of caudal vertebrae seen in anurans (excepting *Leptobrachella* and various other megophryid genera). (Inset) *XHoxc10* expression in a *Xenopus laevis* embryo (Nieuwkoop & Faber stage 35), as visualized by *in situ* hybridization. Somite counts have been adjusted to omit occipital somites (see Table 4.1).

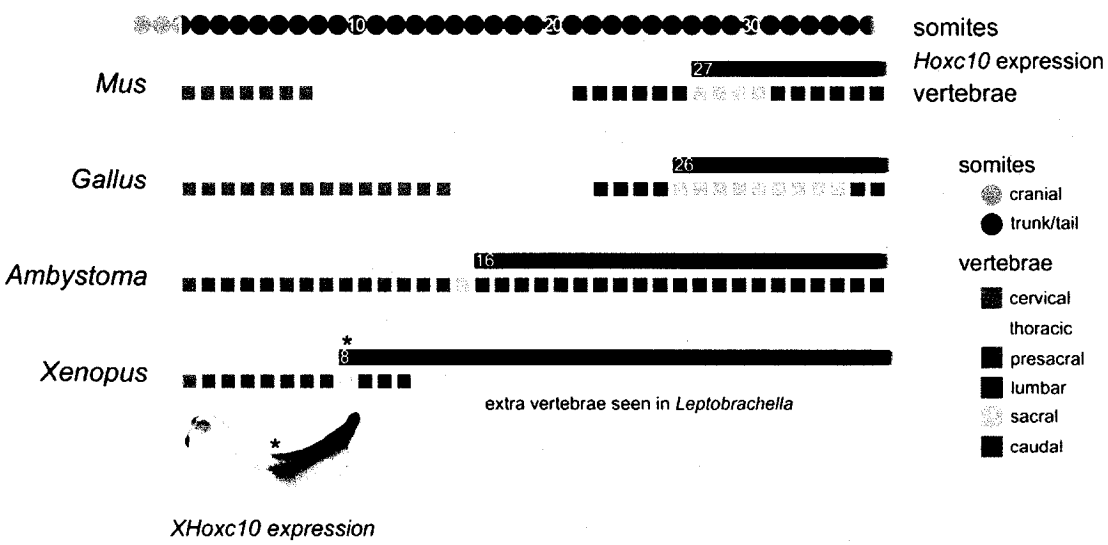

XHoxc10 expression

Table 4.1 Axial level of *Hox* anterior expression boundaries in the vertebrates *Xenopus laevis*, *Mus musculus*, and *Gallus gallus*. *Hox* expression in *Xenopus* (as observed during early tailbud stages, ~30) has been generally anteriorized relative to that of the amniotes. To standardize somite counts between the species represented, I omit occipital/cranial somites and instead enumerate only vertebral-forming (*i.e.*, trunk/tail) somites. Accordingly, Burke and colleagues' (1995) counts were adjusted by subtracting five (the number of cranial somites in amniotes). I opted for this method as the number of cranial somites in amphibians remains controversial. Unless otherwise cited, expression data are taken from Burke *et al.* (1995). Hostikka and Capecchi (1998) reported the anterior expression terminus for *Hoxc10* at prevertebrae 18 in the mouse. Using Burke *et al.*'s (1995) enumeration method (and adjusting for cranial somites), I report the somitic level at a slightly more posterior somitic level of approximately 25.

Hox paralogous group		*Hox* somitic anterior expression termini in...		
		Xenopus laevis	*Mus musculus*	*Gallus gallus*
4	B	3[1]	1-2	2-3
6	C	3-4	7-8	12-15
8	C	4[2]	12-13	18-19
10	C	8/9[3]	~25[5]	25-26
	D	8[4]	26-27	25-26
11	A	9[4]	24[6]	29-30
12	C	13[4]	?	?
13	A	Tailbud[4]	Tailbud	35+
	D	Tailbud[4]	Tailbud[7]	35+

1 – Godsave *et al.*, 1994; 2 - Ko & Chung, 2003; 3 – Christen *et al.*, 2003; 4 – Lombardo & Slack, 2001; 5 – Hostikka & Capecchi, 1998; 6 – Branford *et al.*, 2000; 7 – de Santa Barbara & Roberts, 2002

CHAPTER 5:

DEVELOPMENTAL EXPRESSION AND FUNCTION OF *XlGdf11*

5.1 SUMMARY

The anuran presacral skeleton is shortened relative to other vertebrates. This evolutionary truncation was likely mediated by *Hox* genes, the primary regulators of axial patterning in vertebrates. A potent upstream regulator of *Hox* gene expression in the mouse is *growth/differentiation factor 11* (Gdf11). Mice homozygous for the gene demonstrate an expanded trunk skeleton and a correspondingly reduced tail. This skeletal reorganization is on the scale of that seen in anurans. To investigate a role for *Gdf11* in the truncation of the anuran vertebral column, I have identified a prospective *Xenopus laevis* ortholog, *XlGdf11*, and documented its developmental expression by RT-PCR and *in situ* hybridization analyses. RT-PCR reveals that transcripts are up-regulated during the neural-fold stage, when somite segregation commences. The whole-mount expression pattern is marked by both rostral and caudal domains. At the head end, *XlGdf11* is expressed in the developing brain, the branchial arches, the otic vesicles, and the facial mesenchyme. Caudally, the gene is expressed in the tail bud and the midline tissues emerging from it. This caudal expression pattern is consistent with a role for *XlGdf11* in global axial patterning in *X. laevis*, which I tested directly by genetic gain- and loss-of-function studies. These experiments, however, provide no support for this hypothesis and assign no clear role for *XlGdf11* in axial patterning of the frog *X. laevis*.

5.2 Introduction

Bone morphogenetic proteins (BMPs) are key regulators of early development and organogenesis in vertebrate embryos. They are highly conserved with respect to their sequence, invariably bearing an C-terminal TGF-β domain that is cleaved from a N-terminal propeptide at a characteristic proteolytic processing site. BMP expression and function, however, varies among family members. BMP4, for example, is expressed in the marginal zone of gastrulating *Xenopus* embryos, where it plays an essential role in the specification of the dorso-ventral axis. Another family member, myostatin/Gdf8, has been implicated in myogenesis. The high sequence identity of its close paralog, BMP-11, however, belies its function. The protein, which is encoded by the gene *Gdf11*, instead plays an important role in the global patterning of the axial skeleton.

Nakashima and colleagues (1999) characterized the early expression of *Gdf11* in the mouse. They noted broad expression in mouse embryos, including the brain, limb buds, branchial arches, tail bud, and posterior neural tube. Subsequent gene-targeting experiments in mice determined that BMP-11 functions as a posteriorizing signal in vertebral column patterning by defining the expression domains of *Hoxc6*, *Hoxc8*, *Hoxc10*, and *Hoxc11*, each of which is closely associated with major morphological boundaries of the axial skeleton (*e.g.*, sacral vertebra; McPherron; Lawler & Lee, 1999). Accordingly, mice deficient for *Gdf11* have 6-8 more trunk vertebrae—and correspondingly fewer caudal vertebrae—than their wild-type littermates, and call to mind the dachshund breed of dogs (Gad and Tam, 1999).

In Chapter 4, I suggested that the elongation of the presacral skeleton of the *Gdf11*$^{-/-}$ mouse mutant is the converse of the evolutionary process that led to the truncated axial skeleton of frogs and toads, which bears no more than 9 presacral vertebrae, compared to 30 or so in most other tetrapods. They have correlated this truncation with the generally anteriorized paraxial expression patterns of *Hox* genes in anurans compared to other vertebrates (Lombardo & Slack, 2001). In the frog *Xenopus laevis*, the anterior expression terminus of *Hoxc10* falls at somite 8/9 and marks the future site of the sacrum (Christen *et al.*, 2003). In the mouse and chick, however, the terminus has been dramatically posteriorized, falling at somites 25 and 26, respectively (see Chapter 4 and references cited therein). Accordingly, the sacral vertebrae falls at a far more posterior level in these amniotes compared to *X. laevis*.

Here I hypothesize that it was anteriorization of *Hoxc* expression termini at the hands of *Gdf11* that led to the evolution of the truncated anuran axial skeleton. To directly explore this question, I have identified a prospective *Xenopus laevis* ortholog, *XlGdf11*, and profiled its expression by RT-PCR and *in situ* hybridization analysis. RT-PCR reveals that transcripts are up-regulated during the neural-fold stage, when somite segregation commences. The whole-mount expression pattern is characterized by both rostral and caudal domains. Rostrally, *XlGdf11* is expressed in the developing brain, the branchial arches, the otic vesicles, and the facial mesenchyme. At the tail end, the gene is strongly expressed in the tail bud and the axial tissues emerging from it. This caudal expression pattern corroborates a role for *XlGdf11* in global axial patterning in *X. laevis*, which I

tested by gain- and loss-of-function studies for the gene. These experiments, however, provide no support for this hypothesis and assign no clear role for *XlGdf11* in axial patterning of the frog *X. laevis*.

5.3 Materials and Methods

5.3.1 Clone identification

Querying the NIBB XDB *Xenopus laevis* EST database (http://xenopus.nibb.ac.jp/) by tBLASTx with the *Mus musculus* ortholog of *growth/differentiation factor 11* (NCBI Accession # XM_991698) against yielded two highly similar clones, XL031e11 and XL098j16. Both were derived from cDNA libraries constructed from neurula- and tailbud-staged embryos, respectively. Each cDNA sequence was directionally-cloned with *Eco*RI (5' end) and *Xho*I (end 3') into the plasmid pBluescript SK-. Following completion of a Materials Transfer Agreement, both clones were received from NIBB as desiccated samples on filter paper.

5.3.2 Clone amplification

To generate sufficient template quantities for subsequent sequencing and transcription reactions, subcloning efficiency DH5α competent *E. coli* cells (Invitrogen # 18265-017) were transformed with each clone as per the manufacturer's specifications. The transformed cells were plated on ampicillin-treated agar plates and incubated overnight at

37°C. Individual bacterial colonies were further incubated in Luria-Burtani liquid medium (for this and other solution recipes see Sambrook, Fritsch & Maniatis, 1989) and, on the following day, plasmid DNA was recovered by a mini-prep protocol (as per Sambrook *et al.*, 1989). To confirm success of the transformation and to determine the precise size of the clone inserts, 5μL of each sample was digested for 2 hours using *Eco*RI (Fermentas # ER0271) and then the linearized template examined by electrophoresis on a 1% agarose gel. XL031e11 and XL098j16 represented 2.0 kb and 1.5 kb inserts in pBluescript SK-, respectively. Following further purification using a GFX spin column (GE Healthcare # 27-9602-01), clone stocks were quantified by spectrophotometry (λ = 260nm) and then placed at -20°C for long-term storage.

5.3.3 Sequencing and analysis

Both clones were sequenced using oligonucleotides (Alpha DNA, Montreal, Quebec; http://www.alphadna.com) against the generic M13 primer sites of pBluescript SK- and internal sites of each cDNA. XL031e11 represents a full-lenth clone, replete with open-reading frame and 5' and 3' UTRs. XL098j16 is identical to XL031e11, but is truncated at its 5' end, indicating that it was incompletely derived from the same mRNA transcript.

Sequence data for XL031e11 was assembled and translated in GeneRunner (http://www.generunner.com/). Using the software ClustalX (http://bips.u-strasbg.fr/fr/Documentation/ClustalX/), a multiple sequence alignment of putative XlGdf11 with orthologous proteins was generated (default settings except: multiple gap

opening penalty = 3.0; gap extension = 1.8). Gdf11 sequences from each of the following vertebrates were used: *Bos taurus* (XP_611840), *Canis familiaris* (XP_848358), *Danio rerio* (AAN03678), *Homo sapiens* (NP_005802), *Mus musculus* (NCBI Accession # AAF21633) and *Rattus norvegicus* (XP_343149.2). The basic Clustal alignment was redrawn using the BoxShade Server (http://www.ch.embnet.org/software/BOX_form.html).

5.3.4 Phylogenetic tree construction

Neighbour-joining, UPGMA, parsimony, and maximum likelihood trees were generated based on the comparison of amino acid sequences of vertebrate homologs of Gdf11 and the closely-related protein Gdf8. [**Gdf11s:** *Bos* (XP_611840), *Danio* (AF411599), *Homo* (NP_005802), *Mus* (AAF21633), and *Rattus* (XP_343149). **Gdf8s**: *Alopex* (AAT37502), *Bos indicus* (AAV63982), *Bos taurus* (BAB79498), *Canis* (NP_001002959), *Capra hircus* (AAR12161), *Capra ibex* (AAT40569), *Coturnix chinensis* (AF440864), *Coturnix coturnix* (AAN63522), *Danio* (CAD43439 and AAV30547), *Equus* (BAB16046), *Fugu* (NP_001027843 and NP_001027844), *Gallus* (AAK18000), *Homo* (NP_005250), *Lepus* (AAN87890), *Macaca* (AAL17640), *Mus* (AAI03677), *Oncorhynchus* (AF273035 and AF273036), *Rattus* (NP_062024), *Salmo* (CAC59700), *Sus* (AAO31983), *Taurotargus* (AAT40568), and *Vulpes* (AAT67171). **Outgroup root:** *Drosophila* myoglianin (AAD24472)] All trees were generated with the PHYLIP 3.6 software suite (http://evolution.genetics.washington.edu/phylip.html) using a ClustalX alignment as the initial input.

5.3.5 RT-PCR

Expression of *XlGdf11* transcripts was profiled by relative RT-PCR during early embryonic stages (Nieuwkoop & Faber 11-37). Total RNA was extracted from staged, unfixed *X. laevis* embryos using TRIzol reagent as *per* manufacturer's instructions (Invitrogen # 15596-026), twice precipitated in ethanol, and then dissolved in 30µL of DEPC-treated ddH_2O. Stock concentrations and purities were determined by spectrophotometry, 0.250 ug/uL working stolutions were aliquoted, and all samples were then placed at -80°C for long-term storage. A 289-bp segment of *XlGdf11* mRNA was amplified using the Qiagen OneStep RT-PCR kit (Qiagen # 210210) with the primers 5'-gcccaaacgctacaaagccaac-3' (forward) and 5'-ggtctgtttgtacccttgagag-3' (reverse) and the following reaction conditions: 30 cycles; T_a = 57.1°C; [$MgCl_2$] = 1.5 mM. These conditions also permitted co-amplification of a 189-bp mRNA segment of *Histone H4*, a house-keeping gene routinely used to normalize reactions across stages (Steinbeisser *et al.*, 1995; forward: 5'-cgggataacattcagggt-3'; reverse: 5'-tccatggcggtaactgtc-3'). *XlGdf11* and *Histone H4* amplicons were resolved by electrophoresis on a 3% agarose gel and visualized using SYBR-Green (Applied Biosystems # 4306736).

5.3.6 Embryo collection, culturing, and fixation

In vitro fertilization of *X. laevis* was carried out as per Sive, Grainger & Harland (2000). In brief, mature female frogs were injected with 500-600 units of human chorionic

gonadotropin (Sigma-Aldrich # 8554) to induce ovulation and egg-laying. The next day (~12-16 hours later), unfertilized eggs were gently squeezed from females into a Petri dish. Following a quick wash in 0.4× MMR, 0.2 mL of homogenized testes slurry was added to the eggs for a minute. Within 20 minutes, fertilized embryos were dejellied by washing in 2% L-Cysteine (pH 7.8) for no more than 4 minutes. Once embryos had reached the appropriate stage, they were euthanized in 0.1% MS222 (Sigma-Aldrich # A5040), fixed in MEMFA (0.1M MOPS, 2mM EGTA, 1mM $MgSO_4$, 3.7% formaldehyde) for 2 hours at room temperature or overnight at 4°C and then transferred to 100% ethanol for long-term storage at -20°C.

5.3.7 RNA probe generation and *in situ* hybridization

Approximately 5 µg of extracted, column-purified XL031e11 DNA was linearized in overnight reactions with restriction endonucleases (for sense template: *Apa*I or *Kpn*I; antisense: *Eco*RI). Following digestion, templates were again purified, dissolved in 20 µL DEPC-treated ddH_2O, and quantified by spectrophotometry. *XlGdf11* RNA probes were generated using digoxigenin-labeled nucleotides (Roche # 11277073910) and T7 or T3 polymerases (Fermentas), for antisense and sense transcripts, respectively. A *XHoxc10* probe was generated using a full-length clone acquired from Dr. Jonathan Slack, University of Bath, England. The template was cut with *Bgl*II and transcribed with T7 RNA polymerase. Subsequently, probes were purified by LiCl precipitation, reconstituted in 30 uL of DEPC-treated water and stored at -80°C. To confirm success of each transcription reaction, 2 uL of the stock was visualized on a 3% agarose gel.

Whole-mount *in situ* hybridization was carried out as per Sive, Grainger, & Harland (2000) with the following modifications: RNase T1 was omitted from the stringency washes and CHAPS from the hybridization buffer. Bound probe was localized using an anti-digoxigenin, alkaline-phosphatase-conjugated antibody (Fab fragments, Roche # 11214667001) and visualized by chromogenic reaction with the substrate BM Purple (Roche # 11442074001).

5.3.8 Paraffin and vibratome sectioning

Xenopus embryos were processed for paraffin histology as per Sive, Grainger & Harland (2000). For vibratome-sectioning, embryos were embedded in 8% low-melting agarose (Sigma A9414) and cut at a thickness of 30 μm. Sections were mounted on slides in 100% glycerol, cover-slipped, and then photographed.

5.3.9 Capped RNA synthesis

Sense capped RNA of *XlGdf11* was transcribed using the Amplicap High Yield Message Maker Kit (Epicentre # AC0707) with T3 RNA polymerase (Promega # P2083). Template was prepared in the same manner as for RNA probe generation (*i.e.*, cut with *Apa*I). Success of the transcription reaction was confirmed by running 1 μL on a 3% agarose gel. Prior to injection, the concentration of the capped RNA stock was

determined by spectrophotometry (λ = 260 and 280 nm) and 1.0 ng/nL working samples were aliquoted.

5.3.10 Morpholino design

A splice-blocking morpholino oligonucleotide was targeted against the intron2_exon3 boundary of *XlGdf11*. To obtain the necessary intronic sequence data, the third exon of the gene was first queried (blastn) against the *Xenopus tropicalis* genome assembly (http://genome.jgi-psf.org/Xentr4/), yielding a hit with 100% sequence identity, corresponding to interval 1625394..1625775 of Scaffold_101. Sequence data for the interval plus 300 bp of 5' flank, corresponding to the 3' end of intron 2, were acquired and served as template for designing primers (forward: 5'-tgtttagggacccaactc-3'; reverse: 5'- cttactgtagacttcgaagc-3') to PCR amplify the corresponding sequence from the genome of *X. laevis* (Fig. 5.1). Genomic DNA was extracted as per Sive, Grainger & Harland (2000) and PCR with the *X. tropicalis* primers was carried out. The resulting 500-bp amplicon was subcloned into pGEM-T (Promega # A-3600) and sequenced using the T7 primer site. Sequence data were provided to Gene Tools (USA; http://www.gene-tools.com/), who designed and synthesised a morpholino oligonucleotide ('*XlGdf11i2_e3*') with the sequence 5'-tgtacagaaaagaggcacaagatta-3'. Upon receipt, the morpholino was reconstituted in 300 µL of nuclease-free ddH_2O, heated briefly to ensure dissolution, and stored at -80°C as 10ng/nL working aliquots.

The *XlGdf11i2_e3* morpholino is purported to prevent the normal splicing of the second intron of *XlGdf11*. To detect this perturbed transcript by RT-PCR, primers flanking intron 2 were designed. The forward primer (5'-gtatacttgcggccaatcag- 3') targets exon 2, while the reverse (5'-acaatcaagtcccaagttcc-3') is complementary to exon 3. Template RNA was extracted for morpholino-injected embryos as described above.

5.3.11 Microinjection into *Xenopus* embryos

Reagents were injected into the animal pole of each blastomere at the 2-cell stage using micropipettes calibrated to consistently deliver 4 nL/injection. In brief, needles were pulled with a Narishige PC-10 apparatus (heat = 62.0), broken to a 10-20 μm bore, and sharpened to a 35° bevel (Narishige EG-44). Positive pressure for microinjection was generated by a Nikon PLI-188 picospritzer (period = 30 msec). To ensure solubility, capped RNA was warmed to 37°C and XlGdf11i2_e3 to 65°C for 5 minutes prior to injection. Diffusion of reagents upon injection into embryos was confirmed using the Fluoresceinated Standard Control (5'-cctcttacctcagttacaatttata- 3') morpholino provided by Gene Tools.

Following injection, embryos were cultured in 4% Ficoll:0.1× MMR at 20°C, transferred to 0.1× MMR overnight, and scored for visible phenotypes on the following days.

5.3.12 Determining axial level of *XHoxc10* anterior expression terminus

The precise axial level of the anterior terminus of *XHoxc10* in the somitic mesoderm was determined by enumerating post-otic somites (as per Lombardo & Slack, 2001). Embryos hybridized for *XHoxc10* were subsequently processed for whole-mount immunohistochemistry (as per Size, Grainger & Harland, 2000) with the myotome marker 12/101 (Hybridoma). Primary and secondary antibodies were diluted to 1:1000. At this dilution, myotomes were sufficiently labeled and *XHoxc10* expression signal could be discerned. The otic vesicle was visualized by clearing embryos in glycerol.

5.3.13 Photography

Hybridized specimens were photographed with a Zeiss Axiocam MRc digital camera attached to a Zeiss Stemi 2000-C stereoscope or an Axioplan 2. Fluorescence images were taken using a Oimaging Qican Fast camera with a Leica MZ FL III stereoscope.

5.4 Results

5.4.1 Characterization and orthology

The clone XL031e11 contains a complete 1,155-bp open-reading frame flanked by 5' and 3' UTRs. Conceptual translation yielded a 385-amino acid protein bearing a TGF-β domain at segment 290-384 and a putative proteolytic site (RSRR) at 272-275 (Fig. 5.2).

The presumptive protein shares high overall sequence identity with vertebrate homologs of both Gdf11 and fellow TGF-β member, Gdf8. Phylogenetic analysis based on a comprehensive multiple protein alignment of vertebrate and invertebrate Gdf8/11 homologs was carried out to clarify the likely orthology of the clone. Maximum-likelihood, parsimony and distance methods alike generated trees grouping XL031e11 with vertebrate orthologs of Gdf11 to the exclusion of Gdf8 orthologs (see Fig. 5.3 for a boot-strapped consensus tree and Fig. 5.4 for a representative UPGMA tree; other trees not shown). This strongly corroborates Gdf11 orthology for XL031e11, which will henceforth be referred to as *XlGdf11*. Aligning the putative protein XlGdf11 with vertebrate orthologs reveals complete sequence identity with other orthologs (except *Danio*) in both the proteolytic and TGF-β motifs (Fig. 5.5).

5.4.2 Developmental expression of *XlGdf11*

XlGdf11 transcripts are first detectable by relative RT-PCR at stage 15, the neural fold stage (Fig. 5.6A). With the closure of the posterior neural tube at stage 17, a spike in transcript levels occurs. A similar level of expression is maintained until stage 26, beyond which there appears to be progressive up-regulation.

A whole-mount expression pattern is first visible at stage 19 in tissue laterally flanking the blastopore, corresponding to the location of the presumptive tail bud. In subsequent stages, strong expression is restricted to the tail bud and eventually to the very tail tip even at tadpole stages (Fig. 5.6B). Cross-sectional analysis of *XlGdf11* expression in the

tail tip shows transcripts in the chordoneural hinge, the posterior wall of the neurenteric canal, and the presomitic mesoderm. More proximally, expression can be seen in the derivatives of each of these structures, including the notochord, ventral neural tube, somites, and the post-anal gut (Fig. 5.7A, B, C).

XlGdf11 also shows strong expression at the head end of *Xenopus* embryos. Transcripts are first visible in the brain at stage 22 (Fig. 5.6B). By stage 27, expression is regionalized to the fore-, mid- and hind-brain (Fig. 5.8A). Concurrently, transcripts are up-regulated in the pharyngeal tissue. Additional staining is seen in the otic vesicle, facial mesenchyme, and restricted domains of the forebrain by stage 31 (Fig. 5.8B,C). Pharyngeal expression at this stage is seen within the branchial mesenchyme of rostral arches and the pharyngeal endoderm of caudal pouches (Fig. 5.8C).

5.4.3 *XlGdf11* knockdown by XlGdf11i2_e3 MO

Capped RNA and/or morpholino oligonucleotides were injected into the animal pole of each blastomere of 2-cell *X. laevis* embryos. The efficiency of this delivery method was assayed by injecting a non-functional Fluoresceinated Standard Control MO (Gene Tools) and subsequently examining the distribution of fluorescence. Ubiquitous, apparently non-mosaic, fluorescence was noted in non-yolk tissue into tadpole stages (Fig. 5.9A).

Using this injection protocol, 20 ng of XlGdf11i2_e3 morpholino was injected into *X. laevis* embryos. This amount was empirically determined to give a predominant phenotype that was not lethal in early developmental stages. Relative RT-PCR confirmed a morpholino-induced attenuation in the levels of endogenous *XlGdf11* transcripts (Fig. 5.9B), but could not recover the predicted splice-blocked transcripts, which should include the second intron (of indeterminate size). This is perhaps not surprising as large-sized mRNA transcripts are typically degraded quite promptly in cells (Vicky Prince, pers. comm.).

For experimental trials, two control groups were used. The first group (n = 165) received 20 ng of the Fluoresceinated Standard Control MO from Gene Tools, and the second group was not injected (n = 540). Among those embryos receiving 20 ng of the XlGdf11i2_e3 MO (n = 394), 61.7% of embryos presented a 'torsion' phenotype, characterized by a down-turned tail and lateral torsion (Fig. 5.9C). The phenotype first emerged at tailbud stages (~stages 28) and persisted throughout the rest of embryonic development.

A torsion phenotype was also noted among the control groups albeit at lower frequencies (Fig. 5.10). One-way ANOVA confirmed that the greater frequency observed among experimental embryos (*i.e.*, XlGdf11i2-e3 injection) is statistically significant compared to both control-injected ($p < 0.001$*, $F = 189.57$) and uninjected ($p < 0.001$, $F = 704.76$) embryos, correlating the torsion phenotype with XlGdf11i2_e3 injection.

5.4.4 Gain-of-function studies

The effect of augmenting *XlGdf11* expression was explored by injecting nanogram quantities of capped sense RNA into 2-cell *Xenopus* embryos. Four different quantities were delivered: 0.25 ng, 0.5 ng, 0.75 ng, and 1.0 ng. Control embryos were not injected. Those embryos receiving 0.25 ng displayed no phenotype (n = 74), whereas with the delivery of 0.5 ng (n = 101) and 0.75 ng (n = 81), a novel phenotype was observed at frequencies of 17.8% and 46.9%, respectively (Fig. 5.11). This phenotype, which I will refer to as 'cranial reduction and axial malformation' (CRAM), is characterized by varying degrees of axial truncation, and slight reduction of head structures, including the eyes and the cement gland (Fig. 5.12). Embryos receiving the largest amount of RNA (n = 95), 1.0 ng, displayed the CRAM phenotype at the same frequency (45.3%) as a more severe manifestation of the CRAM phenotype (Fig. 5.11), which is characterized by extreme axial truncation and a down-turned head, bearing massively-reduced or altogether missing eyes, branchial arches, and/or cement gland (Fig. 5.11).

5.4.5 Rescue experiments

To confirm XlGdf11i2_e3 function and to attempt rescue of the torsion and CRAM phenotypes, concurrent morpholino and capped RNA injections were carried out. Experimental embryos were co-injected with 20 ng XlGdf11i2_e3 morpholino and 1.0 ng of capped sense *XlGdf11* RNA (n = 55). Inexplicably, embryos receiving 20 ng XlGdf11i2_e3 along with smaller quantities of capped RNA (0.5 ng and 0.75 ng) showed

extensive mortality. Control embryos (n = 157) were not injected. Double-injected ('rescued') embryos show reduced frequencies of the torsion, mild CRAM and severe CRAM phenotypes relative to the corresponding single-injected treatments (Fig. 5.13). Pairwise one-way ANOVA (summarized in Table 5.1) reveals these differences are statistically significant for the torsion ($p < 0.001$, $F = 61.073$) and severe CRAM ($p = 0.002$, $F = 10.175$) phenotypes, but not for the mild posteriorization ($p = 0.051$, $F = 3.865$). Furthermore, the double-injected treatment showed a greater frequency of normal embryos (38.2%; 21 of 55 embryos) when compared to the 20 ng XlGdf11i2_e3 (24.4%; 96 of 394) and 1.0 ng RNA single injections (7.4%; 7 of 95). These differences are statistically significant as determined by pairwise one-way ANOVA (double-injected vs. 20 ng MO: $p = 0.029$, $F = 4.811$; double-injected versus 1.0ng RNA: $p < 0.001$*, $F = 25.145$). These data suggest that co-injection of capped sense RNA rescued the *XlGdf11i2_e3* phenotype and vice versa.

5.4.6 Effects on *XHoxc10* expression

The role for *XlGdf11* in patterning the future axial skeleton of *X. laevis* was explored by studying the downstream effects on *Hox* gene expression. *Gdf11* is a known regulator of the spatial expression pattern of the *Hox* genes *Hoxc6*, *c8*, *c10*, and *c11* (McPherron *et al.*, 1999). Of these genes, *Xenopus* clones exist for *Hoxc6*, *c8* and *c10*. *XHoxc10* was chosen for this study as its anterior expression boundary is particularly well-defined and its expression is integral to the positioning of the sacrum in vertebrates. In the case of

Hoxc6 and *c8*, it is the relatively poorly-resolved posterior termini that appear to be under the control of *Gdf11* in vertebrates (McPherron *et al.*, 1999; Liu, 2006).

The precise axial level of the anterior expression terminus of *XHoxc10* was determined for embryos having received 20ng XlGdf11i2_e3, 0.5ng RNA, or 0.75 ng RNA. Control embryos (control MO or uninjected) were processed similarly. All enumerated *XHoxc10* termini fell at either post-otic somite 8 or 9, consistent with Christen and colleague's (2003) findings for wild-type expression. One-way ANOVA revealed no significant discrepancies between experimental or control treatments (all p values > 0.250; F values < 1.217; see Table 5.2 for all p values), strongly suggesting that neither XlGdf11i2_e3 MO nor capped RNA injection had an effect on the spatial expression of *XHoxc10*.

5.5 Discussion

XlGdf11, the *X. laevis* ortholog of *Gdf11*, is strongly conserved with respect to its sequence. It bears perfectly conserved proteolytic and TGF-β motifs (Fig. 5.5) and overall protein sequence identity of ~80% with other vertebrate orthologs. It is similarly conserved in terms of its expression profile during *Xenopus* development, showing both rostral and caudal domains of expression. Expression first appears in the prospective tail bud, where it persists into late stages (Fig. 5.6, 5.7). At the head end, *XlGdf11* transcripts were noted in the regions of the brain, the pharynx, otic vesicles, and facial mesenchyme (Fig. 5.6, 5.8). Similarly, Nakashima and colleagues (1999) noted strong initial

expression in the tail bud (at 8.5 dpc), followed by up-regulation in the branchial arches, posterior neural tube, and the brain of the rat.

Disrupting the normal function of *XlGdf11*, however, does not readily corroborate a conserved function for the ortholog in *X. laevis* development. Double homozygous *Gdf11*$^{-/-}$ mutant mice show dramatic reorganization of their vertebral column, to wit, an expansion in the trunk skeleton due to an increase in the number thoracic and rostral vertebrae (McPherron *et al.*, 1999). Whereas I cannot directly analogize the phenotypes described herein with that of the mouse mutant, as embryos were not followed beyond early developmental stages, I can draw some parallels. Embryos receiving the *XlGdf11i2_e3* MO or exogenous *XlGdf11* capped RNA showed strong axial malformations (Fig. 5.9 and 5.11), corroborating a role for the gene in rostro-caudal development. However, the apparent lack of effect of *XlGdf11* knockdown or over-expression on *XHoxc10* expression suggests that the axial defects may not be the result of perturbed rostro-caudal patterning or at least not through the predicted downstream targets.

The observed effects of perturbing normal *XlGdf11* function may instead relate to the protein's demonstrated ability to induce mesodermal and neural formation *in vitro*. Using the *Xenopus* animal cap assay, Gamer and colleagues (1999) showed that applying exogenous Gdf11 protein induced the formation of axial mesodermal tissue, including notochord and muscle, as well as neural tissue. The data presented here, however, appear contradictory to these findings. *XlGdf11* over-expression caused a reduction of neural-

derived head structures and truncation of the long axis. What's more, the torsion phenotype is more in accordance with an overgrowth of axial tissues. Sugimoto, Hayata & Asashima (2005) ascribed a bent axis phenotype evoking the 'torsion' embryos to notochordal overgrowth in their work with the *B-cell translocational gene 2.*

Subsequent analysis of the unusual torsion phenotype of XlGdf11i2_e3-injected embryos may indeed uncover similar overgrowth of midline tissues. Further molecular and developmental studies beyond those presented here, however, are needed to resolve the precise role of *XlGdf11* in the development of the frog *X. laevis* and to ascertain if gene function has diverged relative to other vertebrates.

Figure 5.1. Sequence data for the third exon (in black) of *XlGdf11* and flanking intronic segments. Double-underlined nucleotides represent the complementary sequence to the XlGdf11i2_e3 morpholino (5'-tgtacagaaaagaggcacaagatta-3').

Figure 5.2 Nucleotide and putative amino acid sequences of cDNA clone (NIBB # XL031e11) for *XlGdf11*. The single open-reading frame encodes a polypeptide of 385 amino acids. The predicted proteolytic processing site is double-underlined and the mature TGF-β domain is boxed. Within this domain, there are seven cysteine residues (asterisks) conserved throughout the TGF- β superfamily.

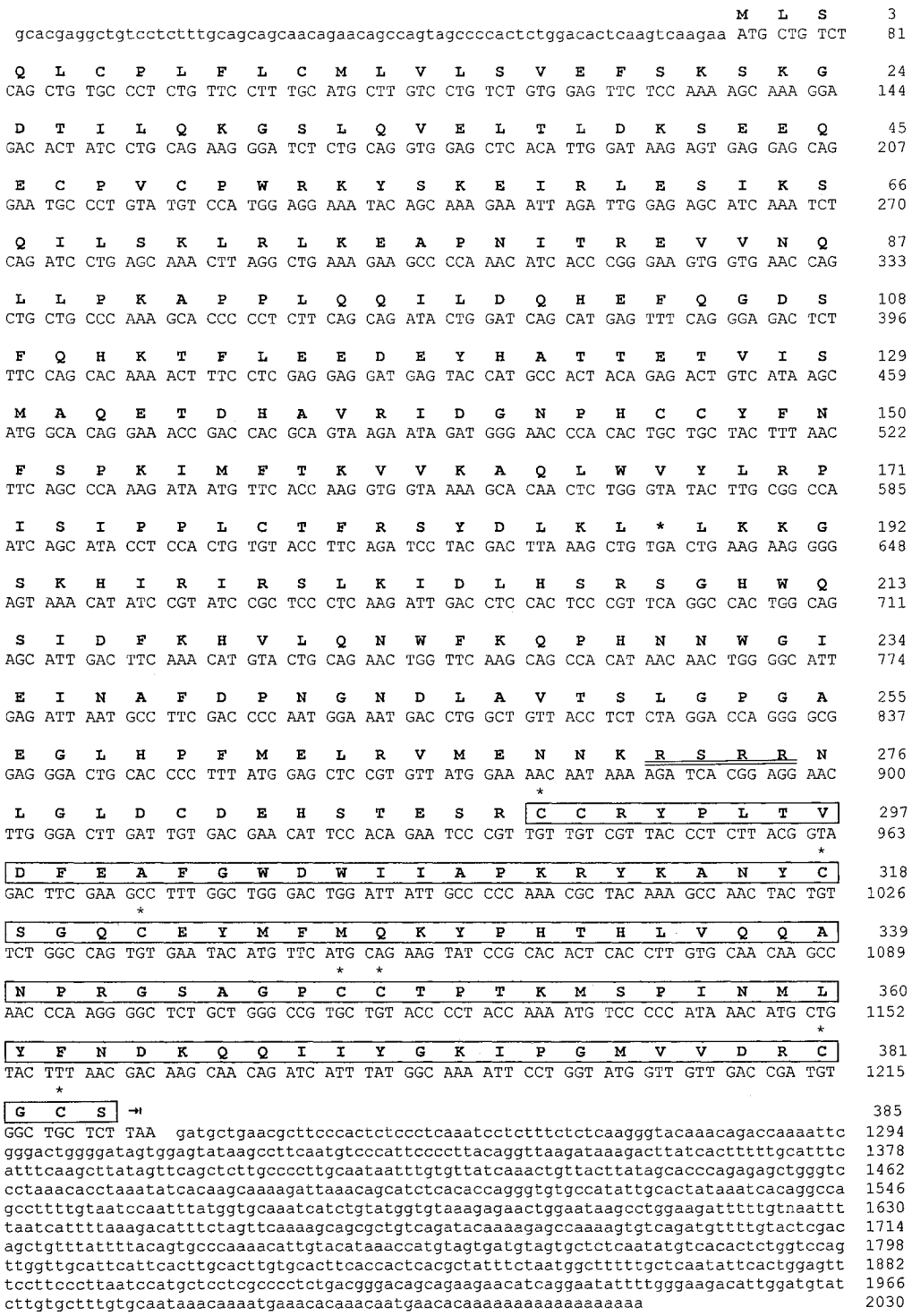
M L S 3
gcacgaggctgtcctctttgcagcagcaacagaacagccagtagccccactctggacactcaagtcaagaa ATG CTG TCT 81
Q L C P L F L C M L V L S V E F S K S K G 24
CAG CTG TGC CCT CTG TTC CTT TGC ATG CTT GTC CTG TCT GTG GAG TTC TCC AAA AGC AAA GGA 144
D T I L Q K G S L Q V E L T L D K S E E Q 45
GAC ACT ATC CTG CAG AAG GGA TCT CTG CAG GTG GAG CTC ACA TTG GAT AAG AGT GAG GAG CAG 207
E C P V C P W R K Y S K E I R L E S I K S 66
GAA TGC CCT GTA TGT CCA TGG AGG AAA TAC AGC AAA GAA ATT AGA TTG GAG AGC ATC AAA TCT 270
Q I L S K L R L K E A P N I T R E V V N Q 87
CAG ATC CTG AGC AAA CTT AGG CTG AAA GAA GCC CCA AAC ATC ACC CGG GAA GTG GTG AAC CAG 333
L L P K A P P L Q Q I L D Q H E F Q G D S 108
CTG CTG CCC AAA GCA CCC CCT CTT CAG CAG ATA CTG GAT CAG CAT GAG TTT CAG GGA GAC TCT 396
F Q H K T F L E E D E Y H A T T E T V I S 129
TTC CAG CAC AAA ACT TTC CTC GAG GAG GAT GAG TAC CAT GCC ACT ACA GAG ACT GTC ATA AGC 459
M A Q E T D H A V R I D G N P H C C Y F N 150
ATG GCA CAG GAA ACC GAC CAC GCA GTA AGA ATA GAT GGG AAC CCA CAC TGC TGC TAC TTT AAC 522
F S P K I M F T K V V K A Q L W V Y L R P 171
TTC AGC CCA AAG ATA ATG TTC ACC AAG GTG GTA AAA GCA CAA CTC TGG GTA TAC TTG CGG CCA 585
I S I P P L C T F R S Y D L K L * L K K G 192
ATC AGC ATA CCT CCA CTG TGT ACC TTC AGA TCC TAC GAC TTA AAG CTG TGA CTG AAG AAG GGG 648
S K H I R I R S L K I D L H S R S G H W Q 213
AGT AAA CAT ATC CGT ATC CGC TCC CTC AAG ATT GAC CTC CAC TCC CGT TCA GGC CAC TGG CAG 711
S I D F K H V L Q N W F K Q P H N N W G I 234
AGC ATT GAC TTC AAA CAT GTA CTG CAG AAC TGG TTC AAG CAG CCA CAT AAC AAC TGG GGC ATT 774
E I N A F D P N G N D L A V T S L G P G A 255
GAG ATT AAT GCC TTC GAC CCC AAT GGA AAT GAC CTG GCT GTT ACC TCT CTA GGA CCA GGG GCG 837
E G L H P F M E L R V M E N N K R S R R N 276
GAG GGA CTG CAC CCC TTT ATG GAG CTC CGT GTT ATG GAA AAC AAT AAA AGA TCA CGG AGG AAC 900
L G L D C D E H S T E S R C C R Y P L T V 297
TTG GGA CTT GAT TGT GAC GAA CAT TCC ACA GAA TCC CGT TGT TGT CGT TAC CCT CTT ACG GTA 963
D F E A F G W D W I I A P K R Y K A N Y C 318
GAC TTC GAA GCC TTT GGC TGG GAC TGG ATT ATT GCC CCC AAA CGC TAC AAA GCC AAC TAC TGT 1026
S G Q C E Y M F M Q K Y P H T H L V Q Q A 339
TCT GGC CAG TGT GAA TAC ATG TTC ATG CAG AAG TAT CCG CAC ACT CAC CTT GTG CAA CAA GCC 1089
N P R G S A G P C C T P T K M S P I N M L 360
AAC CCA AGG GGC TCT GCT GGG CCG TGC TGT ACC CCT ACC AAA ATG TCC CCC ATA AAC ATG CTG 1152
Y F N D K Q Q I I Y G K I P G M V V D R C 381
TAC TTT AAC GAC AAG CAA CAG ATC ATT TAT GGC AAA ATT CCT GGT ATG GTT GTT GAC CGA TGT 1215
G C S →| 385
GGC TGC TCT TAA gatgctgaacgcttcccactctccctcaaatcctctttctctcaagggtacaaacagaccaaaattc 1294
gggactggggatagtggagtataagccttcaatgtcccattccccttacaggttaagataaagacttatcacttttgcatttc 1378
atttcaagcttatagttcagctcttgccccttgcaataatttgtgttatcaaactgttacttatagcacccagagagctgggtc 1462
cctaaacacctaaatatcacaagcaaaagattaaacagcatctcacaccagggtgtgccatattgcactataaatcacaggcca 1546
gccttttgtaatccaatttatggtgcaaatcatctgtatggtgtaaagagaactggaataagcctggaagatttttgtnaattt 1630
taatcattttaaagacatttctagttcaaaagcagcgctgtcagatacaaaagagccaaaagtgtcagatgttttgtactcgac 1714
agctgtttatttttacagtgcccaaaacattgtacataaaccatgtagtgatgtagtgctctcaatatgtcacactctggtccag 1798
ttggttgcattcattcacttgcacttgtgcacttcaccactcacgctatttctaatggctttttgctcaatattcactggagtt 1882
tccttcccttaatccatgctcctcgccccctctgacgggacagcagaagaacatcaggaatattttgggaagacattggatgtat 1966
cttgtgctttgtgcaataaacaaaatgaaacacaaacaatgaacacaaaaaaaaaaaaaaaaa 2030

Figure 5.3 An UPGMA consensus tree based on the comparison of full-length amino acid sequences of vertebrate homologs of Gdf11 and Gdf8. The protein myoglianin (GenBank # AF132814), a designated *Drosophila* homolog of Gdf11 and Gdf8 (Lo & Frasch, 1999), was used as an outgroup root. XlGdf11 groups with other vertebrate orthologs to the exclusion of Gdf8 homologs. The numbers indicate the relative robustness of each node as assessed by boot-strap analysis (based on 100 replicates). See section 5.3.4 for GenBank Accession numbers for all proteins used in this analysis.

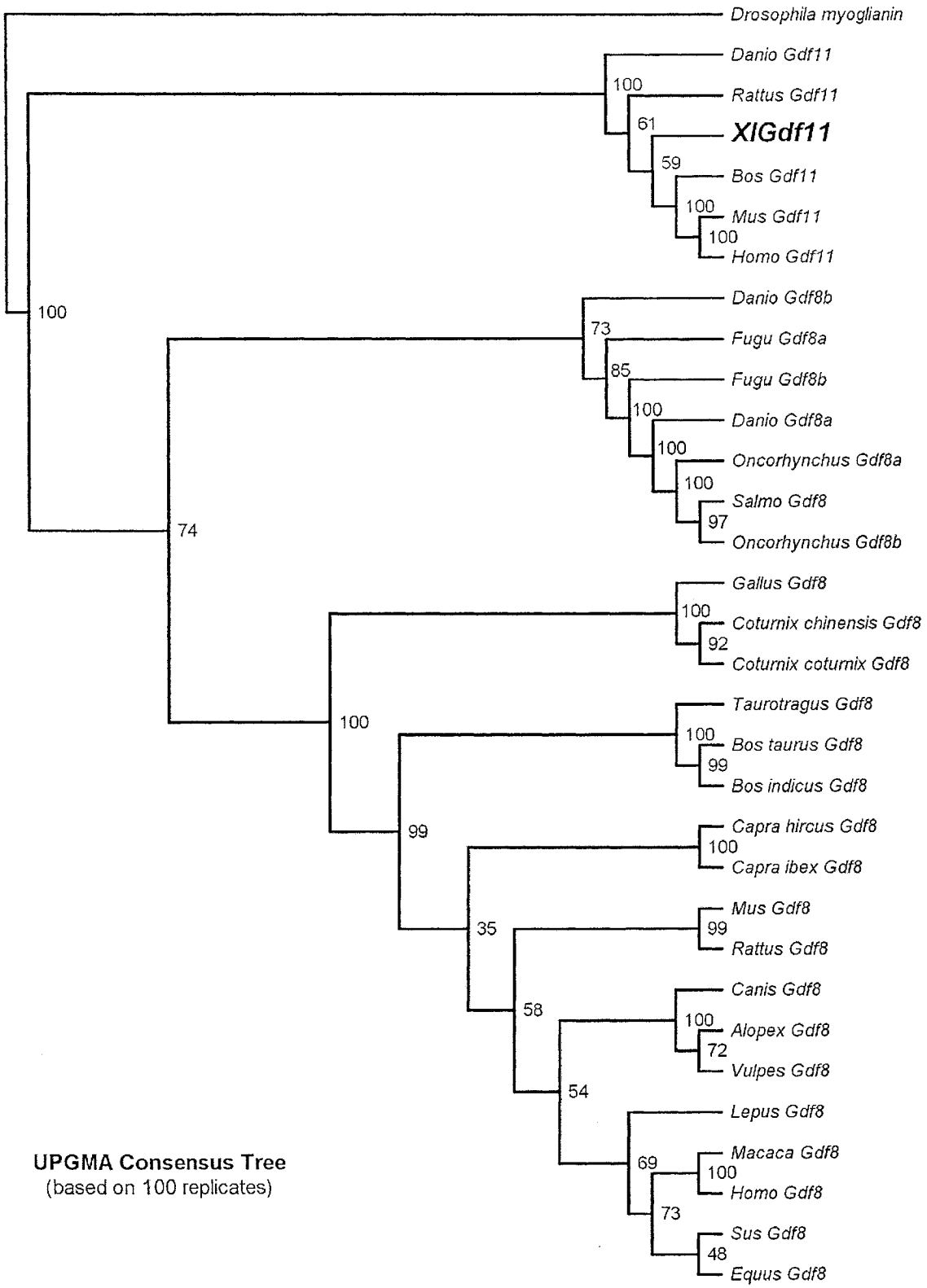

UPGMA Consensus Tree
(based on 100 replicates)

Figure 5.4 An UPGMA distance tree based on the comparison of full-length amino acid sequences of vertebrate homologs of Gdf11 and Gdf8. The protein myoglianin (GenBank # AF132814), a designated *Drosophila* homolog of Gdf11 and Gdf8 (Lo & Frasch, 1999), was used as an outgroup. XlGdf11 groups with other vertebrate orthologs to the exclusion of Gdf8 homologs. The scale bar indicates 0.1 amino acid substitutions per site. See section 5.3.4 for GenBank Accession numbers for all proteins used in this analysis.

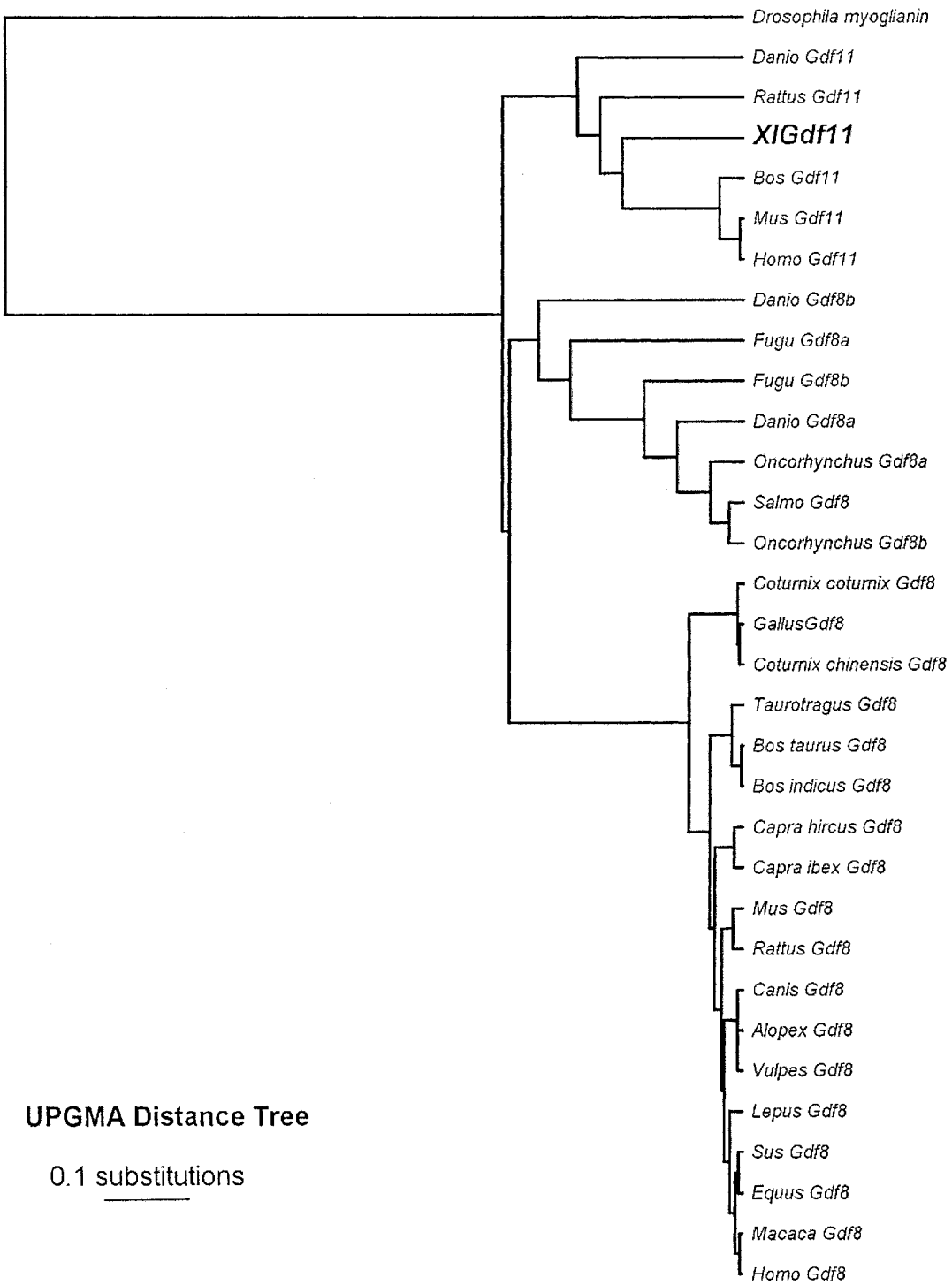
Drosophila myoglianin
Danio Gdf11
Rattus Gdf11
XlGdf11
Bos Gdf11
Mus Gdf11
Homo Gdf11
Danio Gdf8b
Fugu Gdf8a
Fugu Gdf8b
Danio Gdf8a
Oncorhynchus Gdf8a
Salmo Gdf8
Oncorhynchus Gdf8b
Coturnix coturnix Gdf8
GallusGdf8
Coturnix chinensis Gdf8
Taurotragus Gdf8
Bos taurus Gdf8
Bos indicus Gdf8
Capra hircus Gdf8
Capra ibex Gdf8
Mus Gdf8
Rattus Gdf8
Canis Gdf8
Alopex Gdf8
Vulpes Gdf8
Lepus Gdf8
Sus Gdf8
Equus Gdf8
Macaca Gdf8
Homo Gdf8
UPGMA Distance Tree
0.1 substitutions

Figure 5.5 Multiple protein alignment of predicted amino acid sequence of XlGdf11 with orthologous vertebrates proteins. [*Mus musculus* (NCBI Accession # AAF21633), *Rattus norvegicus* (XP_343149.2), *Homo sapiens* (NP_005802), *Canis familiaris* (XP_848358), *Bos taurus* (XP_611840) and *Danio rerio* (AAN03678).] Amino acid residues highlighted in red represent the putative proteolytic processing site. Cleavage at this site releases the active TGFβ domain (highlighted in blue).

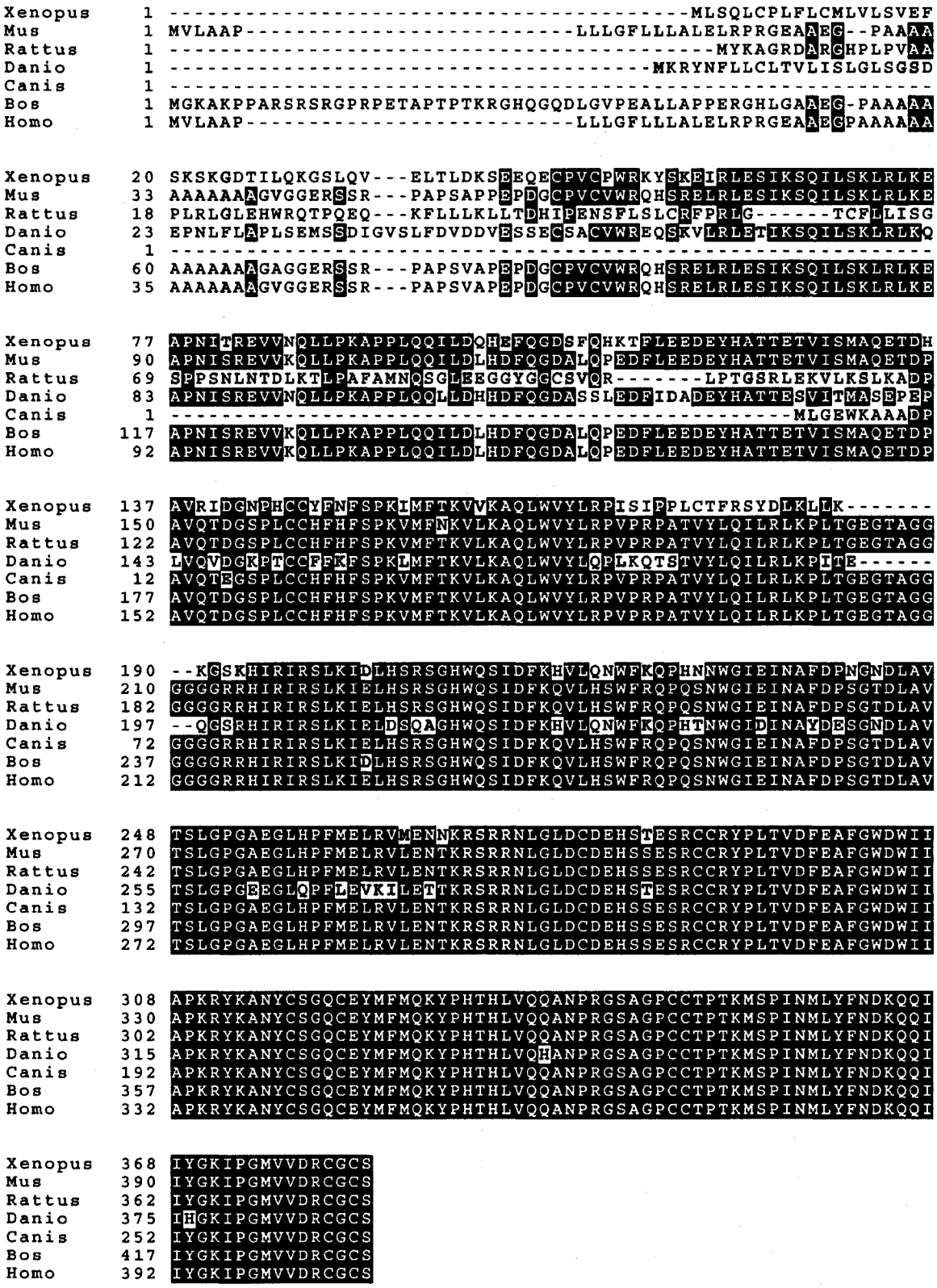
Xenopus 1 ----------MLSQLCPLFLCMLVLSVEF
Mus 1 MVLAAP----------LLLGFLLLALELRPRGEAAEG--PAAAA
Rattus 1 ----------MYKAGRDARGHPLPVAA
Danio 1 ----------MKRYNFLLCLTVLISLGLSGSD
Canis 1 ----------
Bos 1 MGKAKPPARSRSRGPRPETAPTPTKRGHQGQDLGVPEALLAPPERGHLGAAEG-PAAAAA
Homo 1 MVLAAP----------LLLGFLLLALELRPRGEAAEGPAAAAAA
Xenopus 20 SKSKGDTILQKGSLQV---ELTLDKSEEQECPVCPWRKYSKEIRLESIKSQILSKLRLKE
Mus 33 AAAAAAAGVGGERSSR---PAPSAPPEPDGCPVCVWRQHSRELRLESIKSQILSKLRLKE
Rattus 18 PLRLGLEHWRQTPQEQ---KFLLLKLLTDHIPENSFLSLCRFPRLG------TCFLLISG
Danio 23 EPNLFLAPLSEMSSDIGVSLFDVDDVESSECSACVWREQSKVLRLETIKSQILSKLRLKQ
Canis 1 ----------
Bos 60 AAAAAAAGAGGERSSR---PAPSVAPEPDGCPVCVWRQHSRELRLESIKSQILSKLRLKE
Homo 35 AAAAAAAGVGGERSSR---PAPSVAPEPDGCPVCVWRQHSRELRLESIKSQILSKLRLKE
Xenopus 77 APNITREVVNQLLPKAPPLQQILDQHEFQGDSFQHKTFLEEDEYHATTETVISMAQETDH
Mus 90 APNISREVVKQLLPKAPPLQQILDLHDFQGDALQPEDFLEEDEYHATTETVISMAQETDP
Rattus 69 SPPSNLNTDLKTLPAFAMNQSGLEEGGYGGCSVQR-------LPTGSRLEKVLKSLKADP
Danio 83 APNISREVVNQLLPKAPPLQQLLDHHDFQGDASSLEDFIDADEYHATTESVITMASEPEP
Canis 1 ----------MLGEWKAAADP
Bos 117 APNISREVVKQLLPKAPPLQQILDLHDFQGDALQPEDFLEEDEYHATTETVISMAQETDP
Homo 92 APNISREVVKQLLPKAPPLQQILDLHDFQGDALQPEDFLEEDEYHATTETVISMAQETDP
Xenopus 137 AVRIDGNPHCQYFNFSPKIMFTKVVKAQLWVYLRPISIPPLCTFRSYDLKLLK-------
Mus 150 AVQTDGSPLCCHFHFSPKVMFNKVLKAQLWVYLRPVPRPATVYLQILRLKPLTGEGTAGG
Rattus 122 AVQTDGSPLCCHFHFSPKVMFTKVLKAQLWVYLRPVPRPATVYLQILRLKPLTGEGTAGG
Danio 143 LVQVDGKPTCCFFKFSPKLMFTKVLKAQLWVYLQPLKQTSTVYLQILRLKPITE------
Canis 12 AVQTEGSPLCCHFHFSPKVMFTKVLKAQLWVYLRPVPRPATVYLQILRLKPLTGEGTAGG
Bos 177 AVQTDGSPLCCHFHFSPKVMFTKVLKAQLWVYLRPVPRPATVYLQILRLKPLTGEGTAGG
Homo 152 AVQTDGSPLCCHFHFSPKVMFTKVLKAQLWVYLRPVPRPATVYLQILRLKPLTGEGTAGG
Xenopus 190 --KGSKHIRIRSLKIDLHSRSGHWQSIDFKHVLQNWFKQPHNNWGIEINAFDPNGNDLAV
Mus 210 GGGGRRHIRIRSLKIELHSRSGHWQSIDFKQVLHSWFRQPQSNWGIEINAFDPSGTDLAV
Rattus 182 GGGGRRHIRIRSLKIELHSRSGHWQSIDFKQVLHSWFRQPQSNWGIEINAFDPSGTDLAV
Danio 197 --QGSRHIRIRSLKIELDSQAGHWQSIDFKHVLQNWFKQPHTNWGIDINAYDESGNDLAV
Canis 72 GGGGRRHIRIRSLKIELHSRSGHWQSIDFKQVLHSWFRQPQSNWGIEINAFDPSGTDLAV
Bos 237 GGGGRRHIRIRSLKIDLHSRSGHWQSIDFKQVLHSWFRQPQSNWGIEINAFDPSGTDLAV
Homo 212 GGGGRRHIRIRSLKIELHSRSGHWQSIDFKQVLHSWFRQPQSNWGIEINAFDPSGTDLAV
Xenopus 248 TSLGPGAEGLHPFMELRVMENNKRSRRNLGLDCDEHSTESRCCRYPLTVDFEAFGWDWII
Mus 270 TSLGPGAEGLHPFMELRVLENTKRSRRNLGLDCDEHSSESRCCRYPLTVDFEAFGWDWII
Rattus 242 TSLGPGAEGLHPFMELRVLENTKRSRRNLGLDCDEHSSESRCCRYPLTVDFEAFGWDWII
Danio 255 TSLGPGEEGLQPFLEVKILETTKRSRRNLGLDCDEHSTESRCCRYPLTVDFEAFGWDWII
Canis 132 TSLGPGAEGLHPFMELRVLENTKRSRRNLGLDCDEHSSESRCCRYPLTVDFEAFGWDWII
Bos 297 TSLGPGAEGLHPFMELRVLENTKRSRRNLGLDCDEHSSESRCCRYPLTVDFEAFGWDWII
Homo 272 TSLGPGAEGLHPFMELRVLENTKRSRRNLGLDCDEHSSESRCCRYPLTVDFEAFGWDWII
Xenopus 308 APKRYKANYCSGQCEYMFMQKYPHTHLVQQANPRGSAGPCCTPTKMSPINMLYFNDKQQI
Mus 330 APKRYKANYCSGQCEYMFMQKYPHTHLVQQANPRGSAGPCCTPTKMSPINMLYFNDKQQI
Rattus 302 APKRYKANYCSGQCEYMFMQKYPHTHLVQQANPRGSAGPCCTPTKMSPINMLYFNDKQQI
Danio 315 APKRYKANYCSGQCEYMFMQKYPHTHLVQHANPRGSAGPCCTPTKMSPINMLYFNDKQQI
Canis 192 APKRYKANYCSGQCEYMFMQKYPHTHLVQQANPRGSAGPCCTPTKMSPINMLYFNDKQQI
Bos 357 APKRYKANYCSGQCEYMFMQKYPHTHLVQQANPRGSAGPCCTPTKMSPINMLYFNDKQQI
Homo 332 APKRYKANYCSGQCEYMFMQKYPHTHLVQQANPRGSAGPCCTPTKMSPINMLYFNDKQQI
Xenopus 368 IYGKIPGMVVDRCGCS
Mus 390 IYGKIPGMVVDRCGCS
Rattus 362 IYGKIPGMVVDRCGCS
Danio 375 IHGKIPGMVVDRCGCS
Canis 252 IYGKIPGMVVDRCGCS
Bos 417 IYGKIPGMVVDRCGCS
Homo 392 IYGKIPGMVVDRCGCS

Figure 5.6 Early expression of *XlGdf11*. (A) Relative RT-PCR. *XlGdf11* transcripts are first detectable by relative RT-PCR at stage 15, followed by a slight spike at stage 17. A similar level of expression is maintained until stage 26, beyond which there appears to be progressive up-regulation. *Histone H4* transcripts were co-amplified for normalization. (B) Whole-mount expression. Expression is first seen at stage 19 in tissue immediately flanking the blastopore, corresponding to the location of the presumptive tail bud (black arrowhead). In subsequent stages, strong expression is restricted to the tail bud and eventually to the very tail tip. Faint expression can also be seen in posterior somites. Rostral expression is also noted in the pharyngeal tissue (white arrow), regions of the brain (white arrowhead), the otic vesicle and the facial mesenchyme.

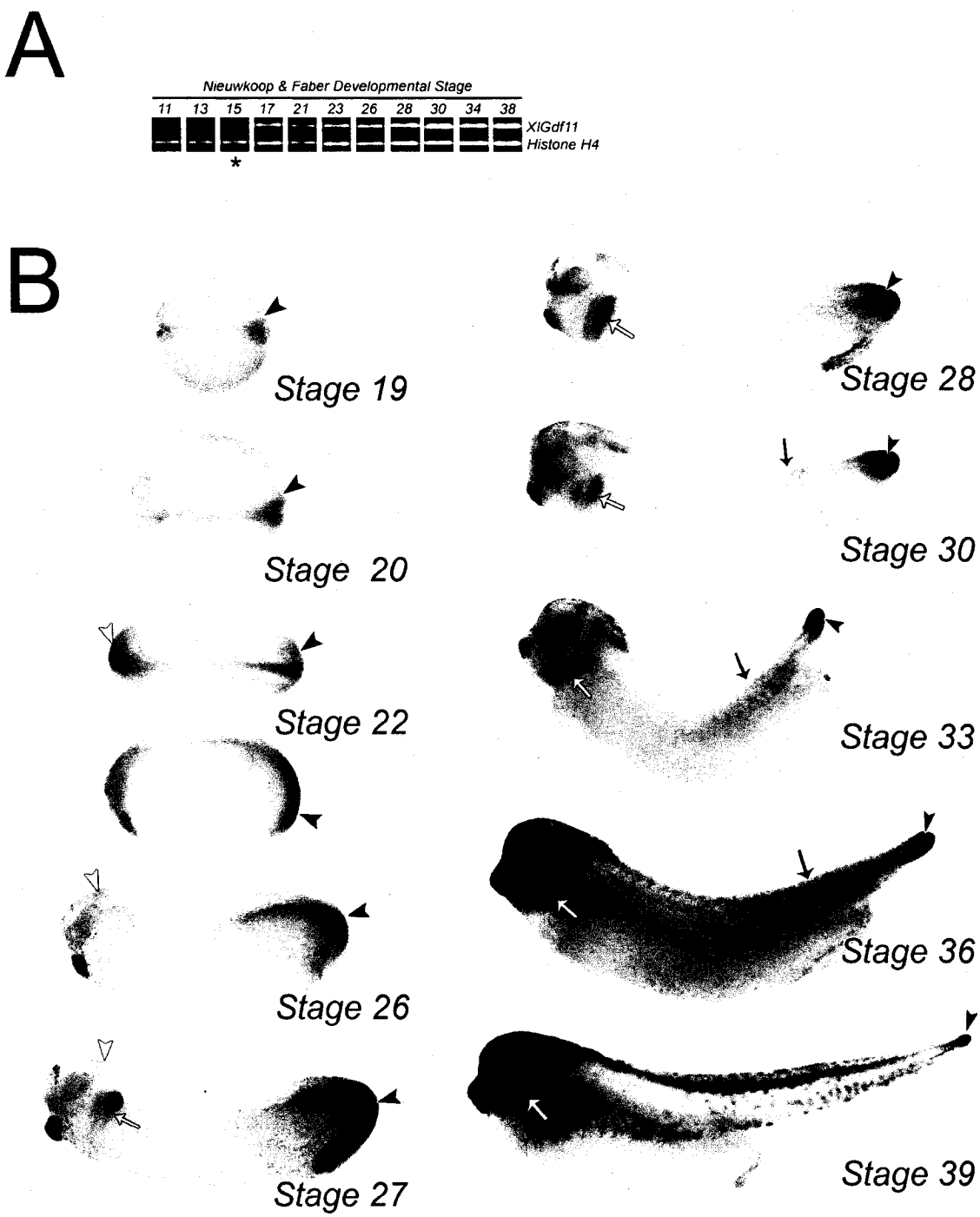
A
Nieuwkoop & Faber Developmental Stage
11 13 15 17 21 23 26 28 30 34 38
XlGdf11
Histone H4
*
B
Stage 19
Stage 20
Stage 22
Stage 26
Stage 27
Stage 28
Stage 30
Stage 33
Stage 36
Stage 39

Figure 5.7 Caudal expression of *XlGdf11*. (A) Tail of stage-31 *X. laevis* embryo (inset) showing expression of *XlGdf11* in the tail bud (tb) and posterior somitic mesoderm (pm). Numbers correspond to the progressively caudal transverse sections shown in B. (B) *XlGdf11* expression in the tail bud (stage 31). At the caudal tip (4), transcripts are found in the tissue encompassing the neurenteric canal (nc), including the posterior wall (pw). More rostrally, expression is obvious in the chordoneural hinge (cnh) and the presomitic mesoderm (3), and their derivative including the notochord (n), ventral neural tube (nt), somites (s), and the post-anal gut (pag). (C) Sagittal section through the tail of stage-28 embryo, showing strong *XlGdf11* expression in the chordoneural hinge (cnh; caudal margin outlined) and the posterior wall (pw), lining the neurenteric canal (nc). (D) Lateral view of tail tip at stage-39 showing persistent *XlGdf11* expression.

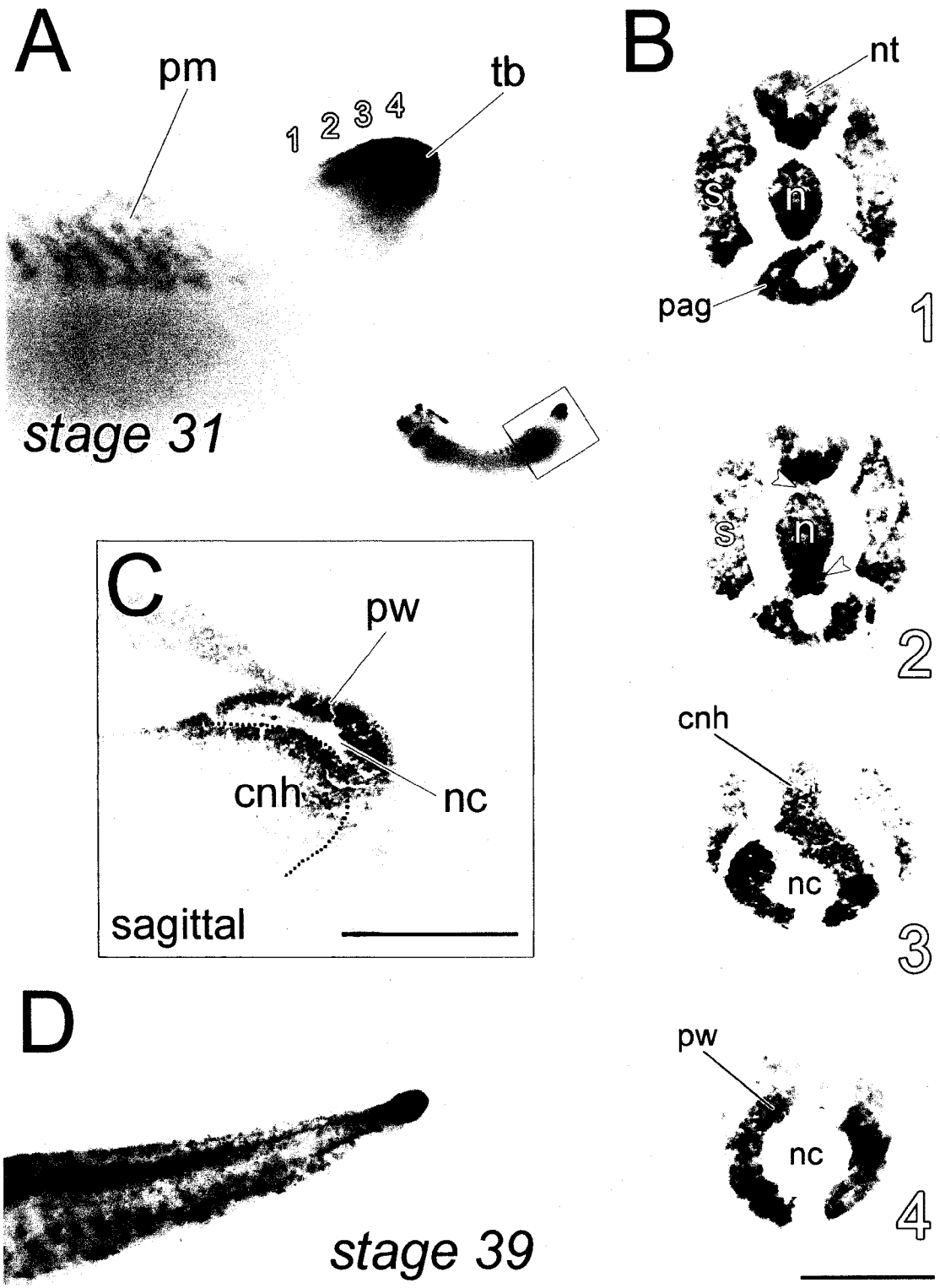
A
pm
tb
1 2 3 4
stage 31
B
nt
s
n
pag
1
s
n
2
cnh
nc
3
C
pw
cnh
nc
sagittal
D
stage 39
pw
nc
4

Figure 5.8 Rostral expression of *XlGdf11*. (A) *XlGdf11* is broadly expressed in the head, including the otic vesicle (ov), the branchial arches (ba), facial mesenchyme (fm), and regions of the brain (also shown in dorsal perspective in inset at top; fb, forebrain; mb, midbrain; hb, hindbrain). Paired insets at bottom show planes of sections depicted in B and C. (B) Transverse sections through head of stage-31 embryo showing *XlGdf11* transcripts in the midbrain, facial mesenchyme (fm), and more caudally, in the hindbrain, otic vesicle, and a branchial arch. (C) Frontal longitudinal sections again showing expression in the brain, otic vesicles, and pharynx. Of note is the restricted expression pattern in the forebrain (indicated by empty arrowheads) and the localization of transcripts to the mesenchyme of the rostral branchial arches (black arrowheads) versus the endoderm of pharyngeal pouches 3 and 4 (P3, P4). S, somites; phx, pharynx. Scale bar equals 0.5 mm.

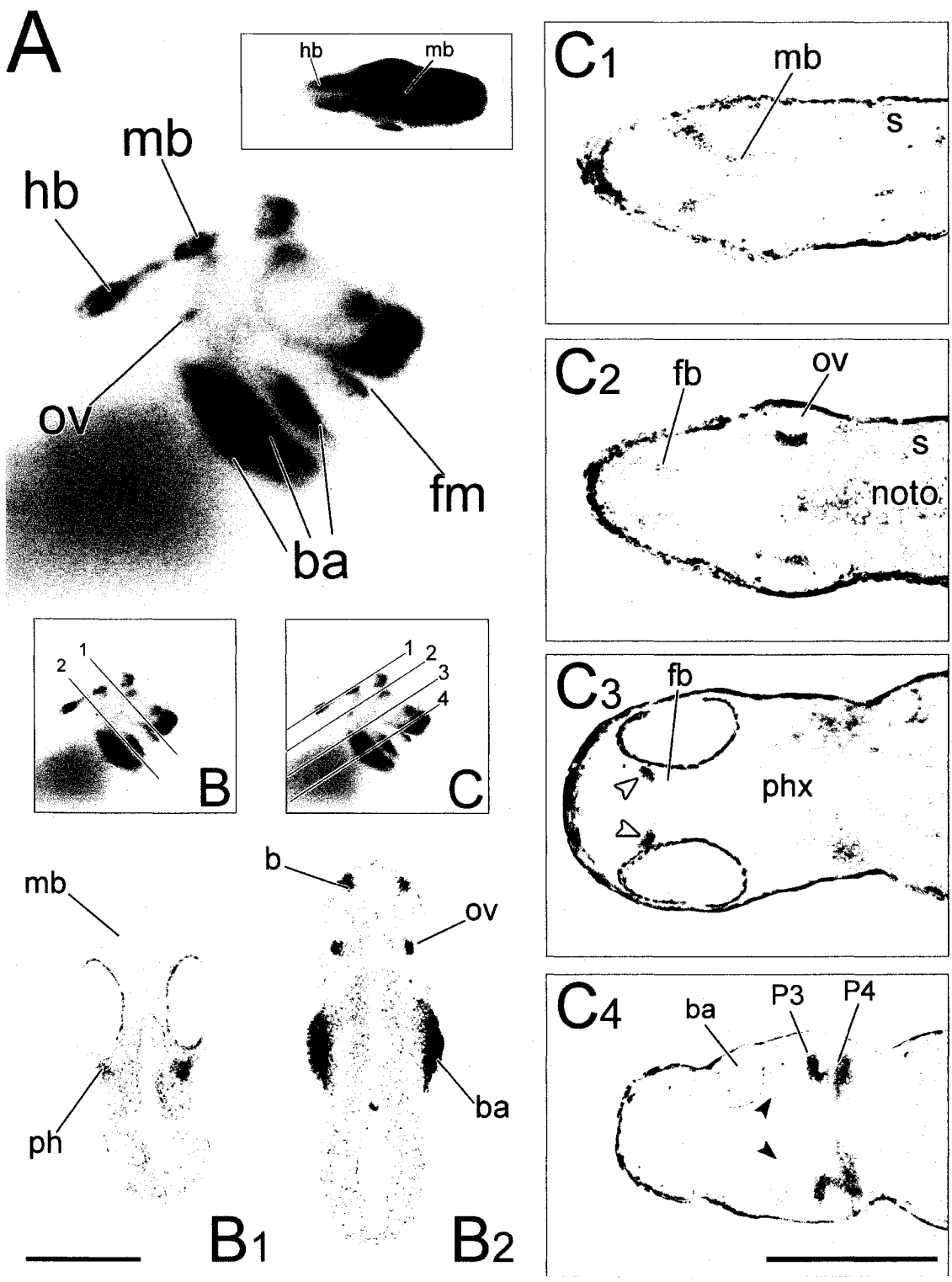
A
hb
mb
mb
hb
ov
fm
ba
B
C
mb
ov
b
ph
ba
B1
B2
C1
mb
s
C2
fb
ov
s
noto
C3
fb
phx
C4
ba
P3
P4

Figure 5.9 Morpholino injection into *X. laevis* embryos. (A) Broad distribution of a fluoresceinated morpholino injected into the animal poles of 2-cell blastomeres, confirming the sufficient diffusion of reagents delivered in this fashion. (B) Relative RT-PCR comparing endogenous *XlGdf11* transcripts in control (uninjected and control MO) and *XlGdf11ie_e3*-injected embryos (20 and 40 ng). Transcripts levels are visibly attenuated in those embryos receiving the experimental morpholino. *Histone H4* transcripts were co-amplified for normalization across treatments. (C) The 'torsion' phenotype. Early (left column) and late (right column) presentations of the 'torsion' phenotype, characterized by a down-turned head and lateral torsion. Embryos are shown in dorsal and lateral perspectives. Stage-matched control embryos are presented at the bottom. (D) *XHoxc10* expression in an embryo (lateral and dorsal views) having received 20 ng of the XlGdf11i2_e3 morpholino and a staged-matched control (in lateral perspective). Arrowheads indicate the well-defined anterior axial terminus of *XHoxc10* expression (shown at higher magnification in inset).

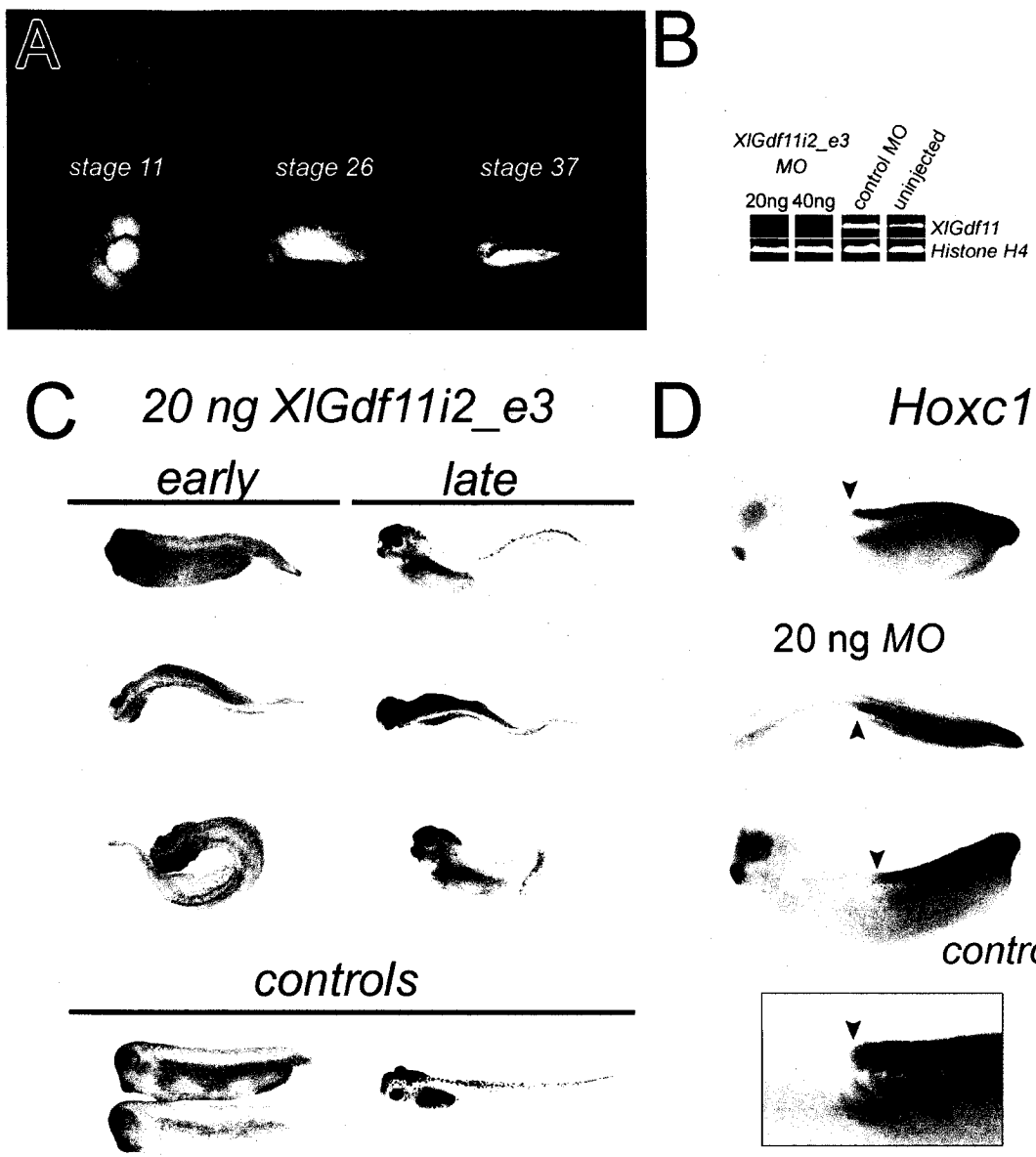
A
stage 11
stage 26
stage 37
B
XlGdf11i2_e3 MO
control MO
uninjected
20ng 40ng
XlGdf11
Histone H4
C
20 ng XlGdf11i2_e3
early
late
controls
D
Hoxc10
20 ng MO
control

Figure 5.11 Mild and severe posteriorization phenotypes observed in *X. laevis* embryos following the injection of capped sense *XlGdf11* RNA. (A) Mildly posteriorized embryos demonstrate a down-turned head with slightly reduced structures and varying degrees of axial truncation. Severely posteriorized embryos (right column), show dramatically reduced or altogether missing head structures and extreme axial truncation. (B) *XHoxc10* expression in posteriorized embryos. Mildly posteriorized embryos (at left) have retained a well-defined anterior terminus of *XHoxc10* expression (arrowhead), whereas it is less resolved in severely posteriorized embryos.

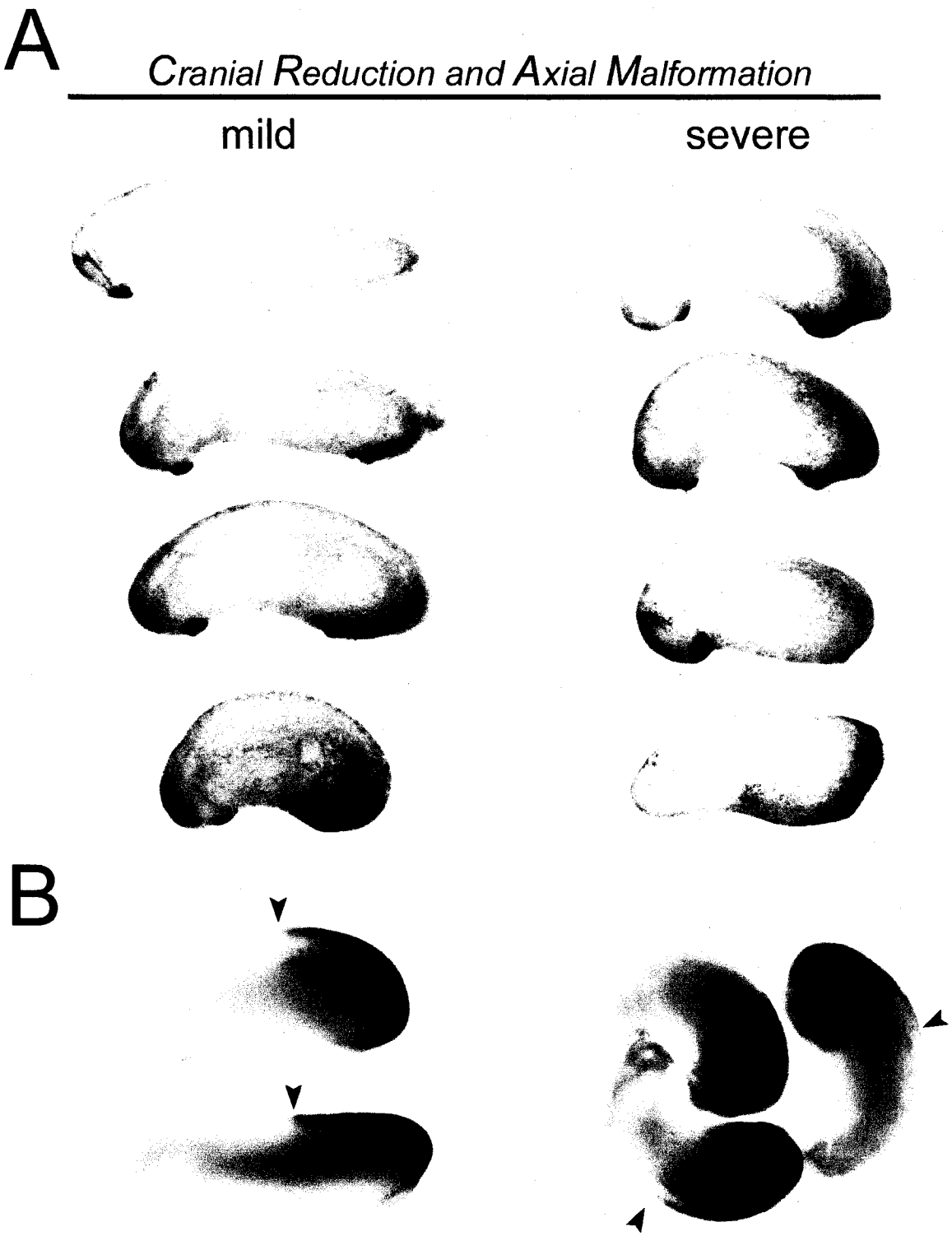
A
Cranial Reduction and Axial Malformation
mild
severe
B

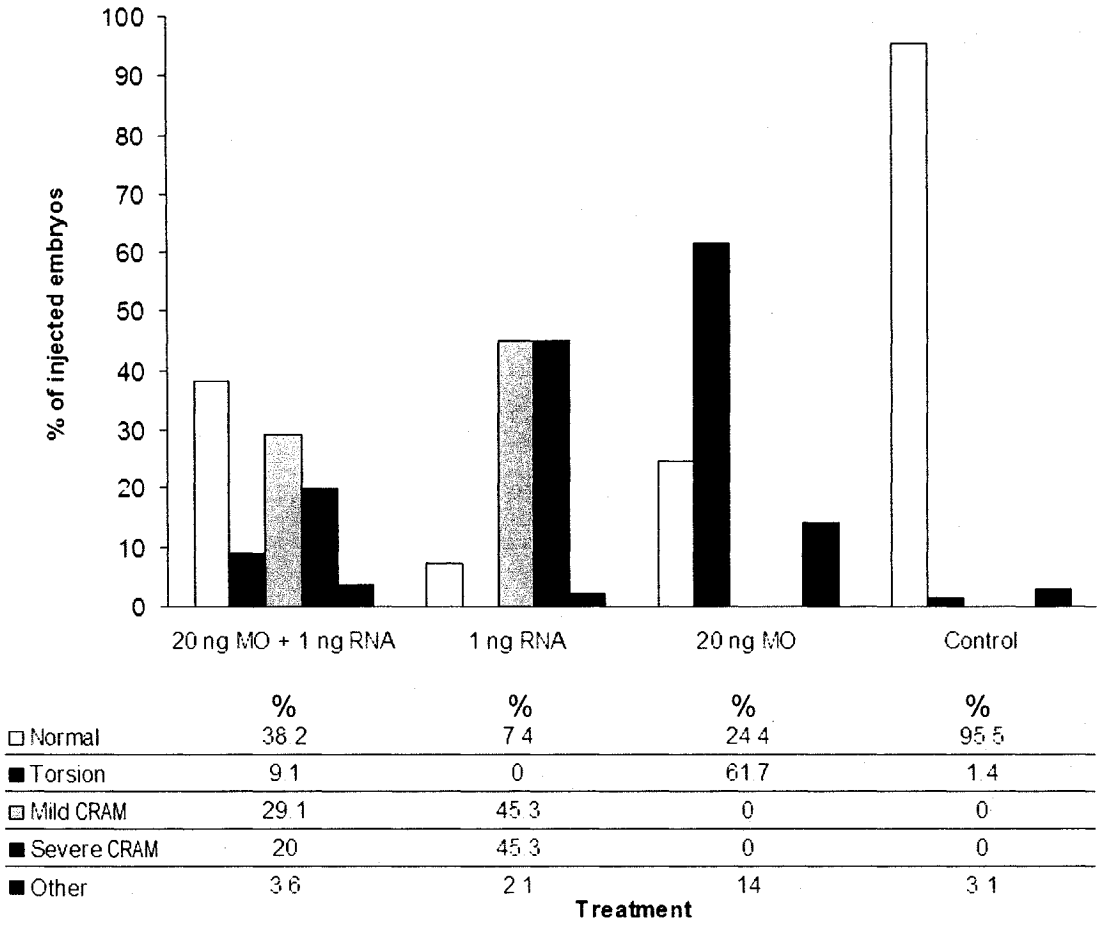

Figure 5.13 Rescue of *XlGdf11* gain- and loss-of-function phenotypes. All three observed phenotypes (*i.e.*, torsion, mild and severe CRAM) occur less frequently in those embryos that were co-injected with 20 ng of XlGdf11i2_e3 MO and 1.0 ng sense XlGdf11 RNA. One-way ANOVA indicates, however, that the differences are only significant for torsion ($p < 0.001$, $F = 61.073$) and severe CRAM ($p = 0.002$, $F = 10.175$). The double-injected treatment differs significantly from corresponding single-injected controls in terms of the frequency of the normal embryos, suggesting that co-injection lead to reverse of the single-injected phenotypes.

Table 5.1 Statistical significance of observed phenotypes as determined by one-way ANOVA.

A. Torsion phenotype between the 20 ng *XlGdf11i2_e3*, 20 ng control MO, and uninjected treatments.

	Treatment		
Treatment	20 ng *XlGdf11i2_e3*	20 ng control MO	uninjected
20 ng *XlGdf11i2_e3*	-	-	-
20 ng control MO	$p < 0.001$ $F = 189.57$	-	-
uninjected	$p < 0.001$ $F = 704.76$	$p = 0.008$ $F=7.022$	-

B. Torsion, CRAM (mild and severe), and normal phenotypes (except 'Other') between the rescue treatment (1 ng sense RNA + 20ng *XlGdf11i2_e3*) and the corresponding single-injected treatments.

		Treatment
Phenotype	**Treatment**	1 ng sense RNA + 20ng *XlGdf11i2_e3*
Torsion	20 ng *XlGdf11i2_e3*	$p < 0.001$ $F = 61.073$
Mild CRAM	1 ng sense RNA	$p = 0.051$ $F = 3.865$
Severe CRAM	1 ng sense RNA	$p = 0.002$ $F = 10.175$
Normal	20 ng *XlGdf11i2_e3*	$p = 0.029$ $F = 4.811$
	1 ng sense RNA	$p < 0.001$ $F = 25.145$
	uninjected	$p < 0.001$ $F = 209.64$

Table 5.2 Statistical significance of variation in *XHoxc10* axial levels as determined by one-way ANOVA.

A. *XHoxc10* expression boundaries between the 20 ng *XlGdf11i2_e3*, 20 ng control MO, and uninjected treatments.

	Treatment		
Treatment	20 ng *XlGdf11i2_e3*	20 ng control MO	uninjected
20 ng *XlGdf11i2_e3*	-	-	-
20 ng control MO	p = 0.275 *F* = 1.217	-	-
uninjected	p = 0.364 *F* = 0.833	p = 0.693 *F* = 0.158	-

B. *XHoxc10* expression boundaries between the 0.5 ng and 0.75 ng sense RNA, and uninjected treatments.

	Treatment		
Treatment	0.5 ng sense RNA	0.75 ng sense RNA	uninjected
0.5 ng sense RNA	-	-	-
0.75 ng sense RNA	p = 0.398 *F* = 0.724	-	-
uninjected	p = 0.820 *F* = 0.052	p = 0.297 *F* = 1.107	-

CHAPTER 6:

THE FORM, FUNCTION AND FATE OF SUPERNUMERARY CAUDAL VERTEBRAE IN LARVAL MEGOPHRYIDS

6.1 SUMMARY

The axial skeleton in most anuran families consists of ≤9 presacral vertebrae, a single sacral vertebra, and the urostyle post-sacrally. Tadpoles from one anuran family, Megophryidae, deviate, however, from this pattern in bearing supernumerary vertebral centra in their tails. At least 5 of 11 genera from this Asian family share this character: *Leptobrachella* (≤30 caudal centra), *Leptolalax* (5-6), *Megophrys* (11-15), *Ophryophryne* (11-14) and *Xenophrys* (≥7). Tadpoles from each genus are typically found in streams, where their extended caudal skeleton anchors muscles that facilitate tadpoles escaping currents and burrowing into the stream bed. The extra centra of megophryids ossify differently in each genus. In *Leptobrachella*, the caudal centra ossify around the entire notochord, whereas in *Megophrys* each centrum develops from dorsal and ventral pairs of ossified anlage that expand to meet each other. At metamorphosis, the most proximal caudal centra are incorporated into the urostyle. The remaining centra are resorbed along with other tail structures, a process assisted by multinucleate, osteoclast-like cells. The presence of caudal vertebrae, a plesiomorphic anuran trait, in megophryids confirms that the machinery for caudal vertebral development has been retained in some modern anurans. A likely driving force in the reappearance of the trait in megophryids is the selective pressure associated with a riparian lifestyle. I suggest that precocious ossification of the axial skeleton relative to the appendicular skeleton, as seen in megophryids and other pelobatoids, may be the underlying developmental mechanism at work. Finally, I speculate as to the molecular bases for the reappearance of caudal

vertebrae in megophryids, implicating Hox genes and the regulators of sclerotome development (*e.g.*, collagen type II).

6.2 Introduction

In his review of anuran phylogeny, Griffiths (1963) referred to frogs and toads as "the most easily diagnosed of all vertebrate groups." The distinctiveness of anurans is readily apparent in their skeleton, which is highly derived in both the axial and the appendicular systems (reviewed in Chapter 2). The anuran vertebral column is dramatically reduced compared to other vertebrates. In the closest common ancestor, the proto-anuran *Triadobatrachus massinoti*, the axial skeleton consisted of at least 21 vertebrae, including 14 presacral and 6 caudal vertebrae (Estes & Reig, 1973; Rage & Roček, 1989). Among true anurans, however, there are at most nine pre-sacral vertebrae, followed by a single sacral vertebra and a greatly reduced caudal skeleton, built from the fusion of 2-4 coccygeal vertebrae with an elongate bony element called the hypochord (Mookerjee, 1931; Mookerjee & Das, 1939; Púgener, 2002; Ročková and Roček, 2005). The latter, located ventral to the notochord, is a mesoderm-derived structure that is somehow induced to ossify (Fig. 2.3).

Anuran caudal vertebrae are incomplete—they consist only of reduced neural arch elements without associated centra. The neural arches and centra arise from separate sub-compartments of the somite and are under separate molecular regulation (Christ, Huang & Scaal, 2000; Christ, Huang & Wilting, 2000). Centra development is predominantly

under the control of the gene *Pax1*, whereas *Uncx-4.1* is the key regulator of neural arch development (Wallin *et al.*, 1994; Ebensperger *et al.*, 1995; Peters *et al.*, 1999; Leitges *et al.*, 2000; Mansouri *et al.*, 2000). The decoupling of dorsal and ventral vertebral development is also manifested in the relative timing of the two events. Along with various cranial bones and the femur, the neural arches are among the first bones of the anuran skeleton to ossify. The centra typically follow in sequence (Carroll, Kuntz & Albright, 1999; Maglia, 2003 and papers cited therein)

Griffiths (1963) also referred to the 'extreme morphological uniformity' of anurans. Indeed, the generalized anuran post-cranial skeleton as described above is found in the vast majority of extant genera. In Chapter 2, I identified three diagnostic features of the anuran *Bauplan*, namely, the truncated axial skeleton, elongate tarsal elements, and the absence of caudal vertebrae. Of these features, only the latter is not perfectly maintained among living species. Against this uniformity Griffiths (1956; 1963) and Haas and colleagues (2006), however, identified two genera—*Megophrys* and *Leptobrachella*—with supernumerary caudal vertebrae in the larval stage. Tadpoles of *Megophrys* bear up to a dozen vertebral centra of varying degrees of completeness; *Leptobrachella* can have over 25 centra in the tadpole tail. Interestingly, the adults of both species appear no different from other anurans with respect to their post-sacral skeleton. It is thus unclear what becomes of the supernumerary caudal vertebrae at metamorphosis.

Both *Megophrys* and *Leptobrachella* belong to the Southeast Asian family Megophryidae, a group of ground-dwelling frogs that take their name from the Greek

'large eyebrows' (*meg* + *ophrys*), an apt description of the pronounced, fleshy outgrowths above the eyes of many *Megophrys* species. The 11 genera currently recognized in Megophryidae can be loosely grouped into two subfamilies (including 11 genera), the Leptobrachiinae and the Megophryinae (Lathrop, 2003; Frost, 2004). The former includes the genera *Leptobrachella*, *Leptobrachium*, *Leptolalax*, *Oreolalax*, and *Scutiger*, the latter *Vibrissaphora*; *Atympanophrys*, *Brachytarsophrys*, *Megophrys*, *Ophryophryne*, and *Xenophrys*. Dubois (1980) favors an alternative taxonomic system for the megophryids, which designates *Atymanophrys*, *Brachytarsophrys*, and *Xenophrys* as sub-genera of *Megophrys*, and *Oreolalax* and *Vibrissaphora* as sub-genera of *Scutiger* and *Leptobrachium*, respectively. This system, however, is based largely on phenetic clustering and is without strong phylogenetic corroboration (Lathrop, 1997; Frost, 2004). While I acknowledge the similarities Dubois' system highlights between megophryid genera, I employ Frost's 11-genera taxonomy throughout.

Adult megophryids are typically found among the leaf litter of montane forests and vary greatly in size and morphology. Similar disparity is seen in the tadpoles, which live in mountain streams of varying depths and rapidity. Among larval megophryids, three general body types can be identified. Megophryine tadpoles have broad funnel-shaped mouths and are modestly elongate. Within the Leptobrachiinae, *Leptobrachella* and *Leptolalax* have a vermiform body that directly contrasts with the larger, globose bodies seen in *Scutiger*, *Oreolalax*, *Leptobrachium* and *Vibrissaphora*. These morphological differences can be correlated with the ecology of each tadpole sub-family. Megophryines occupy relatively slow-flowing, shallow water at the edges of streams, where they feed

on floating debris with their funnel-shaped mouths (Nodzenski, Wassersug & Inger, 1989; Lathrop, 2003). Larger-bodied leptobrachines prefer the calm waters of deep splash pools; however, *Leptobrachella* and *Leptolalax* live among the rocky stream beds of fast-flowing streams.

In a recent paper describing the larval cranial skeleton and musculature of *Leptobrachella*, Haas and colleagues (2006) suggested that the supernumerary caudal vertebrae of this species offer additional attachment area for the tail musculature and facilitate burrowing of tadpoles into the rocky stream bed (see their Fig. 6.1). Highly fossorial tadpoles, similar to *Leptobrachella*, are also found in some neobatrachid families; *e.g.*, the Centrolenidae, Hylidae, Ranidae and Microhylidae (Orton, 1953; Altig & Johnston, 1989; Inger and Wassersug, 1990).

Before the discovery of *Leptobrachella* larvae, the only known tadpoles that forcefully burrowed into sand or gravel were those of the microhylid genus *Otophryne*. These tadpoles live in shallow, relatively slow-flowing, sandy bottom streams in Northern South America (Wassersug & Pyburn, 1987). Their tadpoles, however, are not elongated, but rather have a broad shovel-like head that they actively use to drive their way into sand snout first (A. Lathrop, live footage, pers. comm.). Centrolenid and ranid (*Staurois*) tadpoles converge more closely on the vermiform morphology of *Leptolalax* and *Leptobrachella*. They are also stream-associated, but they sequester themselves in the wet leaf mulch found at the margins of streams rather than the sand or gravel at the bottom of the main channel. Several hylid tadpoles, such as *Hyla bromeliacia*, are

similarly attenuated and fossorial. However, they are concurrently arboreal, living in the decaying organic matter at the base of bromeliads. Haas *et al.* (2006) suggested that the actively burrowing, attenuated tadpoles constitute an 'ecomorphological guild' (as per Altig and Johnston, 1989) with *Leptobrachella*, an extreme representative.

Haas *et al.* (2006) also noted that axial skeletal development is accelerated relative to appendicular skeletogenesis in *Leptobrachella*. Such heterochronic shifts in developmental sequence could have been a fruitful source of morphological divergence during anuran evolution (Chipman, 2002) and key driving forces in the adaptive radiation and success of frogs and tadpoles. In torrent-dwelling bufonid and ranid tadpoles, for instance, Nodzenski and Inger (1990) noted delayed mouth part development relative to tail resorption. They suggested that these tadpoles retain their suctorial mouths, their means of anchoring themselves in fast-flowing water, up until their limbs have fully grown and are functional. Similar shifts in developmental sequence would have likely accompanied the adaptive radiation of megophryid larvae to the streams in which they are found.

Here I describe development of the post-cranial axial skeleton in 9 (of 11) megophryid genera, including *Leptobrachella*, *Leptobrachium*, *Leptolalax*, *Megophrys*, *Ophryophryne*, *Oreolalax*, *Scutiger*, *Vibrissaphora*, and *Xenophrys*. Along with *Leptobrachella* and *Megophrys*, tadpoles of *Leptolalax*, *Ophryophryne* and *Xenophrys* bear supernumerary vertebrae in their tails. There is notable diversity in the osteology as well as the ontogeny of the post-sacral skeleton among these genera. In all five, however,

the caudal skeleton appears to be resorbed at metamorphosis by a common degradative mechanism. I consider ecological, developmental and genetic bases for the expanded caudal skeleton of megophryids and its curious absence in fellow stream-associated anuran species, of which I examined tadpoles of *Heleophryne rosei*, *Osteopilus brunneus*, and the centrolenids *Hyalinobatrachium*, *Cochranella*, and *Centrolenella*. Finally, I consider the appearance of supernumerary caudal vertebrae, a decidedly atypical anuran trait, in megophryids in the context of *Bauplan*, in an attempt to clarify the interaction between developmental constraint and natural selection in driving tadpole evolution.

6.3 Materials and Methods

Megophryid specimens were obtained from various museum and personal collections (see Table 6.1 for catalogue numbers). Generally, specimens had been previously fixed in neutral-buffered formalin (4%) and transferred to 70% ethanol for long-term storage. Prior to processing, standard measurements (total and snout-vent length) were made using an electronic caliper (accurate to 0.01 cm), and specimens were staged as per Gosner (1960). In the case of *Leptobrachella* and other megophryid genera, Gosner stages may not be accurate as hindlimb development appears to be desynchronized with the development of internal structures, particularly the axial skeleton (Haas *et al.*, 2006). For the sake of standardization, however, I refer to Gosner stages throughout.

Whole anuran specimens were eviscerated and then cleared and stained with alcian blue and alizarin red as per Hanken and Wassersug (1981). In cases of poorly preserved or

aged specimens, alcian blue staining was extended up to seven days to maximize mucopolysaccharide labeling. It should be noted that while alcian blue and alizarin red are not definitive stains of cartilage and bone, in the case of the axial skeleton, where bones develop by endochrondral ossification, the "alcian blue equals cartilage" and "alizarin red equals bone" rules of thumb apply. I thus employ this system throughout this paper.

Specimens for histology were decalcified in 10% EDTA for 7 days, dehydrated in an ethanol series (30%, 50%, 70%, 80%, 90%, 95%, 2 × 100%), cleared in Histo-Clear II (National Diagnostics HS-202) and then embedded in paraffin. Serial sections were cut at a thickness of 5-10 μm and then mounted on slides subbed with Haupt's adhesive. Sections were rehydrated in a EtOH series and stained by a Mallory's trichrome protocol. Briefly, sections were stained in 1% acid fuchsin for 15 s, the stain differentiated by two quick dips in fresh distilled H_2O (dH_2O) and then fixed by immersion in 1% phosphomolybdic acid (1-2 min). Following a quick dH_2O rinse, sections were stained in Mallory's (0.5% aniline blue : 2% orange G) for 75 seconds, briefly rinsed, and then dehydrated prior to two 5-minute washes in xylene. The Mallory's trichrome stain rendered connective tissue and cartilage blue (aniline blue), muscle red to orange (orange G), and other tissues plus nuclei pink (acid fuchsin). Sections were photographed with a Zeiss Axiocam MRc digital camera attached to an Axioplan 2 microscope. For cleared-and-stained specimens, a Zeiss Stemi 2000-C stereoscope was used.

6.4 RESULTS

A total of 60 megophryid specimens, ranging from Gosner stage 25 to adult, were examined (see Table 6.1 for comprehensive listing). Two of the 11 megophryid genera, *Atympanophrys* and *Brachytarsophrys*, were unavailable. As a pilot study, I surveyed few members from each genus by whole-mount clearing and bone-staining. Those genera found to have supernumerary caudal vertebrae were studied in greater detail. For each, I tried to obtain multiple species; however, I was limited by the rarity of many of these genera in museum collections. Where possible, I assembled a developmental series of each species.

The megophryid trunk axial skeleton comprises 8 presacral vertebrae (designated I-VIII as per Trueb, 1973) followed caudally by a single sacral vertebra (IX). In all species, presacral vertebrae bear transverse processes, which are particularly elongate on vertebrae II-IV. Towards metamorphosis, the sacral vertebra forms expanded diapophyses that articulate with ilia of the hindlimb skeleton.

Megophryid tadpoles demonstrate great diversity in the morphology of their post-sacral skeleton. Post-sacral vertebrae (numbered proximal to distal as PS1, 2 etc.) all show some degree of reduction of neural arches and/or vertebral bodies. Only rudimentary neural arches are seen on PS1 and 2 in megophryids. There is considerably more variety in the number and degree of completeness of post-sacral centra. Minimally, I define a centrum as any perichordal ossification occurring at myoseptae. In some species, for

example, a single fragmentary ossified anlage of a centrum counted as a post-sacral vertebra.

In the following, I describe vertebral column development in each represented megophryid genus, focusing on the morphological diversity of the post-sacral skeleton.

6.4.1 *Leptobrachella*

6.4.1.1 L. mjobergi

Strong ossification of the axial skeleton is evident from the earliest free-living larval stage (Gosner stage 25; represented by FMNH 157998b and BrachellaM6). The vertebral complement of *L. mjobergi* appears to be fully established during this stage: 8 presacral, 1 sacral, and 29-30 caudal vertebrae. Centra are spool-like, completely encompassing the notochord and narrowing towards their centres; this corresponds to the 'perichordal' type (or 'ectochordal' *sensu* Griffiths, 1963 and Trueb, 1973). Bilaterally, each post-sacral centra bears a small convexity at its middle, which corresponds to the level of the associated myoseptum. Histologically, post-sacral centra consist of collagenous connective tissue around the periphery of the notochordal sheath (BrachellaM2; Fig. 6.1E). Vertebrae I-XI bear neural arches that decrease in height caudally. Conversely, vertebral centra increase in size caudally, abruptly expanding post-sacrally and reaching their greatest size mid-tail before tapering again towards the tip. The most caudal vertebrae are represented as faint ossifications in the perichordal sheath (Fig. 6.1B).

Consistent with a previous observation of relatively delayed hindlimb development (Haas *et al.*, 2006), the appendicular skeleton is not apparent despite the advanced state of the axial skeleton.

In subsequent stages, no further vertebrae are added, while distal caudal centra show signs of ossification and neural arch elements continue to expand rostro-caudally. By stage 39/40 (FMNH 157998a), all but the two most caudal centra are ossified (as visualized with alizarin-red staining). More rostrally, the neural arches of vertebrae I-IX articulate at their zygapophyses; II-IV bear expanded transverse processes. The sacral diapophyses have not yet developed, whereas the long bones of the appendicular skeleton, with the exception of some forelimb digits, all show signs of ossification.

In the adult (FMNH 222857; Fig. 6.1A), the caudal skeleton comprises a caudally-tapered coccyx ankylosed with the hypochord, itself fused to the sacral vertebra (monocondylar). Hypochord development appears to be delayed until late metamorphosis as it is not found in specimens as late as stage 39/40; however, this may be an artifact of poor alcian-blue staining. The sacral vertebra bears longitudinally-expanded diapophyses that articulate with ilia extending rostrally to the level of vertebra V.

6.4.1.2 L. parva

This metamorph (stage 42; FMNH 244079) was fixed in unbuffered formaldehyde and stained poorly with alcian blue, which reduced the visibility of non-ossified tissue. Nevertheless a total of 33 vertebrae, including 8 presacrals, 1 sacral, and 24 post-sacrals, are clearly identifiable. Vertebrae I-XI have neural arches that decrease in height caudally; I-IX articulate at their zygapophyses. The sacral vertebra (IX) bears slightly-expanded diapophyses, extending towards the ilia. A cartilaginous ridge, likely the nascent hypochord, is evident on the ventral surface of PS1 (Fig. 6.1D). The most caudal centra appear fragmented and porous, suggesting that they may be undergoing degradation at this stage (Fig. 6.1C). The appendicular skeleton is well-developed, showing ossification of all long bones, including those of the girdles.

6.4.2 *Leptolalax pelodytoides*

Consistent with what was observed in the closely-related *Leptobrachella*, axial skeleton development in this genus is accelerated relative to appendicular development. By stage 27 (ROM 42275), when the limb buds are mere rudiments, the vertebral column is well-formed, comprising 12 vertebrae of varying degrees of completeness. Vertebrae I-IX are complete, with perichordal centra and articulated neural arches; II-IV bear ossified transverse processes of consecutively lesser length. The three post-sacral vertebrae are progressively more rudimentary. PS1 has reduced dorsal structures, PS2 is a centra, and

PS3, the caudalmost vertebra, consists of a pair of osseous plates superposing the notochord. As in *Leptobrachella*, the circumference of centra increases towards the caudal end, coinciding with the progressive dilation of the notochord.

Two complete post-sacral centra (PS1 and 2) are also seen at stages 30 and 32 (specimens ROM 42276 and 42281, respectively). The rest of the post-sacral skeleton of the younger specimen, however, lacks a clear segmental pattern, particularly in ventral aspect (Fig. 6.2A). Whereas dorsal anlagen coincide with the myoseptae, several ventral anlagen occur between these boundaries. It is not clear to which vertebrae these precursors will eventually contribute. In contrast, three discernible vertebrae follow PS1 and 2 at stage 32; PS3's centrum is nearly complete (discontinuous dorsally), PS4 comprises four discrete anlagen (not unlike the distal post-sacrals of *Megophrys*), and PS5 two anlagen, a ventral plate and a cartilaginous disc on the left dorsal surface. Interestingly, at both stages, the transverse processes of presacral vertebra IV are barely visible and highly reduced compared to the corresponding structures at stage 27. Histological examination of the proximal tail of a stage-31 tadpole (ROM 42280) reveals peri-notochordal bone at three successive myoseptae caudal to PS1 and PS2, for a total of 5 post-sacral centra.

By stage 37 (ROM 42282), a sixth, incomplete post-sacral centra has formed. This represents the terminal number of post-sacral vertebrae as no more than six are seen in subsequent stages. PS1-3 are perichordal centra (only the most rostral bearing neural arches) whereas their caudal neighbors are progressively incomplete: PS4 comprises two lateral bands separated at both dorsal and ventral surfaces of the notochord; PS5 is a

dorsal anlagen pair; and PS6 is a single, unilateral anlage. PS1 and 2 are bridged by a narrow symphysis ventrally.

The appendicular skeleton shows signs of ossification in all long bones except for the most distal digital elements. Earlier stages of limb skeletogenesis are not represented in my developmental series, but would have been expected to occur following stage 32. By stage 40 (FMNH 254546), the appendicular skeleton is ossified throughout and has lengthened considerably. Post-sacral vertebrae 1 and 2 are tightly compacted, and a prominent, bulbous outgrowth is visible on the ventral surface of the former (Fig. 6.2C). This structure will likely contribute to the urostyle in the adult. PS4 flanks the notochord laterally, while PS5 and 6 dorsally superpose it as anlagen pairs (Fig. 6.2B). These vertebrae are noticeably more developed at stage 43 (FMNH 254546): PS4 has fused ventrally, and PS5 and PS6 each extend over the dorso-lateral surface of the notochord. More proximally, PS3 completely encircles the notochord, and PS1 and 2 are joined ventro-medially by the hypochordal rod, which projects caudally from ventral surface of PS2 (Fig. 6.2D). Consistent with a extra-vertebral origin for the rod, a small gap can be seen between it and vertebral body of PS2.

Towards the end of metamorphosis at stage 45 (represented by ROM 42278), all caudal vertebrae have been longitudinally compacted into the sacrum and the notochord has degraded entirely. The remnants of PS1 and 2 are closely articulated dorsally and fused completely as the hypochord ventrally (Fig. 6.2E). Laterally, both vertebrae show signs of degradation. Post-sacral vertebrae 4-6 are displaced ventrally and also shows signs of

degradation. The presacral skeleton is well-developed. The vertebrae are tightly apposed, separated only by cartilaginous intervertebral discs, and appear imbricate from the dorsal perspective. Prominent tranverse processes adorn II-IV, while broad sacral diapophyses extend laterally towards the ilia, but do not articulate with them.

6.4.3 *Megophrys*

6.4.3.1 M. boettgeri

Cartilage-staining is generally poor among this lot of specimens (A-30639). At the earliest stage examined, Gosner 36, 17 vertebrae, including 8 post-sacral centra, are present. Well-formed neural arch pairs adorn vertebrae I-IX and PS1. Thumb-like transverse processes can be seen on vertebrae II and III. On PS2, rounded rudiments project from the dorsal surface of the centrum. Along with the sacral vertebra, PS1 and 2 show expansion of their ventral surfaces, perhaps representing early stages of hypochord development. PS3 and 4 each have fused dorsal and ventral osseous perinotochordal plates. Their caudal neighbors, PS5 and 6 comprise four anlagen (dorsal and ventral pairs), whereas 7 and 8 consist of only dorsal anlagen. Longitudinal staggering of dorsal and ventral anlagen is pronounced in these vertebrae. Within the hindlimb, the femur, tibia, and fibula are slightly ossified at their centers.

By stage 39, a total of 20 vertebrae are present. Presacrally, vertebrae articulate at their zygapophyses and neural arches are fused with the underlying vertebral bodies.

Rudimentary transverse processes adorn II-IV, and dilated diapophyses project laterally from IX, the sacral vertebra. Along with PS1 and PS2, IX has a longitudinal ridge on its ventral surface. This ridge, the hypochord, is continuous with a symphysis joining PS1 and 2 ventro-medially. PS1-5 completely encircle the notochord, while PS6-8 consist of separate dorsal and ventral plates. Further caudally, PS9-11 consist of discrete ossified anlagen. PS10 is missing its left-dorsal anlage, which is noticeably reduced in size in PS9. PS11, the caudalmost vertebra, comprises a single ventral anlage. All elements of the appendicular skeleton show signs of ossification at this stage.

The post-sacral skeleton varies little in subsequent stages. At stage 44 (represented by two specimens), there are 14 post-sacral centra. Only the most proximal 5-7 of these are perichordal, while the two most caudal centra comprise discrete anlagen. Intervening vertebrae consist of paired, longitudinally-staggered dorsal and ventral plates. All vertebral centra—both pre- and post-sacral—are porous, suggestive of early-stage osteoclastic degradation. PS1-3 appear more intact than vertebrae at more rostral and caudal levels. These same vertebrae are bridged ventrally (hypochordal ridge) and dorsally at the neural arches (coccygeal ridges) (Fig. 6.3H). Presacral centra, porous at both their ventral and lateral faces, show the greatest signs of degradation. Coincident with this degradation, the notochord appears deflated and reduced in thickness at trunk levels. Dorsally, laminae circumscribe the spinal cord in vertebrae III-IX and prominent transverse processes adorn II-IV. All long bones of the appendicular skeleton are protracted and strongly ossified at this stage.

The latest specimen of *M. boettgeri* examined, corresponding to Gosner stage 44/45, is atypical with respect to its post-sacral skeleton. Caudal to PS9, many vertebral anlagen occur intrasegmentally (versus at myoseptae), disrupting segmental character within the tail. Otherwise, the axial skeleton is little different from that at stage 44: All vertebral centra show signs of osteoclastic degradation, with PS1-3 the least affected and bridged dorsally and ventrally by symphyses. A longitudinal sliver of ossified tissue can be seen on the ventral surface of PS4, suggesting that the completed hypochord will extend caudally to this level.

6.4.3.2 M. lateralis

A total of 18 vertebrae have formed by Gosner stage 28 (ROM 42357). Vertebrae I-IX bear neural arches that are bridged by faintly-stained cartilage to the underlying vertebral body and articulate at their zygapophyses. Post-sacral vertebra 1 presents paired cartilaginous pedicles and, along with PS2, bows out at the ventral face of its centrum. Centra are perichordal up to the level of PS2, caudal to which they are progressively reduced to discrete dorsal and ventral anlagen pairs. The five most caudal centra are cartilaginous.

Five stages later, at Gosner 33 (ROM 42358), only the three most distal post-sacral centra (of a total of 12) are cartilaginous. Also at this stage, the dorsal and ventral anlagen pairs of PS3-6 are fused as bilobed, ossified plates, whereas, more caudally, adjacent anlagen remain discrete (Fig. 6.3B). The neural arches of PS1 comprise ossified pedicles with

cartilaginous zygapophyses. A second pair of post-sacral neural arches, on PS2, has formed by stage 35 (ROM 42359; Fig. 6.3A). Interestingly, this neural arch pair is barely visible in the next two specimens of my series, corresponding to stages 37 and 41 (ROM 42362 and 42364, respectively). At stage 45 (ROM 42366), however, the arches are again visible and are continuous with those of PS1. There is similar inconsistency in the post-sacral vertebral complement across these stages, with tallies ranging between 11 and 15 (see Table 6.2 for data per stage). Generally, the 4-6 most proximal of these are perichordal, followed by centra comprising either bilobed dorsal and ventral plates or, most caudally, discrete anlagen pairs. The longitudinal staggering of dorsal and ventral anlagen is apparent from lateral inspection of all whole-mount specimens and in progressive transverse cross-sections through the tail at stage 36 (ROM 42361; Fig. 6.3C). In one specimen (stage 41; ROM 42364), the strict segmental pattern of the tail is broken with two ventral anlagen falling in between myoseptae (instead of at them).

Ossification of the proximal hindlimb skeleton, including the ilia, femur, tibia and fibula, is first evident at stage 35 (ROM 42359). Meanwhile, all but the two most caudal centra have ossified in the axial skeleton. By stage 41, all centra of the post-sacral skeleton and long bones of the appendicular skeleton have ossified.

The presacral skeleton is nearly complete at stage 43 (ROM 42365). Sacral diapophyses, first visible at stage 37, now project laterally and appear slightly dilated longitudinally. Laminae have started to form on vertebrae I-IX, and fingerlike transverse processes are found on II-IV (the longest on III and the shortest of IV). At stage 45 (ROM 42366; Fig.

6.3F), laminae completely enclose the neural tube on all but the atlas and II; the sacral diapophyses are triangular in shape, with their bases nearly touching the ilia; and the elongate transverse processes of II-IV are now joined by stumpy processes on V-VIII. Already at this stage, presacral centra show signs of osteoclastic degradation: I-IV persist only at the dorsal face of the notochord, while V and VI show only traces of lateral and ventral tissue. Closer to the sacrum, however, centra remain largely intact, encircling a visibly deflated notochord. A similar phenomenon is demonstrated by the post-sacral skeleton at this stage: distal centra are most porous, while those closest to the sacrum are largely untouched.

At the level of the sacrum, components of the adult caudal skeleton are taking shape. The hypochordal ridge, first seen on PS1 and 2 at stage 28, is now continuous at intervertebral levels with the hypochord proper, which extends caudally to PS4. Dorsally, the post-zygapophyses of PS1 are bridged with the adjacent neural arches of PSII and, in turn, the dorsal surface of the vertebral body of PS3. By stage 46 (ROM 42368), the last of my series, these thin bridges have filled out and constitute the coccyx. Laterally, PS1-3 are in the late stages of degradation, while ventrally, they are continuous with a thickened, ossified hypochord, together forming the urostyle. The notochord has completely disappeared along the entire length of the axial skeleton. Presacral centra, now compact cylinders following the collapse of the notochord, are separated by cartilaginous intervertebral discs. In dorsal perspective, presacral neural arches are imbricate and all bear noticeable transverse processes. The sacral diapophyses are now broad and articulate with the pelvic ilia.

6.4.3.3 M. longipes

At stage 33, the total vertebral count is 21, including 12 post-sacral centra. Vertebrae I-IX and PS1 have well-ossified neural arches bearing cartilage-tipped zygapophyses. A pair of cartilaginous rudiments project from the dorsal surface of PS2. Ventrally, PS1 and 2 bow downwards noticeably. Post-sacral centra circumscribe the notochord up to PS7, beyond which discrete anlagen (dorsal and ventral pairs) can be seen. The most caudal centrum (PS12) comprises only a single ossified anlage (at dorsal left); the other three anlagen are faintly stained with alcian blue. Similar faintly-stained, cartilaginous precursors are found caudal to PS12, indicating that vertebrae are still being added at this stage (and that my vertebral tally is conservative). The longitudinal staggering of dorsal and ventral anlagen pairs seen in other *Megophrys* species is not as pronounced. Accordingly, post-sacral centra form continuous rings around the notochord in transverse histological sections (stage 31; ZRC 1.4079; Fig. 6.3D). PS1 and 2 also show reduced neural arches and a bulbous outgrowth at their ventral surface in cross-section. This is consistent with the 'bowed out' appearance of these vertebrae seen in whole-mount, indicative of early hypochord formation. The ilia, femur, tibia and fibula show signs of early chondrogenesis.

6.4.3.4 M. montana

Nine vertebrae (I-IX) have formed by stage 25 (CAS 138414). All have well-ossified pedicles, but, ventrally, centra only partially envelop the notochord. The atloid centrum is particularly rudimentary, whereas that of vertebra IV is nearly complete. Beyond IV, centra are progressively reduced, with IX merely a bilobed plate on the dorsal face of the notochord (Fig. 6.3A). By stage 36 (CAS 138409), a total of 20 vertebrae, including 11 post-sacral centra, are present. Two stages later, at 38 (CAS 138409), 2 additional post-sacral centra are present. At both stages, all presacral centra circumscribe the notochord, and neural arches bear zygapophyses, but have not yet formed laminae. Post-sacrally, two reduced neural arch elements can be seen; zygapophyses are seen on PS1, whereas PS2 presents only rounded projections atop its centrum. Immediately post-sacral centra (PS1-4 at 36; PS1-5 at 38) completely envelop the notochord and, in the case of PS1 and 2, bow out ventrally, suggesting early formation of the hypochordal ridge. More distally, caudal centra comprise separate dorsal and ventral plates that are closely apposed, but not fused laterally. These anlagen are longitudinally staggered, with dorsal anlagen falling farther rostral than their ventral counterparts. The most caudal vertebra at each stage (PS11 at 36; 13 at 38) consists of discrete dorsal and ventral pairs of anlagen.

Towards the end of metamorphosis (stage 45; CAS 138410; Fig. 6.3G), signs of vertebral resorption are evident. Vertebral centra are generally porous in appearance, indicative of osteoclastic degradation. Histological examination of centra in a late-stage metamorph (stage 44; 138409) reveals multinucleate, osteoclast-like cells occupying cavities in the

bony matrix (Fig. 6.3I). These cells are also readily observed in sagittal sections through the sacral region of the same metamorph, selectively embedded in the vertebral bone while not present in the hypochord (Fig. 6.3J).

Those centra farthest caudal from the sacrum appear the most degraded. Towards the tail tip, centra are completely fragmented and nearly impossible to distinguish from each other (Fig. 6.3G). More proximally, post-sacral vertebrae are largely intact. PS4 and 5 have not yet fragmented and PS1-3 are porous only at their lateral surfaces. PS1-3 have thickened ventral surfaces that appear fused with the ossified hypochord, which spans all three vertebrae. Dorsally, the neural arches of IX, PS1, and 2 are bridged with PS3, forming paired, longitudinal ridges that constitute the coccyx (Fig. 6.3G).

At presacral levels, the rostralmost centra are no longer hollow, having receded dorsally with the collapse of the notochord. Closer to the sacrum, where the notochord is more rigid, centra are missing only their ventral portions (Fig. 6.3G). Dorsally, vertebrae articulate at their zygapophyses, laminae have fused medially on all but the atlas and II, and transverse processes extend laterally from II-VIII. The sacral diapophyses are dilated and in contact with the pelvic ilia, which are strongly ossified along with the rest of the appendicular skeleton.

6.4.3.5 M. nasuta

Our stage-36 specimen (ZRC 1.1543) is poorly stained for alizarin red. The total vertebral count is 23, including 14 post-sacral vertebrae. Post-sacral vertebrae 1-6 encircle the notochord, and 7-14 comprise staggered dorsal and ventral plates that do not meet laterally. All long bones of appendicular skeleton show signs of ossification. Caudal to the sacrum, PS1 and 2 bow out ventrally, suggestive of early formation of the hypochordal ridge. In cross-section, the ridge is visible as a bulbous swelling on the ventral surface of the notochord (stage 27; Fig. 6.3E). In the same section, neural arches partially envelope the neural tube and the notochord is covered by thin connective tissue.

6.4.3.6 M. stejnegeri

Seventeen vertebrae, including eight post-sacral centra are present by stage 26 (FMNH 50950-820). Vertebrae I-VIII, the sacrum, and PS1 all bear rudimentary neural arch pairs, which are not in contact with the underlying centra and lack zygapophyses. Notably, vertebra VIII and the sacrum are joined ventro-medially by a narrow cartilaginous bridge. This is an unlikely location for the hypochordal ridge, however, as it usually extends from the sacral vertebra caudally (to PS2 or PS3). The centra of PS1 circumscribes the notochord, while PS2 and 3 comprise separate ventral and/or dorsal plates. More caudally, where longitudinal staggering of dorsal and ventral structures is particularly pronounced, discrete anlagen make up the centra. PS4-7 comprise 3-4 anlagen and PS8, the caudalmost, is only a single asymmetrical dorso-lateral anlage.

No additional post-sacral centra are found in later stages (FMNH 50950-804). PS1 and 2 are now continuous around the notochord, while PS3 and 4 remain unfused laterally. The most caudal centra, PS5-8, comprise ventral anlagen pairs, with only PS6 having a corresponding dorsal pair.

In cross-section (FMNH 50950-808), post-sacral centra appear as thin osseous tissue around the notochord, alternately expanded at either ventral or dorsal surfaces (consistent with the longitudinal staggering of anlagen seen in whole-mount). Presacrally, the neural arches now bear zygapophyses, but do not yet articulate. There are no signs of ossification in the appendicular skeleton at this stage.

6.4.4 *Ophryophryne microstoma*

Generally, specimens of this series are strongly stained with alcian blue, but weakly stained with alizarin red, giving ossified tissue a plum color. This may be an artifact of fixation or extended storage.

At stage 29 (ROM 42334), the trunk skeleton is well-developed, with vertebrae I-IX bearing neural arches bridged to the underlying centrum by faintly-stained cartilage; III and IV present rudimentary zygapophyses. The post-sacral skeleton comprises 14 vertebrae. PS1-12 completely encircle the notochord (Fig. 6.4C,D), whereas 13 and 14 are dorsal plates. From lateral perspective, PS1 and 2 bow out at their ventral surface,

indicating formation of the hypochordal ridge. The ridge appears as a bulbous swelling on the ventral face of the notochord in cross-section (Fig. 6.4B). The post-sacral vertebral complement appears to be terminally established at this early stage as no more than 14 vertebrae are found in older specimens in the series.

Ossification of the post-sacral skeleton is evident by stage 30 (ROM 42334; Fig. 6.4A). At this and subsequent stages, all but the 2-3 most caudal vertebrae are noticeably stained with alizarin red and do not encompass the notochord. At stage 34 (ROM 42335), a tenth neural arch pair can be seen on PS1. Dorsal bumps are visible on PS2, indicative of the early stages of coccyx formation. Among the presacral neural arches, II-IX all bear prezygapophyses and II and III show transverse processes. Two stages later, at 36 (ROM 42339), a third transverse process, on IV, is visible.

Our stage-37 specimen (ROM 42340) is anomalous with respect to its axial skeleton. One of the presacral vertebrae is missing, for a total of seven, and vertebra VIII is longitudinally protracted so that it is in contact with two myoseptae on the right side. Assuming that vertebra VIII represents the sacrum, there are a total of 14 post-sacral centra at this stage.

Towards the end of metamorphosis, at stage 42 (ROM 42344), the presacral skeleton has seen further development. Transverse processes can be clearly seen on vertebrae II-IV, while III-VIII have fused laminae dorsally. Cartilaginous diapophyses project laterally from the sacrum. At its ventral surface, the sacrum is closely associated with the

cartilaginous hypochord, which extends caudally to PS2 (Fig. 6.4E). The neural arches of PS1 and PS2 are joined by thin cartilaginous symphyses to bumps on the dorsal surface of PS3. Caudal to PS3, centra appear porous.

At the last stage represented, 43 (ROM 42345; Fig. 6.4F,G), laminae are fused dorsally on vertebrae III-IX; II-IX articulate at their zygapophyses; transverse processes adorn II-VIII, and the sacral diapophyses have ossified. Presacral centra have regressed dorsally with the collapse of the notochord. Post-sacrally, PS1-3 are bridged dorsally, continuous with the ossified hypochord ventrally, and noticeably degraded at their lateral faces. More distal centra are in the late stages of osteoclastic resorption, appearing fragmented and porous (Fig. 6.4F).

6.4.5 *Xenophrys* sp.

At stage 25 (MNHN 1998.9166-9167), neural arches adorn vertebrae 1-X and are progressively less ossified towards the sacrum (Fig. 6.5E). Ventrally, the vertebral centra have not yet formed. Along with the stage-25 *Megophrys montana* tadpole examined (Fig. 6.3A), this confirms for megophryids that neural arch ossification precedes vertebral body formation, the generally recognized ossification sequence for the anuran axial skeleton (Maglia, 2003).

Two stages later, at Gosner 27 (Fig. 6.5A), all but the most caudal neural arch pair (on PS1) is ossified. Immediately caudal to this vertebra, on the dorsal surface of

PS2 is a small cartilaginous bump. The centra of vertebrae I-VIII, the sacrum, and PS1 are well-ossified and completely encircle the notochord. Post-sacrally, there are a total of 7 rudimentary centra, which are represented as discrete anlagen towards the tail tip. Anlagen are cartilaginous at their periphery and well-ossified at their centre (Fig. 6.5D). Dorsal and ventral ossified plates are not fused laterally on PS2 and PS3. Longitudinal rods of cartilage appose the ventral face of both vertebrae and extended inter-vertebrally, suggestive of early hypochord formation (Fig. 6.5B,C).

6.4.6 *Leptobrachium*

Three larval specimens, each representing a separate species of *Leptobrachium*, were examined by whole-mount bone-staining. Overall, the tadpoles closely resemble each other as well as *Vibrissaphora boringii*. All bear transverse processes on vertebrae II-IV and share a reduced post-sacral skeleton. Supernumerary post-sacral vertebrae were not observed in any tadpole of *Leptobrachium*.

6.4.6.1 L. hendricksoni

Staging placed this tadpole (ZRC 15945) at Gosner 31. Caudal to the sacrum are two rudimentary neural arch pairs. PS1 is reduced in height but well-ossified, while PS2 consists of bilateral, longitudinally-paired, non-ossified anlagen. Ventrally, the cartilaginous hypochord tapers caudally to the level of PSII. At its rostral surface the hypochord appears to be continuous with a cartilaginous, sub-notochordal rod

spanning the trunk. Vertebra IX is discontinuous ventro-medially with lateral halves of the centrum in close apposition, but not fused. Central development thus appears to proceed from the dorsal to ventral surfaces of the notochord. Laterally, IX bears cartilaginous rudiments of the diapophyses. The appendicular skeleton could not be visualized by either alcian blue or alizarin red at this stage.

6.4.6.2 L. montanum

The presacral skeleton of this specimen (stage 37; FMNH 241683) is well-developed, with all vertebrae articulating at their zygapophyses and elongate, cartilage-tipped transverse processes adorning II-IV. Neural arch laminae have not yet formed at this stage. Post-sacrally, PSI, a rudimentary neural arch pair, lies atop the notochord and is strongly ossified. Ventral to the notochord and extending caudally from PSI into the next segment, the hypochord is ossified. The centrum of vertebrae IX, the sacrum, is not continuous laterally, suggesting that ossification begins at the dorsal and ventral surfaces of the notochord and proceeds laterally (compared to dorsal-to-ventral progression in *L. hendricksoni*). PSII, visible as longitudinally-paired anlagen in *L. hendricksoni* (and *V. boringii*), is not present in *L. montanum*. This, however, might be an artifact of poor cartilage staining due to specimen age or poor fixation. In the appendicular skeleton, all long bones show signs of ossification at this stage.

6.4.6.3 L. nigrops

Vertebrae I-IX of this tadpole (stage 36; ZRC 13403a) comprise perichordal centra with associated neural arches. Centra can be clearly seen from dorsal aspect as the laminae have not formed. Post-sacrally, there is a single pair of axially-elongated neural arches. Unlike both *L. montanum* and *L. hendricksoni*, there is no PS2 in this species. The hypochord, elliptical and in the early stages of ossification, extends caudally from the ventral margin of PSI. The stylopodial and zygopodial elements of the appendicular skeleton are ossified at their centres.

6.4.7 *Oreolalax popei*

On superficial inspection, this specimen (stage 39; FMNH 268756) is virtually indistinguishable from *Scutiger*. It presents a total of 10 vertebrae, including 9 complete, tightly apposed presacrals and one post-sacral neural arch pair. There are no post-sacral centra, only one reduced neural arch pair followed caudally by intermyoseptic, bilateral ossified discs. The ossified hypochord extends from PS1 to the next caudal myoseptum. Rostrally, the hypochord is continuous with a cartilaginous, sub-notochordal rod that appears to extend all the way up the trunk, though interspersed by presacral centra (as seen in *Leptobrachium hendricksoni*). The appendicular skeleton is complete, showing ossification in all elements. Vertebrae II-IV bear elongate transverse processes. The sacral vertebra bears rudimentary diapophyses and its vertebral body does not completely circumscribe the notochord.

6.4.8 *Scutiger*

6.4.8.1 S. glandulatus

At first glance, this specimen (stage 36; FMNH 50985) is virtually indistinguishable from *Oreolalax*. Cartilage-staining is very poor in the post-cranial skeleton of this specimen. There are a total of nine well-formed neural arch pairs, all articulating at their zygapophyses and joined by faint cartilaginous bridges to the underlying centra. Centra of vertebrae I-IV are perfectly cylindrical, whereas V-VIII narrow ventro-medially. The sacral centrum is not continuous ventro-medially as the lateral halves do not meet. This suggests that central development proceeds dorsal-to-ventral in this species. Neural arches of the first post-sacral vertebra are reduced, but with discernible prezygapophyses, and are followed caudally by the cartilaginous rudiments of PS2. Dorsally, the ossified hypochord extends from the level of PS1 to 2.

6.4.8.2 Scutiger sp.

This specimen (stage 35; CAS 90674) is deeply stained with alizarin red. There are no vertebral centra caudal to the sacrum. Presacral centra I-VIII are perichordal. The sacral centrum is not continuous ventro-medially, indicating a dorso-ventral ossification in this species. A second post-sacral pair of neural arches, seen as lightly-stained rudiments in *S. glandulatus*, are not seen in this specimen. Rostrally, the neural arch pair of PS1 lacks

discernible zygapophyses. The cartilaginous hypochord extends caudally from the level of PS1.

6.4.9 *Vibrissaphora boringii*

Superficial examination prior to processing placed this tadpole (GRH Vb1) at stage 25, but the advanced state of its axial skeleton is not consistent with this stage, perhaps suggesting decoupling of axial and appendicular development—as in fellow leptobrachine genera *Leptobrachella* and *Leptolalax.* Overall, its axial skeleton is highly similar to that of *Leptobrachium.* Vertebrae I-IX are well-ossified and complete, with perichordal centra joined dorsally by cartilaginous bridges to neural arches bearing broad zygapophyses; transverse processes extend from the neural arches of II-IV. The centrum of IX, the sacrum, narrows ventrally and lateral halves are joined ventro-medially only by a narrow symphysis. The post-sacral skeleton comprises two rudimentary pairs of neural arches; PS1 is ossified and projects dorsally, whereas PS2 stains only cartilage and consists, on each side, of flat, longitudinally-paired analgen. Immediately ventral to the notochord, an elongate, cartilaginous hypochord spans PS1 and 2 longitudinally.

6.4.10 *Non-megophryid genera*

Larval specimens from the stream-associated neobatrachid species *Heleophryne rosei* and *Osteopilus brunneus* and the centrolenid species *Hyalinobatrachium pulveratum,*

Cochranella granulosa and *Centrolenella prosoblepon* were examined. No supernumerary caudal vertebrae were found in either species.

6.5 Discussion

6.5.1 Megophryid caudal vertebral diversity

Our survey of post-cranial skeletal development in Megophryidae has unveiled surprising diversity in the skeletal ontogeny and larval osteology within the family. Not only does the number of supernumerary vertebrae vary widely in megophryid larvae (anywhere from 0 up to 30), the early ontogeny of these vertebrae is also quite variable. I have identified at least three distinct modes at work in megophryids. In *Leptobrachella* (Fig. 6.1) and *Ophryophryne* (Fig. 6.4), post-sacral centra begin as osseous spools that completely circumscribe the notochord and eventually ossify to form perichordal centra. I refer to this as the 'spool mode.'

Caudal vertebral development occurs by an 'anlagen mode' in both *Megophrys* (Fig. 6.3) and *Xenophrys* (Fig. 6.5). In this mode, centra are assembled as four discrete ossification centres—two dorsal, two ventral—expand to meet each other. Generally, this process goes to completion in the proximal tail, forming perichordal centra. More distally, however, anlagen often fail to come together, leaving centra discontinuous around the notochord (Fig. 6.3B).

In *Leptolalax*, post-sacral centra development seems to draw from both the 'spool' and 'anlagen' modes, constituting a third mode, with proximal centra resembling perfect perichordal spools and distal centra as paired dorsal anlagen, normally coinciding with successive myoseptae. In at least one specimen of *L. pelodytoides*, however, I noted several intrasegmental anlagen that fell in between adjacent myoseptae (Fig. 6.2A). A similar anomaly was presented by specimens of *M. boettgeri* (stage 44/45; A-30639) and *M. lateralis* (stage 41; ROM 42364), suggesting that the 'anlagen mode' may not be as tightly regulated with respect to segmental pattern as the 'spool mode', for which no analogous defects were noted.

Evolutionary affinities inferred from these modes of caudal vertebral development challenge the current hypothesized phylogeny of Megophryidae (Zheng *et al.*, 2004; Frost *et al.*, 2006; Grosjean, 2006), which generally group *Ophryophryne* with *Megophrys* and *Xenophrys*, and *Leptobrachella* with *Leptolalax*. This discrepancy, along with the sheer variety of osteogenic modes and the variation observed in the number of post-sacral centra in megophryids, points to multiple evolutionary origins for supernumerary caudal vertebrae in the family (Fig. 6.6).

At the same time, the predominance of these additional vertebrae within Megophryidae—in all but 4 of 9 genera surveyed—suggests that the general capability to produce extra caudal vertebrae is a megophryid apomorphy that was secondarily lost in *Leptobrachium*, *Vibrissaphora*, *Oreolalax*, and *Scutiger* (Fig. 6.6). It is worth emphasizing that these four genera consistently group together as a clade in phylogenetic analysis (Zheng *et al.*,

2004; Grosjean, 2005) and are quite similar in terms of their ecology and gross body type (Lathrop, 2003). It is also worth noting that *Atympanophrys* and *Brachytarsophrys*, the two megophryid genera missing from this study, share strong phylogenetic affinities with *Megophrys* and *Xenophrys* (Jiang *et al.*, 2003; Zheng *et al.*, 2004), leading me to hypothesize that they too will eventually be found to have supernumerary caudal vertebrae (bringing my total to 7 of 11 genera with the trait). More extensive sampling of the family for morphological, molecular and phylogenetic analyses will help resolve the evolutionary origins of caudal centra in megophryids.

6.5.2 Precocious vertebral development in megophryids

Despite the overwhelming variety in caudal skeletal ontogeny and osteology presented by megophryids, the overall *sequence* of skeletogenesis appears to be tightly conserved among all studied genera: Vertebral column development invariably precedes formation of the appendicular skeleton (Table 6.2). Skeletogenesis is also faithful to this pattern in other studied anurans (Maglia, 2003), but there is decidedly less decoupling of the two events compared to megophryids. The onset of appendicular skeletal development does indeed follow axial development in non-megophryid anurans, but usually in quick succession and with the two processes progressing concurrently (Maglia, 2003). In megophryids, however, the processes show little contiguity in time—the vertebral column is virtually complete by the earliest stages of limb development (Table 6.2).

As limb development is the benchmark of the Gosner staging table (used throughout), direct stage comparisons between megophryids and other anurans cannot be used to determine if vertebral development is accelerated or decelerated relative to appendicular skeletogenesis in one family versus another. A more useful assay is ossification sequence, the order in which individual bones begin to ossify. Typically, the bones of the cranial skeleton are the first to ossify in anurans, followed shortly by the neural arches and femurs and later by the vertebral centra and more distal bones of the appendicular skeleton (*e.g.*, *Ceratophrys cornuta* – Wild, 1997; *Discoglossus sardus* – Púgener & Maglia, 1997; *Pipa pipa* - Trueb, Púgener & Maglia, 2000; *Scaphiopus intermontanus* – Hall & Larsen, 1998; *Spea multiplicata* – Banbury & Maglia, 2006). Not all anuran species, however, follow this sequence of events. In the fire-bellied toad *Bombina orientalis*, for example, the femurs ossify before the neural arches (Maglia & Púgener, 1998), whereas in *Chacophrys pierotti* the cranium, vertebral column and limbs ossify in tandem (Wild, 1999).

The ossification sequence of pelobatid spadefoot toads is of particular relevance here, owing to its congruence with the megophryid model and the close phylogenetic affinities between the two families (García-París, Buchholz & Parra-Olea, 2003; Frost *et al.*, 2006). In megophryids, the vertebral column is essentially complete, showing strongly-ossified centra, neural arches, and associated processes, before any sign of ossification in the femur or other appendicular bones (see Table 6.2 for breakdown by genus). Similarly, Maglia (2003) described precocious ossification of vertebral centra in *Pelobates cultripes*, occurring concurrently with neural arch ossification, but preceding femur

ossification. While all neural arches ossify before the femurs in *P. cultripes*, the centra are slow to follow suit. Maglia (2003) noted ossification of the atloid centrum (I) as early as Gosner stage 31, but the sacral centrum (IX) begins to ossify only by stage 39. At this point, most long bones of the appendicular skeleton, including the femur, are already strongly ossified.

Along with precocious vertebral ossification, *Pelobates* may share with megophryid larvae supernumerary caudal centra. Banbury (2005) reported a single post-sacral centra associated with PSI in half of her stage-43 *P. syriacus* metamorphs. The centra flanks the notochord laterally and is lost by the next Gosner stage, presumably integrated into the coccyx. While it remains to be seen how prevalent the character is throughout the genus and family, its presence in *P. syriacus* nonetheless corroborates the close phylogenetic affinities of megophryids and pelobatids (Frost *et al.*, 2006). Further, it may even suggest that the two families share a common ontogenetic bias towards supernumerary vertebral development. But what then accounts for the large discrepancy in the *number* of supernumerary post-sacral centra between each family and, more topically, the uneven peppering of the character within Megophryidae? In other words, why does *P. syriacus* only form one extra centra, while *Leptobrachella* forms up to 30, and *Leptobrachium* none?

6.5.3 Life history and supernumerary caudal vertebrae in pelobatoids

6.5.3.1 Larval period and body size

Stream-associated or rheophilous tadpoles are generally slow growers due to the reduced primary productivity characteristic of cool stream waters. Megophryids in particular remain as tadpoles for extended periods of time—as long as three years for *Vibrissaphora* (Jinzhong Fu, pers. comm.). A protracted larval period has also been noted for *Leptobrachium*, *Leptolalax*, *Ophryophryne*, *Oreolalax*, and *Scutiger* (Smith, 1917; Liu & Hu, 1960; Chen, Li & Xiao, 1984; Zhao *et al.*, 1994; Grosjean, 2003). It may be intuitive to correlate the extended axial skeleton of megophryids with their long tadpole life, but this reasoning breaks down once we consider *Ascaphus truei*. Tadpoles of this basal species share with megophryids a stream habitat and protracted larval period, but do not bear supernumerary vertebrae in their tails (R. J. Wassersug, pers. obs.).

Perhaps more relevant is a discussion of embryonic period, *i.e.*, the time taken to reach hatching at approximately Gosner stage 24. It is during these early stages that the blueprint for the axial skeleton is established and ossification first occurs. While the duration of embryogenesis is not known for megophryids, it is conceivable that prolonging it (relative to other tadpoles) may afford them the time needed to extend their axial skeleton into the tail. Indeed, as I have emphasized above, the axial skeleton of most megophryids is quite well-developed even at the earliest free-living stages (Table 2).

Among Megophryidae, it is worth highlighting the size discrepancy between those tadpoles with supernumerary caudal vertebrae and those without. Generally, those genera lacking caudal vertebrae (*e.g.*, *Leptobrachium*, *Oreolalax*, *Scutiger*, and *Vibrissaphora*) are larger in size than those bearing centra in their tails. It is possible that small body size among megophryids may predispose tadpoles to forming tail vertebrae (and vice versa). Such a correlation is not substantiated by the current study, but could readily be tested by comparing post-sacral skeletal development in leptobrachine tadpoles—particularly an intermediate form like *Leptolalax*—raised under conditions known to affect larval body size (*e.g.*, including temperature and housing density).

The possibility remains, of course, that the presence of supernumerary caudal vertebrae correlates with neither body size nor developmental period. Instead, all three may be independent products of the unique riparian lifestyle of megophryid tadpoles.

6.5.3.2 A riparian lifestyle

The presence or absence of supernumerary caudal vertebrae among pelobatoid larvae can be readily correlated with their way of life. Pelobatid tadpoles, like most anuran larvae, generally live in ponds and, accordingly, have a generalized morphology, including a reduced caudal skeleton. Megophryid larvae, however, live in streams, where they face the perpetual challenge of avoiding being swept downstream. The various genera have dealt with this by exploiting a broad array of stream microhabitats.

The leptobrachine tadpoles *Leptobrachium*, *Vibrissaphora*, *Scutiger*, and *Oreolalax*, avoid torrents altogether, living in the relatively deep, static waters of splash pools adjacent to streams. These habitats are largely similar to the ponds occupied by *Pelobates* and other anuran larvae and this is manifested in the decidedly generalized morphology of these leptobrachine tadpoles (Nodzenski *et al.*, 1989; Lathrop, 2003). They are wide, deep-bodied, and short-tailed, and, not surprisingly, do not bear supernumerary caudal vertebrae.

The more attenuated tadpoles of *Leptobrachella* and *Leptolalax* are typically found among riffles. They avoid fast-flowing water by burrowing among rocks of the stream bed (Haas *et al.*, 2006; Nodzenski *et al.*, 1989). Their slender bodies and shallow tails allow them to move easily among tight crevices. Supernumerary caudal vertebrae, as Haas *et al.* (2006) point out, increase maneuverability and provide a strong skeleton to anchor muscles that must be recruited to generate thrust for burrowing through resistant substrate.

Megophryine tadpoles, such as *Megophrys*, *Xenophrys*, and *Ophryophryne*, are intermediate when it comes to habitat. They prefer the relatively calm, shallow water at the edge of streams, but are also often found buried among the leafy substrate, where a reinforced tail skeleton may prove useful (Nodzenski *et al.*, 1989). While tempting, it is problematic to correlate the megophryine's habitat with their intermediate number of caudal vertebrae (on a spectrum with *Leptobrachella* and *Leptobrachium* as two poles)—

especially considering that *Leptolalax*, a burrower like *Leptobrachella*, has only half their complement.

6.5.4 Why are extra caudal vertebrae absent in the 'ecomorphs'?

Certain ranids, centrolenids and arboreal hylids with fossorial tadpoles face similar selective pressures as the megophryids. Like *Leptobrachella* in particular, they must be able to generate great thrust to make headway against resistant substrates. However, these species bear no supernumerary vertebrae in their tails. This curious omission may be ascribed to several factors. Firstly, the selective pressures faced by megophryid tadpoles in streams may be different—perhaps more extreme—than those faced by their ecomorphs. Alternatively, megophryids may face similar selective pressure as their ecomorphs, but, as ancestral anurans, may be less susceptible to the constraining effects of phyletic history. In other words, while the plesiomorphic capacity to generate caudal vertebrae is available to megophryids, it may be entirely lost or more tightly constrained in derived frogs, such as centrolenids and other neobatrachids, prevented from emerging even in the face of strong selective pressure.

6.5.5 Reclaiming caudal vertebrae

Other than in megophryids (and *Pelobates syriacus*), the tadpole tails of anurans are practically devoid of osseous peri-notochordal tissue. In Chapter 4, I suggested that chondrogenesis in the tail is precluded at the very earliest stage, to wit, cartilage

condensation formation. Using immunohistochemistry and gene expression analyses, I found no biochemical markers for cartilaginous condensations (*e.g.*, tenascin) or cartilage (*e.g.*, collagen type II and *Sox9*) at appreciable levels in caudal paraxial tissues in *Xenopus laevis*. I did confirm, however, that sclerotomes, the bone-forming compartment of the somite, are properly segregated in the tail of *X. laevis*. Thus, it appears that caudal sclerotomal cells do not form condensations, perhaps due to a failure of cell proliferation (see Chapters 3 and 4).

A molecular model for the appearance of supernumerary caudal vertebrae in megophryids might then involve a heterochronic up-regulation of the expression of *Pax1* and a concomitant increase in cell proliferation within caudal sclerotomes. Such a simple model, however, could not possibly account for the diversity of caudal vertebral development patterns in megophryids. Furthermore, it sheds no light on caudal vertebral preclusion as a *global* patterning phenomenon. That is to say, it can only account for the disappearance or reappearance of vertebrae on a one-by-one basis. In non-megophryid anurans, however, it is a case of loss of an entire *region* of vertebrae, an entire tail's worth. This begs the question of what upstream factors regulate the differential expression of *Pax1* along the length of future axial skeleton (*i.e.*, turn it on/off in the tail).

The most likely candidates for regulating a *global* loss (and perhaps reappearance) of caudal vertebrae in anurans are *Hox* genes, the molecular architects of the axial skeleton in all vertebrates. In gene loss-of-function studies, Economides and colleagues (2003) identified *Hoxb13*, the most 5' gene in the *HoxB* cluster, as a termination signal for tail

outgrowth in the mouse. They showed that the gene represses growth and induces cell apoptosis in the tail bud. Accordingly, the homozygous mouse mutant demonstrated overgrowth of caudal tissues, including vertebrae, the spinal cord, and ganglia. Conversely, in the tail of neobatrachid anuran larvae, these same structures are typically reduced (*e.g.*, the spinal cord of *Rana*; Nishikawa & Wassersug, 1988; 1989) or absent (vertebrae). Morpholino knockdown and transgenic overexpression studies with the African clawed frog *Xenopus laevis* could test the role of *Hoxb13* in the outgrowth of the tadpole tail and, in particular, the premature termination of vertebral formation in all anurans but the megophryids.

6.5.6 Caudal vertebral fate at metamorphosis

An overriding question at the outset of this study concerned the ultimate fate of the supernumerary caudal vertebrae of megophryids at metamorphosis. Given that the megophryid adult axial skeleton is ostensibly indistinguishable from other anurans (Fig. 6.1A), I assumed that the additional vertebrae were either resorbed or somehow incorporated into adult post-sacral skeleton, consisting of the coccyx and hypochord. Careful examination of late-stage metamorphs confirmed both scenarios in different genera. In *Megophrys* (Fig. 6.3G), *Ophryophryne* (Fig. 6.4F,G), and perhaps *Leptobrachella* (Fig. 6.1C) supernumerary caudal vertebrae appear to undergo osteoclastic degradation. Histological examination of caudal vertebrae of *Megophrys montana* in this state showed multinucleate osteoclast-like cells embedded in the bony matrix of centra (Fig. 6.3G, I, J). Interestingly, this is the case for both pre- *and* post-

sacral centra, underlining a hitherto unappreciated role for osteoclasts in metamorphic remodeling of the anuran axial skeleton (Fig. 6.3G). In *Leptolalax*, the additional centra remain intact and do not appear to be degraded. Instead, they appear to compacted and synostotically fused into the urostyle (Fig. 6.2E).

It is not known how the presence of caudal vertebrae affects the resorption of the tadpole tail. The process is likely to be substantially longer than for normal pond tadpoles of comparable size, which, as I point out in Chapter 2, may have serious adaptive consequences for the metamorphosing megophryid. I argue that the persistent tail would diminish jumping performance, primarily by adding dead weight, thus making metamorphs easy targets for predation. The possibility remains, however, that tail vertebrae do not impede tail resorption at all. Documenting the absolute rate of metamorphosis of megophyid tadpoles could readily resolve this question.

As an interesting side note, I should point out that megophryids are not unrivalled in their ability to remodel their axial skeleton at metamorphosis. Metamorphosing 'tenuis' larvae of the pearlfish *Carapus homei* can resorb up to *70* vertebrae on their way to becoming juveniles. Whereas it is not known how long or by what mechanism this massive remodelling process occurs, Parmentier *et al.* (2004) have correlated it with the pearlfish's unique lifestyle. They suggest that the additional vertebrae enable the parasitic larvae to make its first entrance into the body cavity of its benthic host, the sea cucumber, via the anus. As with *Leptobrachella* and other burrowing megophryids, the

additional vertebrae of *C. homei* likely allow for great thrust during burrowing, necessary to progress through a substrate more resistant than water.

6.5.7 Dual origins for the hypochord in megophryids

In most anurans, the hypochord ossifies as a sub-notochordal rod separate from the overlying perichordal tissue (see Fig. 2.3). In megophryids, however, the hypochord is only visible as a discrete structure at intervertebral levels (Fig. 6.2G,H; 6.3E,G). At vertebral levels, it is continuous with the ventral face of the vertebral body, forming a hypochordal ridge (Fig. 6.3H, 6.4E, 6.5C). Accordingly, one cannot distinguish between the two structures in cross-section (Fig. 6.3E, 6.4B). The osseous tissue of the post-sacral centra appears to have been co-opted into forming the future urostyle. At metamorphosis, this tissue is spared while all other portions of the vertebral body are resorbed (with the exception of dorsal tissues forming the coccyx). Thus, in the megophryids at least, the hypochord has a dual origin. This clarifies Griffiths' (1963) inaccurate description of the urostyle of *Megophrys major* as 'a posterior, ventral outgrowth of the first post-sacral intervertebral body.'

6.5.8 Implications for the anuran *Bauplan*

The anuran body plan or *Bauplan* is largely conserved among extant species (see Chapter 2). The presence of supernumerary vertebrae in the tails of megophryid tadpoles demonstrates, however, that this *Bauplan* is not entirely rigid and is flexible in the face of

extreme selective pressure (*e.g.*, fossorality in tadpoles). The developmental processes central to establishing a *Bauplan* may thus be modulated to generate novel morphologies. In the case of supernumerary caudal vertebrae in megophryids, this modulation may have occurred as a heterochronic shift in the ossification sequence of the axial skeleton, effectively clearing a path around the normal obstacles to vertebral formation in the tail.

At metamorphosis, of course, megophryids reclaim the anuran *Bauplan*, replacing their expanded caudal skeleton with the urostyle that characterizes all frogs and toads. This renewed adherence to the anuran *Bauplan* sharply contrasts with the seeming infidelity of the megophryid larval phase, manifested in their supernumerary caudal vertebrae. In this light, megophryids represent a unique system in which to explore the interaction of natural selection and developmental constraint in driving morphological evolution.

Table 6.1 Anuran specimens examined Specimen.s were either cleared and bone-stained ('C&S') or serially-sectioned in paraffin ('Histology').

Species		*Gosner stage*	*Catalogue #*	*Total length* (mm)	*Snout-vent length* (mm)	*Processing*
Leptobrachella	*mjobergi*	25	BrachellaM2	22.3	7.5	Histology
		25	BrachellaM6	25.0	8.8	C&S
		25	FMNH 157998b	35.2	11.2	C&S
		30/31	FMNH 77504	?	11.5	C&S
		39/40	FMNH 157998a	32.1	10.7	C&S
		Adult	FMNH 222857	18.7	18.7	C&S
	parva	42	FMNH 244079	38.4	10.7	C&S
Leptobrachium	*hendricksoni*	31	ZRC 1.5945a	49.0	24.3	C&S
	montanum	37	FMNH 241683	55.3	19.7	C&S
	nigrops	36	ZRC 1.3403a	42.2	19.7	C&S
Leptolalax pelodytoides		27	ROM 42275	52.5	18.1	C&S
		30	ROM 42276	50.6	18.3	C&S
		31	ROM 42280	46.9	18.0	Histology
		32	ROM 42281	44.2	17.3	C&S
		37	ROM 42282	51.7	20.7	C&S
		40	FMNH 254546	58.7	18.7	C&S
		43	FMNH 254546	53.9	21.0	C&S
		45	ROM 42278	20.5	20.5	C&S
Megophrys	*boettgeri*	36	A-30639	42.3	14.8	C&S
		39		86.7	30.6	C&S
		44a		34.9	17.1	C&S
		44b		32.5	16.5	C&S
		44/45		35.7	15.3	C&S
	lateralis	28	ROM 42357	41.6	14.2	C&S
		33	ROM 42358	43.7	13.8	C&S
		35	ROM 42359	44.3	14.8	C&S
		36	ROM 42361	44.7	15.7	Histology
		37	ROM 42362	42	15.3	C&S
		41	ROM 42364	37.3	12.6	C&S
		43	ROM 42365	47.1	14.7	C&S
		45	ROM 42366	31.7	16.0	C&S
		46	ROM 42368	19.0	19.0	C&S
	longipes	33	ZRC 1.4079a	37.5	11.4	C&S
		31	ZRC 1.4079b	38.6	12.0	Histology
	montana	25	CAS 138414	25.8	10.5	C&S
		36	CAS 138409	36.9	12.4	C&S
		38	CAS 138409	32.2	12.9	C&S
		44	CAS 138409	28.5	12.9	C&S
		44	CAS 138409	-	-	Histology
		45	CAS 138410	18.8	14.0	C&S
	nasuta	27	ZRC 1.1543b	36.5	13.5	Histology
		36	ZRC 1.1543a	41.8	15.4	C&S

Table 6.1. (Continued)

	stejnegeri	26	FMNH 50950-820	-	-	C&S
		27	FMNH 50950-804	-	-	C&S
		-	FMNH 50950-808	-	-	Histology
Ophryophryne microstoma		28	ROM 42328	28.5	9.1	C&S
		29	ROM 42330	29.6	10.1	C&S
		30	ROM 42334	26.9	9.1	C&S
		34	ROM 42335	30.3	9.9	C&S
		35	ROM 42337	-	-	Histology
		36	ROM 42339	30.4	10.0	C&S
		37	ROM 42340	25.7	9.7	C&S
		42	ROM 42344	22.8	8.8	C&S
		43	ROM 42345	15.7	10.9	C&S
Oreolalax popei		39	FMNH 268756	86.7	30.6	C&S
Scutiger	*glandulatus*	36	FMNH 50985	49.8	20.0	C&S
	sp.	35	CAS 90674	49.1	22.9	C&S
Vibrissaphora boringii		25	GRH Vb1	50.5	19.7	C&S
Xenophrys sp.		25	MNHN 1998.9166-9167	20.7	7.2	C&S
		27		34.0	11.9	C&S
Heleophryne rosei		40/41	RJW Hr1	57.0	20.4	C&S
Hyalinobatrachium pulveratum		30	GRH Hp1	22.7	7.4	C&S
Osteopilus brunneus		34	RJW Ob1	37.5	12.0	C&S
Cochranella granulosa		41	GRH Cg1	tail portion		C&S
Centrolenella prosoblepon		42/43	GRH Cp1	tail portion		C&S

A, American Museum of Natural History, New York, USA; CAS, California Academy of Science, San Francisco, USA; FMNH, Field Museum of Natural History, Chicago, USA; MNHN, Muséum National d'Histoire Naturelle, Paris, France; ROM, Royal Ontario Museum, Toronto, Canada; ZRC, Raffles Museum of Singapore, Singapore

Table 6.2. Tally of supernumerary caudal centra in surveyed megophryid species during larval development. Outlined cells represent the earliest stage at which appendicular skeletal development (as revealed by whole-mount Alizarin Red-staining) was noted for each species.

Species		Number of supernumerary centra by Gosner stage																				
		25	*26*	*27*	*28*	*29*	*30*	*31*	*32*	*33*	*34*	*35*	*36*	*37*	*38*	*39*	*40*	*41*	*42*	*43*	*44*	*45*	*46*
Leptobrachella	*mjobergi*	30					~29									29							
	parva																		~33				
Leptolalax pelodytoides				3			6		5					5			6			6		5R	
Megophrys	*boettgeri*												8			11					11	?	
	lateralis				?					10		13		12				11		14		15	C
	longipes									12													
	*major**	11																12-13					
	montana	0											11		13						?	R	
	nasuta												14										
	stejnegeri		8	8																	?		
Ophryophryne microstoma					?	14†	14†				14		12	12					14†	~11			
Xenophrys sp.		0‡		7																			
Leptobrachium	*hendricksoni*							0															
	montanum													0									
	nigrops												0										
Oreolalax popei																0							
Scutiger	*glandulatus*												0										
	sp.											0											
Vibrissaphora		0																					

*from Griffiths, 1963; R, vertebrae are being resorbed; C, fused as coccyx; †, approximate vertebral tally given poor staining; ‡, presacral centra not yet formed

Figure 6.1. Ontogeny of the axial skeleton of *Leptobrachella*. (A) A stage-39 metamorph of *L. mjobergi* (FMNH 157998a) cleared and stained for bone (red) and cartilage (blue). Inset shows cleared-and-stained axial skeleton of an adult of the same species (FMNH 222857). Arrowheads indicate the sacral vertebrae. Scale bar equals 5mm. (B) Close-up lateral view of most caudal vertebrae of specimen shown in A. In *L. mjobergi*, supernumerary post-sacral centra are laid down as spools of perichordal cartilage, which eventually ossify (as seen in vertebrae at far left). PS25, the 25th post-sacral centrum. (C) Close-up lateral view of most caudal centra of stage-42 *L. parva* (FMNH 244-79). Vertebrae are porous and fragmented, suggestive of osteoclastic degradation. PS22, the 22nd post-sacral centrum. (D) Lateral view at level of the sacrum (black arrowhead) of *L. parva* (same specimen as in C). A cartilaginous longitudinal ridge (white arrowhead) can be seen on the ventral face of the first post-sacral centrum. This structure will likely contribute to the urostyle of the adult skeleton. Scale bar equals 1mm. (E) Transverse cross-section through a post-sacral vertebra of a stage-25 tadpole of *L. mjobergi*. The centrum (blue stain) is perichordal, completely encompassing the notochord. Section was stained with Mallory's trichrome, rendering osseous tissue blue and the myomeric muscle red. Scale bar equals 250 μm.

Leptobrachella

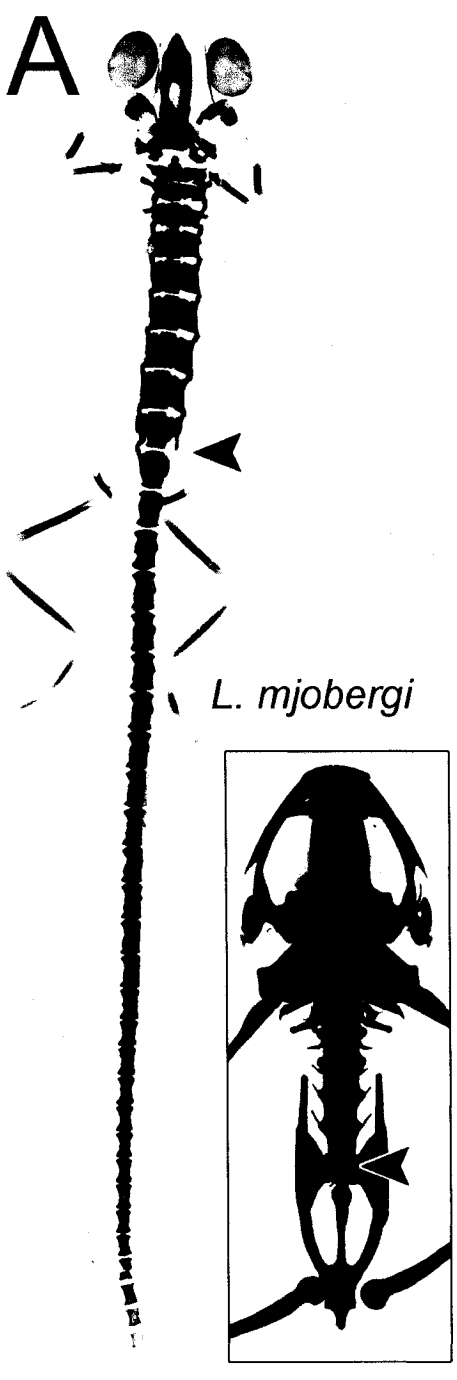

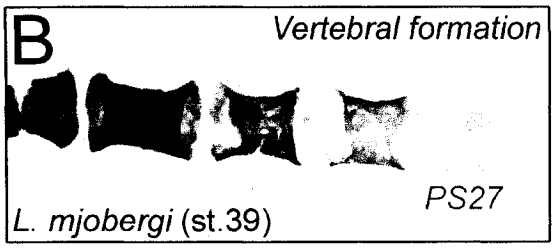

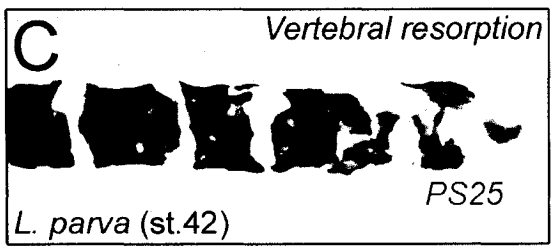

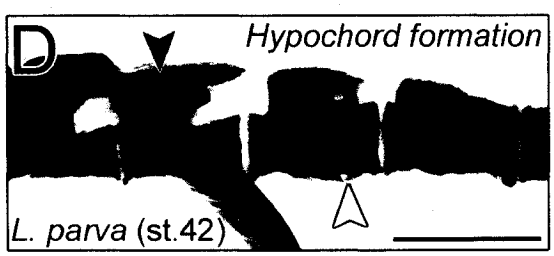

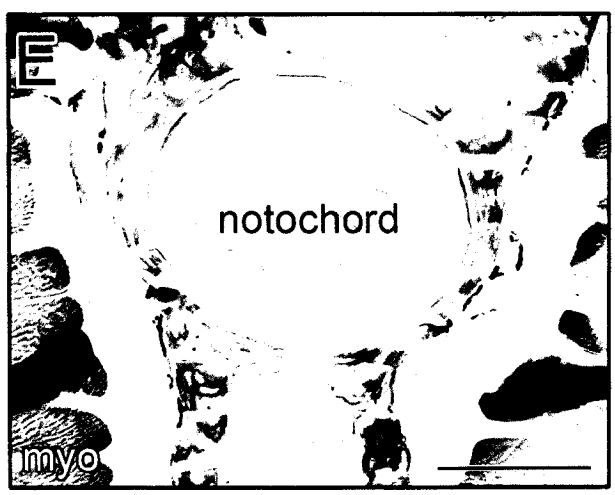

Figure 6.2. Ontogeny of the axial skeleton of *Leptolalax pelodytoides*. (A) Lateral view of a cleared-and-stained tadpole (stage 30; ROM 42276). The presacral skeleton comprises eight complete (centrum + neural arches) and closely-articulated vertebrae. Caudal to the sacrum (black arrowhead), there is one complete vertebra followed by two perichordal centra and then a series of dorsal and ventral anlagen, falling at or between successive myoseptae. The appendicular skeleton has not begun to ossify by this stage. Scale bar equals 4 mm. (B) Dorsal view of the post-sacral skeleton of a stage-40 metamorph (FMNH 2545546). Anlagen typically occur coincident with myoseptae (broken lines) as opposed to those depicted in A. Scale bar equals 2 mm. (C) Lateral view at the level of the sacrum of the same specimen in B. The sacrum (black arrowhead) is followed immediately by two tightly-compressed centra and, more caudally, a perichordal centra and three progressively more rudimentary dorsal anlagen pairs. Scale bar equals 4 mm. (D) Lateral view of immediately post-sacral vertebrae of a stage-43 metamorph (FMNH 254546). Post-sacral centrum 1 is joined to PS2 at its caudal margin by an osseous bridge. Both vertebrae are expanded ventrally, forming the hypochordal ridge. Scale bar equals 2 mm. (E) Lateral view of the caudal skeleton near the end of metamorphosis (stage 45; ROM 42278). Post-sacral vertebrae 1 and 2 are fused both dorsally and ventrally, forming the coccyx and hypochord, respectively. The remnants of PS3 and 4 are displaced dorsally. Intervertebral cartilage (white arrow) can be seen between the sacrum and adjacent vertebrae. Scale bar equals 2 mm.

Leptolalax pelodytoides

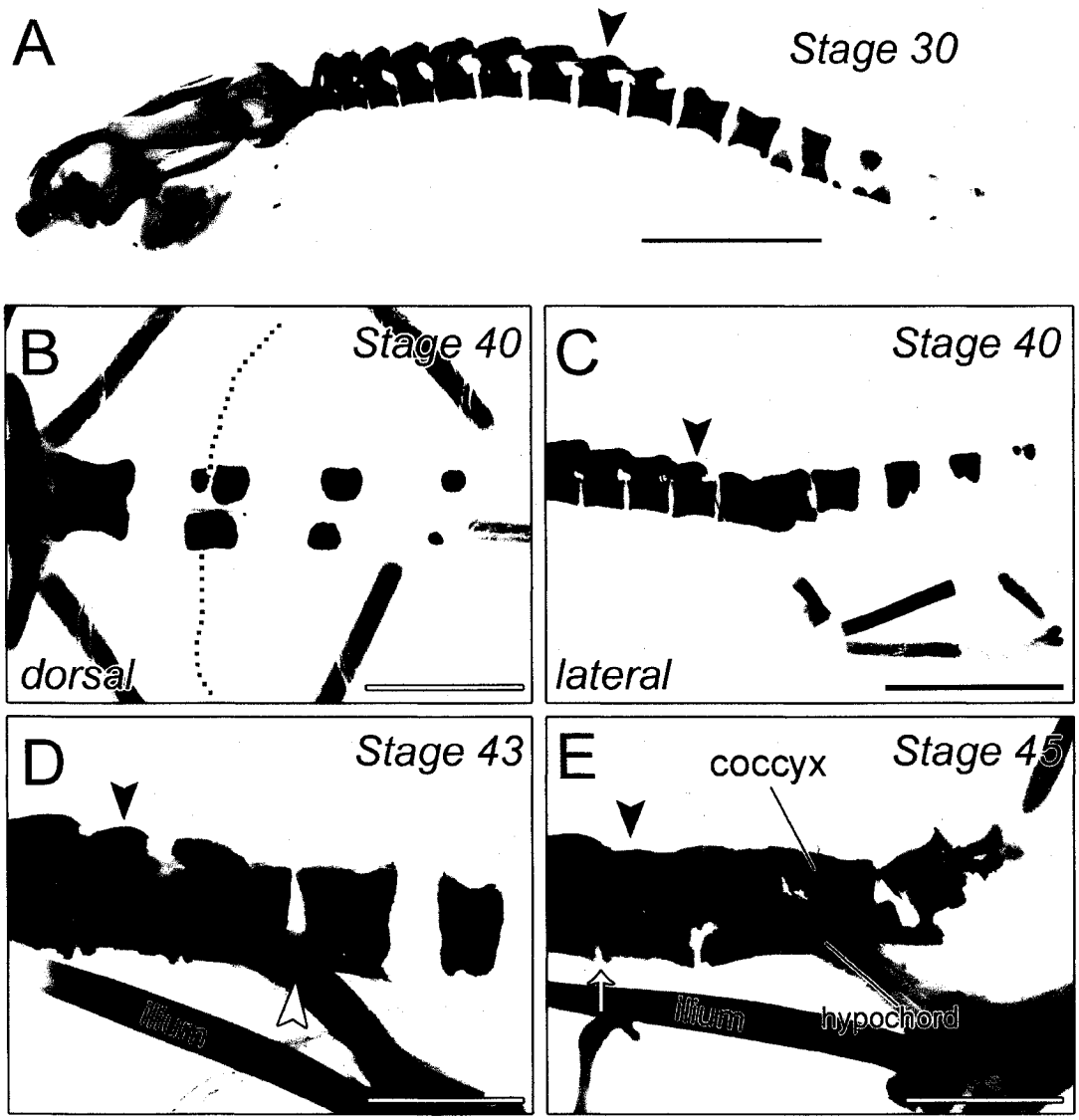

Figure 6.3. Ontogeny of the axial skeleton of *Megophrys*. (A) A cleared-and-stained tadpole (stage 35) of *M. lateralis* in lateral perspective. Caudal to the sacrum (arrowhead), vertebrae are progressively more rudimentary. In the presacral skeleton, centra development follows formation of the neural arches as seen in a stage-25 *M. montana* (inset). Scale bar equals 4mm. (B) Dorsal view of post-sacral vertebrae of *M. lateralis* tadpole (ROM 42359), showing the progressive decoupling of centra into discrete anlagen and the longitudinal staggering of corresponding dorsal and ventral anlagen. Scale bar equals 1 mm. (C) Successive cross-sections (stained with Mallory's trichrome) through a single caudal vertebrae of *M. lateralis* (stage 36; ROM 42361). Dorsal anlagen (indicated by arrowheads in C1) always precede their ventral counterparts (arrowheads in C2). n, notochord. Scale bar equals 250 μm. (D) Cross-section through a perichordal post-sacral vertebra of *M. longipes* (stage 31; ZRC 1.4079b). The centrum, having once comprised discrete anlagen, now completely encompasses the notochord. myo, myomere. Scale bar equals 250 μm. (E) Cross-section through post-sacral vertebra 1 of a stage-27 tadpole of *M. nasuta* (ZRC 1.1543b). Neural arches dorsally appose the notochord and partially envelope the neural tube (nt). The hypochord is visible as a bulbous swelling (arrow) ventral to the notochord. Scale bar equals 250 μm. (F) A cleared-and-stained metamorph of *M. lateralis* (stage 45; ROM 42366). Scale bar equals 4 mm. (G) Lateral view of the axial skeleton (caudal from vertebra IV) of a *M. montana* metamorph (CAS 138410). With the exception of the sacrum (arrowhead) and those post-sacral vertebrae in contact with the hypochord and coccyx, centra are fragmented and porous along the length of the vertebral column, suggestive of osteoclastic degradation. Scale bar equals 2 mm. (H) Close-up lateral view of the immediately post-sacral vertebrae of a *M. boettgeri* metamorph (stage 44; A-30639). PS1-3 are joined ventrally by a longitudinal bridge (white arrow), which extends from the caudal margin of PS3. This structure will go on to form the hypochord in later stages. The dorsal surface of PS2 and 3 are fused as the coccyx. The hindlimb skeleton has been disarticulated from the sacrum (arrowhead), allowing for an unobstructed view. Scale bar equals 2 mm. (I) Parasagittal section through the sacral region of a *M. montana* metamorph (stage 44; CAS 138409), showing multinucleate, osteoclast-like cells (arrows) embedded in peri-notochordal osseous tissue. n, notochord; myo, myomere. Scale bar equals 0.5 mm. (J) Sagittal section through the same specimen in I. Osteoclast-like cells are clearly visible in the peri-notochordal osseous tissue, but absent from the nascent hypochord, lying ventral. Scale bar equals 0.5 mm. (K) Lateral view of the caudal skeleton of *M. lateralis* (ROM 42368) nearing the very end of metamorphosis. Post-sacral vertebrae 1-3 have been incorporated into the urostyle. All other supernumerary centra have been resorbed by this point. Scale bar equals 2 mm.

Megophrys

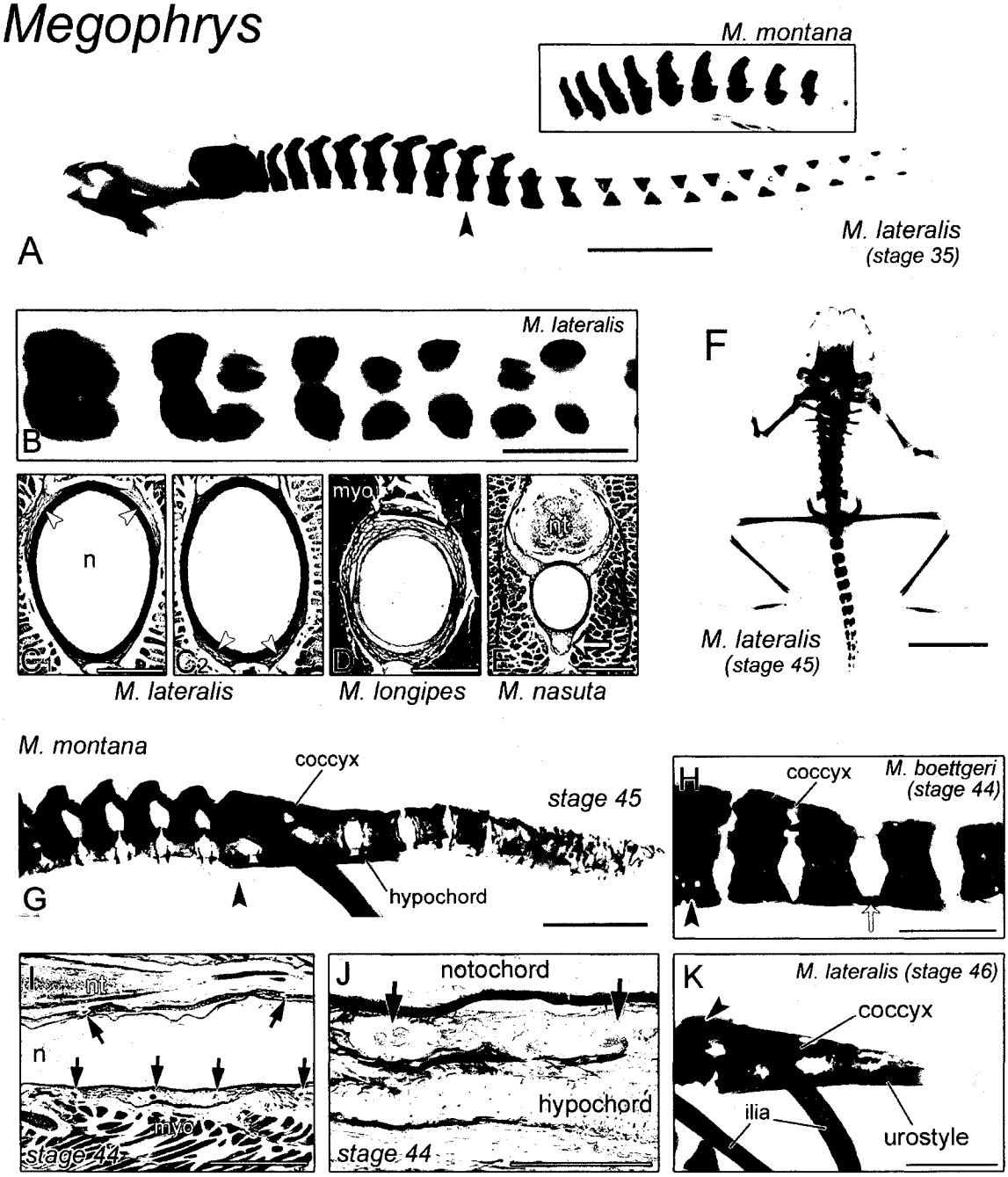
M. montana
A
M. lateralis
(stage 35)
M. lateralis
B
n
myo
nt
C1
C2
D
E
M. lateralis
M. longipes
M. nasuta
F
M. lateralis
(stage 45)
M. montana
coccyx
stage 45
hypochord
G
H
coccyx
M. boettgeri
(stage 44)
I
nt
n
myo
stage 44
J
notochord
hypochord
stage 44
K
M. lateralis (stage 46)
coccyx
ilia
urostyle

Figure 6.4. Ontogeny of the axial skeleton of *Ophryophryne microstoma*. (A) A cleared-and-stained tadpole (stage 30; ROM 42334) in lateral perspective. Caudal to the sacrum (arrowhead), centra form as cartilaginous spools (inset) in this species. A similar developmental mode is seen in *Leptobrachella* (Fig. 6.1). Scale bar equals 2 mm. (B) Transverse section through post-sacral vertebra 1 of a stage-35 tadpole (ROM 42337). Neural arches dorsally appose the notochord (n) and partially envelope the neural tube (nt). The hypochord is visible as a bulbous swelling (arrowhead) ventral to the notochord. myo, myomere (C) Cross-section through a perichordal post-sacral vertebra of the same specimen shown in B. The centrum completely encompasses the notochord (n). myo, myomere. Scale bar equals 250 μm. (D) Frontal section through a post-sacral centrum of the same specimen shown in B. A thin layer of osseous tissue (arrows) can be seen on either side of the notochord, coinciding with myoseptae. Scale bar equals 250 μm. (E) The immediately post-sacral skeleton of a stage-42 metamorph (ROM 42344) in lateral perspective. PS1, 2 and 3 are joined dorsally by thin symphyses, forming the coccyx, and ventrally by the cartilaginous hypochord (arrowhead). Scale bar equals 1 mm. (F) Close-up lateral view of porous post-sacral centra of specimen shown in G. Scale bar equals 0.5 mm. (G) The post-cranial skeleton of a metamorph (stage 43; ROM 42345) in lateral perspective. Centra appear porous and reduced along the entire length of the vertebral column and particularly so at rostral and caudal extremes, indicative of osteoclastic resorption. The hypochord (white arrowhead) extends along the ventral surface of the sacrum (black arrowhead) and post-sacral vertebrae 1-3. Scale bar equals 1 mm.

Ophryophryne microstoma

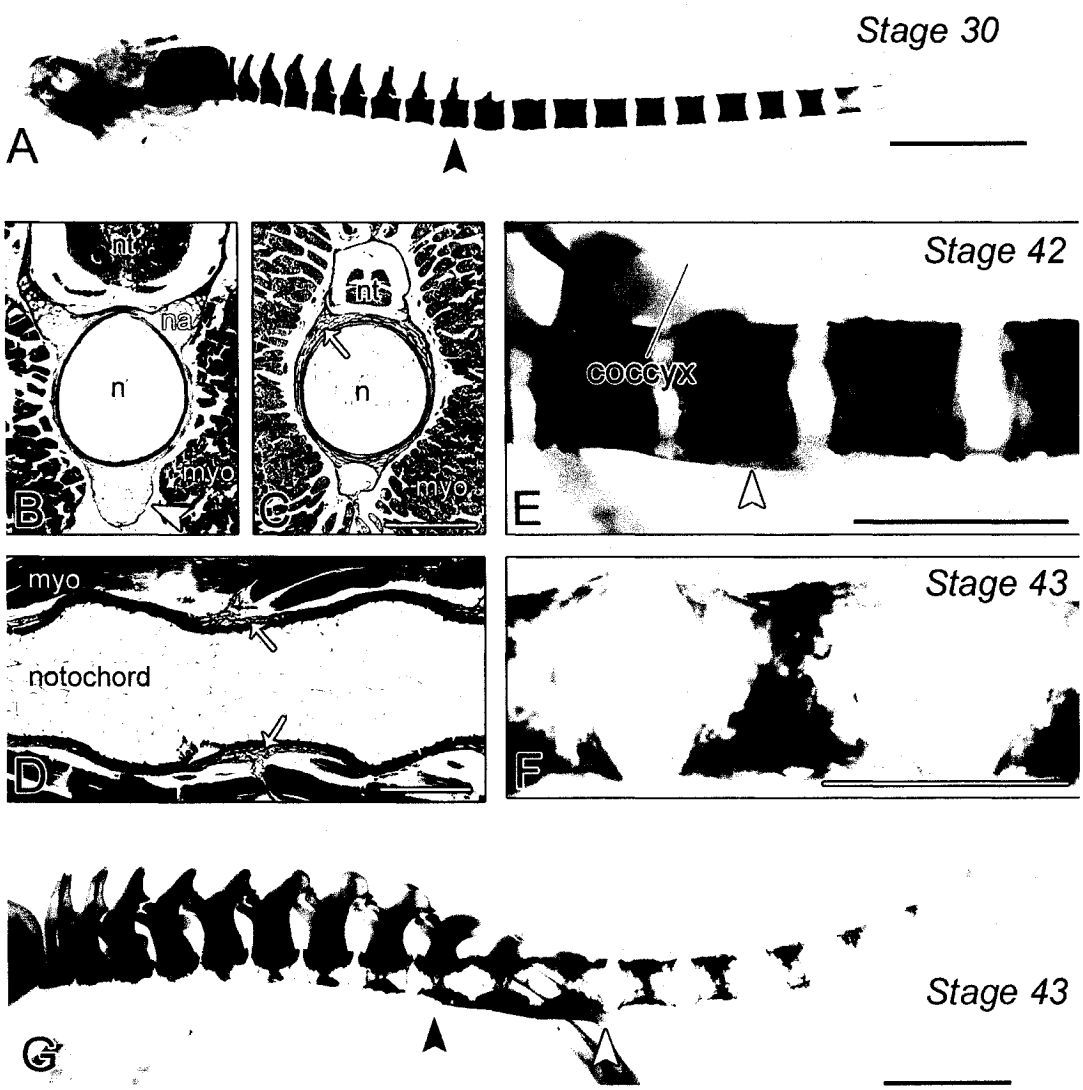

Figure 6.5. Ontogeny of the axial skeleton of *Xenophrys*. (A) A cleared-and-stained tadpole (stage 27; MNHN 1998.9167) in lateral perspective. Scale bar equals 2 mm. (B) Ventral view of the sacrum (asterisk) and post-sacral vertebrae 1-3 of specimen shown in A. Cartilaginous bumps (arrowheads) project longitudinally from the rostral and caudal margins of PS1 and 2. Scale bar equals 1 mm. (C) Lateral view. The bumps visible in B represent the tips of cartilaginous rods at the ventral surface of PS1 and 2. In subsequent stages, these rods will likely converge and ossify to form the hypochord. Scale bar equals 1 mm. (D) Ventral view of caudal centra of specimen shown in A. Dorsal and ventral anlagen are progressively more decoupled towards the tail tip. Anlagen are ossified medially, but remain cartilaginous at their periphery. Scale bar equals 1 mm. (E) Post-cranial skeleton of a stage-25 tadpole (MNHN 1998.9166) in lateral view. Ossification is restricted to the neural arches of vertebrae I-VI. Segmented cartilage lines the ventral surface of the notochord, indicate of early vertebral body formation. Scale bar equals 1 mm.

Xenophrys

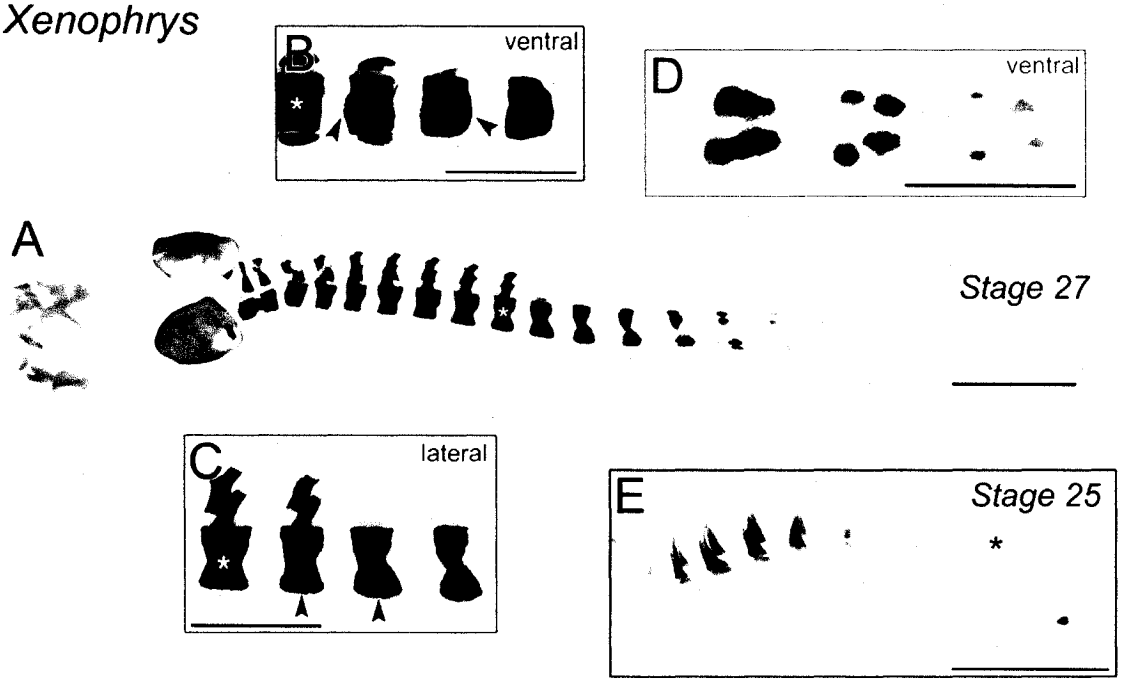

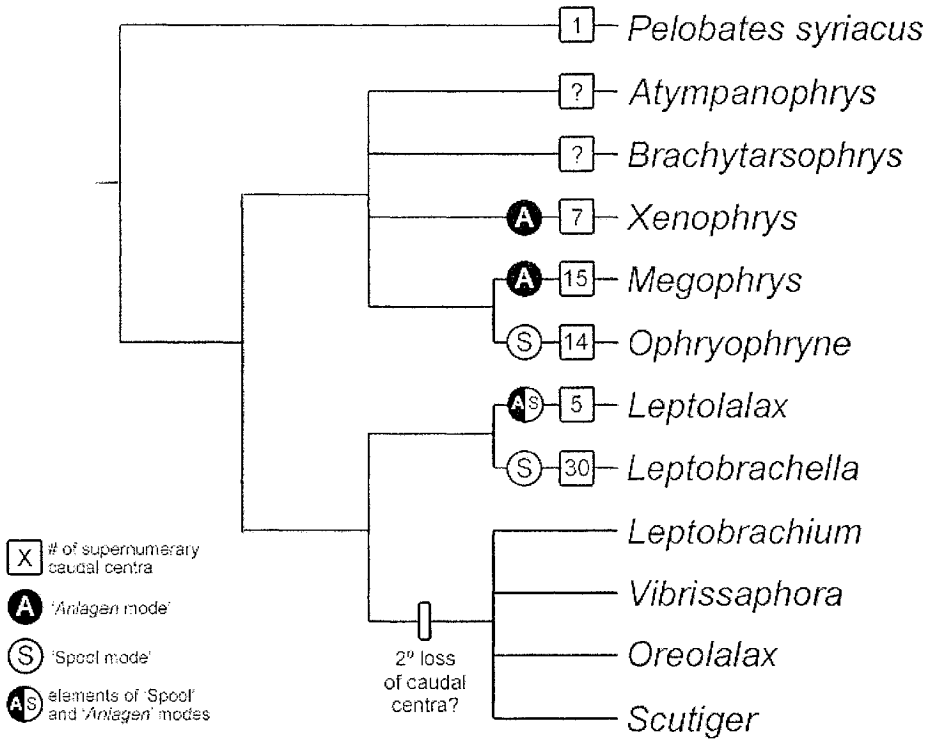

Figure 6.6. A phylogeny for the Megophryidae with *Pelobates syriacus* as an outgroup representative of the closest related anuran family. Mapped on are data for the number of caudal centra (boxed numbers) and mode of caudal vertebral formation (circled letters) by genus. Neither character appears to vary according to a particular phylogenetic trend. The observation of a single post-sacral centrum in metamorphs of *Pelobates syriacus* suggests that the capacity to form supernumerary caudal vertebrae had been either retained or regained in its closest common ancestor with the Megophyridae. The larger-bodied, side pool-dwelling tadpoles of the megophryid genera *Leptobrachium*, *Vibrissaphora*, *Oreolalax* and *Scutiger* all lack supernumerary caudal vertebrae and neatly cluster into a single clade, suggesting a secondary loss of caudal centra in their common ancestor. The phylogeny was adapted from Zheng *et al.* (2004) and Frost *et al.* (2006).

CHAPTER 7:

TARSAL ELONGATION IN ANURANS AND UNRAVELING *BAUPLAN*

The contents of this chapter together with chapters 2 and 4 are currently in press in the journal *Biological Reviews of the Cambridge Philosophical Society* as:

Handrigan, G. R. & Wassersug, R. J. The anuran *Bauplan*: A review of the adaptive, developmental, and genetic underpinnings of frog and tadpole morphology, 100 manuscript pages

AUTHOR'S NOTE

In Chapter 5, I explored a potential role for the gene *XlGdf11*, an upstream regulator of *Hox* genes, in the evolutionary truncation of the anuran axial skeleton. Whereas the work does not reveal a clear link between *XlGdf11* function and *Hox* gene expression in the patterning defects observed, there can be no denying the overarching importance of *Hox* genes to axial patterning in vertebrates, including anurans.

This same set of genes is also integral to the development of the appendicular skeleton in vertebrates and, by extension, may provide a molecular bases for the third and final feature of the anuran *Bauplan*, the elongate tarsal elements of the hindlimb. In Chapter 7, I review an important study by Blanco and colleagues (1998), which identifies one potential *Hox*-mediated route to tarsal elongation in *X. laevis*, along with some complementary amniote literature.

Following this discussion, I broaden my discussion of the anuran body plan, synthesising the specific hypotheses raised for each *Bauplan* character (*viz.* elongate tarsal elements, shortened trunk, and absent caudal vertebrae) into general statements concerning the nature of *Bauplan*. I emphasise the importance of *Bauplan* in directing morphological evolution as well as the value of comparative approaches in dissecting its role in the process. The list of conclusions closing Chapter 7 summarizes the salient findings of the literature review (Chapters 2, 4, and 7 inclusive).

7.1 TARSAL DEVELOPMENT IN ANURANS: A CASE OF MISTAKEN IDENTITY

The generalized tetrapod limb (Fig. 7.1) consists of three segments or elements (moving proximal to distal): stylopodium (femur / humerus), zeugopodium (radius and ulna / tibia and fibula), and autopodium (carpals, metacarpals, tarsals, metatarsals and phalanges). These elements vary greatly in size and shape in vertebrates (Tickle, 2002). In some elongate tetrapods (*e.g.*, cetaceans, skinks, caecilians), for example, hindlimb elements have all but been eliminated. At the other extreme are the dramatically lengthened digits of the bat forelimb, which often are as long as the animal's body and serve as a frame for the broad bat wing (Sears *et al.*, 2006).

Skeletal divergence is also commonly seen between fore and hind limbs of the same animal. For example, the broad, hyperphalanged forelimbs of cetaceans are juxtaposed by their rudimentary hindlimbs (usually only a single reduced pelvic bone; Bejder & Hall, 2002). More topically, the tarsal elements of the anuran hindlimb are elongate relative to the corresponding autopodial bones of the forelimb (*i.e.*, carpal bones; Blanco *et al.*, 1998). These differing morphologies not only point to a decoupling of fore- and hind-limb development, but also to compartmentalization of bone development *within* the limb. The digits of the bat wing and the tarsals of the frog hindlimb have each undergone elongation independent of adjacent bones.

The developmental decoupling of limb elements is first manifested as differential gene expression in the bud. Each podial element appears to be specified by members of a

progressively 5' *Hox* paralogous group, *viz.*, *Hox10* (stylopod), *Hox11* (zeugopod), and *Hox12/13* (autopod; Figure 7.1). Disrupting the normal function of either group (by gene-targeting, bead implantation, electrophoresis, etc.) results in the loss or reduction of the corresponding element. For instance, Wellik and Capecchi's (2003) triple *Hox10* and *Hox11* mutants exhibited reduced stylopodial and zeugopodial elements, respectively. Staggered *Hox* gene expression along the proximo-distal axis of the growing limb bud seems to set the bounds for the bony limb elements. Altering the spatial domain of *Hox* gene expression is thought to produce a 'homeotic transformation' of limb elements. Yokouchi and colleagues (1995) noted nodular elements (resembling tarsals/carpals) in place of the elongate zeugopodial elements when autopodial-specifying *Hoxa13* was expanded proximally in the chick.

The anuran hindlimb exhibits the opposite morphology (*i.e.*, proximal tarsal elements (tibiale and fibulare) have elongated to resemble zeugopodial bones; Figure 2.2, 7.1). Blanco *et al.* (1998) attributed this to a heterochronic prolongation and spatial expansion of *Hoxa11* expression. Unlike the corresponding carpal elements of the anuran forelimb, the tibiale and fibulare of *X. laevis* are laid down as elongate precursors in the expression domain of *Hoxa11*. What is more, both bones ossify in a mode characteristic of the long bones of the anuran limb; *i.e.*, perichondrally. Meanwhile the forelimb carpals and more distal tarsals ossify endochondrally. These discrepancies have led Blanco *et al.* (1998) to suggest that tarsal elongation in anurans represents a qualitative change of state—the elements have been re-specified from an autopodial to a zeugopodial fate.

On the other hand, the massive lengthening of digits in the bat forelimb likely represents a quantitative change of state: the elements have retained their autopodial identity, but are merely larger. Recent work from the Niswander group suggests that BMPs are key players in this process (Sears *et al.*, 2006). Specifically, they have noted increased levels and broadened spatial expression of *BMP2* transcripts in the developing forelimb (compared to the bat hindlimb and mouse forelimb). These changes in expression appear to be correlated with an expanded hypertrophic zone (the site of chondrocyte formation) in the digital anlagen, suggesting that the underlying developmental machinery has been modulated and not replaced.

Sears and colleagues (2006) have not explored a *Hox* gene role in the process, though it is quite likely given the changes in the size of limb elements that consistently accompany 5' *Hox* gene knock-out. These findings have led some to suggest that *Hox* genes function to regulate cell proliferation in the developing limb bud (Duboule, 1995; Hombría & Lovegrove, 2003). Blanco and colleagues' (1999) work with the anuran tarsal elements, however, implies that the *Hox* role is slightly more complicated and may involve global and local—qualitative and quantitative—functions in the limb.

Finally, it is tempting to assign a *Hox* basis to the other relatively elongate bones of the anuran appendicular skeleton, the pelvic ilia. However, there is little evidence to suggest this. Pellegrini and colleagues (2001) downplay the role of *Hox* genes in patterning the girdles, favoring instead the genes *Pax1*, *Emx1* and *Emx2*. This is contradicted, however, by the observation of pelvic abnormalities in *Hox10* and *Hox11* paralogous-group

knockout mice (Wellik & Capecchi, 2003; especially their Fig. 2). Abnormalities appear to be restricted to the distal elements (*i.e.*, ischia and pubis), whereas the ilia are indistinguishable from the wildtype. The role of these genes in patterning the ilia of anurans clearly warrants further investigation.

7.2 UNDERSTANDING *BAUPLAN* AND ITS ROLE IN MORPHOLOGICAL EVOLUTION

I have attempted to frame anuran morphology within the context of contemporary evolutionary developmental biology (evo-devo). The anuran *Bauplan* emerges as a product of modulating generalized vertebrate molecular and developmental machinery. For each of my three diagnostic anuran characters, a fairly unambiguous developmental basis can be extrapolated from comparative analyses: (1) Caudal vertebral agenesis is due to a preclusion of cartilage development, perhaps resulting from altered expression or function of *Pax1*, *Shh*, and *Uncx-4.1* or more likely *Sox9* and Collagen type II; (2) axial truncation, due to rostral shifting of morphological boundaries, is correlated with anteriorized *Hox* gene expression in the paraxial mesoderm; and, (3) the expanded tarsal elements of the hindlimb may be ascribed to spatial and temporal shifts in *Hox* expression. While these explanations (and alternatives presented above) largely await experimental confirmation, none is unfounded. In each case, there is sufficient corroborative data in birds, mammals and fishes to elevate them to 'reasonable hypotheses' status.

7.2.1 Insights into morphological evolution

The conservation of developmental and genetic programs within a group of organisms establishes and maintains its *Bauplan*. These programs are passed from generation to generation along with their inherent constraints. Morphological diversity is permitted only within the range of morphologies that can be generated by the suite of programs. Although vertebrates have a fixed repertoire of such developmental programs, as exemplified by *Hox* patterning and somite compartmentalization, these programs have a certain degree of flexibility. Modulation of the *Bauplan* machinery occurs via evo-devo mechanisms, such as heterochrony and heterotopy (Hall, 1992; Hall & Olson, 2003).

To illustrate: In the face of a selective pressure to maximize saltatory escape (*e.g.*, from faster predators), a vertebrate may evolve a shorter trunk (to reducing torque while jumping) through a reduction in the number of presacral vertebrae. To accomplish this, the animal can turn to its *Hox* program, which has produced a broad array of axial morphologies during vertebrate evolution. A slight perturbation in the timing of the expression of a *Hox* gene (as mediated by *cis*-regulatory elements) or of a suite of *Hox* genes (by an upstream regulator) could readily transpose axial landmarks to produce a shortened trunk as seen in frogs; the opposite effect may also occur, creating the elongate trunk seen in snakes. It is the selective advantage of the former to saltation, however, that ensures it will be seen in future generations.

7.2.2 Probing *Bauplan*'s outer limits

Further understanding of the vertebrate *Bauplan* can be achieved by probing its outer limits—divergent morphological forms. Cohn and Tickle (1999) did just this. By successfully applying the '*Hox* code' (cracked with data gleaned almost exclusively from amniotes) to pythons, they corroborated the universality of the code to vertebrates and its centrality to the vertebrate *Bauplan*. It is perhaps not surprising then that the *Hox* code so readily accommodates the truncated anuran axial skeleton.

This hypothesis and others presented in this review, however, beg for scientific scrutiny. Broad surveying of ontogenetic mechanisms—particularly in morphologically diverse groups such as amphibians and reptiles—would capture the true range of variation and lability possible within the vertebrate *Bauplan*.

Alberch and Gale (1983, 1985) established a good template for such an experimental approach to studying *Baupläne* with their investigation of digital loss in amphibians. By experimentally reducing the number of cells in the early limb buds of frogs and salamanders with the pro-apoptotic agent colchicine, they produced concomitant and predictable changes in the phalangeal formulae of each taxon. Frogs typically lost digit I, whereas salamanders lost IV. Interestingly, these experimentally-generated limb morphologies correlate with the predominant, naturally-occurring digit-deficient morphologies presented by each taxon (*i.e.*, digit I is most frequently lost as a result of naturally-occurring and colchicine-induced digit loss in frogs). These parallels in limb

morphology represented to the authors evidence of the "resilient developmental rules" of limb morphogenesis at work.

Technology is now firmly in place to explore the developmental and genetic mechanisms central to the divergence of anurans and the subsequent maintenance of their *Bauplan* (for detailed discussion of recent advances in *Xenopus* technology see Carruthers & Stemple, 2006; Blitz, Andelfinger & Horb, 2006). *Xenopus* is readily amenable to genetic manipulation by mRNA and morpholino injection as well as transgenesis (for elegant examples of each technique in use see: Blitz, Cho & Chang, 2003; Horb *et al.*, 2003). The construction of extensive expressed sequence tag libraries (*e.g.*, Wellcome Full-Length Database; see Gilchrist *et al.*, 2004) has greatly accelerated the discovery and characterization of genes and, most recently, has opened the door to wide-scale gene expression analysis using microarrays (Altmann *et al.*, 2001; Chalmers *et al.*, 2005). And with the diploid *X. tropicalis* about to usurp its allotetraploid cousin *X. laevis* as the new model anuran species, frog knock-out technology will soon be within reach (Hirsch, Zimmerman & Grainger, 2002). Also close at hand is the complete sequence of the genome of *X. tropicalis* (see www.jgi.doe.gov/xenopus/). Now in its fourth and probably final assembly (with ~8× coverage of 1.5Gb sequence), the *Xenopus tropicalis* genome project is arguably the most important advance in modern anuran biology. This growing suite of experimental tools and genetic data will resolve many unanswered questions about the evo-devo of the anuran *Bauplan.*

7.3 Conclusions

(1) Morphological features such as the lack of a vertebrated tail, elongate tarsal elements and a shortened trunk—along with many other larval and adult characters—characterize the anuran body plan or *Bauplan*, which is nested (*i.e.*, *Unterbaupläne*) in an overarching vertebrate *Bauplan*.

(2) The tadpole tail lacks vertebrae beyond the anus in all anurans except for some megophryids and is ultimately lost at metamorphosis.

(3) Fossil data indicates that the anuran *Bauplan* was established by the Early Triassic as exemplified by *Vieraella herbsti*, which bore ten presacral vertebrae, a coccyx and elongate tarsal elements. The *Bauplan* has seen little modification in the intervening 200 million years.

(4) The anuran *Bauplan*, most notably the short torso, facilitates both jumping in frogs and escape turns in tadpoles. The absence of the tail in the post-metamorphic anuran improves jumping performance. The absence of vertebrae in most of the pre-metamorphic tail facilitates turning in the tadpole because it is so flexible. By lacking vertebrae, the tadpole's tail can furthermore be resorbed quickly at metamorphosis.

(5) Anuran development shares much in common with other vertebrates (*e.g.*, somites), but several non-trivial discrepancies include:

(a) The hypochord ossifies in anurans and is incorporated into the post-sacral skeleton;

(b) Axial and appendicular development have been decoupled by delaying limb bud formation;

(c) Anuran myotome differentiation employs cell-sorting mechanisms that are not seen in amniotes; and,

(d) Somitic compartment sizes in anurans are reversed relative to amniotes (*e.g.*, the anuran sclerotome is proportionately larger than its amniote counterpart).

Whereas the ultimate morphological impacts of *a* and *b* are clear, it is unknown how *c* and *d* may contribute to anuran morphology.

(6) Anurans have lowered their vertebral count by two mechanisms: (i) 2-to-1 or, less frequently, 3-to-1 fusion of vertebrae; and, (ii) the preclusion of ossification of somites. The former is occasionally seen in the most rostral and caudal pre-sacral vertebrae, and always seen in post-sacral vertebrae, which fuse with the hypochord to form the urostyle. The latter mechanism accounts for the lack of osseous elements in the tadpole tail, and it is may be the result of failure of cartilage condensation due to perturbed expression and function of *Pax1*, *Pax9*, *Sonic hedgehog*, *Uncx-4.1*, *Sox9* and/or Collagen type II.

(7) *Hox* genes underlie the divergent axial morphologies of vertebrates. Gene expression data reveal that the anterior expression termini of *Hox* genes have been anteriorly transposed in the paraxial mesoderm of *Xenopus* relative to other vertebrates, corresponding with the rostral shift of the pectoral and pelvic girdles and the shortening of the trunk. These changes in *Hox* expression are likely mediated by *cis*-regulatory elements and/or upstream factors such as *Gdf11*.

(8) Shifts in the spatial and temporal expression of the *Hox* genes are also correlated with the distinct anuran appendicular morphology. Specifically, delayed expression of *Hoxa11* in the limb bud has induced a 'homeotic transformation' of proximal tarsal elements into the likeness of neighbouring zeugopodial elements. The tibiale and fibulare ossify in a manner akin to their zeugopodial counterparts.

(9) The anuran *Bauplan* emerges as a permutation of the overarching vertebrate *Bauplan*. The conservation of developmental and genetic programs ('*Bauplan* machinery') constrains the range of morphologies available to a vertebrate, but is flexible to allow for vertebrates as diverse as snakes and frogs to evolve.

(10) 'Extreme' morphological forms, such as frogs, turtles, and snakes, represent ideal systems in which to gauge the lability of the *Bauplan* machinery. Anurans are particularly amenable as experimental technology is already in place and great advances are being made with respect to their developmental genetics and genomics.

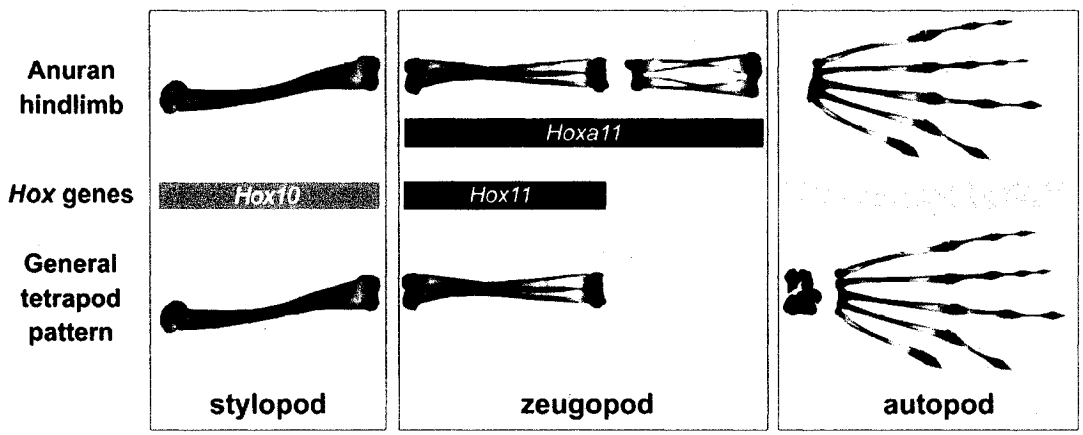

Figure 7.1 *Hox* patterning of the anuran hindlimb. Podial elements of the tetrapod hindlimb (bottom) are specified by particular 5' *Hox* paralogous groups (middle); viz., the stylopod, zeugopod and the autopod are under the control of *Hox10*, *Hox11*, and *Hox12/13* genes, respectively (Wellik & Capecchi, 2003). In anurans, proximal stylopodial bones, the tibiare and fibulare, resemble and develop in a manner akin to the tibia and fibula, which constitute the zeugopod (top). Blanco *et al.* (1998) suggest that the proximal stylopod has been respecified to a zeugopodial fate in the anuran hindlimb. They attribute this to a heterochronic shift in the expression of *Hoxa11*, a *Hox11* paralog, relative to other tetrapods.

CHAPTER 8:

CONCLUSION

The overriding goal of my doctoral research was to elucidate the bases for two defining features of the anuran *Bauplan*, namely, the truncated presacral axial skeleton and the absence of discrete caudal vertebrae. In the literature review, divided among chapters 2, 4, and 7, I focused on the adaptive and developmental bases of each. From an adaptive perspective, the truncated axial skeleton has obvious benefits for both tadpoles and frogs—making them more efficient swimmers and jumpers, respectively, and easing the transition between both locomotor modes at metamorphosis. During ontogeny, the anuran axial skeleton forms by a developmental program (*i.e.*, somite compartmentalization) that differs little from the generalized vertebrate pattern.

The original research presented in Chapters 3 and 5 attempts to uncover the molecular bases for axial truncation in anurans. In Chapter 3, I describe the identification of the gene *XlPax1*, the *Xenopus laevis* ortholog of *Pax1*. Using RT-PCR and *in situ* hybridization, I characterized early developmental expression of *XlPax1*, revealing transcripts in the pharyngeal endoderm and in the sclerotome, the bone-forming portion of the somite. This expression profile is consistent with other vertebrates and also suggestive of a role for *XlPax1* in vertebral development in *X. laevis*. A role for *Pax1* in the evolutionary loss of caudal vertebrae in anurans, however, is less likely given the observation of *XlPax1* transcripts in the vertebra-less tail of *X. laevis* tadpoles.

In Chapter 5, I identified and characterized the expression of a second *X. laevis* gene, *XlGdf11*. In amniotes, *Gdf11* orthologs show strong expression at both rostral and caudal levels. Gene knockout studies with *Mus* have shown that *Gdf11* functions as a potent

posteriorizing factor, delineating *Hox* gene expression and, in turn, determining the global pattern of the mammalian axial skeleton. *XlGdf11* shares its expression pattern with fellow vertebrate orthologs (*i.e.*, head and tail expression), but appears to diverge with respect to its function. Genetic loss-of-function studies in *X. laevis* do indeed point to a role for the gene in axial patterning, but one that does not appear to be mediated by the presumed downstream targets, the *Hox* genes. Instead, *XlGdf11* may be working through an alternative pathway or its function has been co-opted for some other aspect of axial development.

Collectively, these data reflect the conservation of gene expression and, to a lesser extent, gene function across disparate taxa and divergent morphologies. Such conservation is fundamental to the establishment and subsequent maintenance of an overarching *Bauplan*. At the same time, those divergent morphologies in question (*viz.* axial truncation, caudal vertebral agenesis) and, as exemplified by *X. laevis,* could not be readily explained by the predictable effects of either candidate gene. In the case of *XlPax1*, transcripts were found in the paraxial mesoderm of the trunk as well as the tail. For *XlGdf11*, genetic knockdown yielded no qualitative change in *Hox* gene expression. These findings underscore the flexibility of *Bauplan* and, more specifically, indicate that other genetic players must be at work in shaping the divergent axial morphology of *X. laevis*. It does not, however, obviate functions for *Gdf11* and *Pax1* in the development of the truncated axial skeleton in other anuran genera.

In Chapter 6, I dealt with an anuran family, Megophryidae, that does not adhere strictly to the *Bauplan*. Instead, tadpoles from at least 5 megophryid genera bear supernumerary vertebral centra in their tails. These genera demonstate great variety in caudal skeletal osteology as well as in vertebral ontogeny, for which I have identified up to three distinct modes of ossification. This surprising diversity indicates that the underlying molecular and developmental machinery is not tightly buffered (or at least entirely fixed) and that it was probably relatively minor 'tinkering' at these levels that produced the unique post-sacral skeleton of megophryids.

Finally, the appearance of supernumerary caudal vertebrae in Megophryidae also indicates that *Bauplan* is not blind or immune to the selective pressures of the environment. Instead, in the face of extreme selective pressure (*e.g.*, fossoriality in *Leptobrachella*), the conserved *Bauplan* machinery may be redeployed to give rise to novel morphologies.

REFERENCES

ALBERCH, P. & GALE, E. A. (1983). Size dependence during the development of the amphibian foot. Colchicine-induced digital loss and reduction. *Journal of Embryology and Experimental Morphology* **76,** 177-197.

ALBERCH, P. & GALE, E. A. (1985). A developmental analysis of an evolutionary trend: Digital reduction in amphibians. *Evolution* **39**, 8-23.

ALTIG, R. & JOHNSTON, F. (1989). Guilds of anuran larvae: Relationships among developmental modes, morphologies, and habitat. *Herpetological Monograph* **3**, 81-109.

ALTMANN, C. R., BELL, E., SCZYRBA, A., PUN, J., BEKIRANOV, S., GAASTERLAND, T. & BRIVANLOU, A. H. (2001). Microarray-based analysis of early development in *Xenopus laevis*. *Developmental Biology* **236**, 64-75.

ANAND, S., WANG, W. C., POWELL, D. R., BOLANOWSKI, S. A., ZHANG, J., LEDJE, C., PAWASHE, A. B., AMEMIYA, C. T. & SHASHIKANT, C. S. (2003). Divergence of *Hoxc8* early enhancer parallels diverged axial morphologies between mammals and fishes. *Proceedings of the National Academy of Sciences U.S.A.* **100**, 15666-15669.

ARNOLD, S. & WASSERSUG, R. J. (1978). Differential predation on metamorphic anurans by garter snakes (*Thamnophis*): Social behavior as a possible defense. *Ecology* **59**,1014-1022.

AUGIER, M. (1931). Squelette cephalique. In *Traité d'Anatomie Humaine* (eds. P. Poirier & A. Charpy), pp. 89-630, Paris, Masson.

BÁEZ, A. M. & BASSO, N. G. (1996). The earliest known frogs of the Jurassic of South America: Review and cladistic appraisal of their relationships. *Munchen Geowissenschfliche Abhandlungen Reihe (Geologie Palaontologie)* **30**, 131–158.

BANBURY, B. (2005). *Comparative development and osteogenesis of cranial and post-cranial elements in pelobatid tadpoles (Anura: Pelobatidae).* Master's thesis. University of Missouri: Rolla, MO, USA.

BANBURY, B. & MAGLIA, A. M. (2006). Skeletal development of the Mexican spadefoot, *Spea multiplicata* (Anura: Pelobatidae). *Journal of Morphology* **267**, 803-821.

BEJDER, L. & HALL, B. K. (2002). Limbs in whales and limblessness in other vertebrates: Mechanisms of evolutionary and developmental transformation and loss. *Evolution and Development* **4**, 445-458.

BELTING, H. G., SHASHIKANT, C. S. & RUDDLE, F. H. (1998). Modification of expression and cis-regulation of *Hoxc8* in the evolution of diverged axial morphology. *Proceedings of the National Academy of Sciences U.S.A.* **95**, 2355-2360.

BIEKER, J. J. & YAZDANI-BUICKY, M. (1992). Distribution of *type II collagen* mRNA in *Xenopus* embryos visualized by whole-mount *in situ* hybridization. *The Journal of Histochemistry and Cytochemistry* **40,** 1117-1120.

BLANCO, M. J, MISOF, B. Y. & WAGNER G. P. (1998). Heterochronic differences of *Hoxa-11* expression in *Xenopus* fore- and hind limb development: Evidence for lower limb identity of the anuran ankle bones. *Development, Genes and Evolution* **208**, 175-187.

BLITZ, I. L., CHO, K. W. & CHANG, C. (2003). *Twisted gastrulation* loss-of-function analyses support its role as a BMP inhibitor during early *Xenopus* embryogenesis. *Development* **130**, 4975-4988.

BLITZ, I. L., ANDELFINGER, G. & HORB, M. E. (2006). Germ layers to organs: Using *Xenopus* to study "later" development. *Seminars in Cell and Developmental Biology* **17**, 133-145.

BOPP, D., JAMET, E., BAUMGARTNER, S., BURRI, M. & NOLL, M. (1989). Isolation of two tissue-specific *Drosophila* paired box genes, *Pox meso* and *Pox neuro*. *EMBO Journal* **8**, 3447-3457.

BRAND-SABERI, B. & CHRIST, B. (1999). Genetic and epigenetic control of muscle development in vertebrates. *Cell and Tissue Research* **296**, 199-212.

BRAND-SABERI, B., EBENSPERGER, C., WILTING, J., BALLING, R. & CHRIST, B. (1993). The ventralizing effect of the notochord on somite differentiation in chick embryos. *Anatomy and Embryology* **188**, 239–245.

BRAND-SABERI, B., WILTING, J., EBENSPERGER, C. & CHRIST, B. (1996). The formation of somite compartments in the avian embryo. *International Journal of Developmental Biology* **40**, 411-420.

BRANFORD, W. W., BENSON, G. V., MA, L., MAAS, R. L. & POTTER, S. S. (2000). Characterization of *Hoxa-10/Hoxa-11* transheterozygotes reveals functional redundancy and regulatory interactions. *Developmental Biology* **224**, 373-387.

BRENT, A. E. & TABIN, C. J. (2002). Developmental regulation of somite derivatives: Muscle, cartilage and tendon. *Current Opinion in Genetics and Development* **12**, 548-557.

BROWN, H. A. (1989). Developmental anatomy of the tailed frog *Ascaphus truei* a primitive frog with large eggs and slow development. *Journal of Zoology (London)* **217**, 525-538.

BRUNS, R. B. & GROSS, J. (1970). Studies on the tadpole tail. I. Structure and organization of the notochord and its covering layers in *Rana catesbeiana*. *American Journal of Anatomy* **128**, 193-233.

BRUSCA, R. C. & BRUSCA, G. J. (1990). *Invertebrates*. Sinauer Associates, Sunderland, MA.

BRUSTIS, J. J., LANDSMANN, F. & GIPOULOUX, J. D. (1976). The differentiation of the somites in embryos of two anuran amphibians: The common toad (*Bufo bufo* L.) and the frog (*Rana dalmatina* Bon.). *Bulletin Biologique de la France et de la Belgique* **110**, 299-311.

BUCKINGHAM, M. (2001). Skeletal muscle formation in vertebrates. *Current Opinion in Genetics and Development* **11**, 440-448.

BURKE, A. C. (2000). *Hox* genes and the global patterning of the somitic mesoderm. *Current Topics in Developmental Biology* **47**, 155-181.

BURKE, A. C., NELSON, C. E., MORGAN, B. A. & TABIN, C. (1995). *Hox* genes and the evolution of vertebrate axial morphology. *Development* **121**, 333-346.

CALLERY, E. M., FANG, H. & ELINSON, R. P. (2001). Frogs without polliwogs: Evolution of anuran direct development. *BioEssays* **23**, 233-241.

CAPDEVILA, J., TABIN, C. & JOHNSON, R.L. (1998). Control of dorsoventral somite patterning by *Wnt-1* and *β-catenin*. *Developmental Biology* **193**, 182-94.

CARLSON, M. R., KOMINE, Y., BRYANT, S. V. & GARDINER, D. M. (2001). Expression of *Hoxb13* and *Hoxc10* in developing and regenerating Axolotl limbs and tails. *Developmental Biology* **229**, 396-406.

CARROLL, R. L., KUNTZ, A. & ALBRIGHT, K. (1999). Vertebral development and amphibian evolution. *Evolution and Development* **1**, 36-48.

CARRUTHERS, S. & STEMPLE, D. L. (2006). Genetic and genomic prospects for *Xenopus tropicalis* research. *Seminars in Cell and Developmental Biology* **17**, 146-153.

CHALMERS, A. D., GOLDSTONE, K., SMITH, J. C., GILCHRIST, M., AMAYA, E. & PAPALOPULU, N. (2005). A *Xenopus tropicalis* oligonucleotide microarray works across species using RNA from *Xenopus laevis*. *Mechanisms of Development* **122**, 355-363.

CHEN, H.-J., LI, F.-L. & XIAO, H. (1984). Preliminary observations on ecology of *Vibrissaphora ailaonica*. *Acta Herpetologica Sinica*, **3**, 41-45.

CHIANG, C., LITINGTUNG, Y., LEE, E., YOUNG, K. E., CORDEN, J. L., WESTPHAL, H. & BEACHY, P. A. (1996). Cyclopia and defective axial patterning in mice lacking *Sonic hedgehog* gene function. *Nature* **383,** 407-413.

CHIPMAN, A. D. (2002). Variation, plasticity and modularity in anuran development. *Zoology* **105**, 97-104.

CHRIST, B., HUANG, R. & WILTING, J. (2000). The development of the avian vertebral column. *Anatomy and Embryology* **202**, 179-194.

CHRIST, B., HUANG, R. & SCAAL, M. (2004). Formation and differentiation of the avian sclerotome. *Anatomy and Embryology* **208**, 333-350.

CHRIST, B. & ORDAHL, C. P. (1995). Early stages of chick somite development. *Anatomy and Embryology* **191**, 381-396.

CHRIST, B. & WILTING, J. (1992). From somites to vertebral column. *Anatomischer Anzeiger* **174**, 23-32

CHRISTEN, B., BECK, C. W., LOMBARDO, A. & SLACK, J. M. (2003). Regeneration-specific expression pattern of three posterior *Hox* genes. *Developmental Dynamics* **226**, 349-355.

CHUNG, H. M., NEFF, A. W. & MALACINSKI, G. M. (1989). Autonomous death of amphibian (*Xenopus laevis*) cranial myotomes. *Journal of Experimental Zoology* **251**, 290-299.

CLEAVER, O. & KRIEG, P. A. (1998). VEGF mediates angioblast migration during development of the dorsal aorta in *Xenopus*. *Development* **125,** 3905-3914.

CLEAVER, O., SEUFERT, D. W. & KRIEG, P. A. (2000). Endoderm patterning by the notochord: development of the hypochord in *Xenopus*. *Development* **127,** 869-879.

COHN, M. J. & TICKLE, C. (1999). Developmental basis of limblessness and axial patterning in snakes. *Nature* **399**, 474-479.

COSTA, M. L., ESCALEIRA, R., MANASFI, M., DE SOUZA, L. F. & MERMELSTEIN, C. S. (2003). Cytoskeletal and cellular adhesion proteins in zebrafish (*Danio rerio)* myogenesis. *Brazilian Journal of Medical and Biological Research* **36**, 1117-1120.

DE SANTA BARBARA, P. & ROBERTS, D.J. (2002). Tail gut endoderm and gut/genitourinary/tail development: A new tissue-specific role for *Hoxa13*. *Development* **129**, 551-561.

DETWILER, S. R. (1937). Observations upon the migration of neural crest cells, and upon the development of the spinal ganglia and vertebral arches in *Amblystoma*. *American Journal of Anatomy* **61**, 63–94.

DEUTSCH, U., DRESSLER, G. R. & GRUSS, P. (1988). *Pax 1*, a member of a *paired box* homologous murine gene family, is expressed in segmented structures during development. *Cell* **53**, 617-625.

DEVOTO, S. H., MELANCON, E., EISEN, J. S. & WESTERFIELD, M. (1996). Identification of separate slow and fast muscle precursor cells in vivo, prior to somite formation. *Development* **122**, 3371-3380.

DUBOIS, A. (1980). Notes sur la systèmatique et répartition des amphibians anoures de Chine at des régions avoisinantes. IV. Classification generique et subgenerique des Pelobatidae Megophryinae. *Bulletin Mensuel de la Société Linnénne de Lyon* **49**, 469-482.

DUBOULE, D. (1995). Vertebrate *Hox* genes and proliferation: An alternative pathway to homeosis? *Current Opinion in Genetics and Development* **5**, 525-528.

DUDLEY, R., KING, V.A. & WASSERSUG, R. J. (1991). Implications of shape and metamorphosis for drag forces on a generalized pond tadpole (*Rana catesbeiana*). *Copeia* **1**, 252-257.

EBENSPERGER, C., WILTING, J., BRAND-SABERI, B., MIZUTANI, Y., CHRIST, B., BALLING, R. & KOSEKI, H. (1995). *Pax*-1, a regulator of sclerotome development is induced by notochord and floor plate signals in avian embryos. *Anatomy and Embryology* **191**, 297–310.

ECONOMIDES, K.D., ZELTSER, L. & CAPECCHI, M. R. (2003). *Hoxb13* mutations cause overgrowth of caudal spinal cord and tail vertebrae. *Developmental Biology* **256**, 317-330.

EKKER, S. C., MCGREW, L. L., LAI, C. J., LEE, J. J., VON KESSLER, D. P., MOON, R. T. & BEACHY, P. A. (1995). Distinct expression and shared activities of members of the *hedgehog* gene family of *Xenopus laevis*. *Development* **121**, 2337-2347.

EMERSON, S. B. (1979). The ilio-sacral articulation in frogs: Form and function. *Zoological Journal of the Linnean Society* **11**, 153–168.

EMERSON, S. B. (1985). Jumping and leaping. In *Functional Vertebrate Morphology* (eds. M. Hildebrand, D. M. Bramble, K. F. Liem & D. B. Wake), pp. 58-72, Belknap Press, Cambridge.

ERIKSSON, J. & LÖFBERG, J. (2000). Development of the hypochord and dorsal aorta in the zebrafish embryo (*Danio rerio*). *Journal of Morphology* **244**, 167-176.

ESTES, R. & REIG, O. A. (1973). The early fossil record of frogs: A review of the evidence. *In Evolutionary Biology of the Anurans: Contemporary Research on Major Problems* (ed. J. L. Vial), pp. 11-64. University of Missouri Press, Columbia, USA.

FLEMING, A., KEYNES, R. & TANNAHILL, D. (2004). A central role for the notochord in vertebral patterning. *Development* **131**, 873-880.

FLETCHER, R. B., WATSON, A. L. & HARLAND, R. M. (2004). Expression of *Xenopus tropicalis noggin1* and *noggin2* in early development: Two *noggin* genes in a tetrapod. *Gene Expression Patterns* **5**, 225-230.

FOMENOU, M. D., SCAAL, M., STOCKDALE, F. E., CHRIST, B. & HUANG, R. (2005). Cells of all somitic compartments are determined with respect to segmental identity. *Developmental Dynamics* **233**, 1386-1393.

FREUND, R., DORFLER, D., POPP, W. & WACHTLER, F. (1996). The metameric pattern of the head mesoderm--does it exist? *Anatomy & Embryology (Berlin)* **193**, 73-80.

FROST, D. R. (2004). *Amphibian species of the world: An online reference.* Version 3.0. American Museum of Natural History, New York, USA.

FROST, D. R., GRANT, T., FAIVOVICH, J., BAIN, R. H., HAAS, A., HADDAD, C. F. B., DE SÁ, R. O., CHANNING, A., WILKINSON, M., DONNELLAN, S. C., RAXWORTHY, C. J., CAMPBELL, J. A., BLOTTO, B. L., MOLER, P., DREWES, R. C., NUSSBAUM, R. A., LYNCH, J. D., GREEN, D. M., AND WHEELER, W. D. (2006). The amphibian tree of life. *Bulletin of the American Museum of Natural History* **297**, 1-371.

GAD, J. M. & TAM, P. P. (1999). Axis development: The mouse becomes a dachshund. *Current Biology* **9**, R783-R786.

GADOW, H. (1896). On the evolution of the vertebral column of Amphibian and Amniota. *Philosophical Transactions of the Royal Society of London. Series B, Biological Sciences* **187**, 1-57.

GALIS, F. (2001). Evolutionary history of vertebrate appendicular muscle. *BioEssays* **23**, 383-387.

GALIS, F., WAGNER, G. P. & JORKUSCH, E. L. (2003). Why is limb regeneration possible in amphibians but not in reptiles, birds and mammals? *Evolution and Development* **5**, 208-220.

GALLI, L. M., WILLERT, K., NUSSE, R., YABLONKA-REUVENI, Z., NOHNO, T., DENETCLAW, W. & BURRUS, L. W. (2004). A proliferative role for *Wnt-3a* in chick somites. *Developmental Biology* **269**, 489-504.

GAMER, L. W., WOLFMAN, N. M., CELESTE, A. J., HATTERSLEY, G., HEWICK, R. & ROSEN, V. (1999). A novel BMP expressed in developing mouse limb, spinal cord, and tail bud is a potent mesoderm inducer in *Xenopus* embryos. *Developmental Biology* **208**, 222-232.

GANS, C. & PARSONS, T. S. (1966). On the origin of the jumping mechanism in frogs. *Evolution* **20**, 92-99.

GARCIA-GASCA, A. & SPYROPOULOS, D. D. (2000). Differential mammary morphogenesis along the anteroposterior axis in *Hoxc6* gene targeted mice. *Developmental Dynamics* **219**, 261-276.

GARCÍA-PARÍS, M., BUCHHOLZ, D. R. & PARRA-OLEA, G. (2003). Phylogenetic relationships of Pelobatoidea re-examined using mtDNA. *Molecular Phylogenetics and Evolution* **28**, 12–23.

GAUNT, S. J. (1994). Conservation in the *Hox* code during morphological evolution. *International Journal of Developmental Biology* **38**, 549-552.

GAUNT, S. J. (2000). Evolutionary shifts of vertebrate structures and *Hox* expression up and down the axial series of segments: A consideration of possible mechanisms. *International Journal of Developmental Biology* **44**, 109-117.

GILCHRIST, M., ZORN, A. M., VOIGT, J, SMITH, J.C., PAPALOPULU, N. & AMAYA, E. (2004). Defining a large set of full length clones from a *Xenopus tropicalis* EST project. *Developmental Biology* **271**, 498-516.

GODSAVE, S., DEKKER, E. J., HOLLING, T., PANNESE, M., BONCINELLI, E. & DURSTON, A. (1994). Expression patterns of *Hoxb* genes in the *Xenopus* embryo suggest roles in anteroposterior specification of the hindbrain and in dorsoventral patterning of the mesoderm. *Developmental Biology* **166**, 465-476.

GOSNER, K. L. (1960). A simplified table for staging anuran embryos and larvae with notes on identification. *Herpetologica* **16**, 183-190.

GOULDING, M. D., LUMSDEN, A. & GRUSS, P. (1993). Signals from the notochord and floor plate regulates the region-specific expression of two *Pax* genes in the developing spinal cord. *Development* **117**, 1001-1016.

GOULDING, M. D., LUMSDEN, A. & PAQUETT, A. J. (1994). Regulation of *Pax-3* expression in the dermomyotome and its role in muscle development. *Development* **120**, 957-971.

GRIFFITHS, I. (1956). The status of *Protobatrachus massinoti*. *Nature* **177**, 342-343.

GRIFFITHS, I. (1963). The phylogeny of the Salientia. *Biological Reviews of the Cambridge Philosophical Society* **38**, 241-292.

GROSJEAN, S. (2003). A redescription of the external and buccopharyngeal morphology of the tadpole of *Ophryophryne microstoma* Boulenger, 1903 (Megophryidae). *Alytes* **21**, 45-58.

GROSJEAN, S. (2006). Apport des caractères larvaires à la phylogénie des Amphibiens Anoures. Cas de deux familles: Les Megophryidae et les Ranidae. *Mémoires du Muséum national d'Histoire naturelle*, in press.

HAAS, A., HERTWIG, S. & DAS, I. (2006). Extreme tadpoles: The morphology of the fossorial megophryid larva, *Leptobrachella mjobergi*. *Zoology* **109**, 26-42.

HALL, B. K. (1992). *Evolutionary Developmental Biology*. Chapman & Hall, New York.

HALL, B. K. (1996). *Baupläne*, phylotypic stages, and constraint: Why there are so few types of animals. *Evolutionary Biology* **29**, 215-261.

HALL, B. K. & MIYAKE, T. (2000). All for one and one for all: Condensations and the initiation of skeletal development. *BioEssays* **22**, 138-147.

HALL, B. K. & OLSON, W. M. (2003). *Keywords and Concepts in Evolutionary Developmental Biology*. Harvard University Press, Cambridge, MA.

HALL, J. A. & LARSEN, J. H. (1998). Postembryonic ontogeny of the spadefoot toad, *Scaphiopus intermontanus* (Anura: Pelobatidae): Skeletal morphology. *Journal of Morphology* **238**, 179-244.

HAMILTON, L. (1969). The formation of somites in *Xenopus*. *Journal of Embryology and Experimental Morphology* **22**, 253-264.

HAMMERSCHMIDT, M. & MCMAHON, A. P. (1998). The effect of pertussis toxin on zebrafish development: A possible role for inhibitory G-proteins in *hedgehog* signaling. *Developmental Biology* **194**, 166-171.

HANDRIGAN, G. R. (2003). *Concordia discors*: Duality in the origin of the vertebrate tail. *Journal of Anatomy* **202**, 255-267.

HANKEN, J. & WASSERSUG, R. (1981). The visible skeleton. *Functional Photograph* **44**, 22-26.

HIRSCH, N., ZIMMERMAN, L. B. & GRAINGER, R. M. (2002). *Xenopus*, the next generation: *X. tropicalis* genetics and genomics. *Developmental Dynamics* **225**, 422-433.

HOFF, K. V.-S. & WASSERSUG, R. J. (2000). Tadpole locomotion: Axial movement and tail functions in a largely vertebraeless vertebrate. *American Zoologist* **40**, 62-76.

HOMBRÍA, J. C. & LOVEGROVE, B. (2003). Beyond homeosis—*Hox* function in morphogenesis and organogenesis. *Differentiation* **71**, 461-476.

HORB, M. E., SHEN, C. N., TOSH, D. & SLACK, J. M. (2003). Experimental conversion of liver to pancreas. *Current Biology* **13**, 105-115.

HOSTIKKA, S. L. & CAPECCHI, M. R. (1998). The mouse *Hoxc11* gene: Genomic structure and expression pattern. *Mechanisms of Development* **70**, 133-145.

HUTCHINSON, J. R. (2004). Biomechanical modeling and sensitivity analysis of bipedal running ability. I. Extant taxa. *Journal of Morphology* **262,** 421-440.

IIMURA, T. & POURQUIÉ, O. (2006). Collinear activation of *Hoxb* genes during gastrulation controls cell ingression into mesoderm. *Nature*, in press.

INGER, R.F. & WASSERSUG, R. J. (1990). A centrolenid-like anuran larva from Southeast Asia. *Zoological Science* **7**, 557-561.

JACOB, M., CHRIST, B. & JACOB, H. J. (1975). Über die regionale Determination des paraxialen Mesoderms junger Hühnerembryonen. *Verhandlungen der Anatomischen Gesellschaft* **69**, 263-269.

JACOBSON, A. G. (1988). Somitomeres: Mesodermal segments of vertebrate embryos. *Development Supplement* **104**, 209-220.

JENKINS, F. A. & SHUBIN, N. H. (1998). *Prosalirus bitis* and the anuran caudopelvic mechanism. *Journal of Vertebrate Paleontology* **18**, 495-510.

JIANG, J.-P., YUAN, F.-R., FENG, X. & ZHENG, Z.-H. (2003) Phylogenetic relationships of some species and genera in megophryids inferred from partial sequences of mitochondrial 12S and 16S rRNA genes. *Zoological Research* **24**, 241-248.

JOHNSON, A. D., DRUM, M., BACHVAROVA, R. F., MASI, T., WHITE, M. E. & CROTHER, B. I. (2003). Evolution of predetermined germ cells in vertebrate embryos: Implications for macroevolution. *Evolution & Development* **5**, 414-431.

KELLER, R. (2000). The origin and morphogenesis of amphibian somites. *Current Topics in Developmental Biology* **47**, 183-246.

KIEŁBÓWNA, L. (1981). The formation of somites and early myotomal myogenesis in *Xenopus laevis*, *Bombina variegata* and *Pelobates fuscus*. *Journal of Embryology and Experimental Morphology* **64**, 295-304.

KIENY, M., MAUGER, A. & SENGEL, P. (1972). Early regionalization of somitic mesoderm as studied by the development of axial skeleton of the chick embryo. *Developmental Biology* **28**, 142-161.

KO, C. & CHUNG, H. M. (2003). *Xenopus hoxc8* during early development. *Biochemical and Biophysical Research Communications* **300**, 9-15.

KOSEKI, H., WALLIN, J., WILTING, J., MIZUTANI, Y., KISPERT, A., EBENSPERGER, C., HERRMANN, B. G., CHRIST, B. & BALLING, R. (1993). A role for *Pax-1* as a mediator of notochordal signals during the dorsoventral specification of vertebrae. *Development* **119**, 649-660.

KURATANI, S. (2005). Craniofacial development and the evolution of the vertebrates: The old problems on a new background. *Zoological Science* **22**, 1-19.

LATHROP, A. (1997). Taxonomic review of the megophryid frogs (Anura: Pelobatoidea). *Asiatic Herpetological Research* **7**, 68-79.

LATHROP, A. (2003). Asian toadfrogs (Megophryidae). In *Grzimek's Animal Life Encyclopedia*, 2nd ed., vol. 6. Amphibians (ed. W. E. Duellman), pp. 109–117. Gale Group, Detroit.

LATIMER, A. J., DONG, X., MARKOV, Y. & APPEL, B. (2002). *Delta-Notch* signaling induces hypochord development in zebrafish. *Development* **129**, 2555-2563.

LEITGES, M., NEIDHARDT, L., HAENIG, B., HERRMANN, B. G. & KISPERT, A. (2000). The paired homeobox gene *Uncx4.1* specifies pedicles, transverse processes and proximal ribs of the vertebral column. *Development* **127**, 2259-2267.

LIU, C. C. (1960). New Scutigers from China with a discussion about the genus. *Scientia Sinica* **9**, 760-780.

LIU, H., WASSERSUG, R. J. & KAWACHI, K. (1996). A computational fluid dynamics study of tadpole swimming. *Journal of Experimental Biology* **199**, 1245-1260.

LIU, H., WASSERSUG, R. J. & KAWACHI, K. (1997). The three dimensional hydrodynamics of tadpole locomotion. *Journal of Experimental Biology* **200**, 2807-2819.

LIU, J. P. (2006). The function of *growth/differentiation factor 11* (*Gdf11*) in rostrocaudal patterning of the developing spinal cord. *Development*, published online.

LO, P. C. & FRASCH, M. (1999). Sequence and expression of *myoglianin*, a novel *Drosophila* gene of the *TGF-β* superfamily. *Mechanisms of Development* **86**, 171-175.

LÖFBERG, J. & COLLAZO, A. (1997). Hypochord, an enigmatic embryonic structure: Study of the axolotl embryo. *Journal of Morphology* **232**, 57-66.

LOMBARDO, A. & SLACK, J. M. (2001). *Abdominal B*-type *Hox* gene expression in *Xenopus laevis*. *Mechanisms of Development* **106**, 191-195.

LUTZ, G. J. & ROME, L. C. (1994). Built for jumping: The design of the frog muscular system. *Science* **263**, 370-372.

MAGLIA, A. M. (2003). Skeletal development of *Pelobates cultripes* and comparisons of the osteology of pelobatoid frogs. *Scientific Papers, Natural History Museum, University of Kansas* **30**, 1-13.

MAGLIA, A. M. & PÚGENER, L. A. (1998). Skeletal development and adult osteology of *Bombina orientalis* (Anura: Bombinatoridae). *Herpetologica* **54**, 344-363.

MALACINSKI, G. M., NEFF, A. W., RADICE, G. & CHUNG, H.-M. (1989). Amphibian somite development: Constrasts of morphogenetic and molecular differentiation patterns between the laboratory archetype species *Xenopus* (anuran) and axolotl (urodele). *Zoological Science* **6**, 1-14.

MANSOURI, A., VOSS, A. K., THOMAS, T., YOKOTA, Y. & GRUSS, P. (2000). *Uncx4.1* is required for the formation of the pedicles and proximal ribs and acts upstream of *Pax9*. *Development* **127**, 2251-2258.

MARTIN, B. L. & HARLAND, R. M. (2001). Hypaxial muscle migration during primary myogenesis in *Xenopus laevis*. *Developmental Biology* **239**, 270-280.

MARTIN, B. L. & HARLAND, R. M. (2006). A novel role for *lbx1* in *Xenopus* hypaxial myogenesis. *Development* **133**, 195-208.

MCMAHON, J. A., TAKADA, S., ZIMMERMAN, L. B., FAN, C. M., HARLAND, R. M. & MCMAHON, A. P. (1998). Noggin-mediated antagonism of BMP signaling is required for growth and patterning of the neural tube and somite. *Genes & Development* **12,** 1438-1452.

MCPHERRON, A. C., LAWLER, A. M. & LEE, S. J. (1999). Regulation of anterior/posterior patterning of the axial skeleton by *growth/differentiation factor 11*. *Nature Genetics* **22**, 260-264.

MELBY, A. E., WARGA, R. M. & KIMMEL, C. B. (1996). Specification of cell fates at the dorsal margin of the zebrafish gastrula. *Development* **122,** 2225-2237.

MOOKERJEE, H. K. (1931). On the development of the vertebral column of Anura. *Philosophical Transactions of the Royal Society of London. Series B, Biological sciences* **219**, 165-195.

MOOKERJEE, H. K. & DAS, S. K. (1939). Further investigation on the development of the vertebral column in Salientia (Anura). *Journal of Morphology* **64**, 167-209.

MORIN-KENSICKI, E. M., MELANCON, E. & EISEN, J. S. (2002). Segmental relationship between somites and vertebral column in zebrafish. *Development* **129,** 3851-3860.

MULLER, T. S., EBENSPERGER, C., NEUBUSER, A., KOSEKI, H., BALLING, R., CHRIST, B., AND WILTING, J. (1996). Expression of avian *Pax1* and *Pax9* is intrinsically regulated in the pharyngeal endoderm, but depends on environmental influences in the paraxial mesoderm. *Developmental Biology* **178**, 403-417.

MURTAUGH, L. C., CHYUNG, J. H. & LASSAR, A. B. (1999). *Sonic hedgehog* promotes somitic chondrogenesis by altering the cellular response to BMP signaling. *Genes and Development* **13**, 225–237.

MURTAUGH, L. C., ZENG, I., CHYUNG, J. H. & LASSAR, A. B. (2001). The chick transcriptional repressor *Nkx3.2* acts downstream of Shh to promote BMP-dependent axial chondrogenesis. *Developmental Cell* **1**, 411–422.

NAKASHIMA, M., TOYONO, T., AKAMINE, A. & JOYNER, A. (1999). Expression of *growth/differentiation factor 11*, a new member of the BMP/TGFbeta superfamily during mouse embryogenesis. *Mechanisms of Development* **80**, 185-189.

NEUBUSER, A., KOSEKI, H. & BALLING, R. (1995). Characterization and developmental expression of *Pax9*, a paired-box-containing gene related to *Pax1*. *Developmental Biology* **170,** 701-716.

NEWMAN, C. S., GROW, M. W., CLEAVER, O., CHIA, F. & KRIEG, P. (1997). *Xbap*, a vertebrate gene related to *bagpipe*, is expressed in developing craniofacial structures and in anterior gut muscle. *Developmental Biology* **181**, 223-233.

NEWMAN, C. S. & KRIEG, P. A. (1999). The *Xenopus bagpipe*-related homeobox gene *zampogna* is expressed in the pharyngeal endoderm and the visceral musculature of the midgut. *Development, Genes and Evolution* **209**, 132-134.

NEWMAN, C. S. & KRIEG, P. A. (2002) *Xenopus bagpipe*-related gene, *koza*, may play a role in regulation of cell proliferation. *Developmental Dynamics* **225**, 571-580.

NEYT, C., JAGLA, K., THISSE, C., THISSE, B., HAINES, L. & CURRIE, P. D. (2000). Evolutionary origins of vertebrate appendicular muscle. *Nature* **408**, 82-86.

NIELSEN, C. (2003). Defining phyla: Morphological and molecular clues to metazoan evolution. *Evolution and Development* **5**, 386-393.

NIEUWKOOP, P. D. & FABER, J. (1956). *Normal table of* Xenopus laevis *(Daudin)*. North Holland, Amsterdam.

NISHIKAWA, K. & WASSERSUG, R. (1988). Morphology of the caudal spinal cord in *Rana* (Ranidae) and *Xenopus* (Pipidae) tadpoles. *Journal of Comparative Neurology* **269**, 193-202.

NISHIKAWA, K. & WASSERSUG, R. (1989). Evolution of spinal nerve number in anuran larvae. *Brain, Behavior and Evolution* **33**, 15-24.

NODZENSKI, E. & INGER, R. F. (1990). Uncoupling of related structural changes in metamorphosing torrent-dwelling tadpoles. *Copeia* **4**, 1047-1054.

NODZENSKI, E., WASSERSUG, R. J. & INGER, R. F. (1989). Developmental differences in visceral morphology of megophrynine pelobatid tadpoles in relation to their body form and mode of life. *Biological Journal of the Linnean Society* **38**, 369-388.

NOETZEL, W. (1895). Die Rüchbildung der Gewebe im Schwanz der Froshlarve. *Archiv für Mikroskopische Anatomie* **45**, 475-512.

NORNES, S., MIKKOLA, I., KRAUSS, S., DELGHANDI, M., PERANDER, M. & JOHANSEN, T. (1996). Zebrafish *Pax9* encodes two proteins with distinct C-terminal transactivating domains of different potency negatively regulated by adjacent N-terminal sequences. *The Journal of Biological Chemistry* **271**, 26914-26923.

OHYA, Y. K., KURAKU, S. & KURATANI, S. (2005). Hox code in embryos of Chinese Soft-Shelled Turtle Pelodiscus sinesis correlates with the evolutionary innovation in the turtle. *Journal of Experimental Zoology. Part B. Molecular and Developmental Evolution* **304**, 107-118.

O'RAHILLY, R. & MULLER, F. (2003). Somites, spinal ganglia, and centra: Enumeration and interrelationships in staged human embryos, and implications for neural tube defects. *Cells Tissues Organs* **173**, 75-92.

ORTON, G. L. (1953). The systematics of vertebrate larvae. *Systematic Zoology* **2**, 63-75.

PELLEGRINI, M., PANTANO, S., FUMI, M. P., LUCCHINI, F. & FORABOSCO, A. (2001). Agenesis of the scapula in *Emx2* homozygous mutants. *Developmental Biology* **232**, 149-156.

PEPLOWSKI, M. M. & MARSH, R. L. (1997). Work and power output in the hindlimb muscles of Cuban tree frogs *Osteopilus septentrionalis* during jumping. *Journal of Experimental Biology* **200**, 2861-2870.

PETERS, H., DOLL, U. & NIESSING, J. (1995). Differential expression of the chicken *Pax-1* and *Pax-9* gene: *in situ* hybridization and immunohistochemical analysis. *Developmental Dynamics* **203**, 1-16.

PETERS, H., NEUBUSER, A., KRATOCHWIL, K. & BALLING, R. (1998). *Pax9*-deficient mice lack pharyngeal pouch derivatives and teeth and exhibit craniofacial and limb abnormalities. *Genes & Development* **12**, 2735-47.

PETERS, H., WILM, B., SAKAI, N., IMAI, K., MAAS, R. & BALLING, R. (1999). *Pax1* and *Pax9* synergistically regulate vertebral column development. *Development* **126**, 5399-5408.

PFAFF, S. L., MENDELSOHN, M., STEWART, C. L., EDLUND, T. & JESSELL, T. M. (1996). Requirement for LIM homeobox gene *Isl1* in motor neuron generation reveals a motor neuron-dependent step in interneuron differentiation. *Cell* **26**, 309-320.

POURQUIÉ, O. (2001). Vertebrate somitogenesis. *Annual Review of Cell and Developmental Biology* **17**, 311-350.

POURQUIÉ, O., COLTEY, M., TEILLET, M. A., ORDAHL, C. P. & LE DOUARIN, N. M. (1993). Control of dorsoventral patterning of somitic derivatives by notochord and floor plate. *Proceedings of the National Academy of Sciences U.S.A.* **90**, 5242–5246.

PÚGENER, L. A. (2002). *The vertebral column and spinal nerves of anurans*. Doctoral dissertation. University of Kansas: Lawrence, KS.

PÚGENER, L. A. & MAGLIA, A. M. (1997). Osteology and skeletal development of *Discoglossus sardus* (Anura: Discoglossidae). *Journal of Morphology* **233**, 267-286.

RAGE, J.-C. & ROČEK, Z. (1989). Redescription of *Triadobatrachus massinoti* (Piveteau 1936) an anuran amphibian from the Early Triassic. *Palaeontographica Abteilung A* **206**, 1–16.

ROBERTS, T. J. & MARSH, R. L. (2003). Probing the limits to muscle-powered accelerations: Lessons from jumping bullfrogs. *Journal of Experimental Biology* **206**, 2567-2580.

ROČKOVÁ, H. & ROČEK, Z. (2005). Development of the pelvis and posterior part of the vertebral column in the Anura. *Journal of Anatomy* **206**, 17-35.

RODRIGO, I., HILL, R. E., BALLING, R., MUNSTERBERG, A. & IMAI, K. (2003). *Pax1* and *Pax9* activate *Bapx1* to induce chondrogenic differentiation in the sclerotome. *Development* **130**, 473-482.

SAMBROOK, J., FRITSCH, E. F. & MANIATIS, T. (1989). Molecular Cloning: A Laboratory Manual, Second Edition. Cold Spring Harbor Laboratory Press, Cold Spring Harbor, USA.

SATOH, A., SAKAMAKI, K., IDE, H. & TAMURA, K. (2005). Characteristics of initiation and early events for muscle development in the *Xenopus* limb bud. *Developmental Dynamics* **234**, 846-857.

SCHAEREN-WIEMERS, N. & GERFIN-MOSER, A. (1993). A single protocol to detect transcripts of various types and expression levels in neural tissue and cultured cells: *in situ* hybridization using digoxigenin-labelled cRNA probes. *Histochemistry* **100**, 431-440.

SCHOENWOLF, G. C. (1981). Morphogenetic processes involved in the remodeling of the tail region of the chick embryo. *Anatomy and Embryology* **162**, 183-197.

SEARS, K. E., BEHRINGER, R. R., RASWEILER, J. J. & NISWANDER, L. A. (2006). The development of bat flight: Morphologic and molecular evolution of bat wing digits. *Proceedings of the National Academy of Sciences U.S.A.* **103**, 6581-6586.

SEO, H. C., SAETRE, B. O., HAVIK, B., ELLINGSEN, S. & FJOSE, A. (1998). The zebrafish *Pax3* and *Pax7* homologs are highly conserved, encode multiple isoforms and show dynamic segment-like expression in the developing brain. *Mechanisms of Development* **70**, 49-63.

SHASHIKANT, C., BOLANOWSKI, S. A., DANKE, J. & AMEMIYA, C.T. (2004). *Hoxc8* early enhancer of the Indonesian coelacanth, *Latimeria menadoensis*. *Journal of Experimental Zoology. Part B. Molecular and Developmental Evolution* **302**, 557-563.

SHASHIKANT, C. S., KIM, C. B., BORBELY, M. A., WANG, W. C. & RUDDLE, F. H. (1998). Comparative studies on mammalian *Hoxc8* early enhancer sequence reveal a baleen whale-specific deletion of a cis-acting element. *Proceedings of the National Academy of Sciences U.S.A.* **95**, 15446-15451.

SHOOK, D. R., MAJER, C. & KELLER, R. (2004). Pattern and morphogenesis of presumptive superficial mesoderm in two closely related species, *Xenopus laevis* and *Xenopus tropicalis*. *Developmental Biology* **270,** 163-185.

SHUBIN, N. H. & JENKINS, F. A. (1995). An Early Jurassic jumping frog. *Nature* **377**, 49-52.

SIVE, H. L., GRAINGER, R. M., & HARLAND, R. M. (2000). Early development of *Xenopus laevis*: A laboratory manual. Cold Spring Harbor Laboratory Press, Cold Spring Harbor, USA.

SMIT, A.L. (1953). The ontogenesis of the vertebral column of *Xenopus laevis* (Daudin) with special reference to the segmentation of the metotic region of the skull. *Annals of the University of Stellenbosch* **29**, 79-136.

SMITH, M. A. (1917). On tadpoles from Siam. *Journal of the Natural History Society of Siam* **2**, 261-278.

SMITH, W. C. & HARLAND, R. M. (1992). Expression cloning of *noggin*, a new dorsalizing factor localized to the Spemann organizer in *Xenopus* embryos. *Cell* **70,** 829-840.

SPOKONY, R. F., AOKI, Y., SAINT-GERMAIN, N., MAGNER-FINK, E. & SAINT-JEANNET, J. P. (2002). The transcription factor *Sox9* is required for cranial neural crest development in *Xenopus*. *Development* **129,** 421-432.

STEINBEISSER, H., FAINSOD, A., NIEHRS, C., SASAI, Y. & DE ROBERTIS, E. M. (1995). The role of *gsc* and *BMP-4* in dorsal-ventral patterning of the marginal zone in *Xenopus*: A loss-of-function study using antisense RNA. *EMBO Journal* **14**, 5230-5243.

STICKNEY, H. L., BARRESI, M. J. & DEVOTO, S. H. (2000). Somite development in zebrafish. *Developmental Dynamics* **219**, 287-303.

STRACHAN, T. & READ, A. P. (1994). *PAX* genes. *Current Opinion in Genetics and Development* **4**, 427-438.

SU, M. W., SUZUKI, H. R., BIEKER, J. J., SOLURSH, M. & RAMIREZ, F. (1991). Expression of two nonallelic t*ype II procollagen* genes during *Xenopus laevis* embryogenesis is characterized by stage-specific production of alternatively spliced transcripts. *The Journal of Cell Biology* **115,** 565-575.

SUGIMOTO, K., HAYATA, T. & ASASHIMA M. (2005). *XBtg2* is required for notochord differentiation during early *Xenopus* development. *Development, Growth & Differentiation* **47**, 435-443.

TICKLE, C. (2002). Vertebrate limb development and possible clues to diversity in limb form. *Journal of Morphology* **252**, 29-37.

TOWNSEND, D. S. & STEWART, M. M. (1985). Direct development in *Eleutherodactylus coqui* (Anura: Leptodactylidae): A staging table. *Copeia* **2**, 423-436.

TRUEB, L. (1973). Bones, frogs, and evolution. *In Evolutionary Biology of the Anurans: Contemporary Research on Major Problems* (ed. J. L. Vial), pp. 65-132. University of Missouri Press, Columbia, USA.

TRUEB, L., PÚGENER, L. A. & MAGLIA, A. M. (2000). Ontogeny of the bizarre: An osteological description of *Pipa pipa* (Anura: Pipidae), with an account of skeletal development in the species. *Journal of Morphology* **243**, 75-104.

TUCKER, A. S. & SLACK, J. M. W. (1995). The *Xenopus laevis* tail-forming region. *Development* **121**, 249-262.

UNDERHILL, D. A. (2000). Genetic and biochemical diversity in the *Pax* gene family. *Biochemistry and Cell Biology* **78**, 629-638.

VAN DIJK, E. D. (1959). On the cloacal region of Anura in particular of larval *Ascaphus*. *Annals of the University of Stellenbosch* **35**, 169-249.

WACHTLER, F. & JACOB, M. (1986). Origin and development of the cranial skeletal muscles. *Bibliotheca Anatomica* **29,** 24-46.

WAGNER, J., SCHMIDT, C., NIKOWITS, W. JR. & CHRIST, B. (2000). Compartmentalization of the somite and myogenesis in chick embryos are influenced by *wnt* expression. *Developmental Biology* **228**, 86-94.

WAKE, D. B. (1970). Aspects of vertebral evolution in the modern amphibia. *Forma et Functio* **3**, 33-60.

WAKE, D. B. & LAWSON, R. (1973). Developmental and adult morphology of the vertebral column in the plethodontid salamander *Eurycea bislineata* with comments on vertebral evolution in the Amphibia. *Journal of Morphology* **139**, 251-300.

WAKE, M. H. (1980). Morphometrics of the skeleton of *Dermophis mexicanus* (Amphibia: Gymnophiona). Part I. The vertebrae with comparisons to other species. *Journal of Morphology* **165**, 117-130.

WAKE, M. H. & WAKE, D. B. (2000). Developmental morphology of early vertebrogenesis in caecilians (Amphibia: Gymnophiona): Resegmentation and phylogenesis. *Zoology* **103**, 68-88.

WALLIN, J., EIBEL, H., NEUBUSER, A., WILTING, J., KOSEKI, H. & BALLING, R. (1996). *Pax1* is expressed during development of the thymus epithelium and is required for normal T-cell maturation. *Development* **122**, 23-30.

WALLIN, J., WILTING, J., KOSEKI, H., FRITSCH, R., CHRIST, B. & BALLING, R. (1994). The role of *Pax-1* in axial skeleton development. *Development* **120**, 1109-1121.

WANG, W. C., ANAND, S., POWELL, D. R., PAWASHE, A. B., AMEMIYA, C. T. & SHASHIKANT, C. S. (2004). Comparative cis-regulatory analyses identify new elements of the mouse *Hoxc8* early enhancer. *Journal of Experimental Zoology. Part B. Molecular and Developmental Evolution* **302**, 436-445.

WARGA, R. M. & NÜSSLEIN-VOLHARD, C. (1999). Origin and development of the zebrafish endoderm. *Development* **126,** 827-838.

WASSERSUG, R.J. (1989). Locomotion in amphibian larvae (or "Why aren't tadpoles built like fishes?"). *American Zoologist* **29**, 65-84.

WASSERSUG, R. J. (2001). Cover picture and accompanying text. *Herpetological Review* **32**, 74.

WASSERSUG, R.J. & PYBURN, W. F. (1987). The biology of the Pe-ret' toad *Otophryne robusta* (Microhylidae) with special consideration of its fossorial larvae and systematic relationships. *Zoological Journal of the Linnean Society* **91**, 137-169.

WASSERSUG, R.J. & SPERRY, D. (1977). The relationship of locomotion to differential predation on *Pseudacris triseriata* (Anura: Hylidae). *Ecology* **58**, 830-839.

WELLIK, D. M. & CAPECCHI, M. R. (2003). *Hox10* and *Hox11* genes are required to globally pattern the mammalian skeleton. *Science* **301**, 363-367.

WILD, E. R. (1997). Description of the adult skeleton and developmental osteology of the hyperossified horned frog, *Ceratophrys cornuta* (Anura:Leptodactylidae). *Journal of Morphology* **232**, 169-206.

WILD, E. R. (1999). Description of the chondrocranium and osteogenesis of the Chacoan burrowing frog, *Chacophrys pierotti* (Anura: Leptodactylidae). *Journal of Morphology* **242**, 229-246.

WILLIAMS, B. A. & ORDAHL, C. P. (1994). *Pax-3* expression in segmental mesoderm marks early stages in myogenic cell specification. *Development* **120**, 785-796.

WILLIAMS, E. E. (1959). Gadow's arcualia and the development of tetrapod vertebrae. *The Quarterly Review of Biology* **34**, 1-32.

YOKOUCHI, Y., NAKAZATO, S., YAMAMOTO, M., GOTO, Y., KAMEDA, T., IBA, H. & KUROIWA, A. (1995). Misexpression of *Hoxa-13* induces cartilage homeotic transformation and changes cell adhesiveness in chick limb buds. *Genes and Development* **9**, 2509-2522.

YOUN, B. W. & MALACINSKI, G. M. (1981). Comparative analysis of amphibian somite morphogenesis: Cell rearrangement patterns during rosette formation and myoblast fusion. *Journal of Embryology and Experimental Morphology* **66**, 1-26.

YOUNG, J. Z. (1962). *The Life of Vertebrates*. Oxford University Press, London.

ZHAO, E.-M., INGER, R. F., WU, G.-F. & SHAFFER, H. B. (1994). Morphological variation and ecological distribution of co-occuring larval forms of *Oreolalax* (Anura: Pelobatidae). *Amphibia-Reptilia*, **15**, 109-121.

ZHENG, Y.-C., MO, B.-H., LIU, Z.-J. & ZENG, X.-M. (2004). Phylogenetic relationships of megophryid genera (Anura: Megophryidae) based on partial sequences of mitochondrial 16S rRNA gene. *Zoological Research* **25**, 205-213.